Subduction-obduction related petrogenetic and metamorphic evolution of the Semail ophiolite sole in Oman and the United Arab Emirates.

Jon Cox BA (Oxon)



Thesis submitted for the degree of
Doctor of Philosophy (DPhil)
at the University of Oxford

Hertford College
&
Department of Earth Sciences

Hilary term, April 2000

Subduction-obduction related petrogenetic and metamorphic evolution of the Semail ophiolite sole, Oman/United Arab Emirates.

Jon Cox (BA, Oxon)

Thesis submitted for the degree of Doctor of Philosophy (DPhil) in the University of Oxford

Hertford College & Department of Earth Sciences

Hilary term, April 2000

ABSTRACT

Structural field observations, combined with petrological, isotopic and geochemical analysis of metamorphic and igneous rocks associated with the Semail ophiolite of Oman and the United Arab Emirates, have been used in conjunction with geochronology and estimates of metamorphic conditions and PT paths to constrain the ophiolite emplacement history.

The ophiolite metamorphic sole was formed at peak conditions of 840 ± 70°C and 11.6 ± 1.6 kbar (THERMOCALC) and 840-870°C and 11.8-13.9 kbar (conventional thermobarometry) and is characterised by an anticlockwise PTt path. Further analysis and structural constraints imply an apparent inverted sole gradient of ~2°C m^{-1} and ~3.7 MPa m^{-1}. In conjunction with existing geochronology, a peak sole exhumation rate of ~12.5 mm yr^{-1} is indicated. Geochemical analysis and tectonic constraints suggest that the Semail ophiolite sole formed from neo Tethyan MORB crust similar in composition to the preserved Triassic-Jurassic Haybi tholeiites and Masirah ophiolite crust. The Bani Hamid granulite facies sole metamorphism peaked at ~96.5 Ma and exhibits a similar PTt path and peak conditions, but formed from oceanic island igneous, volcanoclastic and sedimentary protoliths.

Anatectic granitoids in the ophiolite mantle sequence have geochemical and isotopic (Rb-Sr and Sm-Nd) characteristics compatible with derivation from the Bani Hamid sole granulites during prograde metamorphism and have ages of 98.8 ± 9.5 Ma, 93.0 ± 10.0 Ma (Sm-Nd) and 105 ± 4 Ma (U-Pb).

The Saih Hatat high pressure metamorphic terrane beneath the ophiolite consists of two contrasting structural levels juxtaposed during exhumation following the subduction of the Arabian continental margin beneath the advancing ophiolite. PT analysis shows the HP event culminated at 450-550°C and 20.0 ± 1.5 kbar (THERMOCALC) and was characterised by a clockwise PTt path. In conjunction with ambiguous existing geochronology, a peak exhumation rate of ~4-12 mm yr^{-1} is indicated, followed by erosion at ~0.5 mm yr^{-1}.

Subduction-obduction related petrogenetic and metamorphic evolution of the Semail ophiolite sole, Oman/United Arab Emirates.

Jon Cox (BA, Oxon)

Thesis submitted for the degree of Doctor of Philosophy (DPhil) in the University of Oxford

Hertford College & Department of Earth Sciences

Hilary term, April 2000

EXTENDED ABSTRACT

The Semail ophiolite of SE Arabia is the largest and most extensively studied ophiolite in the world and is characterised by a complete oceanic crustal and upper mantle stratigraphy. None the less, there are a number of facets of the emplacement tectonics of the ophiolite that have remained unclear.

The ophiolite forms a well exposed allochthonous thrust sheet ~700 km in length, 100 km wide, and 10-15 km thick in the United Arab Emirates (UAE) and Oman, and is of Cenomanian age and formed ~95 Ma ago, undoubtedly at an oceanic spreading centre within Tethys. Evidence from this study suggests the ophiolite formed in a supra-subduction zone (SSZ) setting. The ophiolite exhibits a well developed and exposed range of emplacement related sub ophiolitic metamorphic rocks, as well as leucogranitic material intruded into the base of the ophiolite mantle sequence.

During this study, field structural and tectonic observations and mapping techniques have been combined with petrological, isotopic and geochemical analysis of these metamorphic (HT material in the ophiolite metamorphic sole and the Bani Hamid terrane, and HP material in the Saih Hatat terrane) and igneous (anatectic granitoids in the ophiolite mantle sequence) rocks associated with the Semail ophiolite, in conjunction with geochronology and estimates of metamorphic conditions and PT paths, in order to constrain the ophiolite emplacement history.

Following initial intra-oceanic thrusting and the formation of the highest grade components of the metamorphic sole, the emplacement process lasted ~23 Ma and was completed by the end of the Lower Maastrichtian (~72 Ma) when shallow-marine fossiliferous limestones were deposited unconformably over the entire ophiolite complex. If the Semail ophiolite was emplaced a minimum horizontal distance of 400 km in 23 Ma, an average emplacement rate of ~17 mm yr^{-1} is indicated; if the ophiolite moved 600 km, the average emplacement rate would have been ~26 mm yr^{-1}.

In the southern and central Oman mountains the metamorphic sole along the base of the Semail ophiolite commonly forms an intermittently outcropping but discrete thrust sheet typically ~250 m thick. Major metamorphic sole outcrops mapped and sampled during the course of field work include Wadi Tayin, Al Ajal, Wadi Hawasina, Asjudi, Haybi and Asimah. The sole exhibits a steep, inverted thermal gradient from rare enstatite diopside granulites and garnet diopside hornblende amphibolite granulites at the peridotite contact, downwards through plagioclase hornblende and epidote amphibolites, to a variety of greenschist facies metasediments, mainly quartzites and marbles, with subordinate volcanoclastic and carbonate units. Overprinting of peak assemblages by a greenschist facies assemblage is common and more intense towards the base of the ophiolite. Small volumes of partial melting occur at the highest grade parts of the metamorphic sole where small scale melt veins of hornblende tonalite intrude garnet-diopside amphibolite granulites. Thermobarometry indicates that these tonalitic melts typically formed at 656 ± 17°C and 5.6 ± 0.6 kbar during prograde metamorphism and indicate an anticlockwise PTt path for the metamorphic sole.

The presence of metamorphic sole outcrops beneath both the leading and trailing edges of the ophiolite implies that the sole extends beneath the entire ophiolite. The strong deformational fabrics seen within the metamorphic sole, particularly at higher structural levels, are parallel to the Semail thrust and similar to fabrics in the lower 'banded ultramafic unit' of the ophiolite. This structural evidence is compatible with the contemporaneous formation of the metamorphic sole and initial detachment of the ophiolite. New determinations of peak metamorphic conditions recorded by garnet diopside bearing amphibolites from the metamorphic sole range from 11-13 ± 2 kbar at temperatures of 860 ± 25°C and 11.8 ± 1.5 kbar in Asimah to 748 ± 25 °C and 11.3 ± 1.9 kbar at Al Ajal using both conventional thermobarometry and THERMOCALC, and overlap existing estimates for the recrystallisation of mantle sequence basal mylonites.

Further PT analysis of lower grade metamorphic sole material and structural constraints implies an apparent inverted metamorphic sole gradient of ~2°C m^{-1} and ~3.7 MPa m^{-1} estimated in the Asimah sole locality. In conjunction with existing geochronology, an estimated peak sole exhumation rate of ~12.5 mm yr^{-1} is indicated, which is comparable with estimates of the current and recent exhumation rate of Pacific rim ophiolites. Geochemical analysis of sole garnet-diopside amphibolite granulites and tectonic constraints suggest that the Semail ophiolite sole formed from Neo-Tethyan MORB crust similar in composition to the preserved Triassic-Jurassic Haybi tholeiites and Masirah ophiolite crust.

In the Bani Hamid area of the United Arab Emirates, a sequence of wholly granulite facies material with an apparent structural thickness of ~1 km is found in a different structural position to the classic metamorphic sole. Field mapping indicates that this heavily imbricated sequence was exhumed along a major out of sequence thrust, termed the Bani Hamid thrust, that repeats the entire ophiolite mantle sequence. The presence of abundant enstatite-

cordierite-sillimanite-spinel ± sapphirine quartzites, alkaline and Ti rich mafic enstatite-diopside granulites and wollastonite-scapolite calc-silicate assemblages is unique to Bani Hamid.

The rocks all exhibit granulite facies assemblages, and the steep inverted metamorphic gradient seen in the classic metamorphic sole is absent. Estimated peak conditions of equilibration are 850 ± 25°C at pressures of 10–14 kbar; coronae and symplectites in garnet-diopside-scapolite-plagioclase ± wollastonite calc silicates and marbles are consistent with an anticlockwise PT evolution. Thermobarometry shows that tonalitic melts from mafic granulites formed at 670 ± 25°C and 5.6 ± 0.6 kbar during the prograde evolution of the sole.

Alkali and Ti rich mafic sills, metamorphosed to granulite facies (with ultramafic glimmeritic xenoliths) within metacarbonatite units of the Bani Hamid terrane may be correlated with similar alkalic metavolcanic units described from the Asimah terrane. It is likely that the Asimah (greenschist to granulite facies) and Bani Hamid (granulite facies) sole terranes represent the metamorphosed equivalents of the unmetamorphosed Permo-Triassic and Jurassic Haybi volcanics observed beneath the Semail ophiolite in the Oman mountains. The correlation of the Bani Hamid and Asimah terranes with the Haybi complex implies that Permo-Triassic and Jurassic transitional oceanic crustal material was subducting NE beneath the obducting Semail ophiolite.

Extrapolation of existing cooling ages for the Bani Hamid granulite facies event, in conjunction with thermobarometry, indicate that the Bani Hamid terrane formed at the same time as the 'classic' metamorphic sole at ~96.5 Ma and although characterised by a similar PTt path and peak metamorphic conditions, formed from subducted oceanic island derived sedimentary and igneous material, rather than from subducted oceanic crustal material, due to local palaeogeographical variations.

The timing of the late thrusting and repetition of the Khawr Fakkan ophiolite block along the Bani Hamid thrust is not well constrained although the extrapolation of existing metamorphic sole cooling rates to the Bani Hamid terrane suggests an age of ~94 Ma, which is similar to the age of the greenschist facies overprint seen throughout the Bani Hamid terrane. Subsequent movement along the Bani Hamid thrust, related to the early Tertiary exhumation of the adjacent Musandam culmination along the Hagab thrust, is also entirely possible.

Leucogranitoid intrusions in the Semail ophiolite mantle sequence are widely, albeit sparsely, distributed and are most common in the Khawr Fakkan block of the ophiolite (United Arab Emirates), which exhibits a suite of 10-100 m scale metaluminous to peraluminous granitic intrusions, ranging from cordierite-andalusite-biotite monzogranites to garnet-tourmaline leucogranites, which intrude mantle sequence harzburgites and lower crustal sequence cumulate gabbros. Granitoids in the Hayalyn block of the ophiolite (Oman) are dominated by a ~100 m thick composite sill, comprising quartz diorites, biotite tonalities and leucogranites,

intruded along a shear zone separating mantle sequence harzburgites from crustal sequence cumulate gabbros.

Structural constraints suggest that the subduction of continental sedimentary material beneath the hot proto-ophiolite in an intra-oceanic arc environment led to granulite facies metamorphism at the subduction front and the generation of granitic melts which were emplaced up to the level of the ophiolite Moho. CIPW norm compositions and Al in hornblende geobarometry indicate the analysed granitoids were largely minimum melts that crystallised at variable a_{H_2O} and pressures of 3 to 5 kbar. LILE (Sr, Rb and Ba) covariation modelling suggests that the granitoids formed largely by the dehydration melting of muscovite rich metasediments. Initial $^{87}Sr/^{86}Sr$ ratios of analysed dykes vary between 0.710 and 0.706 at initial ε_{Nd} values of between -6.3 and -0.5.

Cogenetic units of a composite sill from Ra's Dadnah (Khawr Fakkan, United Arab Emirates) yield an Sm-Nd isochron age of 98.8 ± 9.5 Ma (MSWD = 1.18), and a similar sill from Wadi Al Hajar (Hayalyn, Oman) yields an age of 93.0 ± 10.0 Ma (MSWD = 0.33). U-Pb dating of zircons from a garnet-tourmaline leucogranite dyke from Ra's Dadnah yields an age of 105 ± 4 Ma which is incompatible with the accepted ophiolite crustal sequence age of ~95 Ma and suggests that the ophiolite in northern Oman and the UAE may be older than in southern Oman.

Geochemical and isotopic characteristics of the analysed granitic intrusions indicate that the subducted continental material was derived from oceanic trench fill (Haybi complex) sediments, preserved as greenschist (Asimah area) to granulite facies (Bani Hamid area) ophiolitic metamorphic sole terranes. Sr-Nd isotope systematics indicate that hybrid granitic melts were derived from pre-magmatic mixing of two contrasting, quartzofeldspathic and basaltic subduction zone source components. The latter source may represent volcaniclastic sediments derived from volcanic islands on the subducting continental margin.

The northern part of the Saih Hatat window, SE Oman mountains, is characterised by HP metamorphic profile through an exhumed portion of Arabian continental crust, which was subducted to depths of ~80 km during the obduction of the Semail ophiolite. The Saih Hatat terrane is unique is preserving the record of continental subduction beneath an obducting ophiolite. Eclogite barometry in the As Sifah region of the southern Oman mountains has demonstrated the subduction of the Arabian continental passive margin, culminating at 450-550^{o}C and 20.0 ± 1.5 kbar.

The processes governing the formation, exhumation and present day distribution of HP rocks in the Saih Hatat window are proposed to have occurred in two distinct stages, with rapid initial exhumation following subduction of the Arabian continental margin, due to relative extension in the subduction zone hanging wall and driven by buoyancy contrasts, followed by a slower erosion. In conjunction with ambiguous existing geochronology, an estimated peak exhumation rate of ~4-12 mm yr^{-1} is indicated for the As Sifah eclogites during the late Cretaceous, followed by (?) erosional exhumation at ~0.5 mm yr^{-1} during the Tertiary.

Structural mapping in the northern part of the window has shown that tectonometamorphic units, characterised by distinct metamorphic mineral assemblages and structural styles, are bounded by diffuse extensional shear zones or discrete detachments that have juxtaposed during exhumation material originally separated by up to 50 km of original crust. The structures within individual tectonometamorphic units are truncated by the detachments and predate final exhumation.

The Saih Hatat HP terrane comprises two major structural levels, the As Sifah-Wadi Hulw-Rija unit, and the Wadi Adai-Wadi Mayh-Al Khuryan unit, separated by a major, largely west dipping ductile extensional detachment with some evidence of late brittle motion in the development of minor mélanges. Each structural domain is characterised by a distinct metamorphic assemblage and structural evolution, and the contemporary distribution of the two structural domains is controlled by interference between an early N-S trending, E verging and a later NW-SE trending folds.

The higher grade, structurally lower As Sifah-Wadi Hulw-Rija unit reached peak metamorphic conditions of ~20 kbar and ~500°C in metabasic, metavolcaniclastic, semi-pelitic and carbonate material. Metabasic material in the Wadi Hulw and Rija areas does not preserve eclogite facies assemblages but this may be a result of the pervasive retrogression in these areas rather than an indication of substantially lower peak conditions in structurally equivalent units. The lower grade, structurally higher Wadi Adai-Wadi Mayh-Al Khuryan and Ruwi mélange units reached lower peak metamorphic conditions. The Ruwi mélange HP event may represent the result of a later stage in the evolution of the Saih Hatat HP terrane.

Intra-oceanic subduction resulted in the formation of the ophiolite metamorphic sole, characterised by higher temperatures and lower pressures of metamorphism, and the generation of granitoid melts at the subduction front whereas, to the south, the subduction of a (?) continental promontory led to higher pressures and lower temperatures of metamorphism to produce the Saih Hatat HP terrane. These two processes, involving distinct source materials and different tectonometamorphic regimes, cannot have occurred together, at the same time, in a single subduction zone, and hence it is proposed that there were two coeval NE dipping subduction zones during the late Cretaceous in the Oman area: an intra-oceanic subduction zone, along which the metamorphic sole formed and the ophiolite was initially obducted, and a more proximal, deeper subduction zone in which the Arabian passive margin carbonate shelf and basement was subducted.

ACKNOWLEDGEMENTS

This DPhil project was conceived by Mike Searle, whose enthusiasm for the landscape, culture and geology of the Sultanate of Oman is unparalleled. His companionship, encouragement and knowledge of Arabic have all been invaluable during my three field seasons in Oman and the Emirates. In Oxford, welcome games of squash, sessions at the Rose & Crown and Pound Cottage slide shows have occasionally dragged me away from my computer. Bob, Geoff & Pauline Searle were also very generous with hospitality in Dubai and Muscat. My sincere thanks to my co-supervisor Dave Waters for endless discussions and guidance (invariably leaving me with more questions than I started with) about mineralogy, petrography, and THERMOCALC. My time in Rolf Pedersen's geochemistry laboratory at Bergen University, Norway was a wonderful and productive opportunity. Rolf's hospitality, humour and patience in the laboratory provided relief from the cold, as did the weekends snowboarding at Voss. This thesis has benefited greatly from the constructive criticism and reviews of Mike, Dave and Rolf.

David, Judy, Mateo and Miguel Willis were wonderful and hospitable friends in Oman. Without them, my long stays in Muscat would have been harder work. I can only hope my occasional entertainment of the lads in Oxford and London have gone a little way in returning such hospitality. Particular thanks to Mateo and Miguel for the weekends surfing at Al Ashkharah, and Miguel for the oil print.

The technical and support staff of the Department of Earth Sciences here at Oxford have made the preparation of this thesis a much simpler matter. I'm particularly grateful to Steve Baker for the preparation of slides and assistance with photomicrography; Rich McAvoy for showing me how to develop and print films; Dave Sansom for drafting figures (before I learnt to use Corel); Roy Goodwin and Steve Wyatt for assistance in the preparation of geochemical samples; Derek Preston for lending me tools; Phil Jackson and Jeremy Hyde for the preparation of sections and probe slides; Norman Charnley for calm and patient instruction in using the microprobe, and Steve Usher for advice on all matters PC, help in installing and configuring hardware, and rescuing Claire's laptop. The Department Burdett-Coutts fund was very supportive financially, and I'm also grateful to Hertford College for my Carreras senior scholarship. NERC grant GT4/96/226/E is also gratefully acknowledged.

My 6 years in Oxford have been the happiest and most fulfilling times I have known. I owe this largely to my partner Claire, who has been a source of encouragement, love, reassurance and general naughtiness for the last four years. In Earth Sciences, my office mate James Fraser has been a constant distraction, particularly when the possibility of a weekend's surfing has come up. We also shared some wicked times with Simon Gough in Pakistan, dodging rock falls on the KKH, trekking, buying gems and eating mangoes. Thanks to 'all the lads' from STA and everyone at Tuesday 5 a side, for not queuing to buy plane tickets, parties and DJing, and general messiness. Respect to Rich, Jim, Matt, Barney and all the boys from Wycombe and

Oxford for weekend surfing, festival trips, getting me back into drinking and (sometimes) holding down proper jobs. The staff at Oxford Brookes 'Heavy Metal' gym have seen rather a lot of my time and money as well.

I owe everything to my parents Steve and Steph for their love, encouragement, and support. My brothers Pete and Olly have not allowed me to get too full of myself, something I'm very grateful for, and have shown me what it's really like to have travelled the world.

TABLE OF CONTENTS

ABSTRACT i
EXTENDED ABSTRACT ii
ACKNOWLEDGEMENTS vii
CONTENTS ix

Chapter One: Ophiolites

1.1 INTRODUCTION 1
1.2 RECOGNITION OF OPHIOLITES AS OCEANIC CRUST 2
1.3 FORMAL DEFINITION OF THE TERM 'OPHIOLITE' 4
1.4 VARIABILITY OF OPHIOLITE COMPLEXES 5
1.5 OPHIOLITE OBDUCTION MECHANISMS 7
1.5.1 Obduction mechanisms in Cordilleran ophiolites 7
1.5.2 Obduction mechanisms in Tethyan ophiolites 8
1.5.3 Recognising obduction mechanisms 10
1.6 OTHER TETHYAN OPHIOLITES 12
1.6.1 Alpine and Mediterranean ophiolites 13
1.6.2 Eastern Arabian ophiolite belt 13
1.6.3 West Pakistan ophiolite belt 14
1.6.4 Himalayan and Tibetan ophiolites 15
1.6.4.1 Kohistan-Dras island arc ophiolite complex 15
1.6.4.2 Southern Tibetan ophiolites 16
1.6.4.3 Spongtang ophiolite 16

Chapter Two: The geological setting of the Semail ophiolite

2.1 INTRODUCTION 17
2.2 HISTORY OF SEMAIL OPHIOLITE GEOLOGICAL RESEARCH 17
2.3 ECONOMIC GEOLOGY OF THE SEMAIL OPHIOLITE COMPLEX 19
2.4 GLOSSARY OF RELEVANT ARABIC TERMS 19
2.5 REGIONAL TECTONIC FRAMEWORK 20
2.5.1 The Zagros 20
2.5.2 The Makran 20
2.5.3 The Gulf of Oman 21
2.6 TECTONOSTRATIGRAPHY OF THE OMAN MOUNTAINS 21
2.6.1 Crystalline basement and pre-Mesozoic metamorphism 21
2.6.2 Permian to Cretaceous carbonate shelf sediments 22
2.6.3 Sumeini group carbonates 23
2.6.4 Hawasina Group sediments 23
2.6.5 Haybi complex 24
2.6.6 Semail ophiolite 25
2.6.7 Batinah complex 25
2.6.8 Neoautochthonous sediments 26
2.7 THE SEMAIL OPHIOLITE 26
2.7.1 Introduction 26
2.7.2 Semail ophiolite stratigraphy 27
2.7.3 Age of the Semail ophiolite 28
2.7.4 Origin of the Semail ophiolite: mid-ocean ridge or supra-subduction zone? 29
2.8 THE MESOZOIC EVOLUTION OF NEO-TETHYS IN OMAN 30
2.8.1 Continental rifting and formation of Neo-Tethys 31
2.8.2 Passive margin development 32
2.8.3 Syn-obduction and Tertiary tectonostratigraphy 32
2.9 AIMS OF RESEARCH 33
2.10 THESIS OUTLINE 35

Chapter Three: Semail ophiolite metamorphic sole

3.1 INTRODUCTION 38
3.2 METAMORPHIC SOLE TECTONOSTRATIGRAPHY AND STRUCTURES 39
3.2.1 Wadi Tayin 41
3.2.2 Sumeini 42
3.2.3 Al Ajal 42
3.2.4 Asjudi 43
3.2.5 Asimah 43
3.3 GEOCHEMISTRY OF VOLCANIC ROCKS IN THE OMAN REGION 44
3.3.1 Hawasina basin volcanic units 45
3.3.2 Haybi volcanic sequence 45
3.3.3 Semail ophiolite volcanic sequence 46
3.3.4 Masirah ophiolite volcanics 46
3.4 GEOCHEMISTRY OF THE METAMORPHIC SOLE AMPHIBOLITES 47
3.4.1 Northern Oman & UAE 47
3.4.2 Southern & central Oman 47
3.5 PROTOLITHS OF THE METAMORPHIC SOLE AMPHIBOLITES 48
3.6 METAMORPHIC SOLE GEOCHRONOLOGY 49
3.7 PETROGRAPHY AND MINERAL CHEMISTRY 50
3.7.1 Mafic gneisses 50
3.7.1.1 Hornblende 50
3.7.1.2 Garnet 50
3.7.1.3 Clinopyroxene 51
3.7.1.4 Orthopyroxene 51
3.7.1.5 Plagioclase 52
3.7.2 Metasediments and carbonates 52
3.8 PT EVOLUTION AND PROFILES 53
3.8.1 Previous estimates 53
3.8.2 New PT estimates from the Semail ophiolite metamorphic sole 54
3.9 DISCUSSION 59
3.9.1 Experimental evidence 59
3.9.2 Bulk rock composition and mineral assemblages 59
3.9.3 Mineral forming reactions in sole amphibolites 60
3.9.4 Tectonic implications of sole PT results 60
3.9.5 Exhumation rates of the metamorphic sole 62
3.10 SUMMARY 62

Chapter Four: Saih Hatat HP metamorphic terrane

4.1 INTRODUCTION 65
4.2 GEOLOGICAL SETTING OF SAIH HATAT 66
4.3 STRUCTURE AND STRAIGRAPHY OF NORTHERN SAIH HATAT 67
4.3.1 Ruwi mélange 67
4.3.2 Wadi Adai – Wadi Mayh – Al Khuryan unit 70
4.3.3 Wadi Hulw unit 73
4.3.4 As Sifah unit 74
4.4 THERMOBAROMETRY IN THE AS SIFAH UNIT 76
4.5 AGE OF HIGH PRESSURE METAMORPHISM IN NORTHERN SAIH HATAT 77
4.6 BRIEF REVIEW OF UHPM AND THE EXHUMATION OF HP MATERIAL 79
4.7 DISCUSSION 82
4.7.1 Exhumation rates and mechanisms 85
4.7.2 Post tectonic evolution 86

Chapter Five: Bani Hamid metamorphic sole terrane

5.1 INTRODUCTION 88
5.2 TECTONICS OF GRANULITE FACIES METAMORPHISM 89
5.2.1 Tectonic settings of granulite facies metamorphism 89
5.2.2 UHT metamorphism: definitions and principles 91
5.2.3 Formation and preservation of granulite facies terranes 92
5.3 FIELD RELATIONSHIPS, PETROGRAPHY AND MINERAL CHEMISTRY 95
5.3.1 Calc silicate rocks and marbles 95
5.3.2 Quartzites 96
5.3.3 Metabasites and ultramafic sills 98
5.4 TECTONOSTRATIGRAPHY AND STRUCTURE 99
5.5 GRANULITE PROTOLITHS AND SOURCE MATERIALS 102
5.5.1 Trace element geochemistry 102
5.5.2 Isotope geochemistry 103
5.5.3 Structural constraints 104
5.6 PT EVOLUTION OF BANI HAMID 104
5.6.1 Existing data 104
5.6.2 Comparison with classic sole 105
5.6.3 Thermobarometry issues in UHT terranes 105
5.6.4 New PT determinations 106
5.6.5 Microstructural evidence 110
5.6.6 PT profiles through Bani Hamid 112
5.7 AGE OF BANI HAMID METAMORPHISM 113
5.8 SUMMARY 113

Chapter Six: Melt generation beneath the Semail ophiolite

6.1 INTRODUCTION 116
6.1.1 Definition of 'leucogranite' 116
6.1.2 Leucogranitic material in other ophiolite complexes 117
6.1.3 Distribution, recognition and tectonic discrimination of leucogranitoids 117
6.2 DISTRIBUTION AND EXTENT OF LEUCOGRANITES IN THE SEMAIL OPHIOLITE 118
6.3 FIELD RELATIONSHIPS 118
6.4 MINERALOGY, PETROGRAPHY AND MINERAL CHEMISTRY 119
6.4.1 Mineralogy and petrography 119
6.4.2 Mineral chemistry 121
6.4.3 Metamorphic assemblage and distribution 122
6.5 MAJOR AND TRACE ELEMENT GEOCHEMISTRY 124
6.5.1 Analytical techniques 124
6.5.2 Major and trace element rock classification 124
6.5.3 Tectonic discrimination diagrams 126
6.5.4 Characterisation of anatectic processes using LILE covariation 126
6.6 Rb-Sr AND Sm-Nd ISOTOPE GEOCHEMISTRY 127
6.6.1 Analytical techniques 127
6.6.2 Summary of analytical data 128
6.6.3 Comparison with oceanic plagiogranites 128
6.6.4 Granitoid sources and protoliths: mixing modelling and identification of end members 129
6.6.5 Sm-Nd isotope systematics 131
6.6.6 Isotopic disequilibrium in the Rb-Sr system 132
6.7 CONDITIONS OF GRANITOID FORMATION BENEATH THE SEMAIL OPHIOLITE 133
6.8 TIMING OF GRANITOID FORMATION 134
6.8.1 Existing cooling ages 134
6.8.2 Extrapolation of ophiolite cooling rates 135
6.8.3 New U-Pb dating 135
6.8.4 New Sm-Nd dating 135
6.9 SUMMARY 136

Chapter Seven: Summary, tectonic models & conclusions

7.1 INTRODUCTION 139
7.2 EVIDENCE FOR THE TECTONIC SETTING OF THE SEMAIL OPHIOLITE: MID OCEAN RIDGE OR SUPRA-SUBDUCTION ZONE? 139
7.2.1 Constraints from the Semail ophiolite 139
7.2.2 Constraints from the Semail ophiolite metamorphic sole 140
7.2.3 Melt generation beneath the Semail ophiolite 141
7.3 SUBDUCTION-OBDUCTION MODELS FOR THE SEMAIL OPHIOLITE 142
7.3.1 Northern Oman & United Arab Emirates 143
7.3.2 South eastern Oman (Saih Hatat) 144
7.3.3 Timing and duration of subduction-obduction process 144
7.3.4 Post obduction tectonics 145
7.4 FUTURE WORK AND UNRESOLVED ISSUES 146

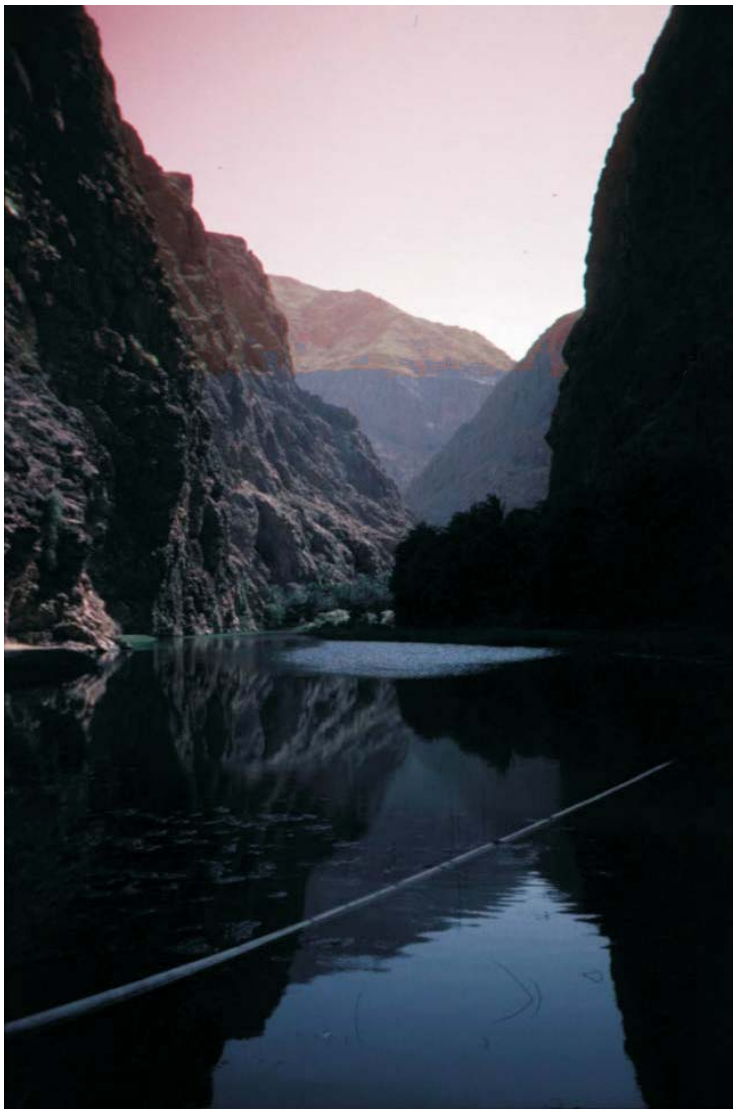
References

REFERENCES 148

Appendices

A: ELECTRON MICROSCOPE MINERALOGY & THERMOBAROMTERY 170
B: X RAY FLUORESCENCE ANALYSIS 173
C: ISOTOPIC GEOCHEMICAL ANALYSIS 175

CHAPTER ONE : OPHIOLITES



The entrance to the Wadi Shab gorge, near the village of Tiwi on the Gulf of Oman coast SE of Muscat.

CHAPTER ONE : OPHIOLITES

1.1 INTRODUCTION

Ophiolites are large scale, structurally coherent and recognisable allochthonous thrust complexes of oceanic lithosphere, crust and associated pelagic to continental margin sedimentary and volcanic sequences that have been emplaced onto continental margins during a process termed obduction (Coleman 1977). Ophiolites have been of particular importance in the reconstruction of ancient plate boundaries ever since their recognition as preserved and obducted fragments of oceanic lithosphere. The internal architecture of well-preserved ophiolite complexes shows that ophiolites are good structural analogues for oceanic crust, providing three-dimensional exposures and age relations to study the nature of extensional tectonics and magmatic construction in oceanic spreading environments.

Ophiolites complement significantly our knowledge of the architecture and generation of oceanic crust that is derived mainly from seismic images and drill holes at mid-ocean ridges. However, the geodynamic setting of many ophiolites remains controversial, as a result of petrological observations and geochemical inferences that imply magmatic affinities to subduction zone settings, rather than mid-ocean ridge environments. Recent multidisciplinary studies of intact ophiolites and drilled core samples of modern oceanic crust from various mid-ocean ridge and subduction zone settings have provided significant information on the mantle heterogeneity, magma chamber processes, melt migration, and geochemical evolution of magma in these modern tectonic settings and in ancient spreading environments, thus leading toward a better understanding of oceanic crust formation and toward resolving the structural-geochemical conundrum.

This chapter introduces the history of geological research into ophiolites and their recognition as examples of preserved oceanic crust, defines the criteria widely used to identify and categorise ophiolites, and reviews recent major developments in global ophiolite research. The techniques used to assign ophiolitic terranes to a variety of formative environments are emphasised, and the mechanisms by which they may be preserved or obducted considered. Evidence from the best described global examples of ophiolite complexes, particularly those formed by the closure of the Tethyan ocean, is reviewed, and possible modern analogues for ophiolite obduction examined.

1.2 RECOGNITION OF OPHIOLITES AS OCEANIC CRUST

Presented here is a review of the history of research into ophiolite complexes, concentrating on the development of a coherent plate tectonic framework to describe the origin and preservation of ophiolitic terranes. More comprehensive reviews of the history of ophiolite research are given in Coleman (1977), Moores (1982), Nicolas (1989) and Peters et al. (1991). Detailed studies devoted to the Semail ophiolite include Coleman & Hopson (1981), Lippard et al. (1986), Boudier & Nicolas (1988) and Robertson et al. (1990).

The term *ophiolite* is derived from the Greek words *ophilos* and *lithos* meaning snake and stone, and was first used by Brongniart (1813) to describe the mottled, shiny green to blue colour of material containing serpentine who subsequently recognised that such serpentinites were generally associated with igneous material including gabbros and basalts, as well as cherts, and inferred an igneous origin for the ophiolites. This breakthrough concept was developed in the Apennine metamorphic ophiolites (*pietre verdi*) until the association of rock types including radiolarite cherts, dolerite, gabbro and serpentinised peridotite was recognised, used widely to denote any material associated with serpentinites, and thought to have a submarine origin (eg Lotti 1886). However, the concept has been generally associated with the rock association known as the 'Steinmann trinity' of chert, dolerite and serpentinite (Steinmann 1927), in which ophiolites were regarded as submarine intrusions emplaced during the development of eugeosynclinal structures at continental margins (use of this term, introduced in the 19th C, has been superceded by plate tectonic theory).

However, acceptance of this theory was not universal, with some authors regarding the peridotites as being distinct plutonic crystal accumulations. For example, Bowen (1927) proposed that the peridotites were produced by fractional crystallisation processes, forming by crystal settling from basaltic melt bodies, and subsequently intruded into the upper crust. Hess (1938) proposed that the presence of H_20 in such ultramafic melts allowed them to be intruded at the low temperatures inferred (for example by the absence of true metamorphic aureoles around many complexes) for ophiolite emplacement. Experimental work by Bowen & Tuttle (1949) showed however that even H_20 bearing ultramafic melts could not exist below 1000°C. Vuagnat (1963) also demonstrated that the commonly observed ophiolitic association of a thick ultramafic sequence with a thinner mafic sequence could not have formed purely by the differentiation of a basaltic parent magma.

By the advent of plate tectonic theories in the late 1960s, the field of ophiolite study was severely hampered by the lack of differentiation by researchers between the occurrence of ultramafic material in widely differing and genetically unrelated tectonic environments. The review of Wyllie (1967) recognized nine different associations of ultramafic rocks:

a) Layered ultramafic-mafic (eg peridotite-norite-gabbro) associations in major intrusive bodies like the Skaegaard and Bushveldt complexes.

b) Concentrically zoned dunite-peridotite associations (eg Duke Island, Urals).

c) Ultramafic material in differentiated small scale mafic intrusions (eg Cuillin complex, Skye).

d) Alpine type peridotite-serpentinite associations or ophiolites *senso stricto* (eg Bay of Islands, Troodos, Oman).

e) Minor components of major batholiths (eg Sierra Nevada).

f) Alkali ultramafic material in ring complexes (eg Kola peninsula).

g) Kimberlite pipes (eg southern Africa, Canada).

h) Archean ultramafic (komatiitic) extrusive igneous material (eg southern Africa, western Australia).

i) Ultramafic xenoliths within extrusive igneous material (eg Hawaii).

This landmark review recognised two distinct formative mechanisms for ultramafic material: by the differentiation of basaltic parental magmas, and by the direct formation of peridotite magmas due to partial melting within the mantle. However, the commonly observed absence of clear contact metamorphic effects around ultramafic rock bodies meant that emplacement mechanisms for many of the above tectonic environments were still obscure.

The new plate tectonic theory of the 1960s allowed a radically new framework in which to consider the formation and emplacement of ophiolitic rock associations, particularly 'Alpine type' peridotites. Despite the noting of structural similarities between the then newly described mid Atlantic ridge and many ophiolites by De Reover (1959) and Brunn (1959), it was not until experimental work on the deformation of peridotites by Den Tex (1969) demonstrated the tectonic origin of many Alpine peridotite structures that the association between oceanic lithosphere and ophiolites was widely accepted, with the key observation being the distinction between the basal metamorphic tectonites and upper igneous cumulate structures commonly seen in Alpine type peridotites.

Subsequent work, including the identification of sheeted dyke complexes in the Troodos complex of Cyprus (Gass 1968; Moores & Vine 1969, 1971), led to the widely accepted conclusion that this and other ophiolite complexes represented oceanic crust and mantle material formed at spreading centres (Moores 1970; Dewey & Bird 1971; Coleman 1971). However, the newly available analytical tools of seismic imaging and ocean drilling showed discrepancies in the composition, thickness and morphology of typical oceanic crust compared to many newly defined ophiolites. This is still a controversial aspect of ophiolite emplacement models today, and the most widely accepted solution proposed invokes the tectonic thinning of

ophiolites by extension during the obduction process (Vine & Moores 1972; Casey & Dewey 1984). The presence of components like plagiogranites in ophiolite complexes not recorded from the oceanic environment, and the lack of identification of magma chambers beneath active spreading ridges, were gradually resolved by the employment of more detailed seismic imaging and the recognition of the limitations of surface based dredging as a representative sampling technique.

1.3 FORMAL DEFINITION OF THE TERM 'OPHIOLITE'

The definition of the term ophiolite used in this work is the widely accepted definition set out in the 'ophiolite manifesto' presented at the 1972 Penrose conference:

'Ophiolite refers to a distinct assemblage of mafic to ultramafic rocks. It should not be used as a rock name or as a petrological unit in mapping. In a completely developed ophiolite, the rock types occur in the following sequence, starting from the base and working up:

1. *Ultramafic complex, consisting of variable proportions of harzburgite, lherzolite and dunite, usually with a metamorphic tectonite fabric (more or less serpentinised).*
2. *Gabbroic complex ordinarily with cumulus textures commonly containing cumulus peridotites and pyroxenites and usually less deformed than the ultramafic complex.*
3. *Mafic sheeted dyke complex.*
4. *Mafic volcanic complex, commonly pillowed.*

Associated rock types include:

a) *An overlying sedimentary section typically including ribbon cherts, thin shale interbeds and minor limestones.*
b) *Podiform bodies of chromite, generally associated with dunite.*
c) *Sodic felsic intrusive and extrusive rocks.*

Faulted contacts between mappable units are common. Whole sections may be missing. An ophiolite may be incomplete, dismembered or metamorphosed. Although

ophiolite is generally interpreted to be oceanic crust and mantle, the use of the term should be independent of its supposed origin.'

1.4 VARIABILITY OF OPHIOLITE COMPLEXES

The realisation of the origin and nature of ophiolites led to the intensive study of many ophiolite complexes, to gain insights into both the processes of the new plate tectonics and the nature of the previously inaccessible oceanic lithosphere and asthenosphere. It was rapidly clear that a great variety of ophiolitic complexes existed, in terms of stratigraphy, morphology, deformation, lithological associations, geochemistry and age. Since the primary control on this variability is clearly the tectonic environment of formation of the ophiolite, comparative studies of the variability of ophiolites can be a powerful means of generating ancient plate tectonic configuration snapshots.

Miyashiro (1973) was the first to suggest, on the basis of the major element geochemistry of the extrusive sequence, that the Troodos ophiolite, Cyprus formed in an island arc setting rather than at the previously standard mid ocean ridge setting. The development and application of basaltic tectonic discrimination diagrams (Pearce & Cann 1971, 1973) similarly demonstrated that many ophiolites had extrusive geochemistry incompatible with an origin at a MORB signature mid ocean ridge. Since this initial recognition of the variability of ophiolite complexes, a variety of petrological, geochemical, and structural techniques have been used to recognise at least 6 distinct tectonic environments in which basaltic extrusive material can form, although in principal these broad groups can be further subdivided:

a) Normal mid ocean ridges;

b) Within plate plume settings;

c) Volcanic arcs;

d) Ocean ridge plume interactions;

e) Marginal basin spreading centres;

f) Attenuated continental lithosphere.

Post plate tectonics research into ophiolite structural and compositional variations has recognised two end member ultramafic compositions in global ophiolites: harzburgitic (ol + opx, more depleted relative to basaltic components) and lherzolitic (ol + opx + cpx, more Ca and Al rich). Initially, it was thought that harzburgitic ophiolite types (HOT) were derived from

suboceanic mantle, whereas lherzolitic ophiolite types (LOT) were derived from sub continental mantle (Nicolas & Jackson 1972). However, subsequent recognition of lherzolitic mantle in oceanic domains showed this distinction to be overly simplistic. Nicolas (1989) identified several clear contrasts between HOT and LOT ophiolites:

a) LOT ophiolites typically have a much thinner (~2-3 km) crustal sequence, with rare or absent cumulate gabbros, and often associated with alkaline rather than tholeiitic extrusive material.

b) Chromite pods are rare or absent in LOT ophiolites.

c) Dolerite dykes in the mantle sequence are more common in LOT ophiolites.

d) Low T plastic deformation is more common in LOT ophiolites, and high T plastic flow structures are typically steeper than in HOT ophiolites.

The fundamental origin of these morphological contrasts is differences in the degree of partial melting and nature of the mantle source material. A higher degree of partial melting produces more basaltic melt from primary mantle, resulting in a thicker crustal sequence and more depleted (harzburgitic) residue. This simple model is complicated by the presence of mantle heterogeneities and the introduction of volatiles to the supra-arc mantle wedge (McKenzie & Bickle 1988). The height reached by any mantle upwelling is limited by the lithospheric front, above which melting rapidly ceases due to the steep conductive gradient in the lithosphere. The faster the upwelling ascends, the further the lithosphere is penetrated, and the greater the degree of melting. The ascent rate of mantle at a ridge can be directly related to the ridge spreading rate (McCulloch et al. 1981; LePichon et al. 1982; Boudier & Nicolas 1985). Although melting paths are complicated by a wide variety of factors ranging from the presence of subduction derived fluids to mantle heterogeneities, melting is generally seen to be maximized at spreading rates of >1-2 cm yr^{-1}, and normal HOT crust is produced, whereas slower ridge spreading rates are associated with LOT crust.

The majority of major ophiolite terranes are HOT, such as the Semail ophiolite (Oman/United Arab Emirates), the Bay of Islands ophiolite, Newfoundland (Church & Stevens 1971), and the Troodos ophiolite, Cyprus (Gass 1968). Examples of LOT ophiolites include the Trinity ophiolite, California (Nicolas 1989). Figure 1.1 depicts the stratigraphic and morphological contrasts between typical HOT and LOT sections.

The identification of relict transform faults within ophiolite complexes is based largely the continuity of crustal structures since dyke complexes are generally rotated into the transform orientation. The presence of transform faults in ophiolites can also be detected in other ways, since the juxtaposition of young, hot and old, cold crust at a transform results in reduced melting, an effect which is magnified at slow spreading rates.

In the Ibra block of the Semail ophiolite a 20 km wide transform domain is exposed in which high temperature mantle structures are orthogonal to the ridge axis and sheeted dykes (Boudier & Coleman 1981). This crustal structure is mirrored away from the transform domain, suggesting that the cooling influence of the transform is attenuated. In contrast, the slow spreading Bogota transform domain in New Caledonia (Nicolas 1989) is only a few km wide, with low temperature plastic flow structures grading into mylonites along axis. In addition, crustal thickness is reduced and hydrous phases are common, and the mantle sequence is characterised by plagioclase lherzolites. Despite the variability in the characteristics and morphology of ophiolite complexes outlined here, most ophiolites have a suite of common characteristics which allow them to be classified in a systematic way, both in terms of their tectonic origin, and the processes that govern their obduction.

1.5 OPHIOLITE OBDUCTION MECHANISMS

Ophiolite obduction (Coleman 1971) may be defined as the process that first emplaces oceanic crust and mantle onto continental crust. Ophiolite emplacement has the same meaning but the term obduction is specific to tectonic emplacement. On the basis of obduction mechanisms, ophiolites can be divided into two broadly defined end member types (Moores 1982, Coleman 1984):

a) Cordilleran ophiolites: those incorporated into continental crust at an active margin. Often subsequently dismembered and incorporated into mélange or accretion terranes.

b) Tethyan ophiolites: those obducted onto continental crust at a passive margin.

1.5.1 Obduction mechanisms in Cordilleran ophiolites

Cordilleran ophiolites are widely observed along the continental margins of the Pacific rim. A wide variety of ophiolitic material is found, reflecting the variety of tectonic environments encountered (often over time, with accreted terranes consisting of ophiolites of oceanwards decreasing age and metamorphic grade) at active margins. It is interesting to note the contrasts between the less active North American continental margin, where accreted ophiolite complexes are common, and the more active South American Andean continental margin, where ophiolite fragments are less common.

High grade blueschist 'knockers' in the Californian Franciscan mélange have been widely used to constrain the burial and exhumation histories of Cordilleran type ophiolitic fragments, and exhibit a complex metamorphic history involving two burial episodes (Moore 1984). Fragments initially accreted to the base of an accretionary prism during subduction were metamorphosed at blueschist facies (~30 km depth) before being exhumed and incorporated into olistostromes in the Franciscan mélange, which were subsequently subducted and metamorphosed again. Platt (1986) however ascribed blueschist facies metamorphism to the hanging wall metamorphic sole.

This controversy highlights the most problematic aspect of Cordilleran ophiolites: the exhumation mechanism of high pressure material. An early model (Lockwood 1972) suggested that the buoyancy of low ρ serpentinites formed in the subduction zone would exhume ophiolitic fragments by diapiric uplift. In contrast, tectonic models of accretionary wedges (Cowan & Silling 1978; Cloos 1982) emphasised the role of return flow due to the geometrical effect of rigid crystalline forearc or continental basement and the mechanical coupling of sediments with the ophiolitic components of the subducting slab.

More recent models (Platt 1986; Jayko et al. 1987) have concentrated on continued underplating at the rear of the accretionary wedge resulting in tectonic uplift; when the weight of the wedge exceeds the strength of its relatively weak component sediments, extensional collapse occurs, and deeper (ophiolitic) material plastered onto the base of the wedge would be exhumed by a combination of extensional faulting and erosion.

1.5.2 Obduction mechanisms in Tethyan ophiolites

The larger and generally more intact and coherent nature of the majority of Tethyan ophiolites compared to Cordilleran ophiolites presents the major problem in contemporary ophiolite research: how large (700 km by 100 km by ~10 km in the case of the Semail ophiolite) slabs of dense (3.0-3.3 g cm^{-3}) oceanic lithosphere can be emplaced onto elevated, less dense (2.7-2.8 g cm^{-3}) continental margins. This topic is a major aspect of ongoing research and only the most presently favoured obduction mechanisms and their application to well constrained ophiolite complex examples will be considered here. Dewey (1976) presented a comprehensive review of ophiolite obduction mechanisms in the light of plate tectonic theory. The models covered in this review fall into three main categories:

a) Gravity sliding onto Atlantic type passive margins.

b) Interference between spreading ridges and subduction zones.

c) Collision of continental or island arc crust with a subduction zone dipping beneath the arc.

The gravity sliding model requires an elevated source region from which a 7 to 20 km thick ophiolitic terrane could slide onto a continental margin (figure 1.2a). Mechanisms for such degrees of uplift are difficult to envisage and an application for the model has yet to be demonstrated on a major scale. The second model is analogous to the concept of 'flake tectonics' (Oxburgh 1972), and requires a subduction zone dipping towards a continental margin (figure 1.2b). Dewey (1976) suggested that the most likely tectonic configuration that would facilitate such a mechanism would be the interaction of a subduction zone and mid ocean ridge, where obduction flaking could occur without impacting on the subduction zone. This mechanism would clearly produce a distinctive ophiolite stratigraphy comprising an arc volcanic sequence overlain by an (in)complete ophiolite stratigraphy and no described ophiolite complexes have such a stratigraphy. Furthermore, only the parallel interaction of a ridge and trench system would produce synchronous obduction.

In the absence of strong evidence supporting the two above described models, Gealey (1980) and Moores (1982) have suggested that the collision of continental or island arc crust with a subduction zone dipping beneath the arc is the only mechanism by which Tethyan ophiolites are obducted. Furthermore, in progress contemporary ophiolite obduction tectonics closely match this model: the Banda arc off the NW margin of Australia is a widely quoted example (Hamilton 1979; Bowin et al. 1980; Searle & Stevens 1984). Seismic reflection profiles show the 35 km thick Australian continental margin and shelf sequence underthrusting the accretionary prisms of the Banda arc in the 3 km deep Timor and Seram trench system. The Weber trough separates the olistostromes and metamorphic sediments of the Banda arc accretionary prism from the active inner arc. Seismic profiles suggest that the Weber trough is formed from forearc oceanic crust and the Banda Sea from back arc oceanic crust.

The nearby Papuan ophiolite represents a comparable tectonic environment in which obduction occurred along the Owen-Stanley fault, interpreted as a Tertiary subduction zone (Davies & Smith 1971). There is also evidence for the development of an early Tertiary arc that formed on oceanic crust prior to continent-arc collision and ophiolite obduction in the Miocene. Searle & Stevens (1984) noted the presence of an emplacement related metamorphic sheet overlying an accretionary prism at the base of the Papuan ophiolite, paralleling the tectonic stratigraphy of other Tethyan ophiolites. Despite the widespread acceptance of this model (which assumes a degree of continuity between the subduction zone and obduction-emplacement surface) for the obduction of Tethyan style ophiolites, it fails to account for the fact that these ophiolites rarely exceed a roughly uniform 10 km in thickness, whatever their lateral extent, rather than forming a wedge rapidly increasing in thickness towards the

ophiolite trailing edge, as well as the depths of subduction beneath the obducting wedge implied by peak metamorphic sole pressures (Gnos 1998).

Modelling the processes that extend and thin ophiolites during their obduction is the major focus of contemporary ophiolite research (Hacker & Gnos 1997). In the model of Casey & Dewey (1984), subduction zone flattening can be accomplished initially by high T solid state flow under low stress conditions, and subsequently by more localised low T solid state flow under higher stress conditions (figure 1.3). Figure 1.4 shows a model, after Dewey & Casey (1984), for the initiation of a subduction zone and the obduction of an ophiolite at a transform margin system that requires a change in relative plate motions across the transform system from strike slip to transpression. Subsequent intra-oceanic thrusting obducts the (relatively) younger and more buoyant oceanic crust.

More recent models have proposed the initiation of intra-oceanic thrusting and subduction along the lithosphere-asthenosphere boundary, which can act as a decoupling zone. Two possible tectonic configurations in which this process may occur are:

1. An oceanic ridge where regional tectonics force a change from an extensional regime to a compressional one within ~2 Ma; the asthenospheric boundary remains at a shallow depth at large spreading rates. This mechanism forms the basis of the MOR model for the origin of the Semail ophiolite (Boudier & Coleman 1981).
2. A subduction zone in which stress differentials at the elastic-plastic boundary in the subducting plate could allow a fracture to develop (Dewey 1976). Field constraints from the Semail and other well exposed ophiolites demand that this boundary occurs typically ~10 km below the Moho of the subducting crust.

The continuity of high T remnant mantle fabrics observable within the Semail ophiolite mantle sequence has been used as evidence for minimal extension during exhumation (eg Ceuleneer 1988). Ophiolite formation by intra-oceanic subduction initiation is a separate tectonic event to the emplacement of oceanic crust onto continental crust (obduction), and ophiolitic nappes would be transported over oceanic crust in the first model, and initially over forearc crust in the second model, until the cessation of subduction and continent-arc collision.

1.5.3 Recognising obduction mechanisms

The interpretation of ophiolite obduction mechanisms requires knowledge of, and contribution from, a broad variety of geological disciplines, and the development of a

coherent, broadly applicable tectonic framework in which observations can easily be compared with those from comparable environments.

Robertson (1994) generated such a framework based around the concept of the *tectonic facies* that 'constitutes the combined lithological and structural features that allow the systematic recognition of past tectonic settings within an orogenic belt'. The concept is simplest to apply to the higher, less deformed and metamorphosed structural levels (typically occupied by ophiolitic allochthons) of orogens. With such a conceptual framework, ophiolite obduction related tectonostratigraphic units may be divided into four main groups, which will be of varying abundance and significance depending on the tectonic environment of ophiolite formation:

a) *Material formed in the same tectonic environment as the ophiolite.* A variety of igneous and sedimentary material, for example volcanogenic, metalliferous or pelagic sediments, may be found associated with ophiolites. An intra-oceanic arc ophiolite would be likely be associated with volcanogenic sediments, whereas a MOR ophiolite would be draped by metalliferous and pelagic sediments.

b) *Allochthonous thrust sheets associated with ophiolite emplacement.* In a typical ophiolite complex, the actual ophiolite is underlain by a sequence of progressively more proximal allochthonous thrust sheets, which, in conjunction with the tectonic facies concept, can be used to restore the different units to their pre-obduction positions. Typically, stacked units may include the following: a series of accretionary mélanges immediately beneath the ophiolite, both tectonic and sedimentary in origin, with blocks (up to ~500 km^3 in size in Oman) including reefal carbonates, oceanic (tholeiitic to alkaline) extrusive rocks, metamorphic sole components, serpentinised ultramafic units and pelagic sediments; a sequence of alkaline extrusive rocks capped by carbonates, representing subducted seamounts, the age, geochemistry and palaeogeography of which can provide valuable constrains on the obduction process. In continental collision zones such as the Himalaya, ophiolitic mélanges are frequently the only preserved relicts of former oceans, whereas when an ophiolite is obducted onto a passive margin, further (more proximal) allochthonous thrust sheets may be preserved.

c) *Basement and cover material onto which the ophiolite was emplaced.* Such units may be considered as a complete tectonic facies, such as a carbonate platform, or may record a more complex tectonic history. In Oman, the carbonate platform records the transition to foredeep sedimentation and deformation associated with the obduction process.

d) *Post emplacement (neoautochthonous) cover material.* The age of the youngest cover material that generally unconformably overlie the ophiolitic allochthon can give a minimum age for emplacement, and the structure and stratigraphy can elucidate post obduction tectonics.

The presence of an emplacement related *metamorphic sole* immediately beneath an ophiolitic complex is probably the most powerful interpretative constraint in the evaluation of the nature and timing of the obduction process. Classic examples include the Bay of Islands ophiolite (Williams & Smyth 1973; Malpas et al. 1973) as well as the Semail ophiolite (Searle 1980; Searle & Malpas 1980, 1982; Ghent & Stout 1981; Gnos 1998). A more detailed evaluation of the interpretative potential of metamorphic soles in the development of ophiolite obduction models will be presented in *Chapter Three*.

Contemporary analogues for the formation of suboceanic crustal metamorphic sheets are restricted to the Western Pacific region. The Yap trench and associated island arc to the east of the Philippines (Hawkins & Batiza 1977) is a widely quoted example, where the Yap arc consists of metamorphic rocks overthrust by ultramafic mylonites and schists, and material dredged from the Yap trench is dominated by foliated metabasaltic amphibolites and marbles, similar to the highest grade components of the classic metamorphic sole examples. Seismic reflection profiles across the arc-trench region show subducting seamounts being accreted to the base of the Yap arc, and the overall tectonics are very similar to those during the obduction of the Semail ophiolite (Searle & Stevens 1984).

1.6 OTHER TETHYAN OPHIOLITES

This section reviews the current state of research and knowledge of the numerous ophiolites related to the final closure of the Neo-Tethyan ocean, concentrating on the identification of tectonic environments of ophiolite formation, the timing of ophiolite formation and obduction, and the mechanisms of subduction.

Definitions of the term 'Tethyan' are after Jenkyns (1980); the large Palaeozoic ocean which broke up Pangea is called Palaeo-Tethys, and the oceanic zone of largely Mesozoic oceanic crust and microcontinents, is termed Neo-Tethys. Rifting in the latter oceanic realm began with the Permian fragmentation of Gondwanaland at the southern margin of Palaeo Tethys and closure occurred diachronously through the Tertiary.

1.6.1 Alpine and Mediterranean ophiolites

Ophiolites from the Alpine, Italian Appennine and Albania and the FYR (figure 1.6) are largely characterised by extrusive sequence MORB geochemistry (eg Bickle & Pearce 1975) and also exhibit the lherzolitic, thin LOT type mantle sequences and poorly developed sheeted dyke complexes characteristic of the thin oceanic crust and mantle found in fractured rift zones (eg Ishiwatari 1985). In contrast to the mid Cretaceous ages common in the eastern half of the Tethyan orogen, Alpine ophiolites are predominantly of lower to mid Jurassic age (eg Ohnenstetter et al. 1981) and many examples have undergone eclogite facies and UHP metamorphism during the closure of Tethys.

The well described Vourinos ophiolite of central Greece exhibits a thick harzburgite mantle sequence, well developed sheeted dyke complex. Its extrusive volcanic sequence has affinities with island arc volcanic units, which suggests that the Vourinos ophiolite formed in a SSZ environment (Pearce 1989), while the adjacent lherzolitic Pindos and Othris ophiolites may have been derived from a similar setting to the LOT ophiolites of the Alps.

The Troodos ophiolite of Cyprus (figure 1.6) is exposed over an area of 30 by 70 km in the Troodos mountains of Cyprus and forms the most well known of the Mediterranean ophiolites (Gass 1968, 1980; Moores & Vine 1971). It is now believed to have formed at several spreading axes in a SSZ environment prior to the collision of the African and Eurasian plates in the late Cretaceous (Pearce et al. 1984). The ophiolite crustal sequence has been dated at 91.6 ± 1.4 Ma (Mukasa & Ludden 1987). Three major geochemical suites are recognized in the Troodos extrusive sequence: an arc tholeiite suite, a depleted tholeiite suite and a highly depleted boninite suite. The upper parts of the ophiolite section are almost undeformed, preserving the original sea floor patterns of low T alteration in the lava sequence.

1.6.2 Eastern Arabian ophiolite belt

The Masirah, Ra's Madrakah and Ra's Jibsch ophiolites of the Batain coast of SE Oman (figure 1.5) are characterised by an absence of subophiolitic metamorphism and a distinctly older age than the Semail ophiolite itself – typically 145-150 Ma (Smewing et al. 1991; Peters et al. 1996; Immenhauser 1996). The absence of emplacement related shear metamorphism led Gnos et al. (1997) to suggest that these ophiolites were obducted by strike-slip accretionary processes from the Owen-Murray basin to the east. Furthermore, all these ophiolites exhibit evidence of renewed alkaline tectonomagmatic activity in the early Cretaceous (123 ± 2 Ma by U-Pb; Nagler & Frei 1994). Accretionary wedge and imbricated flysch type deposits were emplaced with the ophiolites from NW onto the Arabian continental margin. The emplacement

window is narrowly constrained by the presence of Maastrichtian pre-obduction sediments and transgressive neoautochthonous sediments of Palaeocene-Eocene age (Immenhauser 1996; Gnos et al. 1997).

1.6.3 West Pakistan ophiolite belt

The western ophiolite belt of Pakistan (figure 1.5) trends approximately N-S and marks the suture between the Helmand block at the southern margin of Eurasia and the Indian continent along which Neo-Tethys was closed (Gnos et al. 1997). There are a number of well described ophiolites, including the Muslim Bagh, Zhob, Bela (Pakistan) and Waziristan-Khost (Afghanistan) examples.

The Bela ophiolites represent the largest and most complete component of this ophiolite suite, and form a ~450 km long N-S oriented belt which contains two distinct tectonic units: a southern sequence of sediments, basalts and dolerite sills and flows up to a total thickness of 3-5 km, and a more extensive northern block which exhibits all the features of a complete ophiolite complex: metamorphic sole, harzburgites, cumulate and isotropic gabbros and sheeted dykes (Sarwar 1992). At the base of the mantle sequence, leucogranitic intrusions related to oceanic arc subophiolitic anatexis during subduction-obduction have U-Pb ages of 64.6 to 66.6 ± 1 Ma (Ahmed 1993), while sediments intercalated with the crustal sequence extrusive units have an Albian age, suggesting a minimum age for the ophiolite. The Muslim Bagh ophiolites are of similar age and structurally overlie Maastrichtian carbonate turbidites and are unconformably overlain by lower Eocene neoautochthonous sediments. Furthermore, $^{40}Ar/^{39}Ar$ dating of amphibolites from the sole of the Muslim Bagh gives ages of 65.1 ± 4.1 Ma to 70.7 ± 5.0 Ma (Mahmood et al. 1995). The Zhob ophiolites are little studied and poorly known, consisting of a harzburgite-gabbro mantle to crustal sequence containing dolerite dykes and granitoid intrusions which is thrust over incomplete crustal sequences to form the cores of a number synclines NNE of the Muslim Bagh ophiolite (Gnos et al. 1997). The Waziristan (Pakistan) and Khost (Afghanistan) ophiolites are thought to have been obducted by the underthrusting of the Eurasian continental margin in the Albian-Cenomanian, dated by $^{40}Ar/^{39}Ar$ (sole amphibolites) methods at 100 ± 5 Ma (Cassaigneau 1979), and consist of a complete but strongly sheared and dismembered ophiolite sequence thrust over a Maastrichtian autochthon and covered by Eocene (~55Ma) neoautochthonous sediments (Beck 1996).

All these ophiolites exhibit a similar internal stratigraphy and age, ranging from Albian to Senonian. All are underlain by a well developed and preserved accretionary wedge containing lower to mid Cretaceous pelagic sediments which grade up into emplacement related calcareous turbidites (Gnos et al. 1997). The tectonic setting of these ophiolites, determined by extrusive geochemistry, coupled with the nature of sub ophiolitic metamorphic

sole material, suggests a common origin as SSZ ophiolites (Mahmood et al. 1995). Emplacement onto the Indian continental passive margin generally occurred during the late Cretaceous and is marked as completed by the widespread occurrence of neoautochthonous Palaeocene-lower Eocene shallow marine carbonates (Alleman 1979).

1.6.4 Himalayan and Tibetan ophiolites

Ophiolites in the Karakoram-Himalaya-Tibet sector of the Tethyan suture and orogen fall into two categories: ophiolites associated with the India-Eurasian suture, and ophiolites emplaced southwards onto the Indian passive margin prior to continental collision. The Kohistan-Dras island arc and the Indus-Tsangpo suture ophiolites of southern Tibet are well known examples of the former, while the Spongtang ophiolite of Ladakh is the largest and best preserved Indian passive margin ophiolite in the Himalayan orogen.

1.6.4.1 Kohistan-Dras island arc ophiolite complex

In northern Pakistan and Ladakh, the Kohistan-Dras island arc separates the Indian plate from the Eurasian plate, and was accreted to the southern margin of the Eurasian plate between 95 Ma and 75 Ma along the Shyok suture (Treloar et al. 1989, 1996). Collision related tectonic features are truncated by the Jutal suite of basic dykes that have been dated ($^{40}Ar/^{39}Ar$) at 75 ± 1 Ma, giving a minimum age of collision (Treloar et al. 1989). The Kohistan and Dras island arc sequences are linked by a highly attenuated but continuous outcrop around the Nanga Parbat syntaxis, and major tectonic units can be correlated across the syntaxis. At the base of the Kohistan arc, the Main Mantle thrust and suture is marked by a subduction related serpentinite and sedimentary mélange characterised by blocks of blueschist to eclogite facies metabasites of uncertain age.

The base of the arc is dominated by upper mantle and lower crustal oceanic material of varying metamorphic grade that may represent Tethyan ophiolites derived from the Kohistan arc forearc region (Searle et al. 1987). Structurally above these ultramafic units lie the Kamila amphibolites, which are cut by peraluminous leucogranitic intrusions most likely derived from the melting of subducted Indian passive margin sediments beneath the arc, and have been variously interpreted as the metamorphosed equivalents to the overlying Chalt volcanics (Coward et al. 1986), a back arc basin sequence (Khan et al. 1996) or an oceanic basement (Treloar et al. 1996). The Chilas complex consists of extensive gabbro norites representing the island arc magma chamber (Khan et al. 1989) and has a formation age (U-Pb) of 84 ± 0.5 Ma

(Zeitler et al. 1981). The overlying Chalt volcanics are thought to be island arc volcanic units (Coward et al. 1986) and are intercalated with Aptian-Albian sediments.

This extensive arc crust is intruded by the collision related calc alkaline components of the Karakoram batholith, which has a range of ages that both pre and post-date suturing of the arc to Eurasia, and document the development of a Cordilleran style active continental margin to Eurasia following the accretion of Kohistan (Coward et al. 1986).

1.6.4.2 Southern Tibetan ophiolites

The largest and best described of the southern Tibetan ophiolites is the Xigaze ophiolite (figure 1.6) that remains rooted in the Indus-Tsangpo suture and has not been transported any appreciable distance south onto the Indian passive margin. The ophiolite sequence is complete but strongly dismembered and the mantle sequence appears to be characteristic of LOT rather than HOT crust (Nicolas et al. 1981). The ophiolite has a U-Pb age of 120 ± 10 Ma (Gopel et al. 1984) and is thought to have been preserved as the forearc crust to the trans Himalayan batholith prior to Indian-Eurasian collision.

1.6.4.3 Spongtang ophiolite

The Spongtang ophiolite of Ladakh lies ~30 km south of the Indus-Tsangpo suture and structurally overlies deformed Indian passive margin sediments of Permian to middle Eocene age. It exhibits a full ophiolite stratigraphy comprising harzburgitic mantle material, gabbros, sheeted dykes and extrusive units of MORB affinity (Corfield 1998) up to a total thickness of ~5-7 km. It comprises Neo-Tethyan crust of mid Jurassic age (174 ± 2 Ma; Pedersen et al. in prep) and is overlaid by arc related extrusive volc40anic rocks and volcaniclastic material of Cenomanian age (Corfield 1998), suggesting the presence of a mid Cretaceous intra oceanic arc in Neo-Tethys. Emplacement of the ophiolite must have predated India-Eurasian collision and is constrained by structural evidence to have occurred in the mid Cretaceous. The ophiolite was subsequently rethrusted over younger Eocene sediments (Searle 1986; Searle et al. 1987; Corfield et al. 1999).

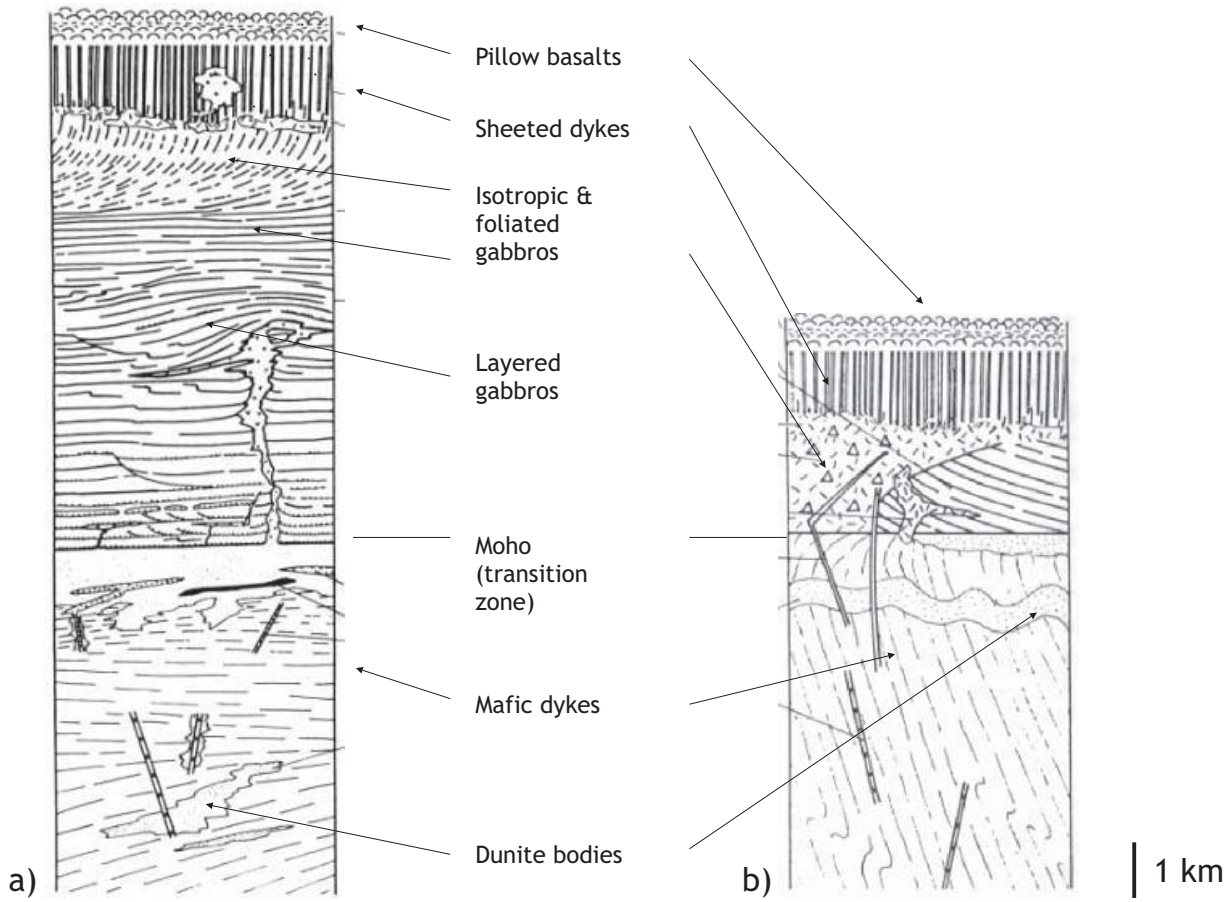
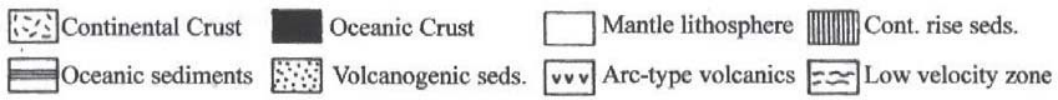
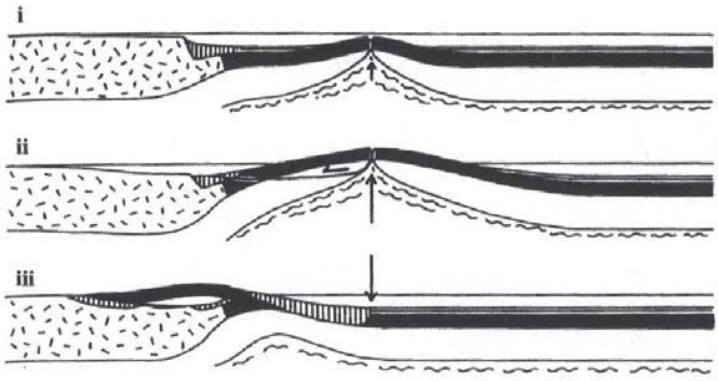


Figure 1.1 Comparative sections through idealised harzburgite (a,HOT) and lherzolite (b,LOT) type ophiolites demonstrating the characteristic contrasts in thickness and morphology. HOT ophiolites have a mantle sequence composed of harzburgite, with clinopyroxene and plagioclase common only at the top of the mantle sequence, in the mantle transition zone, which may be up to ~1 km thick and is dominated by dunites with associated chromite pods. LOT ophiolites exhibit a much thinner and more homogeneous plagioclase lherzolite dominated mantle sequence with rare dunites and a very sharp and thin Moho transition zone. In addition, HOT ophiolites generally exhibit a thicker and more coherent crustal sequence than LOT ophiolites, which may, as in the Piedmont and Ligurean examples, have ultramafic material forming the ocean floor. From Nicolas (1989), after Boudier & Nicolas (1985).

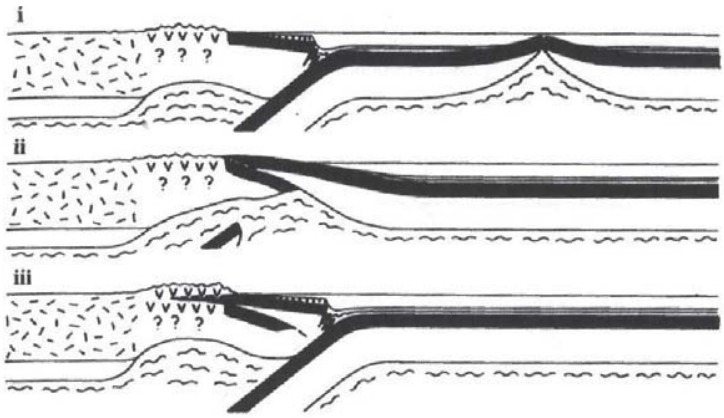
Figure 1.2 Proposed obduction and emplacement models for Tethyan type ophiolites, after Dewey (1976).



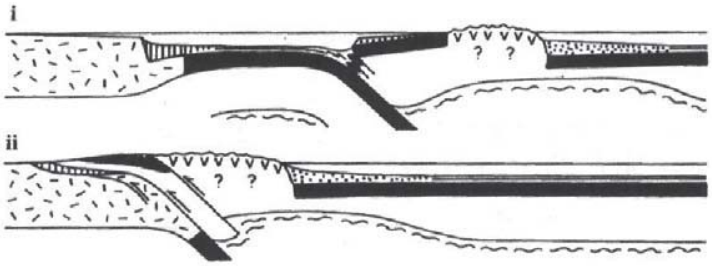
a) Obduction and emplacement of an ophiolite onto a passive Atlantic type margin by gravity from an uplifted ridge. Although proposed for the Semail ophiolite by Glennie et al. (1974), the model is widely dismissed as improbable by recent researchers.



b) Flaking of subducting oceanic lithosphere after the collision of a mid ocean ridge and an subduction zone, resulting in ophiolite obduction and emplacement.



c) Flaking of subducting oceanic lithosphere after the collision of a mid ocean ridge and an subduction zone, resulting in ophiolite obduction and emplacement.



d) Obduction of an arc-trench gap ophiolite due to the collision of a volcanic arc and a passive continental margin. Variations could include the obduction of an immature or back arc ophiolite, or MORB crust from the hanging wall of a young subduction zone.

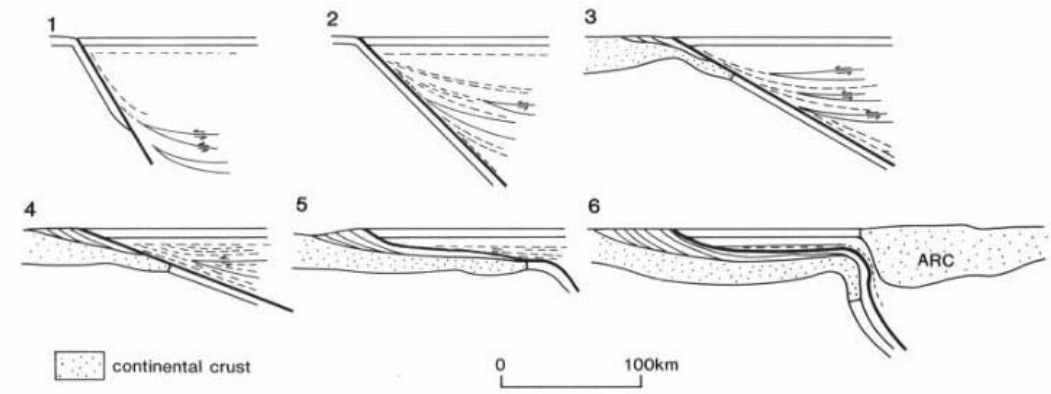


Figure 1.3 Sequential model, from Dewey & Casey (1984), showing the 'flattening' of an ophiolite obduction related subduction zone. The progressive shallowing of the dip of the subduction zone and associated structural thinning and extension of the obducting ophiolite may account for the presence of metamorphic sole material (represented by the thick black line in the diagram) metamorphosed at pressures of >10 kbar (Jamieson 1981; Gnos 1998; this study) occurring beneath ophiolite complexes <20 km thick.

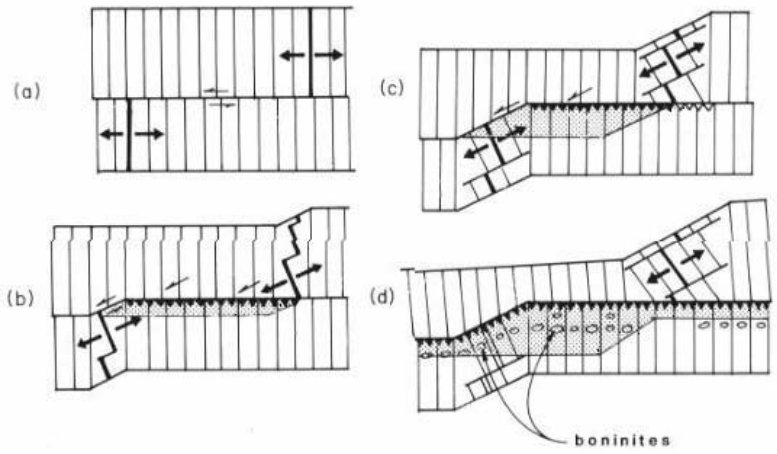


Figure 1.4 Model, after Dewey & Casey (1984), for the initiation of a subduction zone and the obduction of an ophiolite at a transform margin system. The model requires a change in relative plate motions across the transform system from strike slip to transpression, and subsequent intra-oceanic thrusting obducting the (relatively) younger and more buoyant oceanic crust. The absolute age and heat of the obducting oceanic crust will govern the presence, nature and extent of any subophiolitic metamorphism, which can be used to evaluate ophiolite complexes in terms of this model (eg Gnos et al. 1997).

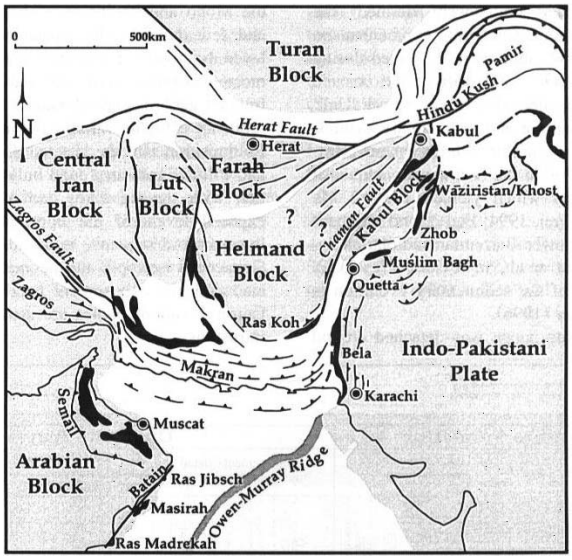


Figure 1.5 Tectonic map of eastern Arabia and SW Asia showing the Semail, Batain and Pakistani ophiolite complexes discussed in the text, from Gnos et al. (1997).

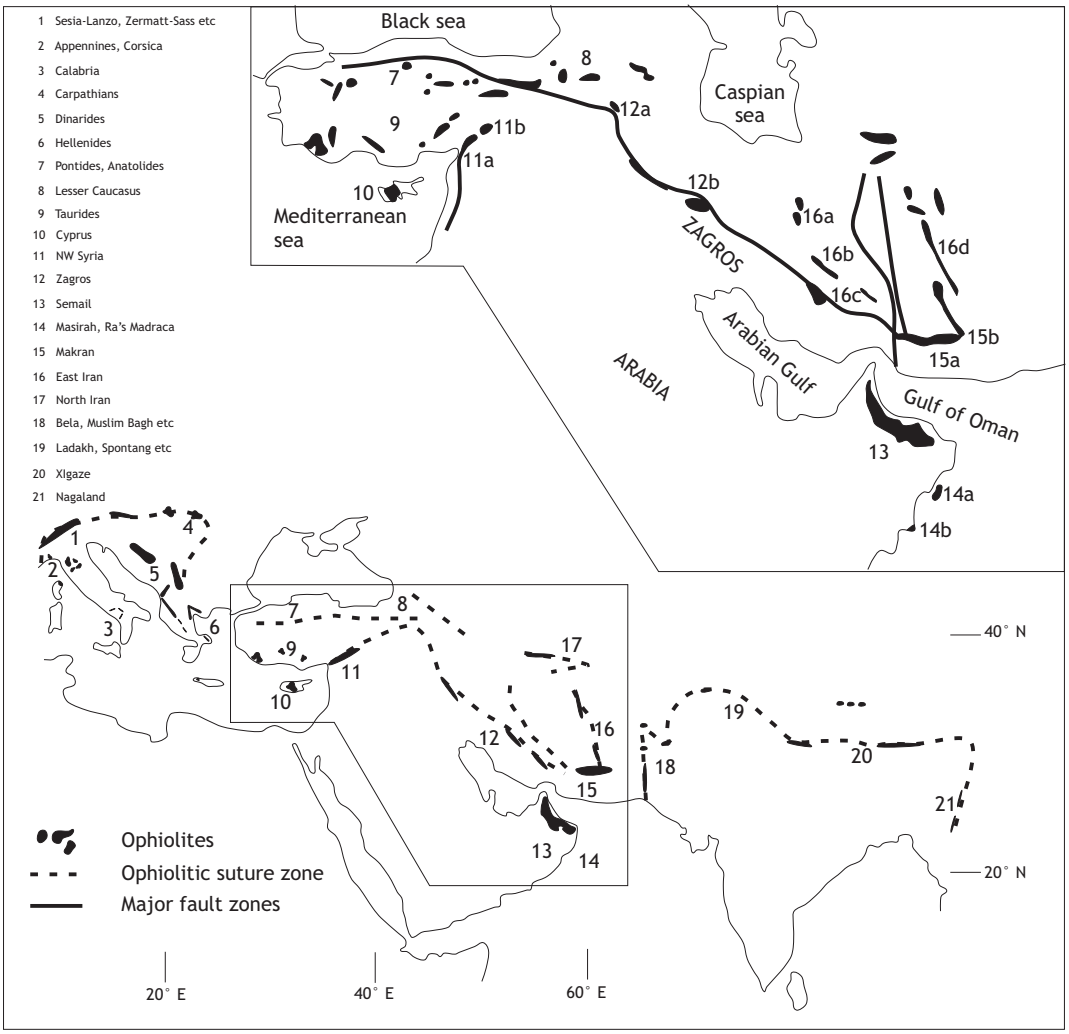


Figure 1.6 Distribution and nomenclature of the ophiolite complexes along the Tethyan orogen, after Lippard et al. (1986).

CHAPTER TWO : THE GEOLOGICAL SETTING OF THE SEMAIL OPHIOLITE



Dark, jagged chocolate brown hills of
mantle sequence harzburgite form the backdrop to
the Gulf of Oman beach of Ra's Dadnah, United Arab Emirates

CHAPTER TWO : GEOLOGICAL SETTING OF THE SEMAIL OPHIOLITE

2.1 INTRODUCTION

The Semail ophiolite of SE Arabia (figure 2.1 and 2.2) is the largest and most extensively studied ophiolite in the world. It forms a thrust sheet ~700 km in length, up to 100 km wide, and 10-15 km thick well exposed over an area of >10,000 km^2 in the United Arab Emirates (UAE) and Oman (Glennie et al. 1974; Coleman & Hopson 1981; Lippard et al. 1986). The ophiolite is of Cenomanian age and formed ~95 Ma ago (Tilton et al. 1981). Following intra-oceanic thrusting, it was transported up to 400-500 km SW (Lippard et al. 1986; Cooper 1988; Béchennec et al. 1988) over the Neo-Tethyan Hawasina basin and was emplaced onto the Permian-Mesozoic passive continental margin of the Arabian plate during the late Cretaceous.

The ophiolite complex was undoubtedly formed at an oceanic spreading centre within Neo-Tethys and it is generally accepted that obduction related thrusts propagated structurally downwards, towards the Arabian shelf margin, as the emplacement process progressed generally in a WSW-SW direction. The ophiolite was emplaced as one internally consistent thrust sheet, but has been subsequently disrupted by faulting and late thrusting (eg Searle 1985). The entire obduction process lasted ~23 Ma and was completed by the end of the Lower Maastrichtian (~72 Ma) when shallow marine fossiliferous limestones were deposited unconformably over all allochthonous units (Glennie et al. 1974).

2.2 HISTORY OF SEMAIL OPHIOLITE GEOLOGICAL RESEARCH

The politics, tribal culture, limited infrastructure and climate of the Sultanate meant that geological exploration of the Oman mountains was difficult and rarely accomplished prior to the accession of Qaboos bin Said in 1970. However, reconnaissance work was carried out in the Muscat area during the late 19^{th} and early 20^{th} C by a number of Indian Geological survey workers, including Pilgrim (1908), who distinguished only Tertiary and pre-Tertiary ('Oman series') units. Lees (1928) was able to make a survey throughout the then accessible parts of the *hajar* mountains and interior of Oman, and developed a stratigraphic framework composed of seven major units. Lees noted the presence of serpentinite, gabbro, diorite and lavas in the 'Semail igneous series' and recognised that the igneous rocks formed a huge coherent thrust sheet, termed the 'Semail nappe'. Despite this work, later research in the 1950s and 1960s, particularly that of Morton (1959), adhered to the then popular geosynclinal concept (in which

the 'Steinmann trinity' of serpentinite, basalt and chert was considered characteristic of the formation of deep basins in previously stable cratons), and regarded the Semail igneous series and the underlying Hawasina sediments as part of an essentially conformable Mesozoic stratigraphy, despite the presence of metamorphic rocks at the base of the Semail igneous series (Wilson 1969).

The present geological framework for the Semail ophiolite allochthon, in which the autochthonous model was discarded, was laid by Reinhardt (1969), the first to describe the Semail nappe as an ophiolite complex. Glennie et al. (1973, 1974), Petroleum Development Oman/Shell geologists, were responsible for producing the first detailed geological map and biostratigraphic framework for the Semail allochthon. This interpretative shift was greatly influenced by the emerging plate tectonic theories of the late 1960s and early 1970s. At the same time, Alleman & Peters (1972), working in the UAE, laid down a clear framework for the nature and timing of metamorphism related to the obduction of the ophiolite. Figure 2.5 shows a detailed tectonostratigraphic column for the allochthon, modified after Glennie et al. (1974) to reflect current knowledge. In the late 1970s and early 1980s, groups from the UK (Open University) and the US (USGS), carried out detailed research in the Oman mountains, the former in the central and northern mountains, the latter in the southern mountains. This research culminated in two major publications, Coleman & Hopson (1981) and Lippard et al. (1986). During the 1980s, the Omani Directorate General of Minerals commissioned the French BRGM (Bureau de Recherches Géologiques et Minières) to produce geological maps of the entire Sultanate. These new maps (LeMetour et al. 1986) have been based on a substantially revised stratigraphy and nomenclature that is not universally accepted (eg Robertson & Searle 1990). Further work on the mantle sequence structures, dynamics and evolution of the Semail ophiolite has consolidated knowledge of the dynamic processes apparent in the oceanic lithosphere.

Recent publications on the Semail ophiolite have concentrated on the age, depth of burial, and exhumation of the Saih Hatat high pressure metamorphic terrane beneath the Semail ophiolite itself (El-Shazly et al. 1990; El-Shazly & Lanphere 1992; Searle et al. 1994; El-Shazly et al. 1997; McMiller et al. 1998, 1999). The unresolved, yet fundamental to the elucidation of the ophiolite subduction-obduction history, tectonic, temporal and spatial relationships between the 'classic' subophiolitic metamorphism of the Semail ophiolite and this unique HP metamorphic terrane will form a major component of this thesis.

The age, nature and duration of sub-ophiolitic sole metamorphism in Oman and the UAE has been addressed (Hacker 1990, 1991, 1994; Hacker et al. 1996; Hacker & Gnos 1997; Gnos 1998) and the search for further field and thermobarometric evidence to constrain the PT evolution of the ophiolite sole forms part of the scope of this thesis. The mineral chemistry of a variety of granulite facies subophiolitic metamorphic rocks from the Bani Hamid terrane, in the UAE has been studied (Gnos & Kurz 1994; Gnos & Peters 1995; Gnos et al. 1996) and yet the

age, origin and emplacement tectonics of the unique granulite facies material of the Bani Hamid terrane, and its relationship to the 'classic' metamorphic sole of the ophiolite, are still poorly understood and controversial.

2.3 ECONOMIC GEOLOGY OF THE SEMAIL OPHIOLITE COMPLEX

Economic geology, in the form of mining, was a major component of the trading power of the Sultanate long before the discovery of oil and natural gas in the Sultanate in the early 1960s. Copper and iron smelting equipment and slag deposits dating back several thousand years have been discovered adjacent to contemporary mines, and today only copper, iron, chromite (with reserves estimated at 2 million tons), gold and silver are mined in the Sultanate, controlled by the government-owned Oman Mining Company and Oman Chrome Company. Coal reserves of 22 million tons, a figure considered adequate for domestic use but not for export, have been reported from Al Kamil, near Sur. Limestone for cement production is mined from extensive Mesozoic carbonate sequences throughout the Sultanate.

Normally accounting for 70-80% of total government revenues and more than 40% of GDP, oil remains critical to the Sultanate's economy. Petroleum Development Oman (PDO), a consortium dominated by the Omani government and Shell, is the country's second largest employer after the government and holds over 90% of the country's oil reserves, accounting for about 94% of production. With relatively small oil reserves, Oman is important to world oil markets primarily because of its strategic location overlooking the Strait of Hormuz. However, a sharp decrease in world oil prices during the late 1990s encouraged Oman to capitalise on its significant natural gas reserves, largely located in deep geological structures.

2.4 GLOSSARY OF RELEVANT ARABIC TERMS

Geomorphologically descriptive Arabic words that will be encountered repeatedly throughout this study, including *jebel* (mountain, singular or range), *wadi* (dry river course), *ra's* (headland or point), *bani* (sons of or tribe), and *khawr* (lagoon).

2.5 REGIONAL TECTONIC FRAMEWORK

The Semail ophiolite allochthon of Oman and the United Arab Emirates forms a 700 km long mountain range parallel to the Gulf of Oman coast on the NE margin of the Arabian plate (figure 2.3), which is bounded to the south and southwest by the active spreading ridges of the Gulf of Aden and Red Sea, and to the west and east by the major transform systems of the Levant fault system and the Owen Fracture zone respectively. To the north, a complex situation exists, in which the actively subducting oceanic-continental margin of the Makran zone becomes the continental collision zone of the Zagros at the Straits of Hormuz syntaxis.

2.5.1 The Zagros

The Zagros fold belt in Iran (figure 2.3) extends for ~1600 km NW-SE, from Turkey to the Makran, and has a very similar Mesozoic tectonic and depositional history to the Oman part of the Arabian continental margin. The Zagros consists of a series of shallow to deep water Mesozoic sedimentary sequences, comprising Permian to Eocene spectacularly folded shallow marine limestones unconformably overlying an older sequence of limestones and clastic sediments. These carbonates are themselves overthrust along the main Zagros thrust by a series of sedimentary and ophiolitic mélanges that represent preserved remnants of Neo-Tethys. As in Oman and the UAE, all these thrust sheets are unconformably overlain by neoautochthonous Tertiary marine limestones. To the NE of the Zagros fold belt, a suite of Cordilleran type calc alkaline plutons and volcanic complexes occurs intruding Precambrian and Palaeozoic basement (Berberian & King 1981). The published ages of these complexes span most of the Mesozoic (Berberian et al. 1982) suggesting that subduction beneath the Zagros has been continuous throughout the Mesozoic. These basement blocks of central Iran (figure 2.3) are thought to have originated as components of Gondwanaland that were separated by rifting in the Permian. The tectonics and chronology of this accretion process have only recently been elucidated (Sengor et al. 1993).

2.5.2 The Makran

The Makran coastal range of SE Iran and Pakistan (figure 2.3) is bounded to the north by Precambrian basement of the Lut block of central Iran and to the west by the Zendan fault bounding the Zagros fold belt. The northern, inner Makran consists of ophiolitic fragments,

pelagic sediments and Mesozoic carbonate platform sediments thrust south over a wide (~200 km) zone of Eocene to Miocene flysch deposits and interpreted as a developing accretionary prism related to the ongoing, shallow, north dipping subduction of the Gulf of Oman oceanic crust beneath the continental margin. The related calc alkaline volcanic arc is ~450 km to the north (figure 2.3) and exhibits magmatism that has been continuous since the late Cretaceous (Berberian et al. 1982), suggesting that subduction and the formation of the Makran has also been continuous for the last ~85 Ma.

2.5.3 The Gulf of Oman

The Gulf of Oman is 3 to 3.5 km deep and reaches such depths only 30 km off the coast of NE Oman. The oceanic crust is thickly covered with 4-6 km of sediments but seismic and heat flow data (Hutchison et al. 1981) demonstrate that the underlying crust is oceanic and at least 70 Ma in age. Recent gravity anomaly and seismic interpretation has demonstrated that the offshore, remnant Semail ophiolite is isolated from the Tethyan oceanic lithosphere in the Gulf of Oman by a continental basement ridge, a NW prolongation of the Saih Hatat window (Ravaut et al. 1997). The tectonic boundary between the continental collision zone of the Zagros and the oceanic subduction-arc system of the Makran in the Gulf of Oman is marked by the N-S trending juxtaposition of the Arabian and Iranian continental shelves west of 58°E. The Zendan fault system (Shearman 1976, figure 2.3) marks the surface boundary between the two zones in SE Iran and shows both westward directed thrust and dextral strike slip components.

2.6 TECTONOSTRATIGRAPHY OF THE OMAN MOUNTAINS

A simplified geological map of the Oman mountains is presented in figure 2.4 and the tectonostratigraphy of the area, modified after Glennie et al. (1974) to reflect the current state of knowledge, is represented in figure 2.5. Figure 2.4 shows two cross sections through the entire allochthon.

2.6.1 Crystalline basement and pre-Mesozoic metamorphism

The crystalline basement of the Arabian continental margin is rarely exposed in Oman although it is inferred to underlie the entire eastern Arabian area. In NE Oman, it is best

exposed around Jebel Ja'alan near Sur and consists of a terrane containing both ortho and paragneisses, intruded by synmetamorphic granitoids. Glennie et al. (1974) obtained an Rb/Sr whole rock age of 858 ± 16 Ma for an intrusive granitoid from Jebel Ja'alan. These compositions and ages are consistent with other regionally distributed examples of Pan African orogeny gneisses (eg Gass et al. 1990).

Infracambrian and Palaeozoic low grade metamorphic rocks of a different paragenesis are exposed in the core of tectonic uplifts in the Huqf, Saih Hatat and Jebel Akhdar windows (figure 2.4) and consist of up to 3.5 km of continental and shallow marine sediments, comprising the Huqf (Infracambrian), Haima (Ordovician-Devonian) and Haushi (Carbonifereous-Permian) groups (Lovelock et al. 1981; Gorin et al. 1982). In the Saih Hatat window, dolomites and limestones of the Infracambrian Hijam dolomite are overlain by ~3 km of Ordovician Amdeh quartzites (Lovelock et al. 1981). The Saih Hatat sequence is completed by middle Permian carbonates (Saiq formation) and intercalated volcanic units that unconformably overlie the Amdeh quartzites and in the NE part of Saih Hatat form the protoliths of the HP terrane described in *Chapter Four*.

Glennie et al. (1974) obtained a Rb-Sr whole rock age of 327 ± 16 Ma from a metavolcanic greenstone from NE Saih Hatat that is independent of the now widely accepted late Cretaceous age (Searle et al. 1994; Hacker et al. 1996) for the Saih Hatat HP event and implies a Hercynian age for the deformation of these Palaeozoic units. However, Sengor (1990) regarded this event as independent from the European Hercynides and instead related it to regional retro-arc fold and thrust belt development. Furthermore, Würsten et al. (1991) used a variety of geochronological techniques to demonstrate major uplift of the Arabian crystalline basement in the Jebel Ja'alan area during the late Palaeozoic.

2.6.2 Permian to Cretaceous carbonate shelf sediments

The autochthonous middle Permian to Cenomanian Hajar supergroup (Glennie et al. 1974) is well exposed in the Jebel Akhdar (figure 2.6c,d), Saih Hatat and Musandam ranges (figure 2.4) of the Oman mountains, and forms extensive subsurface oil bearing source rocks and reservoirs throughout eastern Arabia. This 3 km thick carbonate platform sequence comprises the Saiq (Permian), Mahil (Triassic), Sahtan and Kahmah (Jurassic) and Wasia (Cretaceous) formations and represents a long period of largely aseismic passive margin shallow marine sedimentation.

2.6.3 Sumeini group carbonates

The allochthonous Sumeini group (Glennie et al. 1974; Watts & Garrison 1986), interpreted as a continental slope sequence, formed along the Arabian continental passive margin and carbonate shelf, has a maximum thickness of some 2 km and is exposed in the core of several anticlinal domes along the leading edge of the Semail ophiolite allochthon (figure 2.4). It consists of Triassic to Cenomanian limestones and although the base is not exposed, the Sumeini group is overthrust by the distal and pelagic sediments of the Hawasina group.

2.6.4 Hawasina Group sediments

The Hawasina allochthon (Lees 1928; Glennie et al. 1974; Cooper 1988) is exposed within erosional windows in the Oman mountains and also forms mountain ranges (Hamrat Al Duru, figure 2.4) in the leading portion of the Semail ophiolite allochthon, SW of the ophiolite itself. It is composed of a variety of Triassic to Cretaceous marine sediments, mostly turbidites, which form a complexly deformed and repeated sequence of thrust sheets, which Glennie et al. (1974) divided into five main tectonostratigraphic units:

a) Hamrat Al Duru group: the thickest (1 km) and most extensive of the tectonostratigraphic units, consisting of Triassic to Cenomanian proximal sediments dominated by quartzose turbiditic sandstones, siltstones and cherts. Palinspastic reconstructions of the Mesozoic Neo-Tethys of the area, coupled with the facies types evident, suggest that these sediments were deposited in a more distal, semi-pelagic environment to the Sumeini group carbonates found at the top of the Neo-Tethyan continental rise (Cooper 1990).

b) Wahrah formation: ~200 m of Jurassic to Cretaceous limestone turbidites which are generally finer grained and more siliceous than units of similar age in the Hamrat Al Duru group, and therefore somewhat more distal in origin (Glennie et al. 1974).

c) Al Ayn formation: dominated by middle Triassic to lower Jurassic quartzose sandstones, with subordinate cherts, limestones and shales with a maximum thickness of ~350 m; their high tectonic position suggests they may be derived in part from basinal highs within a marine environment (Glennie et al. 1974).

d) Halfa and Haliw formations: thin sequences of fined grained, distal Triassic to lower Cretaceous limestones and cherts that are highly deformed and are intruded

by a variety of basaltic and alkali ultramafic sills of mostly Triassic age (Glennie et al. 1974; Lippard & Rex 1982; Searle 1984; Hacker et al. 1996).

e) Al Aridh and Ibra formations: consist of up to ~125 m of coarse grained conglomerates, containing clasts mainly of shallow marine carbonate and basalts. Glennie et al. (1974) interpreted these formations as having been formed adjacent to volcanic islands within a relatively distal environment.

In its type locality in the Hawasina window, the Hawasina outcrop is dominated at lower structural levels by thick (~2 km) imbricate sheets of proximal Hamrat Al Duru group turbidites, which are overthrust by more distal turbidites and pelagic sediments of the Halfa and Haliw formations associated with redeposited limestone conglomerates of the Al Aridh formation and large Triassic 'exotic' limestone masses (Graham 1980).

2.6.5 Haybi complex

The 'Haybi complex' was introduced by Searle (1980) to describe in structural terms the thrust bound sequence found between the Hawasina sediments (Haybi thrust) and the ophiolite (Semail thrust), and incorporates units described in part by Glennie et al. (1974) as the 'Oman mélange'. However, the recent BRGM maps do not use this term and the Haybi outcrops are reassigned to the new Umar group of the Hawasina allochthon (Béchennec 1987), a purely stratigraphic definition that does not reflect the influence of thrusting on the structural position, thickness and composition of the lithologies it encompasses.

The Haybi complex includes a variety of thrust slices and olistoliths of Triassic to Cretaceous volcanic rocks as well as large masses of 'exotic' Permo-Triassic limestones, Hawasina type sediments, and entrained metamorphic sole components in a fine grained pelitic matrix. This diverse assemblage is now recognised as forming in a variety of tectonic situations throughout the Mesozoic, ranging from pre-obduction subduction zone mélanges to syn-emplacement tectonic mélanges and sediments.

The Permo-Triassic shallow water 'exotic' limestones (Glennie et al. 1974; Searle & Graham 1982) form large allochthonous masses or klippen below the base of the Semail ophiolite and may be up to 600 km^3 in size (Jebel Khawr; Glennie et al. 1974) and form individual mountains (figure 2.6c). The exotics are widely associated with alkaline basalts volcanics and are interpreted to have formed around oceanic islands within a tropical environment (Glennie et al. 1974).

The Haybi volcanics form a sequence up to ~700 m thick of tholeiitic, transitional and alkaline basaltic volcanics (Searle et al. 1980). Their geochemistry, origin, age and relationship to the tectonic evolution of the Oman Neo-Tethys is detailed in *Chapter Three*. The Haybi mélange consists of megaconglomerates and breccias containing large blocks of all the other Haybi complex components, with a largely sedimentary matrix, containing mid Cretaceous radiolaria, suggesting an origin as an olistostrome. The Haybi complex also includes a basal serpentinite, derived from the ophiolite during the emplacement process (Searle 1980) that in some places (Asjudi for example) dominates the sub ophiolitic tectonic zone and may replace the metamorphic sole entirely. The entire complex is strongly and complexly deformed, with wide variations in internal stratigraphic sequence and thickness, ranging from over ~1 km in the type locality in the Haybi corridor, to complete excision.

2.6.6 Semail ophiolite

The Semail ophiolite (figure 2.7, 2.8) has an outcrop area of some 20,000 km^2, broken into a number of major structural blocks by syn and largely post emplacement (Tertiary) tectonic processes. The greatest observed stratigraphic thickness of the ophiolite is ~20 km although geophysical profile data (Shelton 1984) demonstrates that the maximum structural thickness of the nappe is 5-10 km, suggesting that that the Semail thrust cuts through the ophiolite itself. Along the SW (leading) edge of the ophiolite, imbricate thrusting and repetition of the ophiolite is common, and out of sequence thrusting is also locally of importance (Searle 1985; *Chapter Five*). Cross strike extensional faulting is seen in the Wadi Jizi and Wadi Ahin structures. Many of the tectonic structures in the mantle sequence of the ophiolite can be shown to be brittle reactivations of primary ductile mantle structures (eg Smewing et al. 1977). The lowest km of the mantle sequence exhibits a strong basal fabric and widespread serpentinisation and has been termed the 'banded ultramafic unit' (Searle 1980). Despite this, the Semail nappe represents a largely complete and unaltered ophiolitic terrane.

2.6.7 Batinah complex

The Batinah complex (Woodcock & Robertson 1982a) consists of number of thin thrust sheets overlying the Semail ophiolite on the edge of the Batinah coast. At its base, a mélange containing blocks of all the underlying allochthonous units is locally in depositional contact with the ophiolite. This mélange is overthrust by a sequence of thin Mesozoic (Triassic to Cretaceous) pelagic sedimentary thrust sheets (Woodcock & Robertson 1982b).

2.6.8 Neoautochthonous sediments

All the allochthonous units of the Oman mountains are unconformably overlain by a sequence of upper Maastrichtian (~73 Ma) to Eocene sediments (Pilgrim 1908; Lees 1928; Morton 1959; Glennie et al. 1974), mainly shallow water fossiliferous limestones (Simsima formation) and subordinate fluviatile conglomerates and sandstones (Qahlah formation), marked at the base by a conglomeratic horizon containing clasts derived from the Semail ophiolite. In the Ibra block area, the presence of a laterite horizon at the base of the sequence implies a period of subaerial ophiolite erosion prior to the Maastrichtian sedimentation (Coleman 1981).

2.7 THE SEMAIL OPHIOLITE

2.7.1 Introduction

The Semail ophiolite of SE Arabia is the largest and most extensively studied ophiolite complex in the world, forming a thin but largely undeformed and coherent thrust sheet ~700 km in length, 100 km wide, and 10-15 km thick well exposed over an area of >10,000 km^2 in the United Arab Emirates (UAE) and Oman (Glennie et al. 1974; Coleman & Hopson 1981; Lippard et al. 1986). This thesis will concentrate on the structural, temporal and petrogenetic aspects of the different metamorphic processes and regimes that the Semail ophiolite has undergone during its subduction-obduction history, from its formation in the mid Cretaceous to its emplacement onto the NE part of the Arabian continental passive margin at the end of the Cretaceous. Different tectonometamorphic units of the Semail ophiolite complex can be used to elucidate different aspects of the subduction-obduction evolution of the Semail ophiolite, and are briefly introduced and described here.

The Semail ophiolite, in common with other globally distributed and well described ophiolite complexes, exhibits a thin and discontinuous *metamorphic sole* at its base, consisting of oceanic crustal and sedimentary material plastered to the base of the ophiolite along the hanging wall of the Semail (emplacement) thrust.

In the Saih Hatat area of SE Oman, a more regionally extensive and distinctive sub ophiolitic metamorphic terrane consists of a complex of *high pressure blueschist-eclogite* facies material metamorphosed at lower temperatures and higher pressures than the 'classic' ophiolite metamorphic sole.

Yet another type of sub ophiolitic metamorphic terrane found beneath the Semail ophiolite is restricted to the Bani Hamid range on the northern border of Oman with the United Arab Emirates (UAE), where a thick sequence of *granulite facies*, largely metasedimentary material, is found apparently imbricated within the ophiolite mantle sequence in a different structural position to the metamorphic sole.

Throughout the mantle sequence of the Semail ophiolite in Oman and the UAE, but particularly abundant adjacent to the Bani Hamid metamorphic terrane, a suite of small scale *granitoid intrusions* (dykes and small stocks) are found and have received little attention and less understanding in the considerable body of research published on the Semail ophiolite.

2.7.2 Semail ophiolite stratigraphy

The tectonostratigraphy of the Semail ophiolite is represented in figure 2.7. Most of the mantle sequence is composed of tectonised harzburgite that represents the residual mantle from partial melting of fertile primary spinel lherzolite at pressures in excess of 20 kbar. Early high temperature orthopyroxene fabrics in the harzburgites (figure 2.8a) probably represent mantle flow patterns that appear to show the presence of mantle diapirs below the ridge (Ceuleneer et al. 1988; Nicolas et al. 1988). Mantle diapirs represent the feeders for the ridge segment and magma chambers must presumably be centred above the diapirs (Boudier & Nicolas 1995). High-temperature lineations were formed by plastic flow of upwelling mantle that diverge away from the ridge axis below the Moho (figure 2.8b). These earlier mantle fabrics have been overprinted along the base by a strongly banded harzburgite-lherzolite-dunite unit (termed the banded ultramafic unit by Searle & Malpas 1980, 1982) showing emplacement related fabrics. Dunite pods and lenses with small chromite bodies (figure 2.8c) occur towards the upper levels of the mantle sequence. The petrological Moho is the base of the crustal sequence and is marked by the incoming of plagioclase. Melts generated in the upper mantle were formed in linear magma chambers in which convecting magma was being fed in batches from below and generating melts feeding upwards through the sheeted dykes above.

Tholeiitic to picritic melts generated the crustal sequence comprising up to 4 km of layered mafic and ultramafic rocks of the cumulate sequence overlain by isotropic gabbros, diorites and trondhjemites. The cumulate sequence layered peridotites and gabbros represent the floor of the magma chamber and are composed of a variety of rocks containing the primary minerals olivine, orthopyroxene, chrome spinel, clinopyroxene, hornblende and plagioclase (figure 2.8d). Rhythmically layered dunites, wehrlites, olivine gabbros, gabbros and gabbronorites show gravity settling cumulate textures. Late intrusive wehrlites have discordant contacts and intrude higher levels of the crustal sequence (Juteau et al. 1988). The

cyclic nature of the cumulate layered series at the base of the crustal sequence suggests open system fractionation of a continually replenished magma chamber (Browning & Smewing 1981). Numerous magma chamber models have been proposed based on field mapping of the cumulate sequence and high level intrusives (Pallister & Hopson 1981; Browning & Smewing 1981; Nicolas et al. 1988; Boudier & Nicolas 1995). The Semail ophiolite is generally thought to represent a fast-spreading ridge with an open, continually replenished magma chamber. The along strike continuity of the cumulate sequence peridotites and gabbros suggest a long, linear magma chamber. Trondhjemites or plagiogranites, composed of quartz and plagioclase with minor ferromagnesian minerals, represent the final end products of magmatic differentiation (Pedersen & Malpas 1984).

Magma generated in the magma chamber at the base of the crust fed the extrusive volcanic sequence via the sheeted dyke complex (figure 2.8e). At the top of the magma chamber dykes can be seen coalescing in between gabbroic screens, and at higher structural levels dykes indicate 100% crustal extension. The dykes trend parallel to the ridge axis and are roughly arcuate along the strike of the Oman mountains with little segmentation of cross-cutting transform fault structures (MacLeod & Rothery 1992). The upper part of the Semail ophiolite consists of up to 2 km of extrusive lavas that in northern Oman have been sub-divided into four major units (Pearce et al. 1981; Alabaster et al. 1982). The lower Geotimes unit (figure 2.8f) comprises clinopyroxene and plagioclase phyric basalts, slightly depleted relative to N-type MORB. The overlying Lasail unit comprises up to 500 m of a basalt-andesite-dacite-rhyolite fractionation sequence, strongly depleted relative to N-type MORB and interpreted as an immature island arc sequence, erupted at discrete volcanic centres above a subduction zone (Pearce et al. 1981). Highly depleted clinopyroxene phyric basalts are overlain by about 100 m thickness of mildly alkaline transitional within-plate basalts (Salahi unit) erupted off-axis, probably along small fissures. The highest levels of the ophiolite show Fe-Mn rich metalliferous sediments or umbers within, and on top of, the volcanic sequence, overlain by pelagic sediments including radiolarian mudstones.

2.7.3 Age of the Semail ophiolite

The age of the Semail ophiolite lithosphere is still not accurately constrained. U-Pb zircon ages from plagiogranites (late stage differentiates) in the Semail ophiolite crustal sequence range from 97.3-93.5 ± 0.25 Ma with a mean age of 94.8 ± 0.1 Ma (Tilton et al. 1981), interpreted as recording the time of formation of the ophiolite. Radiolarian ages from pelagic sediments interbedded within the upper volcanic units are Cenomanian-Turonian (Tippit et al. 1981) and correlate closely with the igneous zircon ages. Gabbro Sm-Nd whole rock ages from the Ibra area of 100 ± 20 Ma, 128 ± 50 Ma and 150 ± 40 Ma (McCulloch et al. 1981), despite

overlapping the Tilton ages, have errors too large to be useful. Accurate, spatially well constrained and widespread dating of the ophiolite using U-Pb or $^{40}Ar/^{39}Ar$ techniques should resolve the age of the ophiolite clearly. The Cenomanian marks the timing of final stable carbonate sedimentation on the Arabian platform and along the shelf margin (Sumeini Group rocks) before the shelf margin collapsed to form the Aruma foreland basin, into which the allochthonous thrust sheets were to become emplaced (Glennie et al. 1973, 1974).

2.7.4 Origin of the Semail ophiolite: mid ocean ridge or supra subduction zone?

Controversy exists as to whether the Semail ophiolite formed at a mid ocean ridge (MOR, figure 2.10) (Coleman 1981; Boudier et al. 1985, 1988; Hacker 1991; Hacker et al. 1996) or a supra subduction zone (SSZ, figure 2.9) setting (Searle & Malpas 1980; Pearce et al. 1981; Lippard et al. 1986; Searle & Cox 1999; Cox et al. 1999). It is possible that an earlier tectonic setting (oceanic ridge) was superceded by a later intra oceanic arc setting.

Any conclusion hinges on the interpretation of the volcanic sequence geochemistry, the structural restoration of the thrust sheets, and the timing of ophiolite formation related to the timing of metamorphism in the amphibolite facies sole. The volcanic units at the upper levels of the Semail ophiolite are most complete in northern Oman where Pearce et al. (1981) and Alabaster et al. (1982) determined the volcanic stratigraphy and, using trace element geochemistry, proposed an immature island-arc setting for the Lasail unit volcanics. Although the upper volcanic units are well exposed along the northern Oman mountains, detailed studies of the crustal sequence in the SE Oman mountains show only the lower MORB basalts, and hence Coleman (1981), Hopson & Pallister (1981) and Boudier et al. (1985, 1988) interpreted the ophiolite as having being generated at a mid-ocean ridge.

If the Semail ophiolite originated at a mid-ocean ridge and obduction was initiated at the ridge, then preserved subduction zone footwall components (metamorphic sole and Haybi complex) should be the same age as the ophiolite itself. The Haybi complex is composed dominantly of older ocean floor material such as Triassic alkali basalts, as well as tholeiitic volcanic rocks (Searle et al. 1980), late Permian and Triassic 'exotic' limestone blocks (Searle & Graham 1982), Cretaceous mélanges and the metamorphic sole. Geochemistry of the amphibolites in the metamorphic sole shows that the amphibolites were not the same as the Semail ophiolite volcanics, nor the Haybi alkali basalts. Immobile trace element geochemistry clearly shows that the amphibolites are closest compositionally to the Neo-Tethyan Haybi tholeiitic volcanics of Triassic age (Searle 1980; Searle & Malpas 1982) and Masirah ophiolite MORB crust (*Chapter Three*). Volcanic material subducted along the footwall of the Semail

thrust was considerably older and colder than the Semail ophiolite crust, and obduction cannot have been initiated at the mid-ocean ridge that formed the ophiolite.

The overlap between plagiogranite U-Pb zircon ages and metamorphic sole $^{40}Ar/^{39}Ar$ hornblende ages (Hacker 1994) also point to subduction of Haybi basalts beneath the ophiolite to depths at least 40 km (Gnos 1998; *Chapter Three*) at the same time as the ophiolite crustal sequence was forming. Clearly obduction cannot have been initiated at the site of the ridge that must have been to the NE of the site of initiation of the Semail thrust (Searle & Malpas 1980).

The only remaining hypothesis whereby older, colder material could be juxtaposed against young, hot ophiolite would be a transform fault setting. However, this model requires a continental margin parallel transform fault to have formed the site of subduction initiation. Only minor transform faulting, such as in the Wadi Jizi and Wadi Hatta areas, has been identified (MacLeod & Rothery 1992). Both the mid ocean ridge setting and the transform fault setting can therefore be rejected. The Semail ophiolite must have been formed in a marginal basin above a NE dipping subduction zone, dipping away from the continental margin. The initiation of obduction along the Semail thrust must have occurred where Triassic to Jurassic Neo-Tethyan crust was being subducted NE beneath the Semail ophiolite during or immediately after formation of the Semail crustal sequence.

This conclusion is backed up by regional tectonic considerations that also suggest that the Semail ophiolite formed by NE directed intra-oceanic subduction in Neo-Tethys. The Mesozoic evolution of the Neo-Tethyan oceanic domain was dominated by N or NE dipping subduction zones (Sengor 1979), a process that is still ongoing beneath the Aegean and Makran. Furthermore, Dewey et al. (1973) suggested that the formation of the Atlantic ocean caused rapid mid Cretaceous convergence in the eastern Neo-Tethyan domain. The emplacement of late Cretaceous calc alkaline arc complexes in the hinterland of the Makran implies shallow dipping northwards directed subduction of Neo-Tethyan crust dating from at least this time (Berberian et al. 1982), and it is most likely that this subduction was initiated shortly after the obduction of the Semail ophiolite onto the Arabian continental margin, a process that was complete by ~72 Ma (Glennie et al. 1974).

2.8 THE MESOZOIC EVOLUTION OF NEO-TETHYS IN OMAN

Neo-Tethys (Jenkyns 1980) is the name commonly given to the ocean that formed in the late Palaeozoic and early Mesozoic by rifting between the NE margin of Gondwanaland (including Arabia) and numerous microplates (including Anatolia, central Iran, and the Lhasa block). The older palaeo Tethyan ocean lay to the north of these rifted microplates and was

largely consumed by subduction beneath the southern Asian continental margin, followed by the accretion of the rifted microplates and associated island arcs, a process that was largely complete by the mid Jurassic (Sengor 1979). Subsequently, northwards subduction of Mesozoic Neo-Tethyan oceanic material beneath oceanic island arcs (eg Spong arc; Corfield 1998) led to the eventual southward obduction of the Himalayan ophiolites (eg Spontang, Corfield 1998) onto the Indian plate passive margin sequence. Figures 2.11 and 2.12 show a reconstruction of the NE Arabian continental margin and adjacent Neo-Tethyan ocean during the Cenomanian, ~95 Ma, immediately prior to the obduction of the Semail ophiolite.

2.8.1 Continental rifting and formation of Neo-Tethys

Permian sedimentation in the Oman area was dominated by a variety of carbonate platform type facies, varying from shallow marine limestones and intertidal sabkha deposits (autochthonous shelf sequence) to more open marine and oceanic island related deposits ('exotic' limestones). Similar limestones occur as allochthonous masses throughout the Tethyan orogen from the Alps to the Zagros and have been interpreted as forming due to the breakup of 'external' carbonate platforms on rifted continental margins (Bernoulli & Jenkyns 1974) or as oceanic island cappings (Glennie et al. 1974). The homogeneity of the sedimentation throughout the Mesozoic following Permian rifting and the creation of a NE facing passive margin clearly implies that aseismic passive margin tectonics dominated this period (Searle et al. 1983, 1994).

Triassic sediments in the Oman area are more diverse than the Permian sequences and range from carbonates of a similar range in facies type to those of the Permian to deep water turbidites and pelagic sediments of the Hawasina allochthon. The Triassic Mahil formation, which overlies the Permian components of the shelf sequence, also represents part of a shallow marine shelf, while the time equivalent Sumeini group sediments were deposited on the continental slope and most of the Hawasina sediments were deposited in deeper, pelagic Tethyan environments.

The Haybi volcanic sequence (Searle 1980) evolved over time in the Triassic to Jurassic from alkaline to transitional to tholeiitic geochemistry and documents the initiation and progression of rifting in the Permian carbonate platform to produce a passive continental margin and true Neo-Tethyan oceanic crust. Similar sequences throughout the Neo-Tethyan domain are found from Greece to Turkey and also have a stratigraphic and geochemical evolution consistent with the development of a rifted continental margin.

2.8.2 Passive margin development

By the late Permian, the Oman area had developed into a NE facing passive continental margin with well defined shelf, slope and pelagic facies environments. Igneous activity was much reduced after the late Triassic (Béchennec et al. 1991), with only minor volumes of alkaline volcanics intruded into the more distal parts of the basin during the Jurassic and Cretaceous. Alkaline ultramafic intrusions in the passive margin sequence (Searle 1984; Hacker et al. 1996) were emplaced during the mid Triassic (~220 Ma) and again during the Cenomanian (~92 Ma).

Igneous activity through the Mesozoic continental margin carbonate and clastic successions was dominated by alkaline basaltic to ultramafic sills, with the latter forming very distinctive bodies up to 30 m thick (Searle 1984). K-Ar and $^{40}Ar/^{39}Ar$ dating of these alkaline ultramafic intrusions suggests they were formed both during the mid Triassic, at ~220 Ma, and during the mid Cretaceous (92-94 Ma), although some sills were subsequently reset with respect to K-Ar and $^{40}Ar/^{39}Ar$ during the Cenomanian emplacement of the ophiolite (Hacker et al. 1996), rather than being emplaced throughout the entire Mesozoic, as suggested by Lippard & Rex (1982).

Minor uplift of the Arabian carbonate platform at the end of the Triassic was followed by Jurassic subsidence and the return of shallow marine carbonate conditions, typified by the Sahtan group limestones, with an increasing terrigeneous input over time reflecting uplift in sediment source areas (Glennie et al. 1974). Similar shallow marine conditions were dominant until the late Cretaceous, when the obduction of the ophiolite and its advancement onto the continental shelf led to the development of a rapidly deepening forearc basin which drowned the carbonate shelf and was filled by limestone conglomerates, olistostromes and marls of the Coniacian to Campanian Aruma group (Glennie et al. 1974; Robertson 1987a,b). The absence of ophiolitic debris within the Aruma group (except at the very top of the sequence) suggests that the source of these flexural basin deposits was the Arabian continental margin.

2.8.3 Syn-obduction and Tertiary tectonostratigraphy

The tectonic processes governing the subduction-obduction history of the Semail ophiolite will be discussed in detail in *Chapter Seven*, using a variety of techniques and new data to produce a model for the subduction-obduction process than accommodates all the existing and new structural, metamorphic and geochronological evidence, and hence here a brief summary of details not covered elsewhere will be presented.

The emplacement of the Semail ophiolite allochthon has several features in common with other well described 'foreland type' fold and thrust belts like the Moine of NW Scotland (Elliot & Johnson 1980) in that thrusting developed in a classic piggy back style, and hence the furthest travelled allochthon (the Semail ophiolite) is the structurally highest, while the least travelled and last transported unit, the Sumeini carbonates, are found at the base of the allochthon. However, Searle (1985) demonstrated the presence of localised 'break back' thrusting in the allochthon; the thrusting of Batinah complex continental margin sediments over the ophiolite is a good example.

Extensive neoautochthonous Maastrichtian-Eocene shallow marine carbonates were deposited after the emplacement of the Semail ophiolite and were deformed after the Eocene in upright to overturned (in the Musandam peninsula; Searle et al. 1983) folds that trend parallel to the Oman mountains: N-S in the Musandam area and generally E-W in the Muscat area. This regional deformational event is thought to have caused the doming and exhumation of the Jebel Akhdar and Saih Hatat windows.

2.9 AIMS OF RESEARCH

Any investigation of the nature, extent and duration of the processes related to the subduction–obduction history of the Semail ophiolite allochthon will have major implications for general models of ophiolite obduction, the tectonic evolution of the Alpine–Himalayan orogen and an understanding of the nature of Jurassic to Cretaceous plate tectonic processes and motions in the Neo-Tethyan domain. An understanding of the origin and nature of the metamorphic and anatectic materials and processes preserved beneath the Semail ophiolite is fundamental to constraining subduction zone processes and may have parallels with processes in contemporary subduction–obduction environments.

Despite the large body of work published on all aspects of the age, petrography, geochemistry, tectonic evolution and metamorphism of the Semail ophiolite (eg Glennie et al. 1974; Searle & Malpas 1980,1982; Coleman & Hopson 1981; Lippard et al. 1986), a number of key issues stemming from the subduction–obduction processes occurring during the emplacement history of the ophiolite remain unresolved. In outline, these major issues include:

a) Controversy exists as to whether the ophiolite formed at a mid-ocean ridge (MOR) (Coleman 1981; Boudier et al. 1985, 1988; Hacker 1991; Hacker et al. 1996) or in an oceanic arc or supra-subduction zone (SSZ) setting (Searle & Malpas 1980; Pearce et al. 1981; Lippard et al. 1986; Searle & Cox 1999; Cox et al. 1999).

b) The pressure and temperature evolution of the well preserved 'classic' ophiolitic metamorphic sole is very poorly constrained (eg Searle & Maplas 1980, 1982; Ghent & Stout 1981; Gnos 1998).

c) The origin and tectonic evolution of the unique Bani Hamid sub-ophiolitic metamorphic terrane, which differs substantially from other metamorphic sole localities in terms of grade, thickness and structural position in the allochthon.

d) The tectonic processes governing the preservation, exhumation and subsequent evolution of the Saih Hatat high pressure metamorphic terrane beneath the ophiolite are poorly understood.

e) The age of the peak (eclogite facies) metamorphic event seen in the Saih Hatat terrane is controversial, with estimates ranging from ~80 Ma (Michard et al. 1994) to ~130 Ma (El-Shazly & Lanphere 1992).

f) The tectonic controls governing the distribution of the contrasting high temperature (amphibolite–granulite) and high pressure (blueschist–eclogite) metamorphic regimes observed beneath the ophiolite have not been adequately addressed in the literature.

g) The origin, nature, age and distribution of leucocratic material within the mantle sequence of the ophiolite has received limited attention despite the unusual occurrence and potential for constraining subduction–obduction processes that these intrusions represent.

h) To develop a clearer understanding of subduction zone rates and processes using thermochronological modelling techniques in conjunction with new and existing PT and geochronological estimates.

Studies of the metamorphic sole of the Semail and other ophiolites are key to the development of models of subduction zones processes and ophiolite emplacement tectonics, as an understanding of the rate, extent, duration and nature of metamorphic processes occurring in a subduction zone or intra oceanic thrust beneath an obducting ophiolite is fundamental to the development and constrain of any obduction model. Furthermore, such a study can address all the major outstanding issues in the emplacement tectonics of the Semail ophiolite, by combining detailed structural, geochemical, petrological and metamorphic analyses of sub-ophiolitic metamorphic and anatectic material into a wider scale tectonic framework. Therefore, within this initial framework, several key research aims of the project were identified:

a) Detailed and comparative structural mapping and sampling of the major 'classic' metamorphic sole outcrops at the base of the Semail ophiolite in order to accurately constrain the nature, deformation, origin and pressure temperature evolution of the metamorphic sole of the ophiolite.

b) Detailed structural mapping of the Bani Hamid metamorphic sole terrane, to attempt to account for its unusual tectonic setting within the ophiolitic allochthon and elucidate the tectonic and deformational evolution of the terrane. Thermobarometry of the metamorphic assemblages will allow the pressure temperature evolution of the terrane to be determined, and geochemical analysis will enable identification of protolith material.

c) Detailed structural mapping and sampling, coupled with macro and micro-kinematic studies, of the northern part of the Saih Hatat high pressure terrane to attempt to distinguish different structural and deformational events and relate these events to the exhumation and post tectonic evolution of the high pressure material.

d) Use of petrographic and thermobarometric techniques, coupled with U-Pb (monazite & titanite) dating to elucidate the pressure temperature evolution of the As Sifah eclogites.

e) Investigation of the nature, distribution, age and origin of leucogranitic material found in the mantle sequence of the ophiolite using field, geochronological, petrographic and geochemical techniques.

From the results of these individual investigations it is intended to reconstruct the subduction–obduction and subsequent tectonic evolution of the Semail ophiolite in terms of an integrated model of obduction that accounts for all the observed features described in this work. The significance of the inferred tectonic processes in terms of existing and general models of ophiolite formation and obduction will be considered throughout, and the results contrasted with work on comparable Neo-Tethyan and other ophiolite terranes.

2.10 THESIS OUTLINE

Chapter 1 presented a review of the history of ophiolite research and a synthesis of current thinking, concentrating on the development of ophiolite obduction models and mechanisms. The term ophiolite was introduced and its subsequent and current usage defined by reference to numerous standard models. Published models and mechanisms used to account for the obduction of ophiolites were discussed and critically compared. The wide range of

geological techniques used to identify and characterise the various rock types and tectonic environments commonly recognised from global ophiolitic terranes are introduced and critically assessed. Major global examples of ophiolitic terranes were introduced and compared to demonstrate both the diversity and similarity, in terms of origin, geochemistry and formative mechanisms, of ophiolites of different ages. The temporal and spatial distribution of ophiolites was also discussed. The value of studies of the Semail ophiolite to the understanding of a wide variety of global tectonic processes was shown, from subduction zone metamorphism to the nature of oceanic spreading centres.

Chapter Two has introduced the Semail ophiolite itself and the general aspects of its historical geology, morphology, stratigraphy, geochemistry and economic geology have been considered. Various techniques have been used to shed new light on the controversial tectonic environment of formation of the Semail ophiolite. Regional (Tethyan) tectonics, coupled with a summary of Arabian tectonics and the stratigraphy of the Semail ophiolite allochthon, has provided a framework within which the subduction-obduction related petrogenetic and metamorphic evolution of the Semail ophiolite sole itself may be interpreted.

Chapter 3 introduces and briefly reviews the concept of ophiolitic metamorphic soles and outlines the key insights an understanding of these rocks can give to models of ophiolite formation and obduction. A series of detailed structural maps and metamorphic profiles through the major metamorphic sole localities of Oman and the United Arab Emirates are introduced and the stratigraphy, structure and petrography of the sampled sole rocks discussed. New and existing thermobarometric analyses of the sole, when coupled with existing geochronology, enable a synthesis of the pressure temperature and deformational evolution of the various sole localities to be developed. This knowledge is used in the final chapter to constrain a new model for the obduction process and environment of the Semail ophiolite.

In *Chapter 4*, the structure, tectonic evolution and metamorphism of the Saih Hatat high pressure metamorphic terrane is considered. The major concepts, models and global examples of (ultra) high pressure metamorphism are reviewed and their relevance to Saih Hatat considered. Detailed structural maps of the northern part of Saih Hatat are presented. Macro and microstructural and kinematic techniques, coupled with thermobarometric analyses, are used to differentiate various deformational and metamorphic regimes during the formation, preservation and exhumation of the high pressure material.

Chapter 5 introduces the Bani Hamid granulite facies subophiolitic metamorphic terrane and compares and contrasts it to the 'classic' metamorphic sole localities described in *Chapter 3*. A detailed structural map and metamorphic profiles across the terrane are presented, and new Rb/Sr and Sm/Nd isotopic analyses and thermobarometric and petrographic results are presented to elucidate the unusual structural position, internal stratigraphy, and thickness of the terrane. New and existing geochemical and geochronological

data are used to constrain the origin, age and tectonic evolution of this unique metamorphic terrane.

Chapter 6 discusses the nature, origin, distribution and age of rare leucocratic granitoid material found as small scale intrusions within the mantle sequence of the ophiolite. Key formative environments and processes of granitoid genesis, and the techniques used to differentiate these tectonic settings, are introduced, with particular reference to processes occurring in ophiolitic terranes. The field relationships, petrography, structure, distribution and stratigraphic position of the Semail ophiolite leucogranites are discussed. Granitoid mineral chemistry, major and trace element geochemical data, and Rb/Sr & Sm/Nd isotopic analyses, are all used to model the protoliths and origin, crystallisation conditions and melt evolution, and age and metamorphism of the observed granitoids. Such techniques can provide great insights into subduction zone processes and rates during the subduction-obduction process.

Chapter 7 draws together and synthesises the material presented and analysed in the preceding chapters and produces tectonic models to account for the origin, formation, PT evolution, exhumation and post tectonic history of the contrasting types of igneous and metamorphic rock associated with the emplacement of the Semail ophiolite allochthon. Two complementary tectonic models accounting for the subduction-obduction history of the Semail ophiolite in the northern Oman-UAE and SE Oman/Saih Hatat areas of the ophiolite belt are presented and the potential for future work not addressed in the present study is also discussed.

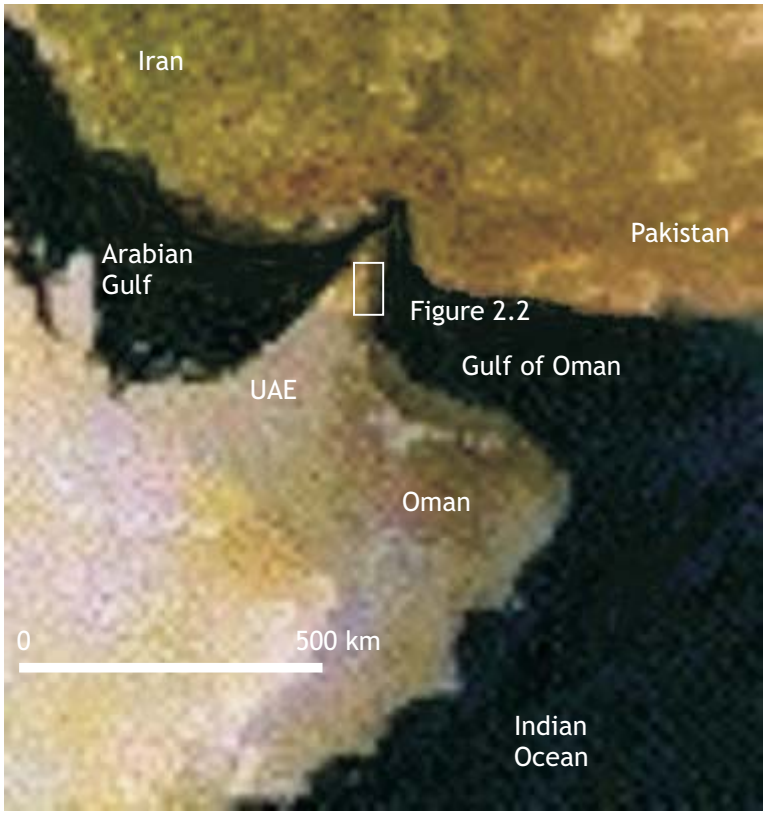


Figure 2.1 Landsat image of eastern Arabia and SW Asia, including Oman. The Oman mountains form an arcuate range adjacent to the Gulf of Oman. The dark outcrops form the Semail ophiolite itself, while paler colours represent the autochthonous shelf carbonates, allochthonous sediments, and post emplacement limestones.



Figure 2.2 Detailed Landsat image of the northern part of the Semail ophiolite in Oman and the United Arab Emirates; north is at the top of the image, which is dominated by the Mesozoic limestones of the southern Musandam peninsula, separated from the dark ophiolite mantle sequence and paler crustal sequence to the south by the faulted Dibba zone. Grey outcrops in the lower centre of the image represent subophiolitic metamorphic material. Base of image is ~100 km.

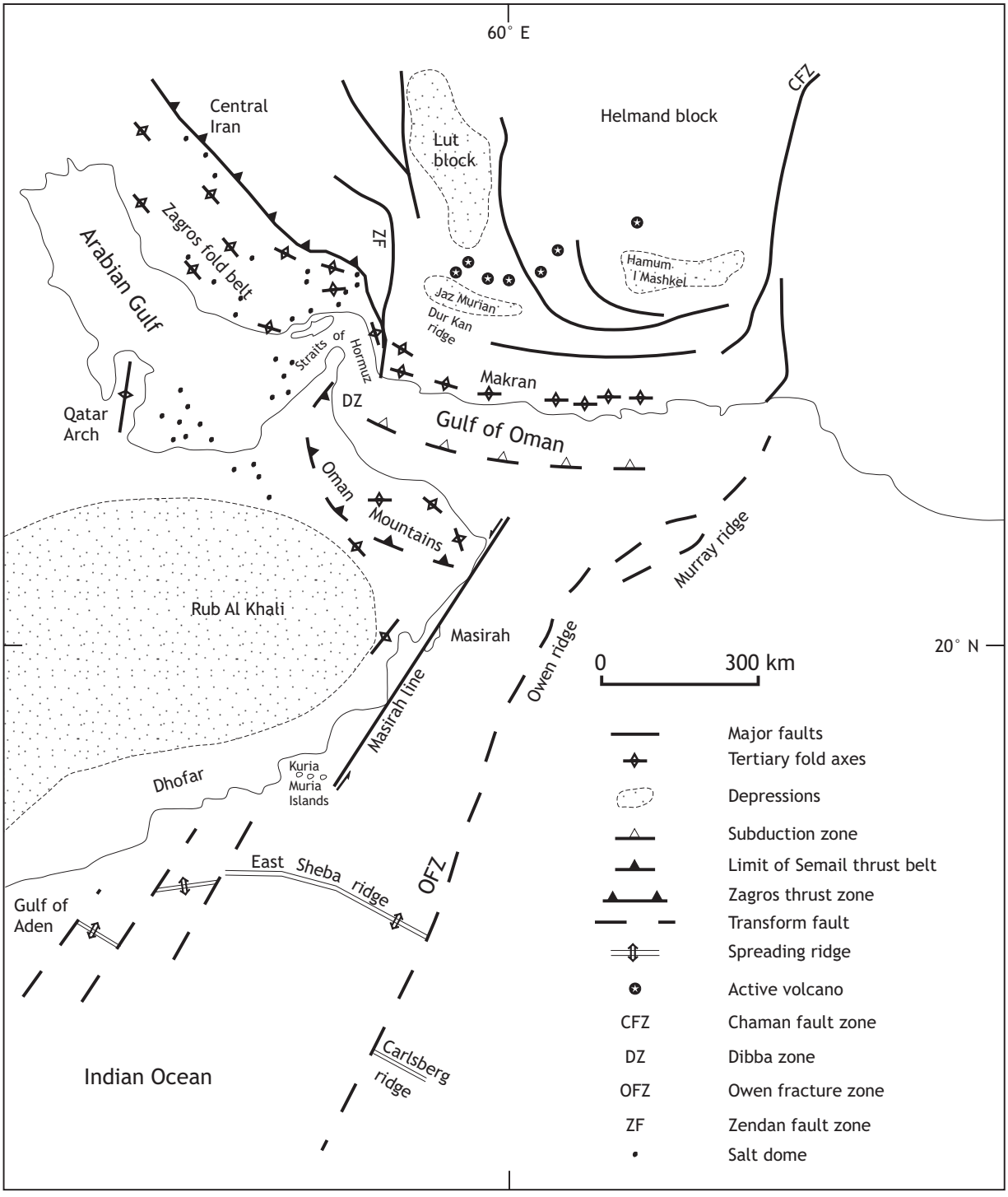


Figure 2.3 Regional tectonics of the Arabian plate and the surrounding Middle East, showing the major structural domains and elements described in the text, after Lippard et al. (1986).

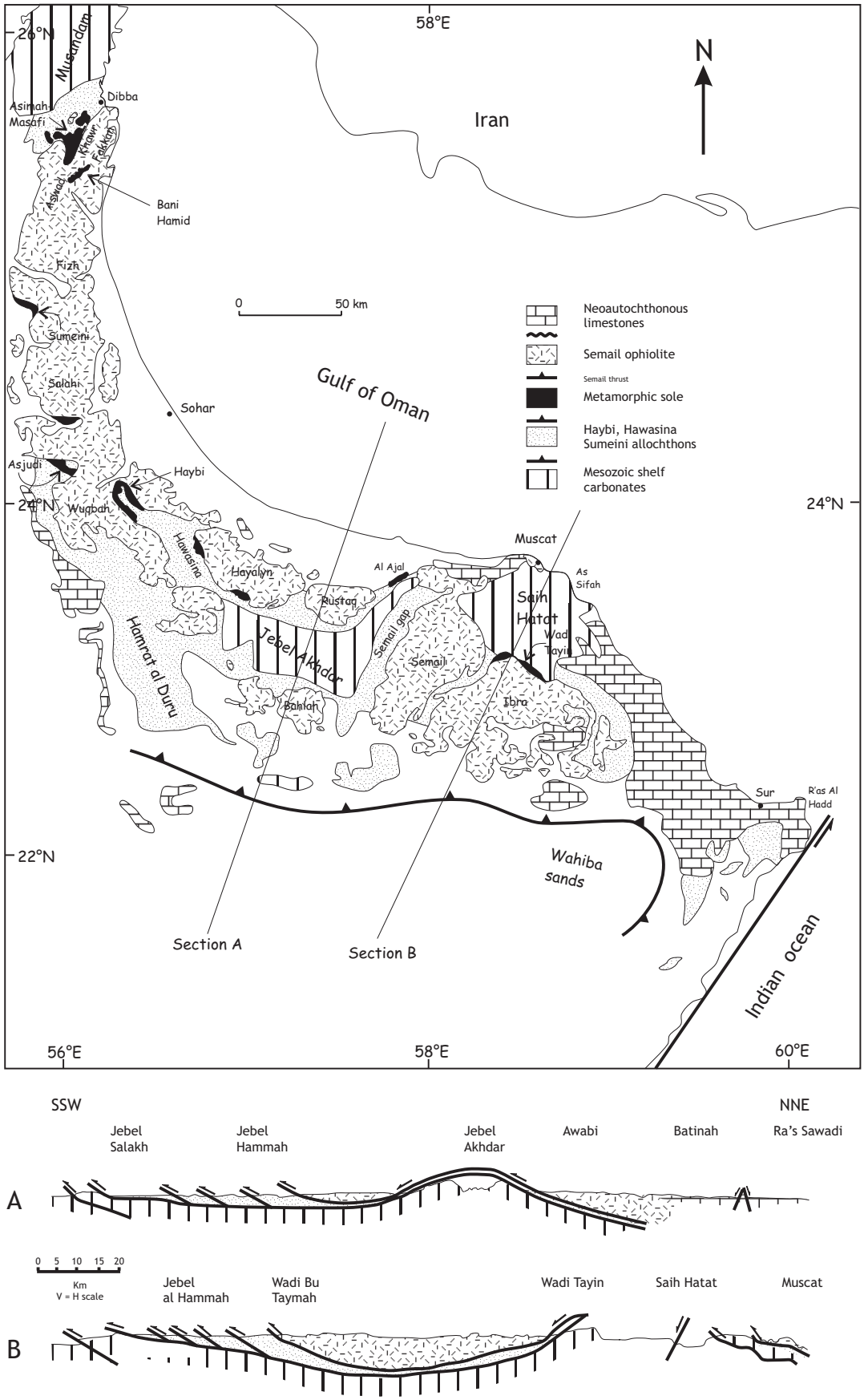


Figure 2.4 a) Geological map of NE Oman, showing the Semail ophiolite allochthon, after Glennie et al. (1973, 1974). The major autochthonous and allochthonous units are shown, along with the separate structural blocks of the Semail ophiolite, the Saih Hatat high pressure metamorphic terrane, and the classic metamorphic sole localities. b) sections through the Saih Hatat and Jebel Akhdar windows exhibit all the thrust sheets of the Semail ophiolite allochthon. Legend as map.

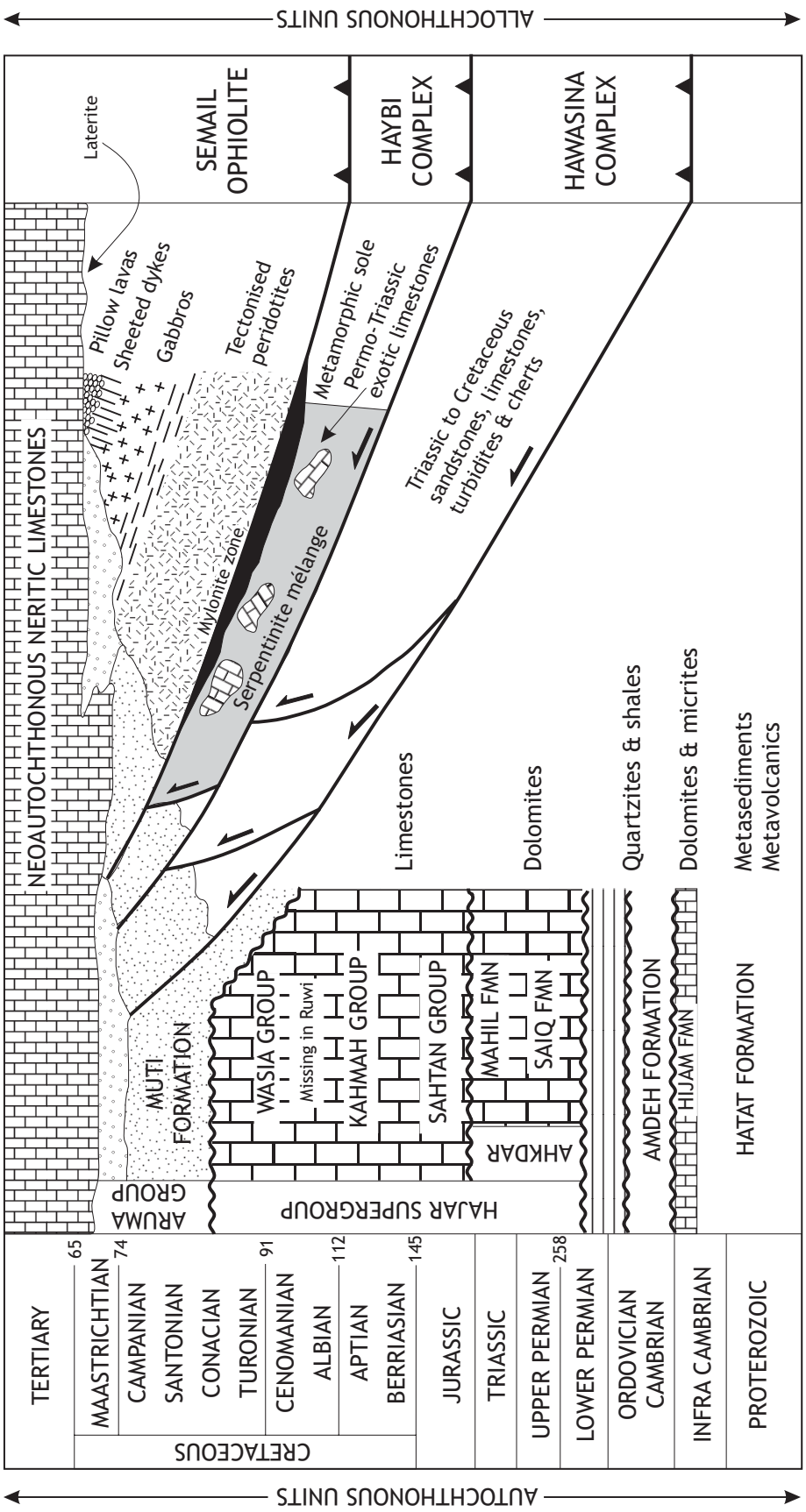


Figure 2.5 Tectonostratigraphic summary of the northern Oman mountains and Semail ophiolite allochthon, after Glennie et al. (1973, 1974) and Searle et al. (1994).

Figure 2.6 Photographs showing the typical field occurrence and relationships of some of the major rock units associated with the Semail ophiolite allochthon.



a



b

a) view of the Semail ophiolite mantle sequence in the Khawr Fakkan block of the United Arab Emirates. Serpentinised harzburgites of the mantle sequence form steep, jagged and well exposed peaks with up to ~1500 m of relief. b) pillow lavas of the lowermost Geotimes unit of the Semail ophiolite crustal sequence, Wadi Jizzi, Oman. See figure 2.4.



c



d

c) the peak of Jebel Misht is an example of the 'Oman exotic' Permo-Triassic limestones which occur in the Haybi complex beneath the Semail ophiolite. d) view from the Semail gap of the autochthonous limestones of the Jebel Akhdar window, which form a major anticlinal dome and reach an elevation of ~3000 m at Jebel Shams on the inner wall of the window. See figure 2.4.

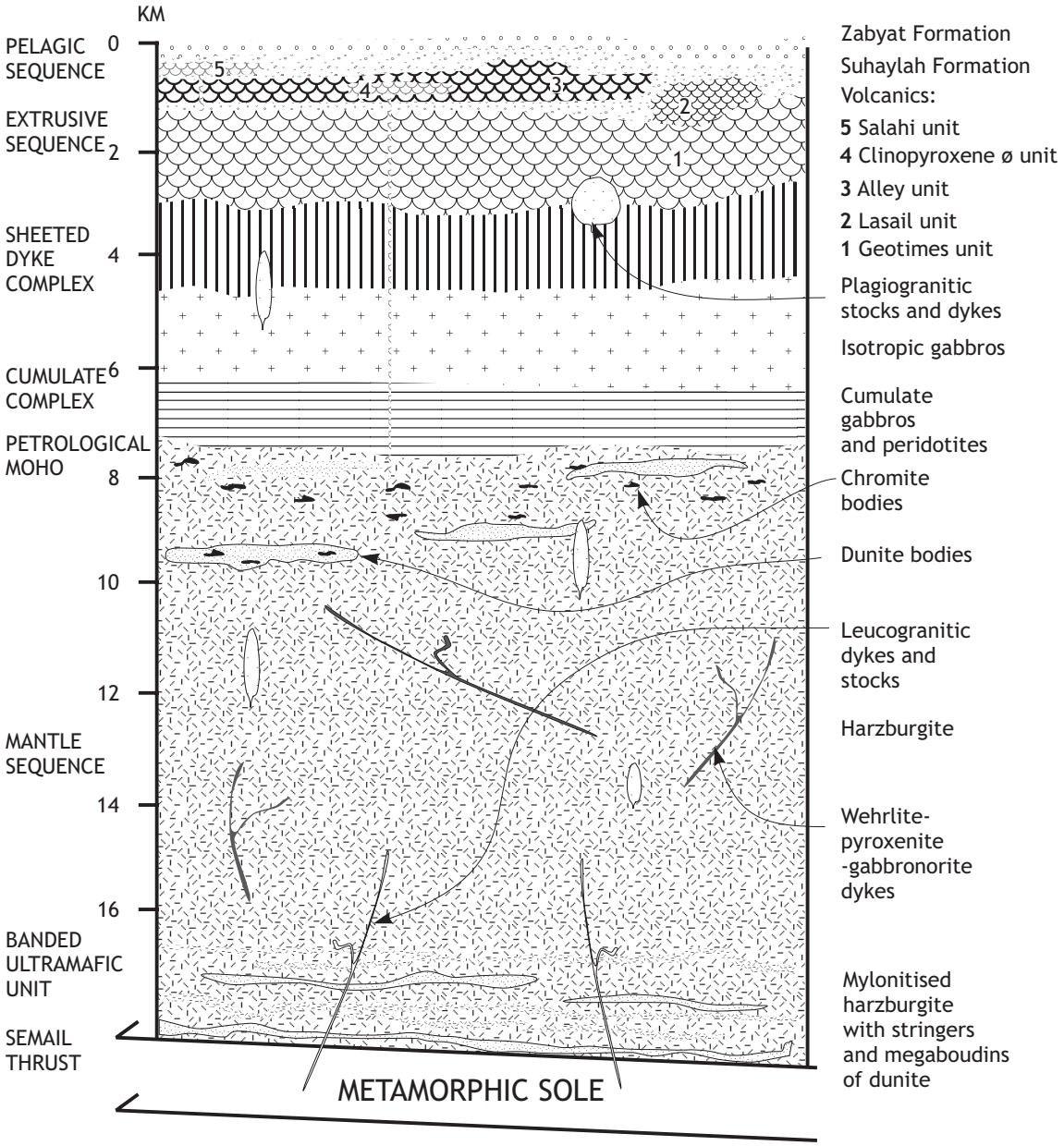


Figure 2.7 Petrography and stratigraphy of a composite, idealised section through the Semail ophiolite, after Lippard et al. (1986). Syn and post emplacement imbricate and out of sequence thrusting (Searle 1985), coupled with extensional faulting, has disrupted the ophiolite complex and produced separate tectonic blocks. The ophiolite reaches its maximum observed stratigraphic thickness of ~18 km in the Ibra block (figure 2.4) although geophysical data (Shelton 1984) demonstrates that the structural thickness of the Semail thrust sheet is at most ~10 km.

Figure 2.8 Field views of the different components of the Semail ophiolite.



a



b

a) Typically severe relief and excellent exposure in the Semail ophiolite mantle sequence, Khawr Fakkan block. b) Cumulate gabbros and peridotites overlying mantle sequence harzburgites at a sharply defined Moho, Wadi Al Abyad. Palm tree is ~6 m tall.

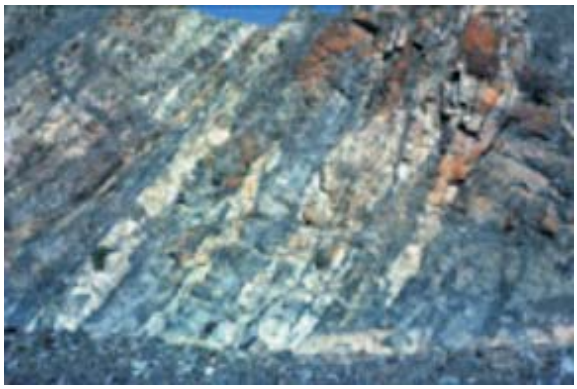


c



d

c) Chromite pod, ~10 m in size, in mantle sequence dunites and harzburgites. d) Cumulate gabbros and peridotites of the mantle transition zone intruded by leucogranitic dykes, Ra's Dadnah, Khawr Fakkan block. Cliff height is ~30 m.



e



f

e) Sheeted dolerite dykes, indicating 100% extension, in the crustal sequence of the ophiolite. Each dyke is ~2 m across. f) Well formed pillow lavas of the lower Geotimes unit of the ophiolite crustal sequence, Wadi Jizzi. Figure for scale.

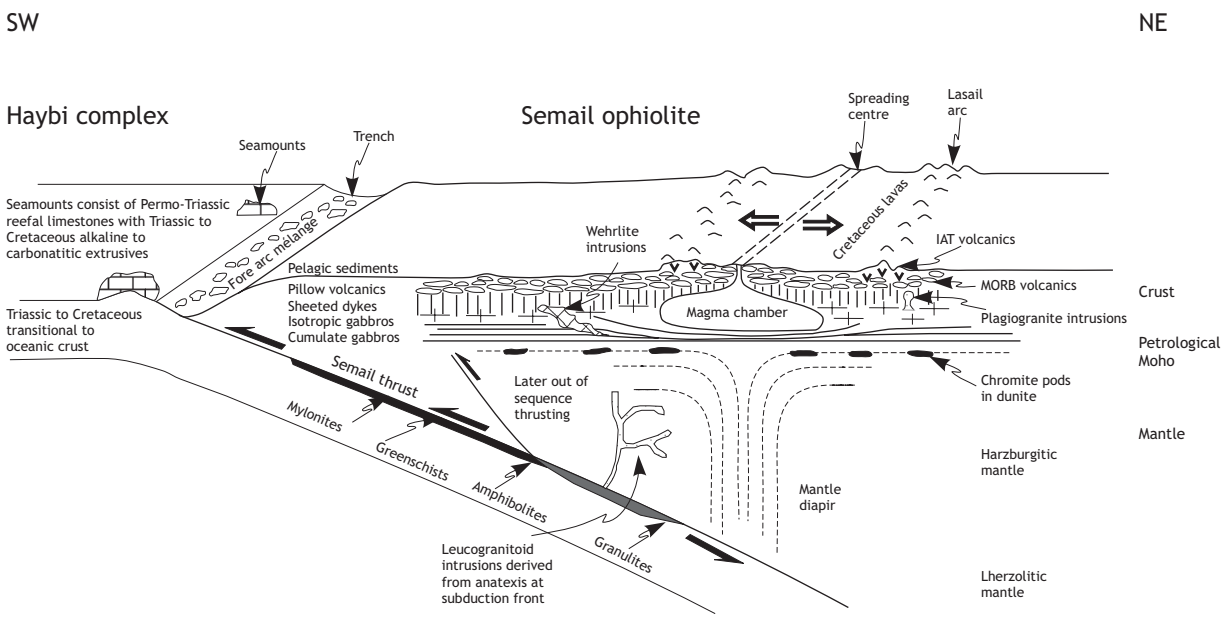


Figure 2.9 Model summarising the supra-subduction zone (intra-oceanic arc) origin hypothesis for the Semail ophiolite shortly after its formation at ~95 Ma. From Searle & Cox (1999), after Searle & Malpas (1980, 1982), Pearce et al. (1981) and Lippard et al. (1986).

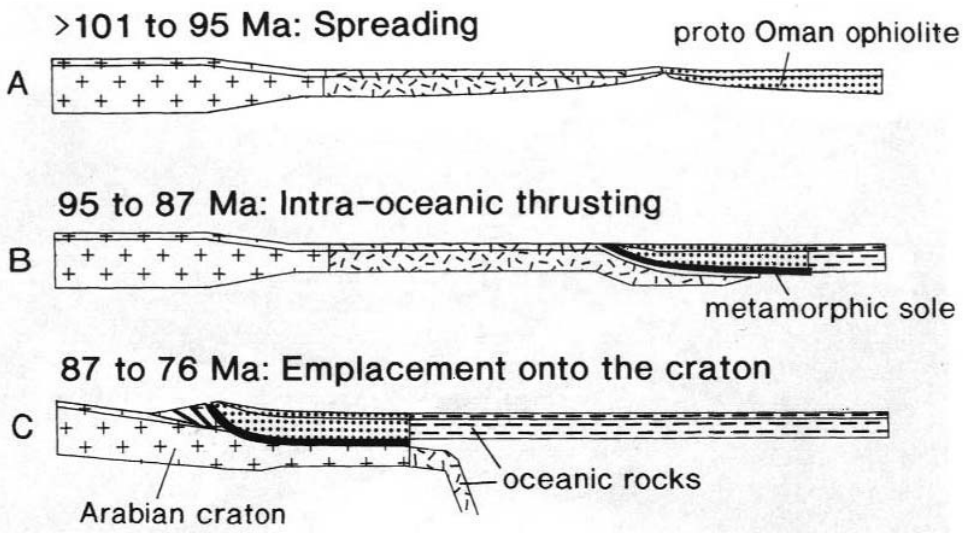


Figure 2.10 The MOR model for the formation and obduction of the Semail ophiolite, from Hacker (1994), after Hopson et al. (1981), Pallister & Hopson (1981) and Boudier & Coleman (1981) *inter alia*.

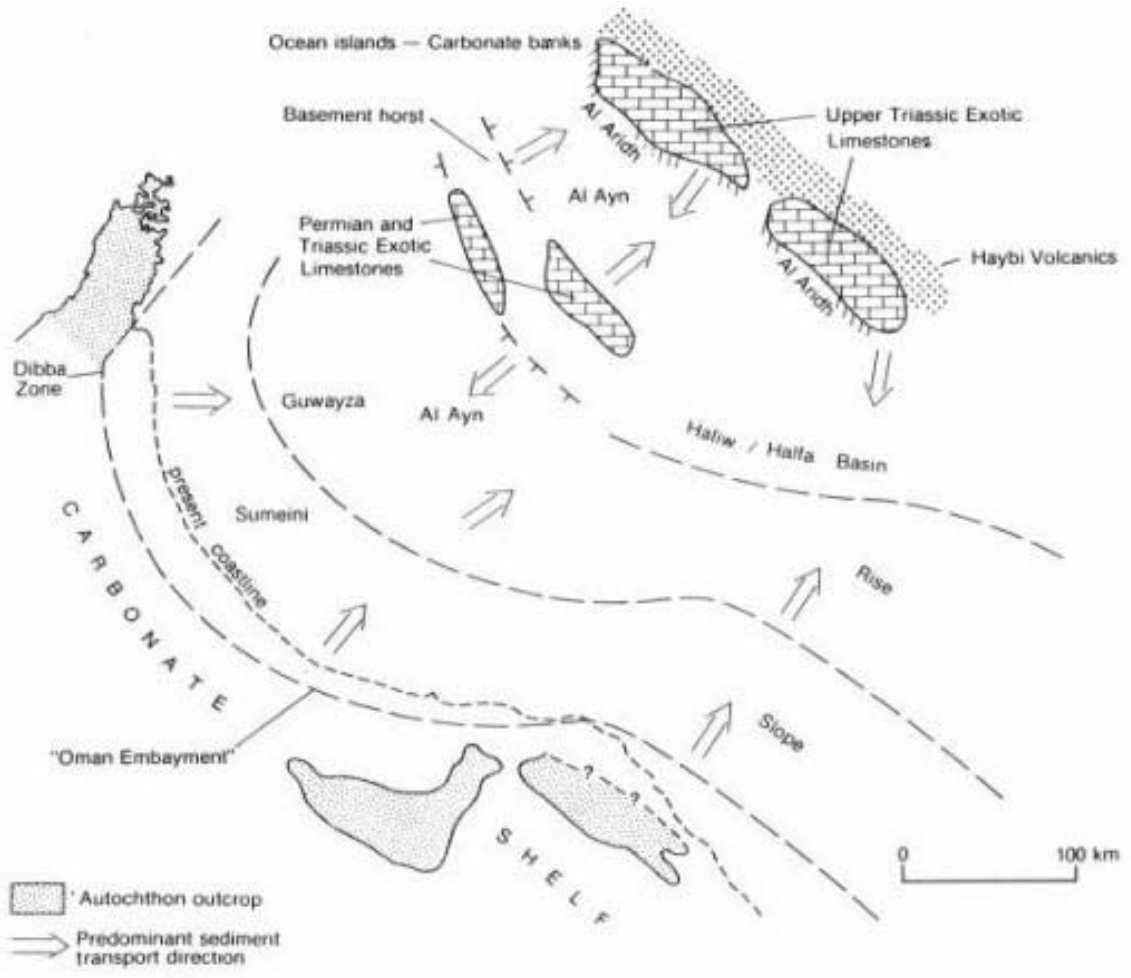


Figure 2.11 Schematic palaeogeographic reconstruction of the Arabian continental passive margin during the mid Cretaceous, prior to the obduction and emplacement of the Semail ophiolite, from Lippard et al. (1986). A section through the Arabian continental margin and Hawasina basin of the Neo-Tethyan ocean is shown in figure 2.12.

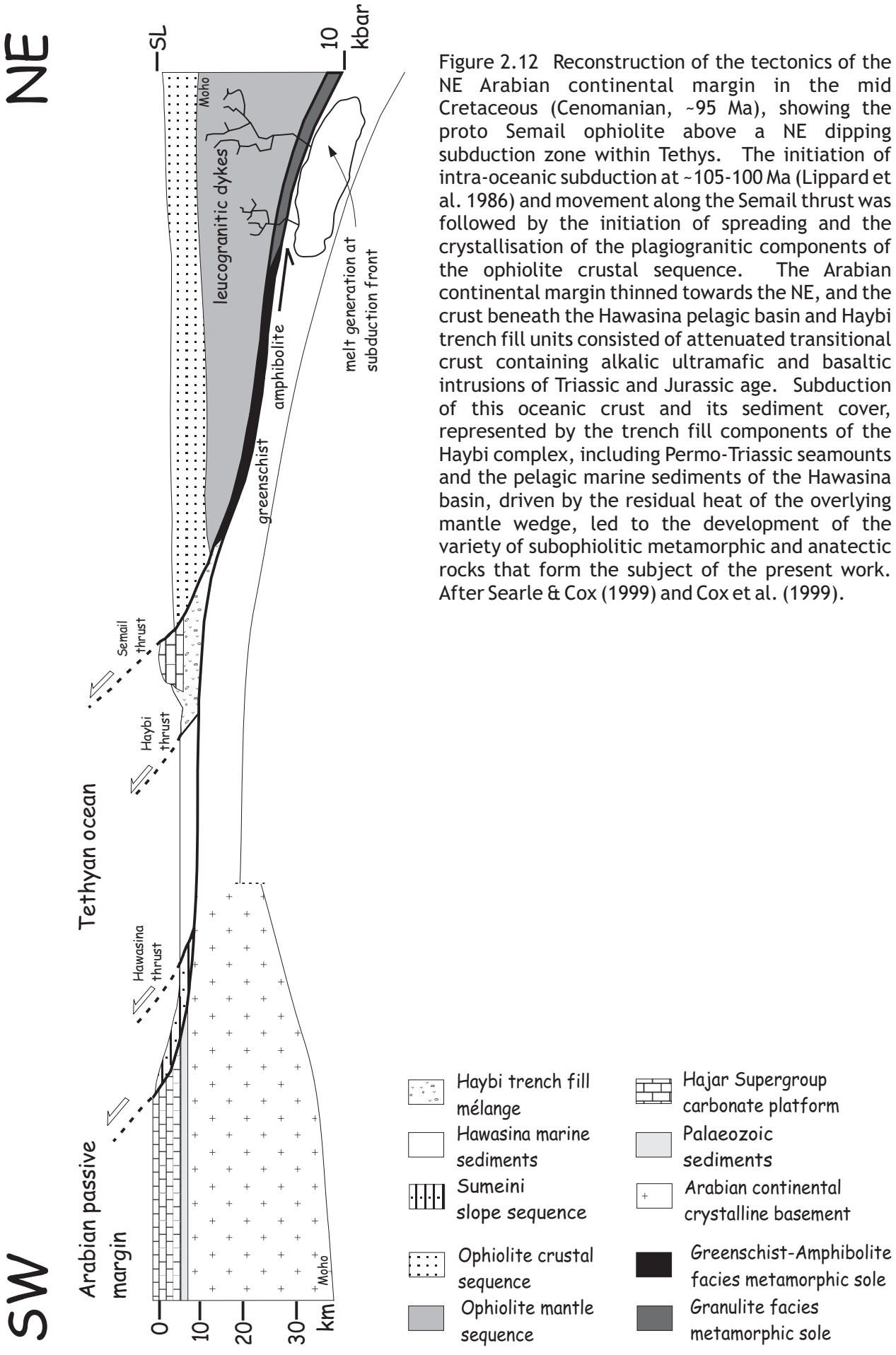


Figure 2.12 Reconstruction of the tectonics of the NE Arabian continental margin in the mid Cretaceous (Cenomanian, ~95 Ma), showing the proto Semail ophiolite above a NE dipping subduction zone within Tethys. The initiation of intra-oceanic subduction at ~105-100 Ma (Lippard et al. 1986) and movement along the Semail thrust was followed by the initiation of spreading and the crystallisation of the plagiogranitic components of the ophiolite crustal sequence. The Arabian continental margin thinned towards the NE, and the crust beneath the Hawasina pelagic basin and Haybi trench fill units consisted of attenuated transitional crust containing alkalic ultramafic and basaltic intrusions of Triassic and Jurassic age. Subduction of this oceanic crust and its sediment cover, represented by the trench fill components of the Haybi complex, including Permo-Triassic seamounts and the pelagic marine sediments of the Hawasina basin, driven by the residual heat of the overlying mantle wedge, led to the development of the variety of subophiolitic metamorphic and anatectic rocks that form the subject of the present work. After Searle & Cox (1999) and Cox et al. (1999).

CHAPTER THREE : SEMAIL OPHIOLITE METAMORPHIC SOLE



The sun doesn’t always shine in the Sultanate...
Wadi flood, near Rustaq.

CHAPTER THREE : SEMAIL OPHIOLITE METAMORPHIC SOLE

3.1 INTRODUCTION

As noted in *Chapter Two*, the presence of emplacement related metamorphic rocks, forming a *metamorphic sole* or *dynamothermal aureole* accreted to the base of the Semail ophiolite is crucial to elucidating the nature and timing of the ophiolite obduction process in Oman and the United Arab Emirates. The structure, deformation, distribution and stratigraphy of the metamorphic sole can provide powerful constraints on shearing and deformation conditions both during intra-oceanic subduction and post-obduction tectonic events. The metamorphic petrology and PT evolution of ophiolite metamorphic sole material can provide valuable information on the thermal conditions during intra-oceanic thrusting.

The geochronology of metamorphic sole material can potentially accurately date the attainment of mineral closure temperatures in the K-Ar and Ar-Ar systems, and date crystallisation events in associated anatectic material using the U-Pb and Sm-Nd (whole rock) systems. When used in conjunction with metamorphic PT histories, geochronology can accurately model the conditions throughout the emplacement process. The extent, grade, age and thermal evolution and peak conditions of metamorphic sole components, while difficult to accurately constrain due to the presence of structural breaks and the polyphase nature of the Semail ophiolite sole, can provide an indication of the age and thermal properties of the ophiolite during obduction.

Studies of the metamorphic soles of numerous ophiolite complexes (eg Williams & Smyth 1973; Searle & Malpas 1980, 1982; Ghent & Stout 1981; Jamieson 1981, 1986) have indicated that a number of features are commonly observed:

1. There is a lithological and structural zonation through the sole, with mantle sequence peridotites thrust over tholeiitic metagabbros and amphibolites with marbles and pelagic cherts of oceanic provenance, which in turn are thrust over metasediments, tuffs and metavolcanic material of continental margin provenance.
2. Metamorphic isotherms are inverted and telescoped, with amphibolite to granulite facies conditions prevailing at the peridotite contact and grading structurally down through epidote amphibolite and greenschist over a thickness that rarely exceeds ~500 m.

3. Metamorphic isobars are similarly inverted and telescoped, with the pressure contrasts between the top and the base of the sole larger than the structural thickness.
4. Temperature gradients averaged over the sole greatly exceed those in typical thermal models of subduction zones.
5. Intense polyphase ductile deformation of all structural levels within the sole is common. Internal, major brittle structures are less common and post-date peak conditions.
6. Overprinting of peak metamorphic assemblages by lower grade assemblages is common and generally more intense at higher structural levels within the sole.
7. It is widely accepted that the main heat source for sole metamorphism is the residual heat of the young, hot, overthrust mantle wedge, with minimal contribution from shear heating during subduction.
8. Peak pressures computed in metamorphic sole metabasites commonly exceed 10 kbar (Jamieson 1981; Gnos 1998; this study) despite overlying ophiolite complexes rarely exceeding 20 km in thickness (equivalent to ~6 kbar).

In this chapter, new geological mapping, PT determinations and structural analysis from the major metamorphic sole outcrops beneath the Semail ophiolite will be used in conjunction with existing age constraints to model changing subduction zone conditions during ophiolite obduction.

3.2 METAMORPHIC SOLE TECTONOSTRATIGRAPHY AND STRUCTURES

The metamorphic sole along the base of the Semail ophiolite (figure 3.1) commonly forms, in the southern and central Oman mountains, a discrete thrust sheet typically ~200-300 m thick (Searle 1980). In its most complete and best preserved examples, such as the Sumeini locality shown in figure 3.2-3, the sole exhibits a steep, inverted thermal gradient from rare medium to coarse grained mafic granulite (?) two pyroxene and garnet-diopside amphibolite gneisses at the peridotite contact, downwards through plagioclase-hornblende and epidote amphibolites, to a variety of lower amphibolite and greenschist facies metasediments, mainly quartzites, with subordinate volcaniclastic and carbonate units. The oceanic metabasites are always separated from the continental metasediments by a thrust, which may be regarded as the preserved subduction zone plate boundary. Small volumes of partial melting occur at the

highest grade parts of the metamorphic sole where cm to m scale melt pods and veins of hornblende tonalite melts intrude garnet-diopside amphibolites (Searle & Malpas 1980, 1982).

The presence of metamorphic sole outcrops beneath both the leading and trailing edges of the ophiolite as well as in tectonic windows eroded through the centre of the ophiolite thrust sheet, implies that the sole extends beneath the entire ophiolite. The strong deformational fabrics seen within the metamorphic sole, particularly at higher structural levels, are parallel to the Semail thrust and similar to fabrics in the lower 'banded ultramafic unit' of the ophiolite (Searle 1980), implying synchronous formation of the fabrics under similar conditions. This structural evidence is reinforced by recent geochronological data (Hacker et al. 1996) and is compatible with the contemporaneous formation of the metamorphic sole and initial detachment of the ophiolite. The ubiquitous nature of the deformation of the metamorphic sole has repercussions for the accuracy of any modelling of the thermal and deformational evolution of the obduction process based on thermobarometry and geochronological studies of 'complete' metamorphic sole sections, although Hacker et al. (1996) suggested peak values of up to ~4000°C km^{-1} and ~100 MPa for the thermal gradient and shear stress within the Semail ophiolite sole.

The typical morphology of the numerous metamorphic sole localities in the Semail ophiolite (figure 3.1) is rarely as clear as the ideal outlined above, with most outcrops incomplete, resulting in highly variable stratigraphy and a lack of continuity between and within major sole outcrops.

The homogeneity of the sole components, coupled with its highly sheared nature particularly at high structural levels (Hacker et al. 1996 estimated shear strains of ~8000 in the upper garnet-diopside amphibolites of the Wadi Tayin sole), and the lack of clear stratigraphic markers to correlate between localities, precludes any clear identification and characterisation of brittle deformation structures within the sole, making precise estimates of the absolute stratigraphy of the sole impossible. Existing ophiolite displacement profiles derived from sole geochronology and tectonostratigraphy (Hacker 1990; Hacker 1991; Hacker & Mosenfelder 1996) have assumed zero repetition or excision within discrete sole sequences, which is demonstrably incorrect (figure 3.4, 3.5).

While the determination of PT values within individual outcrops is possible, any accurate correlation between present structural position and absolute stratigraphic depth beneath the Semail thrust during emplacement is virtually impossible; the construction of meaningful PT profiles through the sole is also difficult, and the metamorphic sole may be regarded as a syn-subduction shear zone that juxtaposes different lithologies and grades of subducted material accreted to the subduction zone hanging wall.

3.2.1 Wadi Tayin

The classic section through the metamorphic sole in SE Oman occurs in the 'green pool' area of Wadi Tayin (figure 3.1), where about 250 m of amphibolite facies mafic amphibolites and quartzites occur beneath the peridotite (Ghent & Stout 1981; Hacker & Mosenfelder 1996). Both upper (Semail ophiolite) and lower (unmetamorphosed sediments of the Haybi complex) contacts are late, brittle, detachment surfaces. Here the uppermost few meters are also composed of garnet-diopside-hornblende gneiss with rare pods of tonalitic to monzodioritic partial melt composed of plagioclase-quartz-apatite-epidote-hornblende, as well as diopside-andradite bearing metasedimentary lenses of carbonate material.

The grain size of these metabasic gneisses reaches ~2 mm at the Semail thrust but decreases to <0.5 mm within ~50 m. Garnet persists only to ~10 m below the Semail thrust, and structurally below are hornblende-plagioclase-epidote amphibolites and Mn garnet and piemontite bearing quartzites (meta-cherts) in a sequence similar to that at Sumeini. Ghent & Stout (1981) reported greenschist facies assemblages below the amphibolites but Hacker & Mosenfelder (1996) presented new petrographic analyses that indicated that these rocks were lower amphibolite facies, thrust over unmetamorphosed sediments without intermediate greenschists. High grade assemblages have been largely overprinted by greenschist and prehnite-pumpellyite facies assemblages, particularly towards the top of the sequence (figure 3.18a).

A new geological sketch map of the 'green pool' locality is presented in figure 3.6 that shows the distribution of sole components, the major structural elements and sample profiles. Figure 3.7 is a cross section through the outcrop, and a structural and petrographic log section through the entire sole in Wadi Tayin is shown in figure 3.10.

The Semail thrust here dips to the SW, parallel to the vergence of asymmetric folds within garnet and piemontite bearing quartzites (figure 3.5), and is cut by a steep late extensional fault. Internal truncation of the Semail thrust parallel, SW dipping, amphibolite foliation within the sequence suggests the presence of brittle imbricate structures (figure 3.4).

The structural aspects of the Semail ophiolite metamorphic sole that preclude any clear assessment of the true sole thickness and pressure & temperature profiles are well seen in Wadi Tayin; the sole has an apparent stratigraphic thickness of ~250 m but there is evidence for brittle imbricate structures that truncate earlier ductile fabrics and repeat lithological units within the sole. The presence of large scale sheath folding within the green pool outcrop is also clear from the outcrop pattern and repetition of a major metachert horizon within the sole (figure 3.3).

3.2.2 Sumeini

The Sumeini area of the northern Oman mountains (figure 3.1) is remote but contains a thick and largely well preserved metamorphic sole section with an outcrop width of up to ~2.5 km that represents the most complete sole sequence in the Oman mountains. Figure 3.2 shows the disposition of the key tectonometamorphic units in the Sumeini area including the 'banded ultramafic unit' at the base of the ophiolite (Searle 1980).

Late stage calcium metasomatism has produced rodingites composed of hydrogrossular, diopside, micas and calcite adjacent to the Semail thrust at the base of the ophiolite. The studied section of the Sumeini area, reproduced in figure 3.10, shows some 60 m of fine to medium grained hornblende-plagioclase amphibolites immediately below the mylonitised basal harzburgites of the ophiolite sequence. The upper ~40 m also contains almandine and diopside; epidote is abundant at lower horizons. At the highest structural levels within the metamorphic sole partial melting has produced small stromatic monzodioritic to tonalitic melt pods. Thin bands and lenses of marble with hornblende, grossular and diopside and muscovite-piemontite-diopside quartzites are intercalated within the amphibolites as well as phyllitic, fine grained amphibolites.

New structural mapping has produced the section and structural log through the entire metamorphic sole in the NW part of the Sumeini area presented in figure 3.10. The logged sequence is thicker than the clearly imbricated Wadi Tayin section and although only one obvious brittle structure was observed in the logged section, imbricate structures in other parts of the Sumeini sequence have shown that it has been thickened in a similar manner (Searle 1980).

3.2.3 Al Ajal

The metamorphic sole outcrop at Al Ajal (figure 3.1) forms a thin (~20 m thick and several km in extent), dismembered and altered thrust sliver detached from the base of the ophiolite and juxtaposed against a lower structural unit (Triassic shelf carbonates of the Mahil limestone formation) by Tertiary extensional movement on the Semail allochthon thrusts, related to the exhumation of the Saih Hatat high pressure terrane. It remains the only noted occurrence of high grade garnet bearing sole metabasites from the trailing, NE margin of the Semail ophiolite (Gnos 1992). The outcrop consists of ~20 m of high grade metabasic amphibolite gneisses, containing garnet and diopside towards the 'top' of the sequence. Lower grade and metasedimentary material is entirely absent but may well be present beneath wadi gravels. The Al Ajal amphibolites are heavily altered, with very little fresh garnet

(pseudomorphed by aggregates of chlorite and magnetite, figure 3.18c) and plagioclase grains present.

3.2.4 Asjudi

In many areas of the central Oman mountains, the metamorphic sole amphibolites and greenschists along the base of the Semail ophiolite are present, but the original structural sequence has been disrupted by strong shearing associated with emplacement. Intact sequences do occur, notably along the NE margin of the Hawasina Window (Searle & Cooper 1986) where a similar section to the Sumeini area is present.

A thick mélange zone containing blocks of amphibolite and greenschist sole components encased within a serpentinite matrix mark the base of the ophiolite and few primary structural features are preserved. The serpentinised harzburgites acted as a ductile detachment horizon on which the ophiolite was emplaced, breaking up and incorporating the sole beneath.

The metamorphic sole outcrops of the Asjudi area (figure 3.1, 3.11) of northern Oman form variably oriented steep sided peaks within a low relief serpentinite terrane (figure 3.12). Few primary tectonic contacts are preserved, absolute tectonostratigraphic depths below the Semail thrust cannot be reliably estimated, and no garnet bearing mafic gneisses were sampled. However, sample OM 71 (figure 3.18f), found as a wadi boulder at the base one of the major amphibolite blocks, contains fresh plagioclase, enstatite and diopside with a well developed granoblastic texture, and may represent a relict sole two pyroxene sole assemblage from the base of the Semail ophiolite. Jamieson (1981, 1986) noted the presence of similar, relict, coarsely granoblastic two pyroxene granulites preserved in low strain zones of the upper sole of the St Anthony ophiolite complex, Newfoundland.

3.2.5 Asimah

The metamorphic sole beneath the Semail ophiolite is thicker and more widespread in the heavily imbricated and folded Dibba zone and Masafi corridor in the UAE (figure 3.1) than anywhere else beneath the Semail ophiolite. An outcrop width of ~6 km of sub-ophiolite metamorphic rocks has been described (Alleman & Peters 1972; Searle 1980) consisting of normal garnet-diopside amphibolite facies metabasalts and lower grade metasedimentary and volcanic units (mostly metacherts with lesser volumes of metabasic and metacarbonate rocks) which form an open anticlinal structure with an upright fold axial plane that trends N-S.

Intermediate high pressure assemblages (glaucophane and crossite bearing meta-basalts) have been recognised in the Dibba zone although the garnet-diopside amphibolites appear to be very similar to the sole rocks elsewhere in Oman (Searle 1980; Searle & Malpas 1980,1982). However, the unique presence of kyanite bearing metabasaltic amphibolites from the Asimah-Masafi sole has recently enabled peak pressures of 11 $\pm$ 2 kbar to be estimated (Gnos 1998). True pelitic horizons intercalated within metacherts and amphibolites in the Asimah area are also unique.

A sketch geological map of the southern part of the Asimah area, showing the location of the sampled sole materials, is presented in figure 3.13.

3.3 GEOCHEMISTRY OF VOLCANIC ROCKS IN THE OMAN REGION

The Semail ophiolite allochthon contains a wide variety of basaltic volcanic material, ranging from abundant Permian to Cretaceous extrusive volcanism in the pelagic and carbonate shelf sediments of the Hawasina basin and in the arc-trench fill complex of the Haybi thrust sheet beneath the ophiolite, to the unaltered late Cretaceous volcanic stratigraphy of the ophiolite itself. The tectonically distinct Masirah ophiolite of SE Oman also contains oceanic crustal material of MORB affinity but is ~40 Ma older than the Semail ophiolite (Smewing et al. 1991; Peters et al. 1996; Immenhauser 1996). All these regionally associated mafic volcanics are possible precursors to the HT metamorphic sole amphibolites. Any tectonic model of the subduction-obduction mechanism process in the Oman mountains must consider the geochemistry, origin, age and provenance of the variously metamorphosed volcanic rocks in the ophiolite metamorphic sole outcrops and the identification of the origin of these metavolcanics enables the nature and precise tectonic configuration of the obduction process to be constrained.

Clearly post magmatic bulk chemical changes during metamorphism can alter rock compositions, hindering clear correlation between structural units and any interpretations of the original tectonic environment of formation of the volcanic rocks. Bulk chemical changes can occur by reaction with sea water during hydrothermal (seafloor) metamorphism and during other tectonic or metamorphic events which may promote chemical exchange with other rock compositions. The LILE (Sr, K, Rb, Ba, Th) are readily mobilised in fluids during alteration and any tectonic conclusions drawn from methods using these elements is subject to error when altered rocks are examined. It is generally reasonable to assume that the HFSE (Zr, Nb, Y, Hf etc) and REE (Ce, Sm, Nd etc) are immobile up to amphibolite facies conditions, although in a subduction environment, some HFSE (Ce, Sm) can become mobile (Pearce 1983). New major and trace element analyses of metamorphic sole metabasalts from the Semail ophiolite are shown in tables 3.1 and 3.2.

3.3.1 Hawasina basin volcanic units

Volcanic mafic to acidic sills are fairly abundant within the Permian to Cretaceous marine sediments of the autochthonous and allochthonous units of the Oman mountains, both in the shelf carbonates of the Hajar supergroup and the pelagic sediments of the Hawasina thrust sheet. These units are widely exposed in the unmetamorphosed Hawasina window and Hamrat Duru range, and also in the Saih Hatat HP metamorphic terrane, where the volcanic rocks exhibit metamorphic assemblages characteristic of greenschist, blueschist and eclogite facies (eg El-Shazly et al. 1994). Permian extrusive rocks in the Hamrat Duru pelagic basin and Hajar Supergroup range from tholeiitic dolerites through transitional and alkaline basalts to rhyolitic tuffs. Abundant Triassic volcanism exhibits a clear magmatic evolution, with alkali basalts, phonolites and trachytes at the base of the Triassic overlain by transitional to tholeiitic basalts. This magmatic evolution has been interpreted as recording progressive extension and attenuation of the Arabian continental passive margin and resulting in the development of true oceanic crust (Neo-Tethys) in the late Triassic (Béchennec et al. 1991). Similar Triassic volcanics are also found in the Haybi complex. Volcanic material is rare in the upper Jurassic and Cretaceous components of the Hawasina basin and is dominated by massive and pillowed tholeiitic basalts.

3.3.2 Haybi volcanic sequence

The Haybi volcanic sequence (Searle 1980) is present throughout the Oman mountains and forms part of a distinct thrust sheet beneath the metamorphic sole. It comprises a sedimentary mélange containing abundant Triassic limestone blocks underlain by volcanic rocks with an alkaline basaltic basal sequence, dominated by pyroclastic material, overlain by transitional and tholeiitic basaltic lavas (Searle et al. 1980). Alkaline ultramafic (jacupirangites to biotite wehrlites) sills intrude all lithologies (Searle 1984). The volcanics are associated with Triassic reefal limestones at the base and a Cenomanian-Turonian sedimentary mélange at the top of the sequence. These biostratigraphic ages are confirmed by K/Ar and $^{40}Ar/^{39}Ar$ dating (Lippard & Rex 1982; Hacker et al. 1996) which date the alkaline volcanics at ~220 Ma and the upper tholeiitic units at ~92 Ma. Numerous authors (Searle 1980; Searle & Malpas 1980, 1982; Pearce et al. 1981) have interpreted the volcanic stratigraphy of the Haybi sequence as reflecting within plate oceanic island sequences associated with the development of rifting and extension in the Arabian continental passive margin and the formation of attenuated transitional and eventually true oceanic crust over the Triassic to Jurassic. Spider

diagrams for Haybi volcanic basalts from Searle & Malpas (1980, 1982) are presented in figure 3.14b.

3.3.3 Semail ophiolite volcanic sequence

The upper part of the Semail ophiolite consists of up to 2 km of pillow lavas that in northern Oman form a distinct volcanic stratigraphy (Pearce et al. 1981; Alabaster et al. 1982). The lowest (Geotimes) unit directly overlies the sheeted dyke complex and comprises clinopyroxene and plagioclase-phyric basalts, slightly depleted relative to MORB. It is generally accepted that the Geotimes unit represents spreading axis volcanism. The overlying Lasail unit consists of discrete volcanic centres forming a ~500 m fractionation sequence evolving from basalts through andesites to dacites and rhyolites, which are strongly depleted relative to MORB and have been interpreted as immature island arc tholeiites, erupted at discrete volcanic centres or seamounts above an intra oceanic arc (Pearce et al. 1981). The overlying and intercalated Alley unit contains highly depleted clinopyroxene phyric basalts, representing the rifting phase in the development of the volcanic arc. The volcanic stratigraphy of the Semail ophiolite is completed by ~100 m of mildly alkaline transitional within-plate basalts (Salahi unit) erupted off-axis, probably along small fissures. The Salahi volcanics are enriched in LILE (figure 3.14a) and represent late 'syn-collision' products of the enrichment of the sub-arc mantle by subducted arc derived crustal material (Pearce et al. 1981).

3.3.4 Masirah ophiolite volcanics

The Masirah island ophiolite of SE Oman is now generally accepted as being tectonically distinct from the Semail ophiolite. It consists of a thin mantle and crustal section of MORB tholeiites of Neo-Tethyan origin which have been dated, both by radiometric and biostratigraphic techniques, at ~145-150 Ma (Smewing et al. 1991; Peters et al. 1996; Immenhauser 1996). At higher stratigraphic levels in the Masirah ophiolite, extensive alkaline basaltic to rhyolitic flows, dated at 123 ± 2 Ma (U-Pb; Nagler & Frei 1994) occur intercalated with Barremian pelagic sediments. These have a distinctive geochemistry, as well as a similar morphology to the Lasail sequence of the Semail crustal section, suggesting that they also formed as discrete seamounts on older oceanic crust. The development of these alkaline volcanic piles in existing MORB oceanic crust has been taken to indicate the passage of the proto-Masirah ophiolite close to a mantle plume during the early Cretaceous (Meyer et al.

1996). Spider diagrams normalised to Masirah ophiolite basalts (Meyer et al. 1996) are presented in figure 3.18.

3.4 GEOCHEMISTRY OF THE METAMORPHIC SOLE AMPHIBOLITES

3.4.1 Northern Oman & UAE

The ophiolite metamorphic sole attains its widest extent in the Khawr Fakkan block of the ophiolite, in the UAE. Normal garnet-diopside amphibolite facies metavolcanics and lower grade metasedimentary and volcanic units (mostly metacherts with lesser volumes of alkaline basaltic and carbonatitic rocks), occur in the heavily imbricated and folded Dibba zone and Masafi corridor, where an outcrop width of ~6 km of sub-ophiolite metamorphic rocks has been described (Alleman & Peters 1972; Searle 1980). In the Bani Hamid area a sequence of wholly granulite facies rocks with an apparent structural thickness of ~1 km occurs in a different structural position to the Asimah sole. Field mapping suggests that this imbricated sequence was exhumed along a major out of sequence thrust that repeats the entire ophiolite mantle sequence of the Khawr Fakkan block (Searle & Cox 1999). The rocks all exhibit granulite facies assemblages, and the steep inverted metamorphic gradient seen in the classic metamorphic sole is absent. The presence of abundant alkaline mafic granulites and alkaline ultramafic (apatite rich glimmerites) xenoliths in greenschist to granulite facies meta-carbonatites is common to the Bani Hamid and Asimah metamorphic sole terranes and suggests that they had the same protoliths (Cox et al. 1999). Normal garnet-diopside amphibolite facies metavolcanics from the Asimah terrane have flat MORB normalised trace element patterns (figure 3.18c, d), with limited enrichment of LILE, similar to tholeiitic sole amphibolites from sole locations in the southern Oman mountains, and distinct from the LILE enriched upper units of the Semail ophiolite volcanic sequence.

3.4.2 Southern & central Oman

The geochemistry of the numerous ‘classic’ metamorphic sole outcrops in the central and southern Oman mountains is well described by Searle (1980) and Searle & Malpas (1980, 1982). These sole localities (Wadi Tayin, Wadi Hawasina, Sumeini, Asjudi, Haybi) commonly form a discrete, highly sheared, thrust sheet typically ~200 m thick and exhibit a steep inverted thermal gradient from garnet-diopside bearing tholeiitic (olivine or nepheline

Sample:	OM 63	OM 71	detection limits (ppm)
	Sole Metabasites		
Major Elements (Wt %)			
SiO_2	44.47	50.32	500
TiO_2	2.13	0.07	50
Al_2O_3	13.24	10.73	500
Fe (total)	16.30	9.96	50
MnO	0.25	0.19	50
MgO	7.69	16.66	300
CaO	11.83	11.64	100
Na_2O	2.22	0.17	400
K_20	0.34	0.01	100
P_2O_5	0.22	0.01	100
H_20 etc	1.28	0.02	-
Total	99.96	99.79	-
Trace Elements (ppm)			
Rb	4.4	0.3	2.0
Sr	120	36	2.0
Y	45.9	2	2.0
Zr	125	3	2.0
Nb	12	1.4	1.5
Ba	100	10	12.0
Pb	3	1	5.0
Th	2	0	4.0
U	2	1	3.0
Sc	53	64	5.0
V	451	239	5.0
Cr	201	1092	4.0
Co	59	79	2.0
Ni	105	188	3.0
Cu	146	4	3.0
Zn	122	42	3.0
Ga	17	8	3.0
Mo	0	0	2.0
As	0	0	5.0
S	1189	30	50.0

Sample:	OM 63	OM 71
	Sole Metabasites	
CIPW Norms (Wt%)		
Q	-	-
Or	2.01	0.06
Ab	15.81	1.44
An	25.15	28.47
C	-	-
Ac	-	-
Ne	1.60	-
SMS	-	-
Di	26.64	23.45
Ol	19.44	1.90
Wo	-	-
Hy	-	42.04
Mt	3.55	2.17
Il	4.05	0.13
Ap	0.48	-
Total	98.73	99.66
Mineralogy (Vol%)		
Di	15	45
En	-	25
Pl	25	30
Hbl	50	-
Grt	10	-
Other	-	-

Table 3.1 Major and trace element geochemistry of the metamorphic sole metabasites analysed.
Table 3.2 Modal mineral assemblages and CIPW norms of the metamorphic sole metabasites analysed.
OM 63 was from the Sumeini sole sequence shown in figure 3.8 and OM 71 was from the Asjudi area, found as a wadi boulder.

normative; Searle 1980; Stössel & Zeigler 1985) basalts downwards to a variety of greenschist facies metasediments, mainly quartzites and marbles, with subordinate volcaniclastic and carbonate units. Metabasalts with alkaline affinities are largely absent, and while variations in metamorphic assemblage may in part be due to differences in protolith bulk chemistry, published analyses of metabasalts from these localities clearly represent MORB tholeiites (Searle & Malpas 1980, 1982; Ghent & Stout 1981). Normal garnet-diopside amphibolite facies metavolcanics from the Wadi Tayin and Sumeini terranes have flat MORB normalised trace element patterns (figure 3.18c,d), with limited enrichment of LILE, which is not compatible with their protoliths being from the Semail ophiolite crustal sequence as required by the MOR model for the origin of the ophiolite.

New major and trace element analyses for Semail ophiolite metamorphic sole metabasites are used to complement existing data from Searle & Malpas (1980, 1982) and Zeigler et al. (1991b) and are presented in tables 3.1 and 3.2.

3.5 PROTOLITHS OF THE METAMORPHIC SOLE AMPHIBOLITES

Metamorphic sole terranes in the Khawr Fakkan block in the UAE uniquely contain alkali basaltic and associated carbonatites and alkali ultramafic xenoliths intercalated with metasediments. The Asimah (greenschist) and Bani Hamid (granulite) terranes have been convincingly correlated with the alkaline volcanic successions of the Haybi complex (derived from the Triassic rifting related volcanism of the Hawasina basin) through isotopic and geochemical work on the Asimah metavolcanic sequence (Zeigler et al. 1991).

Reconstruction of the tectonic environment in which the Haybi volcanics and the associated Hawasina sediments were formed (Béchennec et al. 1987; Cooper 1988), on the basis of volcanic geochemistry, sedimentary facies and biostratigraphy, suggests that the 'Hawasina basin' was underlain by rifting, attenuated continental to transitional oceanic crust margin crust.

Since the Haybi thrust sheet represents the oceanic arc trench fill formed during the intra-oceanic subduction that accompanied the obduction of the Semail ophiolite, the age and nature of the volcanic and sedimentary material preserved in such a tectonic environment will therefore correlate closely with the material subducted beneath the intra-oceanic arc and subsequently preserved as the Semail ophiolite metamorphic sole.

The majority of the Semail ophiolite metamorphic sole metavolcanic material exposed in the classic outcrops is clearly of E and N type MORB origin (figure 3.15-17). The source of these tholeiites preserved in the classic metamorphic sole localities of the southern and central Oman mountains is less clear. Tholeiitic extrusive rocks are uncommon within the Hawasina

basin, and are largely restricted to the Permian (pre-rifting). However, Béchennec et al. (1991) noted the presence of late Triassic to late Jurassic tholeiites in the most distal facies of the Hawasina basin, which may be equivalent to the Jurassic Neo-Tethyan oceanic crust preserved in the Masirah ophiolite.

Figures 3.15-17 show analyses from all the described metabasites plotted on a variety of widely used and accepted ternary basalt discrimination diagrams. The Sumeini, Asimah tholeiitic and Wadi Tayin sole amphibolites are typically classified as MORB (N or E type) or IATs and correlate most closely with Masirah MORB crust. The (?) two pyroxene granulite from Asjudi (OM 71) does not give a consistent result between different discrimination diagrams but also correlates more closely with the sole metabasalts than with the ophiolite volcanic sequence basalts.

The sole metabasalts have very similar trace element profiles to both the tholeiitic components of the Haybi volcanics and the MORB crust of the Masirah ophiolite, which are of late Triassic (~220 Ma; Lippard & Rex 1982; Hacker et al. 1996) to late Jurassic (145-150 Ma; Smewing et al. 1991; Peters et al. 1996; Immenhauser 1996) age respectively and which both represent preserved Neo-Tethyan oceanic crust largely consumed at the NE dipping subduction zone that emplaced the Semail ophiolite in the Cenomanian.

3.6 METAMORPHIC SOLE GEOCHRONOLOGY

Geochronology of metamorphic sole material is a powerful tool in the application of modelling to the subduction-obduction history of the Semail ophiolite. Existing geochronology has been largely in the $^{40}Ar/^{39}Ar$ and K-Ar system, particularly using hornblende. Many ages from Semail ophiolite metamorphic sole amphibolites have been determined (Alleman & Peters 1972; Lanphere et al. 1981; Lippard et al. 1986; Montigny et al. 1988; Gnos & Peters 1993; Hacker et al. 1996) with results ranging from 101 to 89 Ma and clustering around 98 Ma, and therefore apparently predating the formation of the Semail crust.

The geochronology of many of these published ophiolitic metamorphic sole ages is however too imprecise to accurately enable measurement of the time interval between the igneous crystallisation of the ophiolite and the initiation of intra-oceanic thrusting, marked by the formation of the metamorphic sole, with 2σ errors typically >6 Ma (Hacker et al. 1996) – greater than the difference between the mean age of sole metamorphism measured by this data and the accepted age of crystallisation of the ophiolite.

Recent $^{40}Ar/^{39}Ar$ ages of hornblendes from amphibolites in the metamorphic sole have a mean of 94.9 $\pm$ 0.2 Ma in the UAE (Asimah terrane) and a slightly younger mean of 93.5 $\pm$ 0.1 Ma in the Wadi Tayin area of SE Oman (Hacker et al. 1996). The age of the granulite facies

Bani Hamid metamorphic sole sequence relative to the adjacent 'classic' Asimah sole terrane is unclear. A K/Ar hornblende age of 95.3 ± 0.5 Ma (Gnos & Peters 1993) from a Bani Hamid metabasic granulite overlaps the mean hornblende age of 94.9 ± 0.2 Ma for the amphibolite facies metamorphism in the Asimah area (Hacker et al. 1996).

Existing ages of the metamorphic sole metamorphism are restricted to the $^{40}Ar/^{39}Ar$ hornblende system, which dates sole metamorphism to ~94-95 Ma (Hacker et al. 1996). The closure temperature of hornblende in the $^{40}Ar/^{39}Ar$ system is ~550°C, and utilising metamorphic sole cooling rates of ~200°C Ma^{-1} before 93.5 Ma (Hacker et al. 1996), it can be estimated that peak temperatures of ~850°C in the sole would therefore have been attained at ~96 Ma, implying that sole metamorphism, at depths of ~40 km, was synchronous with crystallisation of the ophiolite crustal sequence.

3.7 PETROGRAPHY AND MINERAL CHEMISTRY

3.7.1 Mafic gneisses

3.7.1.1 Hornblende

Amphiboles are a major phase throughout the upper mafic components of the metamorphic sole, forming hornblendites and amphibolites which contain foliation defining brown to brown-green pleochroic subidiomorphic amphibole grains typically 2-3 mm in size (figure 3.18a) at the Semail thrust although grain size falls to <0.5 mm within ~50 m.

Mineral analyses show a compositional trend with increasing temperature (measured by garnet-clinopyroxene thermometry; figure 3.19-20) and structural height within the sole from edenitic hornblende, through ferroan pargasitic hornblende to ferroan pargasite. The trend produced is roughly parallel to the Tr-Parg join, equivalent to tschermakite and Fe-Mg exchanges. Individual grains are generally compositionally homogeneous, with insignificant core-rim variations.

3.7.1.2 Garnet

The occurrence of garnet in the mafic amphibolite gneisses of the metamorphic sole is restricted to the upper sections of the sole, and its distribution is influenced by protolith bulk composition (Ca content) as well as metamorphic grade. Commonly, garnet is concentrated in

thin horizons within a garnet free hornblendite amphibolite. Garnet forms syn to post kinematic subidiomorphic to poikiloblastic grains up to ~20 mm in size although size attained appears to be independent of paragenesis and distance beneath the Semail thrust.

A typical garnet composition is $Alm_{0.49}Grs_{0.31}Prp_{0.16}Sps_{0.04}$ and garnet is always unzoned, suggesting that the metamorphic peak was above the garnet closure temperature (figure 3.21). Hornblende, diopside, quartz, Fe-Ti oxides and plagioclase are found as inclusions (figure 3.18b). Garnets associated with diopside have slightly higher grossular contents, reflecting the higher CaO contents of diopside bearing amphibolites. Garnet is frequently altered to chlorite and Fe oxide along cracks and in some cases may be completely pseudomorphed by chlorite (figure 3.18c).

3.7.1.3 Clinopyroxene

The clinopyroxene found in the upper part of the metamorphic sole is diopside (Morimoto et al. 1988) and forms pale green unzoned xenomorphic grains up to 5 mm in size (figure 3.18a), and has a typical mean composition of $Ca_{0.86}Mg_{0.68}Fe_{0.28}Al_{0.08}Fe^{3+}_{0.04}Na_{0.05}Mn_{0.01}[Si_{1.91}Al_{0.09}]O_6$. Individual grains are generally compositionally homogeneous. Diopside tends to occur associated with plagioclase within ~40-50 m of the Semail thrust and is absent from hornblendite units in the sole, suggesting that its presence and distribution is a function of bulk chemistry as well as grade. The presence of diopside in garnet free hornblende-plagioclase assemblages may indicate equilibration at peak temperatures of at least 775°C (Spear 1981) in homogeneous bulk compositions but in the field more is probably controlled primarily by protolith Ca abundance.

3.7.1.4 Orthopyroxene

The first described orthopyroxene bearing (true) granulite from the metamorphic sole of the Semail ophiolite is tentatively here reported, from a wadi boulder at the base of a high grade sole sequence in the Asjudi sole locality in the northern Oman mountains. The orthopyroxene forms part of a coarse grained granoblastic gneiss, and is an enstatite with a mean composition of $Mg_{1.43}Fe_{0.46}Ca_{0.04}Al_{0.03}Fe^{3+}_{0.02}Mn_{0.01}[Si_{1.96}Al_{0.04}]O_6$. It forms fresh idiomorphic grains, producing a granoblastic rock texture, with a pale green to pink pleochroic scheme and a typical size of 0.5-1 mm (figure 3.18f), coexisting with unaltered plagioclase and diopside.

3.7.1.5 Plagioclase

Plagioclase in the mafic amphibolite gneisses is largely altered and replaced by a combination of epidote group minerals and sericite (figure 3.18a). Albite (An_{5-10}) is common as part of a greenschist facies retrograde assemblage. Rare unaltered plagioclase has a typical composition of An_{50-60} in garnet free assemblages (Searle 1980; Ghent & Stout 1981) and An_{20-30} in garnet bearing sole assemblages and has enabled the determination of accurate metamorphic sole PT estimates.

3.7.2 Metasediments and carbonates

Metasedimentary material is rare in the highest parts of the Semail ophiolite metamorphic sole and is generally restricted to thin discontinuous lenses and pods of calc silicates and marbles intercalated with garnet and/or diopside bearing amphibolites. Coherent units of piemontite-muscovite quartzites are present in the sole outcrops and are most well developed in the Wadi Tayin, Sumeini and Asimah areas.

Small metre scale pods and lenses of carbonate material are rare but widespread in the upper parts of the Semail ophiolite metamorphic sole, and are most abundant in the Sumeini area (Searle 1980). Typical assemblages include Ca garnet and diopside (figure 3.18c) in a calcite-dolomite matrix. The structural relationships of these units and their relationship to the surrounding metavolcanic material suggest that they are derived from sedimentary material intercalated with subducted extrusive volcanics.

Mn garnet-piemontite-muscovite bearing metacherts (figure 3.5) are abundant throughout the metamorphic sole, although the limited abundance of true pelitic assemblages has been a major problem in the elucidation of the PT evolution of the sole (Searle & Malpas 1980; Ghent & Stout 1981; Gnos 1998). Rare, thin (typically ~1 m) and strongly sheared, often protomylonitic true pelite layers within amphibolite facies metacherts and carbonates have been found in the Asimah area (figure 3.1, 3.13) and commonly contain the assemblage quartz-plagioclase(~An_{28})-hornblende-garnet-biotite ± clinozoisite (figure 3.18e). The sampled metapelite layer occurs approximately ~100 m structurally below the Semail thrust with no obvious brittle imbricate structures in between. The mineral chemistry of hornblende, biotite, plagioclase and garnet (table 3.7) grains from sample OM 131 used to compute THERMOCALC activities is summarized in (figure 3.22-25) and the results of PT calculations using THERMOCALC presented in table 3.8.

3.8 PT EVOLUTION AND PROFILES

3.8.1 Previous estimates

Peak temperatures within the metamorphic sole have previously been well constrained at ~775-875ºC using garnet-clinopyroxene exchange thermometry (Searle & Malpas 1980; Ghent & Stout 1981; Hacker & Mosenfelder 1996; Gnos 1998) although peak pressures are less well constrained due to an absence of true pelitic assemblages. Pressure estimates from the mafic amphibolites in Sumeini and Wadi Tayin, based on the jadeite component in diopside (Searle & Malpas 1980; Ghent & Stout 1981) were imprecise due to the high Fe^{3+} levels in diopside, coupled with the absence of quartz and unaltered plagioclase. Thermobarometry and structural considerations indicate minimum pressures of ~5 kbar at Wadi Tayin (Ghent & Stout 1981). However, the presence of kyanite and quartz in metabasaltic amphibolites from the Asimah-Masafi sole in the UAE has recently enabled higher peak pressures of 11 $\pm$ 2 kbar to be estimated (Gnos 1998) which imply the attainment of greater depths of burial beneath the obducting Semail ophiolite than demanded by the preserved structural thickness of the ophiolite, which is <20 km.

An independent measure of the peak pressure and temperature conditions attained within the metamorphic sole can be obtained from thermobarometry of recrystallised mantle sequence harzburgite mineral grains found in the basal 'banded ultramafic unit' (figure 3.2a,b) (Searle 1980) of the Semail ophiolite. The presence of diopside in basaltic garnet free amphibole-plagioclase assemblages indicates equilibration at peak temperatures of at least 775°C (Spear 1981). Browning (1982) used the experimental data and single pyroxene thermobarometric calibration of Mercier (1980) to suggest clinopyroxene recrystallisation conditions of 844-906ºC and 5-11.8 kbar in harzburgitic mylonites from the base of the Hayalyn block of the ophiolite, which overlaps the recent higher suggested pressures for the metamorphic sole.

Numerous authors (eg Hacker 1990; Hacker 1991; Hacker & Mosenfelder 1996) have calculated (inverted) exponential metamorphic temperature gradients of up to 4000ºC km^{-1} within the upper metamorphic sole of the Semail ophiolite, orders of magnitude larger than those suggested by conventional thermal modelling of subduction zones. As already noted, these estimates have little real value since they assume structural and metamorphic coherence and continuity throughout the metamorphic sole, which is demonstrably incorrect.

3.8.2 New PT estimates from the Semail ophiolite metamorphic sole

New PT determinations from a variety of metamorphic sole localities and tectonostratigraphic horizons are presented here, and have been derived using a variety of geothermometers, geobarometers, and the DOS program THERMOCALC (v 2.75), based on the internally consistent thermodynamic dataset of Holland & Powell (1998). Typical analyses used in PT determinations from a variety of sole outcrops sampled are presented in table 3.4.

The classic approach to the estimation of pressure conditions in garnet amphibolites is to use a garnet-quartz-plagioclase-hornblende barometer (Kohn & Spear 1990), or a garnet-quartz-plagioclase-diopside barometer (Moecher et al. 1988). The former uses the equilibrium:

$$6\ An + 3\ Tr = 2\ Grs + Pyp + 3\ Tsch + 6\ Qtz$$

and its Fe end member equivalent coupled with the anorthite activity model of Hodges & Royden (1984), the garnet component activity model of Hodges & Spear (1982), and the amphibole activity model of Kohn & Spear (1989). Similar results are obtained using the garnet-quartz-plagioclase-diopside barometer (Moecher et al. 1988). The results obtained are shown in table 3.3; typical errors are quoted as ± 0.5 kbar.

Table 3.3 Results of Kohn & Spear (1990) grt-hbl-pl-qtz barometry.

Sole location	Sumeini	Wadi Tayin	Asimah
Sample	OM 56-63	OM 29	OM 129
Powell (1985) temperature	838	839	868
Pressure (Mg) kbar	11.82	12.85	11.85
Pressure (Fe) kbar	12.72	13.92	11.85

The ophiolite metamorphic sole was formed at peak conditions of 840-870°C and 11.8-13.9 kbar using these conventional thermobarometers. The similarity in peak conditions in widely dispersed metamorphic sole localities suggests that similar subophiolitic subduction zone conditions were widespread during the formation of the metamorphic sole. These results are also comparable with the recent results of Gnos (1998), who computed peak sole conditions of 800 ± 100°C and 11 ± 2 kbar.

Table 3.4 Microprobe mineral analyses used in PT calculations (na, not analysed).

Sample	OM 143				OM 144				OM 129				OM 56 etc				OM 29			
Location	Al Ajal				Al Ajal				Asimah				Sumeini				Wadi Tayin			
Mineral (wt%)	Grt	Di	Amph	Plag	Grt	Di	Amph	Plag	Grt	Di	Amph	Plag	Grt	Di	Amph	Plag	Grt	Di	Amph	Plag
SiO_2	37.42	49.51	42.38	57.44	38.09	49.41	43.96	57.01	38.39	49.60	41.45	60.13	38.49	49.03	42.65	57.35	38.77	49.77	41.28	57.35
TiO_2	0.15	0.55	1.81	na	0.14	0.43	1.54	na	0.14	0.28	1.53	na	0.12	0.48	1.79	na	0.21	0.44	1.63	Na
Al_2O_3	19.76	4.65	12.43	26.57	20.67	4.08	10.93	25.70	20.47	4.15	12.70	24.81	20.67	4.59	11.57	26.23	21.02	4.31	13.40	26.23
Cr_2O_3	Na	Na	na	na	na	na	na	na	na	na	na	na	na	na	na	na	na	na	na	Na
Fe_2O_3	Na	Na	na	1.06	na	na	na	0.33	na	na	na	0.03	1.67	1.79	3.29	0.36	1.67	2.51	4.14	0.36
MnO	2.45	0.27	0.29	na	2.51	0.31	0.24	na	1.99	0.30	8.26	na	24.02	9.91	12.75	na	22.44	10.53	12.98	Na
FeO	23.51	9.99	14.63	na	22.36	10.37	14.82	na	23.84	11.53	0.25	na	1.63	0.27	0.17	na	1.68	0.31	0.21	Na
MgO	2.93	10.62	10.76	na	4.48	10.68	11.01	na	4.49	9.84	19.38	na	5.08	10.63	10.22	na	3.09	9.60	9.41	Na
CaO	12.70	21.70	11.28	2.15	10.98	21.91	11.52	5.71	9.73	20.56	11.50	6.85	8.72	20.65	11.28	6.76	13.19	21.65	10.88	6.76
Na_2O	Na	0.83	2.15	5.71	na	0.97	1.95	6.34	0.00	0.94	1.87	7.48	0.03	0.73	1.81	6.32	na	0.91	1.76	6.32
K_2O	Na	Na	0.18	4.65	na	na	0.18	1.89	0.01	na	0.61	0.17	0.03	0.02	0.47	1.39	na	na	1.24	1.39
Total	98.91	98.12	95.91	97.58	99.22	98.16	96.15	96.99	99.05	97.20	97.53	99.47	100.47	98.10	96.00	98.41	102.08	100.03	96.94	98.41
Oxygens	12	6	23	8	12	6	23	8	12	6	23	8	12	6	23	8	12	6	23	8
Si	2.977	1.892	6.346	2.643	2.992	1.887	6.565	2.631	3.029	1.924	6.249	2.689	2.998	1.884	6.439	2.611	2.985	1.889	6.222	2.611
Ti	0.009	0.016	0.204	na	0.008	0.012	0.173	na	0.008	0.008	0.172	na	0.007	0.014	0.203	na	0.012	0.013	0.185	Na
Al	1.853	0.209	2.194	1.441	1.914	0.184	1.924	1.399	1.904	0.190	2.243	1.308	1.898	0.208	2.059	1.408	1.908	0.193	2.381	1.408
Cr	Na	Na	na	na	na	na	na	na	na	na	0	Na	na	na	na	na	na	na	na	Na
Fe^3	0.173	0.037	0.400	0.037	0.084	0.090	0.328	0.012	0.021	0.017	0.525	0.001	0.098	0.052	0.373	0.012	0.097	0.072	0.470	0.012
Fe^2	1.391	0.283	1.432	na	1.385	0.241	1.523	na	1.552	0.357	1.937	Na	1.565	0.319	1.610	na	1.445	0.334	1.637	Na
Mn	0.165	0.009	0.037	na	0.167	0.010	0.030	na	0.133	0.010	0.032	Na	0.108	0.009	0.022	na	0.110	0.010	0.027	Na
Mg	0.347	0.605	2.401	na	0.524	0.608	2.450	na	0.528	0.569	1.861	Na	0.590	0.609	2.300	na	0.355	0.543	2.114	Na
Ca	1.084	0.889	1.810	0.106	0.925	0.896	1.843	0.282	0.823	0.855	1.842	0.328	0.728	0.850	1.825	0.330	1.089	0.880	1.757	0.330
Na	Na	0.062	0.624	0.509	na	0.072	0.565	0.567	na	0.071	0.546	0.649	0.005	0.054	0.530	0.558	na	0.067	0.514	0.558
K	Na	Na	0.034	0.273	na	na	0.034	0.111	0.001	na	0.117	0.010	0.003	0.001	0.091	0.081	na	na	0.239	0.081
Sum	8.00	4.00	15.48	5.01	8.00	4.00	15.44	5.00	8.00	4.00	15.52	4.99	8.00	4.00	15.45	5.00	8.00	4.00	15.55	5.00

Table 3.5 presents new THERMOCALC PT determinations from the highest grade parts of the classic metamorphic sole from a variety of outcrops beneath the Semail ophiolite. Using THERMOCALC and the internally consistent thermodynamic dataset of Holland & Powell (1998), the ophiolite metamorphic sole was formed at peak conditions of 840 ± 70°C and 11.6 ± 1.6 kbar, values which correspond closely with both the results obtained on the same samples using conventional thermobarometry (table 3.3) and previously published estimates (Gnos 1998).

Peak temperatures may also be constrained using a variety of calibrations of the Fe^{2+}-Mg exchange thermometer between garnet and clinopyroxene, as well as the garnet-hornblende Fe^{2+}-Mg exchange thermometer of Graham & Powell (1985), and the hornblende-plagioclase thermometer of Holland & Blundy (1994). Results obtained are shown in table 3.6.

Table 3.5 THERMOCALC average PT mode results for metamorphic sole amphibolites.

Location	Wadi Tayin	Sumeini	Al Ajal	Asimah
Sample	OM 29	OM 56	OM 144	OM 129
PT stage	Peak	Peak	Peak	Peak
Rock type	Amphibolite	Amphibolite	Amphibolite	Amphibolite
Peak assemblage (qtz as inclusions)	grt-di-hbl-pl-qtz-H_2O	grt-di-hbl-pl-qtz-H_2O	grt-di-hbl-pl-qtz-H_2O	grt-di-hbl-pl-qtz-H_2O
Average garnet-clinopyroxene T	832°C	826°C	774°C	859°C
Independent reactions	6	6	6	7
Best fit av PT result	835 ± 91°C 12.1 ± 2 kbar	829 ± 61°C 11.1 ± 1.3 kbar	766 ± 69°C 11.5 ± 1.9 kbar	853 ± 66°C 11.5 ± 1.4 kbar
Corr	0.65	0.424	0.721	0.525
Fit	1.35	0.84	1.13	0.83
a_{H2O}	0.75	0.5	0.5	0.35
End members excluded	cats, fact	cats, fact	cats, tr	cats, fact

The garnet-clinopyroxene exchange thermometer calibrations of Ellis & Green (1979), Ai (1994), Krogh (1988) and Powell (1985) all produce consistent results, with the Ellis & Green calibration producing results typically 60°C higher than the lowest calibration (Ai). The Powell (1985) thermometer is perhaps the most rigorous and reliable of these calibrations (Waters 2000 pers. comm.).

Table 3.6 Results of Fe^{2+}-Mg exchange thermometry for metamorphic sole amphibolites at 10 kbar (reference pressure).

Sole location	Sumeini	Wadi Tayin	Asimah	Al Ajal	Asjudi
Sample	OM 56-63	OM 29	OM 129	OM 144	OM 71
Krogh (1988) garnet-clinopyroxene	832	826	867	781	-
Ai (1994) garnet-clinopyroxene	780	787	821	720	-
Ellis & Green (1979) garnet-clinopyroxene	853	874	881	805	-
Powell (1985) garnet-clinopyroxene	838	839	868	789	-
Holland & Blundy (1994) hbl-pl	-	758	747	-	-
Graham & Powell (1984) grt-hbl	746	752	822	732	-
Lindsley (1983) opx-cpx	-	-	-	-	~920
Brey & Kohler (1990) opx-cpx	-	-	-	-	976

The Graham & Powell (1984) garnet-hornblende thermometer yields temperatures typically 40-60°C lower than the garnet-clinopyroxene thermometer average, which may be due to the low X_{Mn} (typically $Sps_{0.04}$) of the analysed garnets (Graham & Powell 1984).

Throughout the highest grade parts of the metabasic metamorphic sole, stromatic (foliation parallel) leucocratic partial melt pods and lenses are found within the amphibolites; a typical monzodioritic to tonalitic assemblage includes coarse grained plagioclase (~An_{30}), quartz, hornblende and biotite with occasional K feldspar. An estimate of the PT conditions at which tonalitic partial melts were extracted may be obtained using the hornblende-plagioclase thermometer of Holland & Blundy (1994) coupled with the Al in hornblende barometer of Anderson & Smith (1995).

Structural and petrographic constraints demand that these leucocratic lenses formed during the prograde evolution of the sole, and they appear to record relict prograde conditions despite the host amphibolite recording much higher peak conditions. New thermobarometry on samples from the Sumeini sole locality is presented in table 3.7 and indicates that tonalitic melts derived from garnet-diopside amphibolites typically formed at 656 ± 17°C and 5.6 ± 0.6 kbar, at lower grades than the metamorphic peak, during the prograde evolution of the sole.

Table 3.7 PT results for metamorphic sole partial melt segregations (analysis from Searle 1980).

Location	Sumeini
Sample	OM 1533
PT stage	Prograde melting
Rock type	Tonalite partial melt
Assemblage	Pl-qtz-hbl-bt-kfs
Hbl-Pl temperature (Holland & Blundy 1994)	656 ± 17°C
Al in hbl pressure (Anderson & Smith 1995)	5.6 ± 0.6

A rare pelite from the Asimah sole locality, intercalated with piemontite-muscovite quartzites approximately ~100 m below the Semail thrust, contains the strongly sheared and deformed peak assemblage quartz-plagioclase(~An_{28})-hornblende-garnet-biotite ± clinozoisite. The mineral chemistry and stoichiometry of the analysed minerals is shown in figure 3.22-25. Fe^{2+}-Mg garnet-biotite exchange thermometry using the calibration of Bhattacharya et al. (1992) yields a result of 642°C.

THERMOCALC in average PT mode, at an a_{H_2O} value of 0.5, yields a peak result of 642 ± 89°C and 7.8 ± 2.7 kbar. The a_{H_2O} value was chosen to obtain good agreement between the exchange thermometry and THERMOCALC temperature estimates.

Table 3.8 Asimah pelite sample (OM 131) mineral analyses used to generate PT data

Mineral	Hornblende	Plagioclase	Garnet	Biotite
SiO_2	42.12	59.52	37.78	35.93
TiO_2	0.57	0.00	0.34	0.72
Al_2O_3	14.85	24.13	20.99	18.96
Cr_2O_3	0.00	0.00	0.00	0.00
Fe_2O_3	5.14	0.29	0.98	2.20
MnO	9.17	0.00	23.16	11.21
FeO	0.48	0.00	6.44	0.29
MgO	10.57	0.00	5.50	12.03
CaO	10.51	5.16	4.68	0.18
Na_2O	1.66	7.22	0.00	0.23
K_2O	0.48	1.09	0.00	4.89
Total	95.55	97.41	99.87	86.65
Oxygens	23.0	8.0	12.0	11.0
Si	6.284	2.717	2.976	2.822
Ti	0.064	0.000	0.020	0.043
Al	2.612	1.299	1.949	1.756
Cr	0.000	0.000	0.000	0.000
Fe^3	0.577	0.010	0.058	0.130
Fe^2	1.144	0.000	1.526	0.736
Mn	0.061	0.000	0.430	0.019
Mg	2.350	0.000	0.646	1.408
Ca	1.680	0.252	0.395	0.015
Na	0.480	0.639	0.000	0.035
K	0.091	0.064	0.000	0.491
Sum	15.343	4.980	8.000	7.455

This pelite occurs approximately 100 m structurally below sample OM 129, with no clear intervening structural breaks. Assuming structural coherence in this sole section, this implies an average inverted temperature gradient of ~2°C m^{-1} and an average inverted pressure gradient of ~3.7 MPa m^{-1}, integrated over the observed section, much greater than would be expected from the structural thickness of the sole. Gnos (1998) calculated similar figures of ~1°C m^{-1} and ~0.3-2 MPa m^{-1} for the Asimah sole using data from Bucher (1990).

Analyses used in THERMOCALC to calculate these PT estimates were obtained by microprobe analysis and are shown in table 3.8, and the results of THERMOCALC PT analysis are presented in table 3.9.

Figure 3.26 is a composite PT evolution diagram for the classic metamorphic sole of the Semail ophiolite, using new PT determinations from this study and $^{40}Ar/^{39}Ar$ ages of the metamorphic peak from Hacker et al. (1996). The inferred sole anticlockwise PT evolution and peak temperatures of 840 ± 70ºC are consistent with an origin in a high geotherm environment derived from the heat of the overlying young and hot Semail ophiolite during intra oceanic

subduction, and is similar in form to paths presented by Jamieson (1986) for the St Anthony complex and to those suggested by modelling (Hacker 1990, 1991).

Table 3.9 THERMOCALC average PT mode results for a metamorphic sole metapelite.

Location	Asimah
Sample	OM 131
PT stage	Peak
Rock type	Pelite
Peak assemblage	Grt-bi-hbl-pl-qtz-H_2O
Average Grt-bt temp	642
Independent reactions	5
Best fit average PT result	642 ± 89°C 7.8 ± 2.7 kbar
Corr	0.609
Fit	2.06
a_{H_2O}	0.5
End members excluded	parg, fact

3.9 DISCUSSION

3.9.1 Experimental evidence

Experimental studies on quartz undersaturated and saturated metabasaltic amphibolites under a variety of H_2O activities (eg Ito & Kennedy 1971; Rapp et al. 1991; Poli 1993; Wyllie & Wolf 1993; Wolf & Wyllie 1994; Patiño Douce & Beard 1995) have demonstrated that garnet is absent below 7 kbar at 800 ± 50°C in the quartz undersaturated system, or below 9 kbar in the quartz saturated system.

3.9.2 Bulk rock composition and mineral assemblages

Experimental evidence suggests that in quartz undersaturated and saturated systems of similar bulk composition to the analysed amphibolites (eg Liu et al.1996), partial melting was common at or before temperatures similar to those attained in the Semail ophiolite sole, a

conclusion which is compatible with the PT estimates of crystallisation of tonalitic partial melts from the sole obtained in this study. Such anatectic processes would remove protolith components (commonly SiO_2 and CaO in quartz and plagioclase) and mean that is it difficult to reconstruct protolith bulk compositions. Since prograde reactions in the metabasic system tend to liberate SiO_2 (Yardley 1989), it is likely that melt extraction from originally SiO_2 saturated tholeiites from the Neo-Tethyan crust preserved in the Haybi tholeiitic and Masirah ophiolite crust produced SiO_2 undersaturated sole amphibolites. Garnet-diopside amphibolites from the Asimah (Stössel & Zeigler 1985) and Sumeini (Searle 1980) sole outcrops are olivine or nepheline normative and this is reflected in the presence of quartz only as rare inclusions within garnet. Calcium and silica rich melts have been produced experimentally as low melt fractions from similar bulk compositions (Wyllie & Wolf 1993; Patiño Douce & Beard 1995).

3.9.3 Mineral forming reactions in sole amphibolites

THERMOCALC uses an internally consistent thermodynamic dataset (Holland & Powell 1998) to generate independent reactions from a set of mineral activity data derived from electron microprobe analyses, and in garnet-diopside amphibolites from the upper parts of the Semail ophiolite metamorphic sole these reactions can include:

1. py + 2gr + 3q = 3di + 3an
2. 2gr + alm + 3q = 3hed + 3an
3. 3tr + 2py + 4gr = 12di + 3ts
4. 6tr + 7gr = 27di + 6an + py + $6H_2O$

At lower grades, prograde reactions consume quartz, amphibole and diopside to produce garnet (Gnos 1998). Experimental data (Lui et al. 1996) suggests that garnet and diopside forming reactions consume epidote group minerals, common at structurally lower levels in metabasic sole sequences, and produce SiO_2 rich melts.

3.9.4 Tectonic implications of sole PT results

Peak metamorphic conditions, averaged over the whole Semail ophiolite outcrop, of 840 ± 70°C and 11.6 ± 1.6 kbar in the metamorphic sole are similar to those reported from the

Mont Albert (Jamieson 1986), Bay of Islands (McCaig 1983) and Palawan (Encarnacion et al. 1995) ophiolites and imply the metamorphism and preservation of Neo-Tethyan oceanic crust that accreted to the hanging wall of the Semail thrust at depths of ~40 km at 94-95 Ma (Hacker et al. 1996). The stratigraphic thickness of the Semail ophiolite is ~20 km (Boudier & Coleman 1981) and the typical structural thickness is only ~5-10 km (Shelton 1984) yielding peak sole pressures of only ~6 kbar if simple overburden is assumed, and early sole pressure estimates (Searle 1980; Ghent & Stout 1981) used such a figure in the absence of clearer results. The discrepancy was discussed by Hacker & Gnos (1997), who suggested three explanations:

1. Another (structurally repeated) 15-20 km thick ophiolitic thrust sheet overlay the present ophiolitic thrust sheet (Nicolas 1989).
2. The ophiolite was a single ~40 km thick sheet and the metamorphic sole has been exhumed by normal faulting and juxtaposed against a thinner ophiolite section.
3. The originally ~40 km thick ophiolite has been thinned to its present thickness during the obduction and emplacement processes.

The geophysical data of Shelton (1984), which constrains the structural thickness of the ophiolite to <10 km along its NE, trailing, edge disproves the first two models, and furthermore there is no evidence in the Semail ophiolite for the burial of the crustal sequence to depths of ~20 km, which would imply the development of greenschist-amphibolite facies assemblages. The presence of late ($^{40}Ar/^{39}Ar$ age of 93.7 ± 0.8 Ma; Hacker et al. 1996) dolerite dykes cutting the Semail thrust in Wadi Tayin suggests that thinning related motion on the thrust was minimal during the early stages of obduction. Thinning of the ophiolite from ~40 km to <15 km, or by ~270%, may have been accommodated using the sequential model proposed by Casey & Dewey (1984), who postulated the 'flattening' of an ophiolite obduction related subduction zone in which the progressive shallowing of subduction zone dip and the associated structural thinning and extension of the obducting ophiolite may account for the presence of metamorphic sole material metamorphosed at pressures of >10 kbar (Jamieson 1981; Gnos 1998; this study) occurring beneath ophiolite complexes <20 km thick.

Furthermore, large scale extensional thinning of the ophiolite during emplacement is consistent with the common excision of the highest grade garnet-diopside amphibolite to granulite sole units, the discontinuous sole outcrop, the discontinuous and variable thickness of the 'banded ultramafic unit' basal mantle sequence mylonites, and the variable structural thickness of the wedge shaped ophiolite itself, which is typically very thin at its leading edge but ~15 km thick at its trailing edge.

Faults and shear zones are abundant throughout the ophiolite mantle sequence, although many are related in part at least to Tertiary thrust culmination and the formation of

tectonic windows beneath the Semail thrust. Displacements along these extensional faults are poorly constrained (Kusky et al. 1998) and such intra-ophiolitic extension does not appear to have greatly disrupted remnant mantle fabrics within the ophiolite (eg Ceuleneer et al. 1988). The difficulty in reconciling this apparent absence of clear internal deformation within the ophiolite with the conflicting evidence that may require major intra-ophiolitic extension to exhume the metamorphic sole suggests that the model can, at best, represent a partial solution until the age, nature and extent of intra-ophiolitic extension can be better constrained.

3.9.5 Exhumation rates of the metamorphic sole

Exhumation rates in the Asimah section of the metamorphic sole may be estimated using a combination of new thermobarometric and structural data with existing geochronological and cooling rate estimates for the northern Semail ophiolite. Peak metamorphism in the Asimah sole has been estimated as occurring at 94.9 ± 0.2 Ma (Hacker et al. 1996) and can be used in conjunction with metamorphic sole cooling rates (~200°C Ma^{-1} before 93.5 Ma, ~90°C Ma^{-1} between 93.5 Ma and 92.6 Ma and ~20°C Ma^{-1} until biotite closure at 89.2 Ma; Hacker et al. 1996) to estimate sole exhumation rates.

Using the Asimah sole cooling rates and ages of Hacker et al. (1996), a 'back extrapolated' peak metamorphic age of ~94 Ma can be estimated for the amphibolite facies metapelite (table 3.6). Pressure contrasts suggest that the sole was exhumed at a rate of ~0.38 GPa Ma^{-1} during this time interval, equivalent to a rate of ~12.5 mm yr^{-1} assuming an ophiolite density of 3.0 g cm^{-3}. This estimate may be regarded as a peak value, and is consistent with peak estimates (>10 mm yr^{-1}) of the exhumation of Indonesian ophiolites (Linthout & Helmers 1994). Exhumation rates of the Semail ophiolite metamorphic sole have been estimated at 3.6-4.5 mm yr^{-1}, integrated over the period 95-90 Ma, when the sole was rapidly cooling, by Gnos (1998).

3.10 SUMMARY

The Semail ophiolite metamorphic sole was formed at peak conditions of 840 ± 70°C and 11.6 ± 1.6 kbar (THERMOCALC) and 840-870°C and 11.8-13.9 kbar (conventional thermobarometry). These conditions suggest temperatures in the hanging wall of the Semail thrust were perhaps ~1000°C at ~40 km depth during intra-oceanic subduction. Timing constraints from peak sole $^{40}Ar/^{39}Ar$ geochronology (Hacker et al. 1996) suggest that the

subducting oceanic crust was at least 50 Ma old, and, in conjunction with ophiolite crustal sequence U-Pb ages (Tilton et al. 1981), are most compatible with an original tectonic configuration characterised by 'thrusting of the ophiolite away from a more easterly ridge' – that is, in a SSZ arc with east directed subduction beneath the proto-ophiolite.

Coupled with an analysis of the geochemistry of the metamorphic sole metabasalts, it is proposed that late Triassic (~220 Ma) to Jurassic Neo-Tethyan MORB crust similar to that preserved in the Masirah ophiolite (~145-150 Ma) best represents the protoliths of the Semail ophiolite metamorphic sole. The identity, nature, origin and age of the oceanic crustal material forming part of the transitional crust subducted beneath the intra oceanic arc that initiated obduction is fundamental to any tectonic model of the subduction-obduction and emplacement process. The available evidence, such as the presence of volcanic units with subduction derived arc geochemistry at the top of the Semail crustal sequence, the coincident timing of ophiolite crustal sequence formation and subduction to depths of ~40 km beneath the ophiolite, the intrusion of granitic material derived from the anatexis of subducted arc sediments into the base of the preserved mantle wedge (*Chapter Six*), the restoration of the allochthonous thrust sheets and the lack of geochemical correlation (figures 3.14-17) between the ophiolite volcanics and the metavolcanics of the metamorphic sole, suggests that the Semail ophiolite represents a relict obducted SSZ oceanic crust and sub-arc mantle section (Searle & Cox 1999; Cox et al. 1999).

The occurrence of possibly the first reported two pyroxene sole metabasite from the Semail ophiolite, although found as a wadi boulder, may record peak metamorphic temperatures of >900°C and exhibits an undeformed granoblastic texture characteristic of recrystallisation in a static environment and trace element patterns consistent with derivation from the subducted Neo-Tethyan MORB crust rather than the Semail ophiolite itself. Jamieson (1986) recorded the presence of analogous rare residual two pyroxene assemblages in sole metabasites from the St Anthony complex, Newfoundland, preserved in low strain zones and surrounded by recrystallised amphibolite assemblages.

Significant contrasts of ~65°C between garnet-clinopyroxene exchange metamorphic temperature peaks measured between the leading and trailing edge metamorphic sole outcrops beneath the ophiolite of 839°C (leading edge average value from Asimah, Sumeini and Wadi Tayin outcrops) and 774°C (trailing edge average value from Al Ajal) match the prediction made by Hacker (1991) on the basis of thermal modelling of the evolution of the Semail ophiolite metamorphic sole.

Calculated PT evolution paths (figure 3.26) for the Semail ophiolite sole have a similar anticlockwise form to those suggested by thermomechanical modelling of subduction zone conditions (Hacker 1990, 1991) and new PT determinations from the Asimah sole section in the UAE have been used to calculate an average sole inverted temperature gradient of ~2°C m^{-1} and an average inverted pressure gradient of ~3.7 MPa m^{-1}, assuming structural coherence in

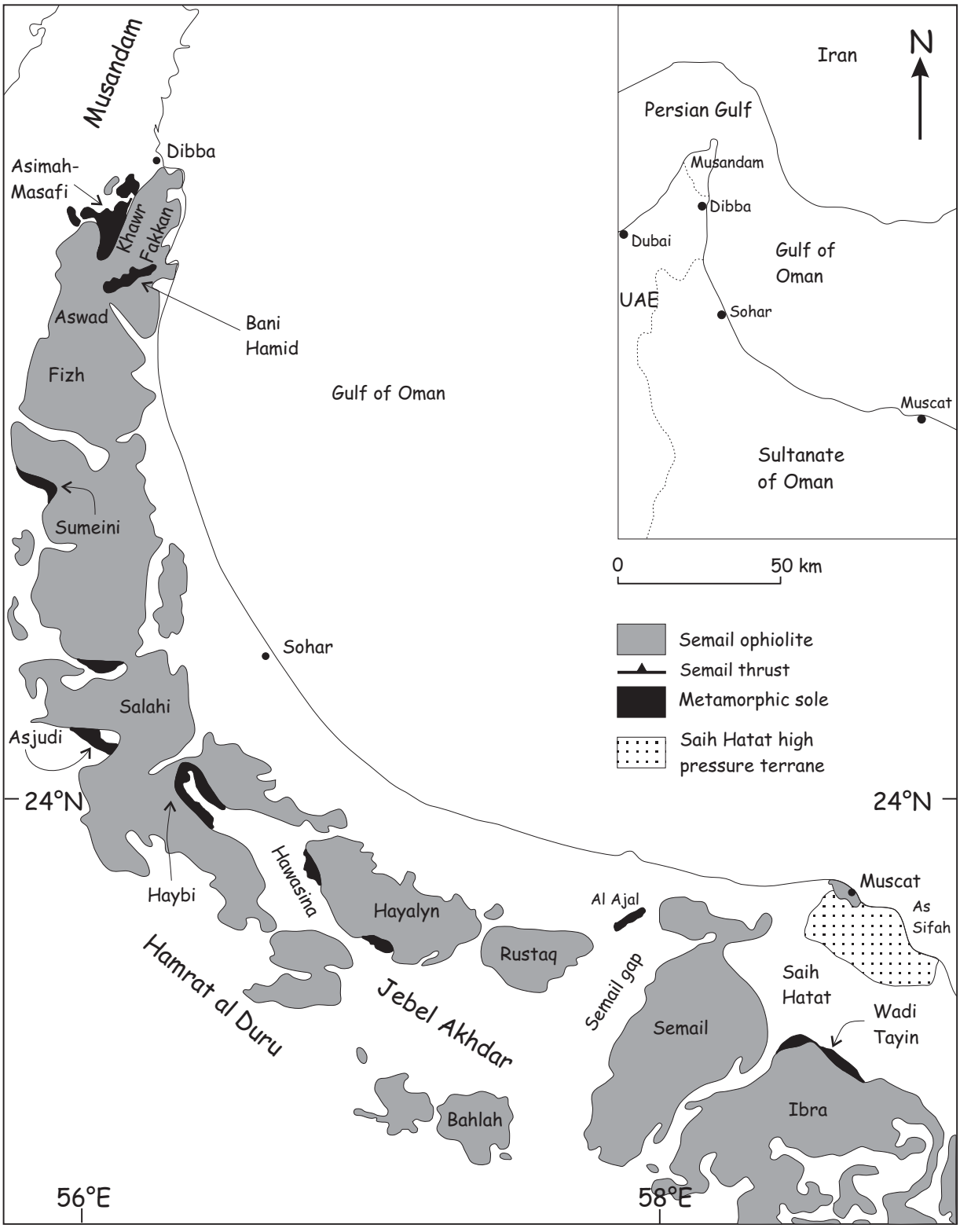


Figure 3.1 Geological sketch map of the Oman mountains, showing the distribution of the major metamorphic sole outcrops beneath the Semail ophiolite that are described in the text. Note that sole outcrops occur beneath both the leading and trailing edges of the SW thrusted ophiolite, as well as in tectonic windows eroded through the centre of the ophiolite. After Glennie et al. (1974), Searle & Malpas (1980) and Cox et al. (1999).



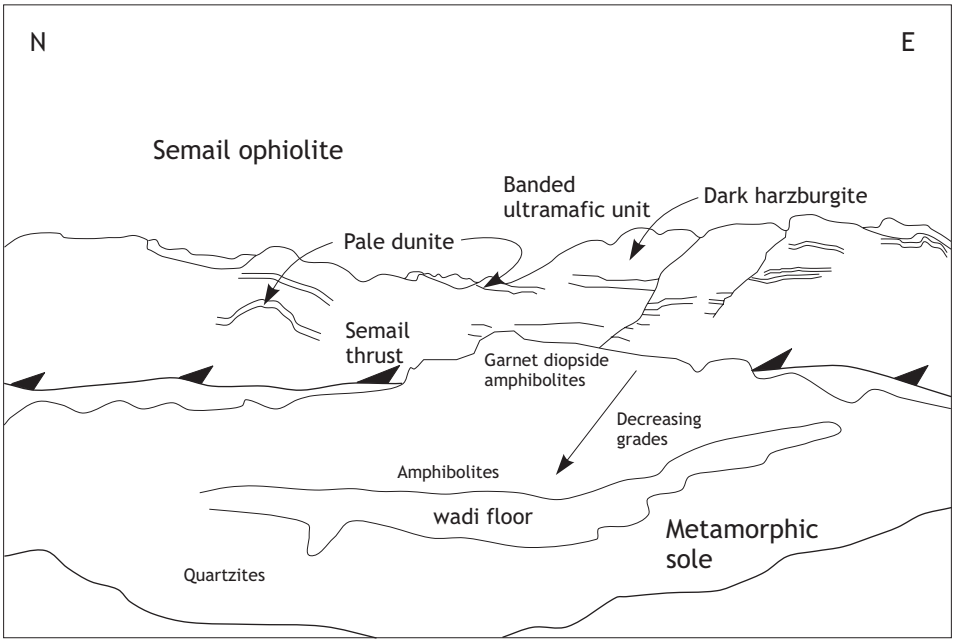


Figure 3.2a,b View and annotated sketch of the basal banded ultramafic unit and metamorphic sole of the Semail ophiolite, in the NE sector of the Sumeini area, northern Oman. The ultramafic mylonites of the mantle sequence 'banded ultramafic unit' (Searle 1980) are banded on a 10 cm to 10 m scale, with pale serpentinised dunite and dark harzburgite bands thrust over the ophiolite metamorphic sole by the Semail thrust. The metamorphic sole decreases in grade with structural depth beneath the ophiolite and is up to ~300 m thick in the Sumeini area.

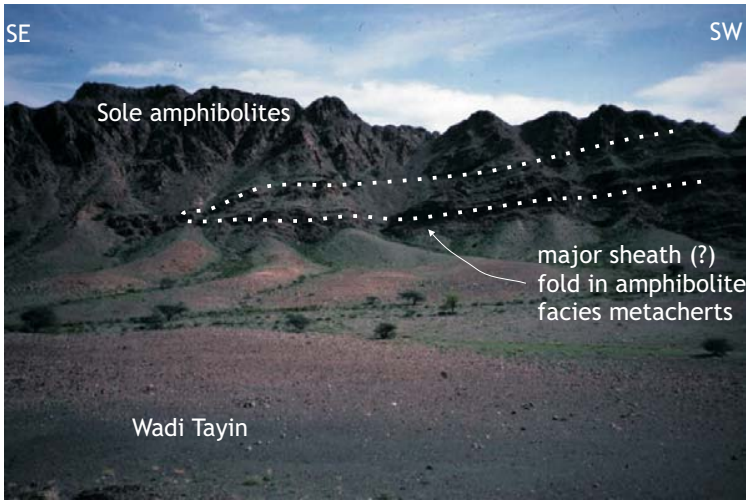


Figure 3.3 View of the Wadi Tayin 'green pool' classic sole outcrop, looking south in the direction of thrusting. The photo is taken at the base of the sole thrust sheet, looking upsection. The skyline ridge consists of coarse grained garnet-diopside amphibolites, and the major fold outlined is formed in amphibolite facies metacherts.

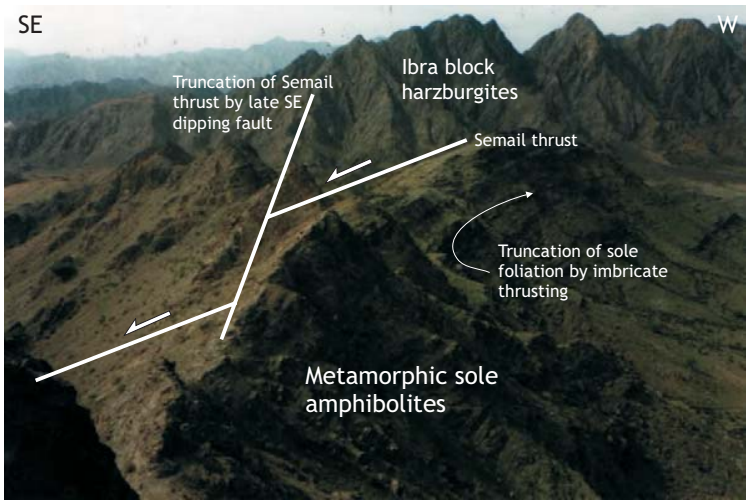


Figure 3.4 View looking WSW from the summit of the ridge shown in figure 3.3, towards the mantle sequence harzburgites of the Ibra block of the ophiolite. In places, truncation of the sole amphibolite foliation (dipping at ~25° SE) can be observed, suggesting repetition of the sole sequence by late, brittle imbricate thrusts.



Figure 3.5 Asymmetric minor folds, verging SW, in piemontite-muscovite metacherts from the upper limb of the folded quartzite unit shown in figure 3.3. Compare with figure 3.9.

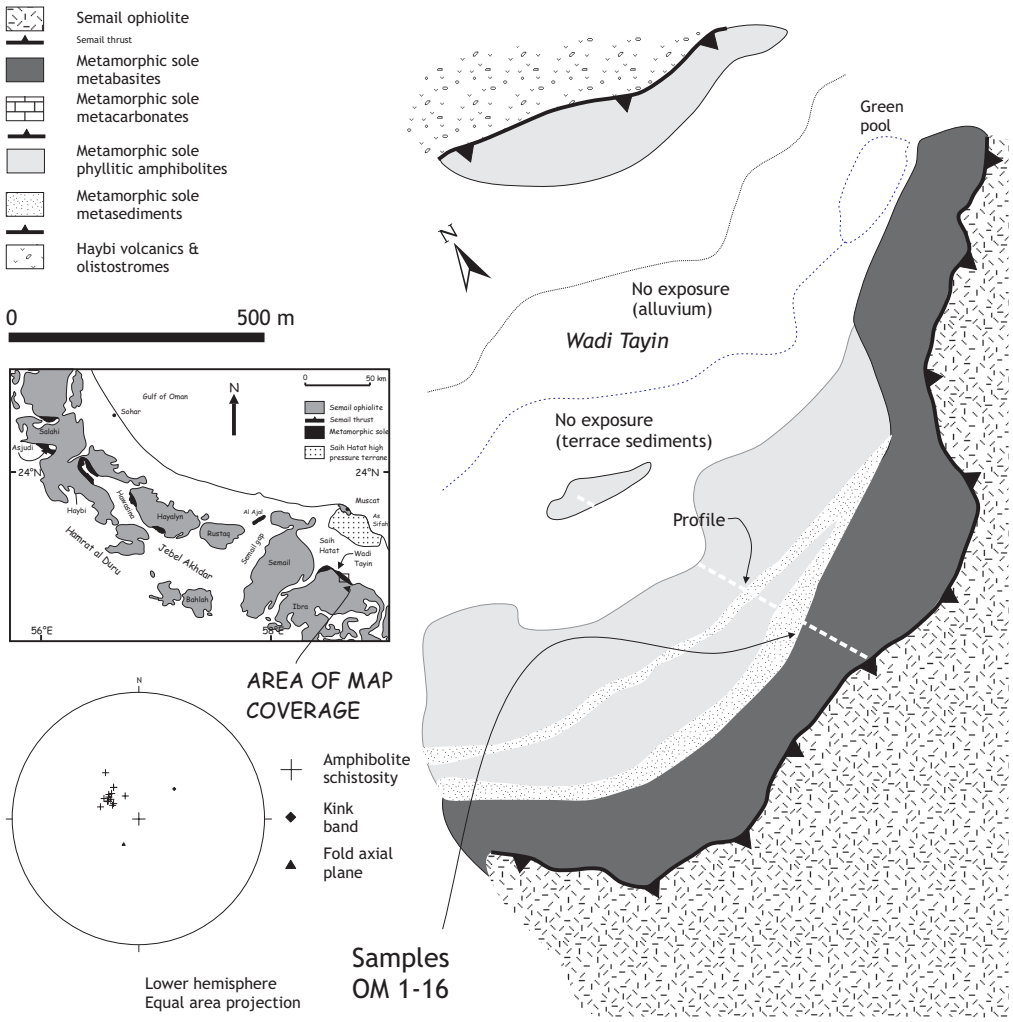


Figure 3.6 Geological sketch map of the Wadi Tayin 'Green pool' sole locality, after Ghent & Stout (1981) and Hacker et al. (1996), showing the section presented in figure 3.7 and the samples referred to in the text.

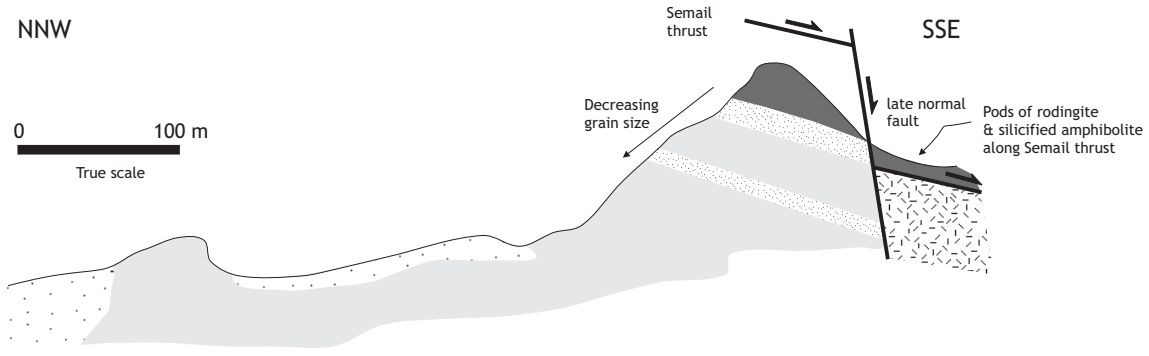


Figure 3.7 Section through the Wadi Tayin 'Green pool' sole locality, after Ghent & Stout (1981) and Hacker et al. (1996). A petrographic and structural log through the section is presented in figure 3.10. Legend as in figure 3.6.

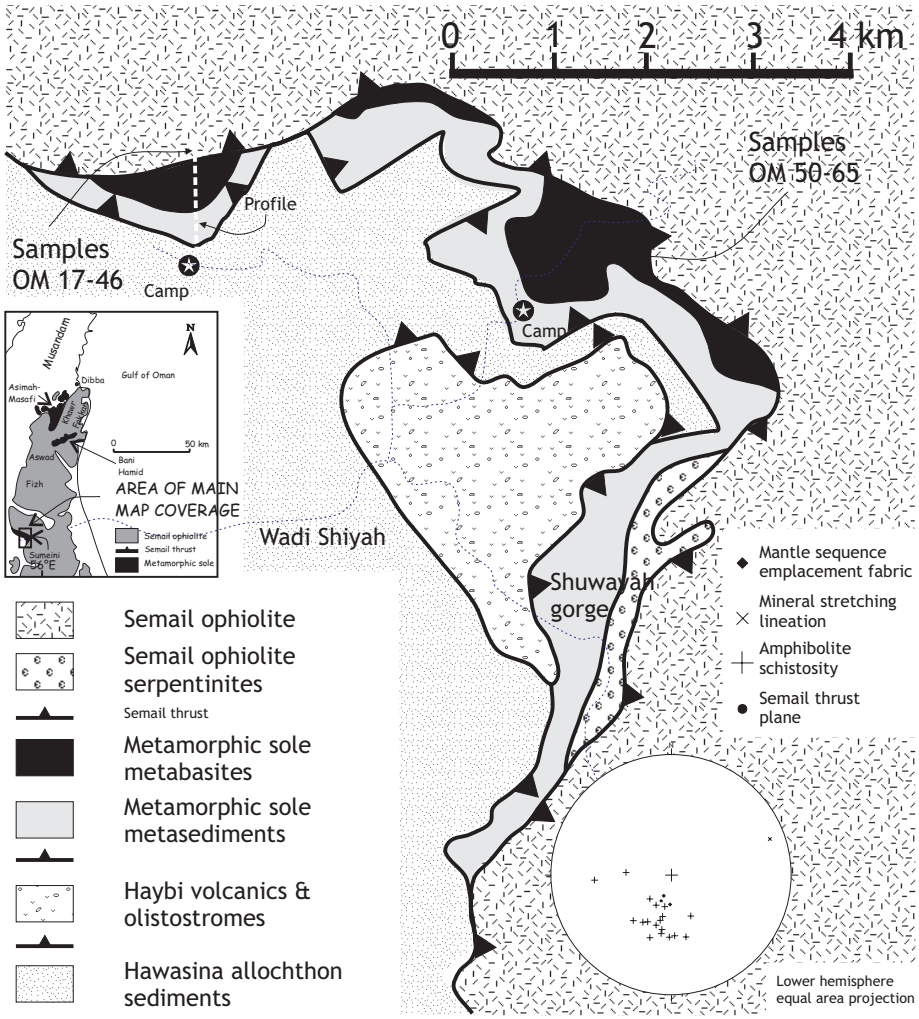


Figure 3.8 Geological sketch map of the Sumeini area, northern Oman, after Searle (1980), showing the distribution of collected samples, the location of the structural section and metamorphic profile presented in figure 3.9 and 3.10, and the structural data from the sampled section represented on a stereographic projection. See text for discussion.

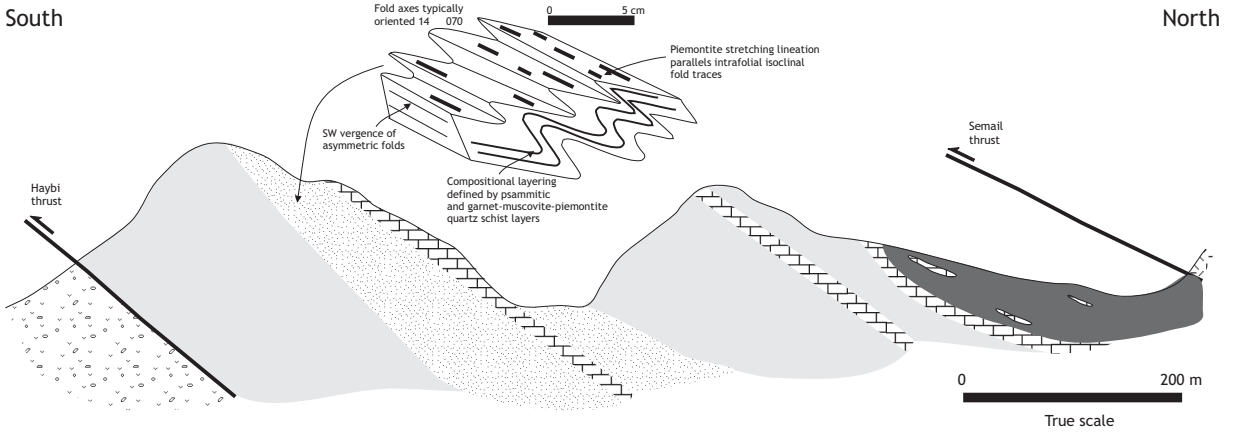


Figure 3.9 Section through the Sumeini metamorphic sole in the location marked above. See figure 3.10 for a log section. Inset: sketch showing fold vergence and microstructural relationships in a lower amphibolite facies metachert from the Sumeini area metamorphic profile described in figure 3.9 and 3.10.

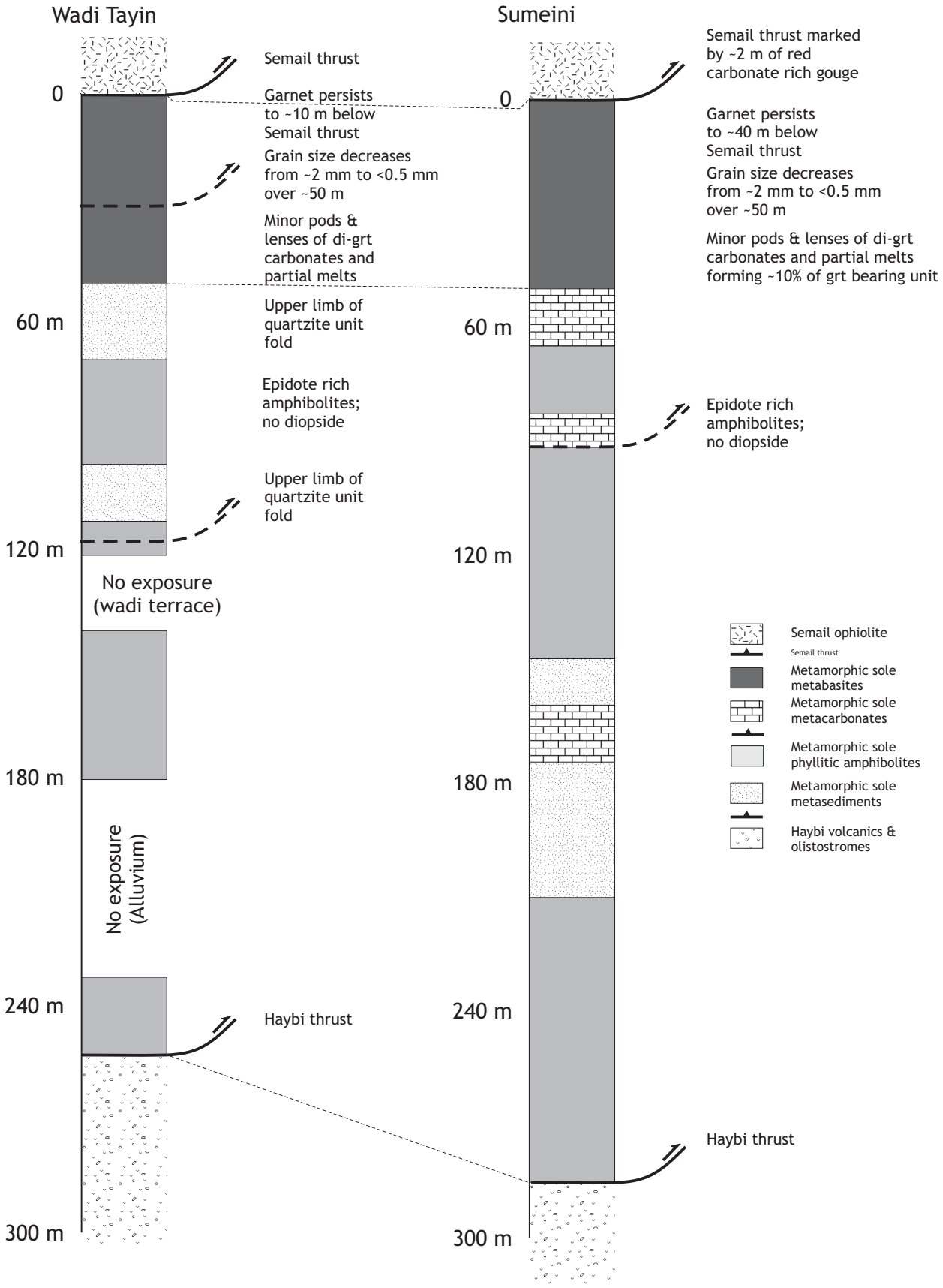


Figure 3.10 Comparative log sections through complete Semail ophiolite metamorphic sole sequences from the Wadi Tayin and Sumeini areas. See figures 3.6 and 3.8 for the location of the sections. The lack of clear correlation between the two sections demonstrates the structurally controlled variability within the metamorphic sole.

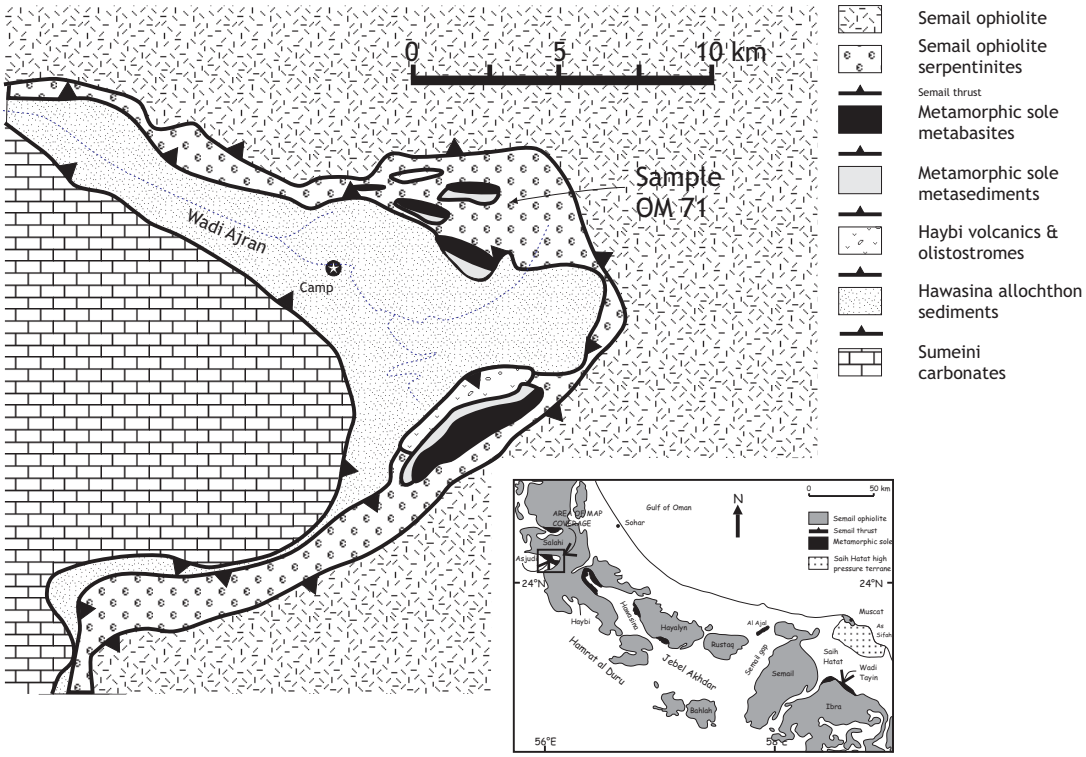


Figure 3.11 Geological sketch map of the Asjudi metamorphic sole locality, after Searle (1980). The location of sample OM 71, found as a wadi boulder at the base of a major dismembered sole outcrop, is shown.

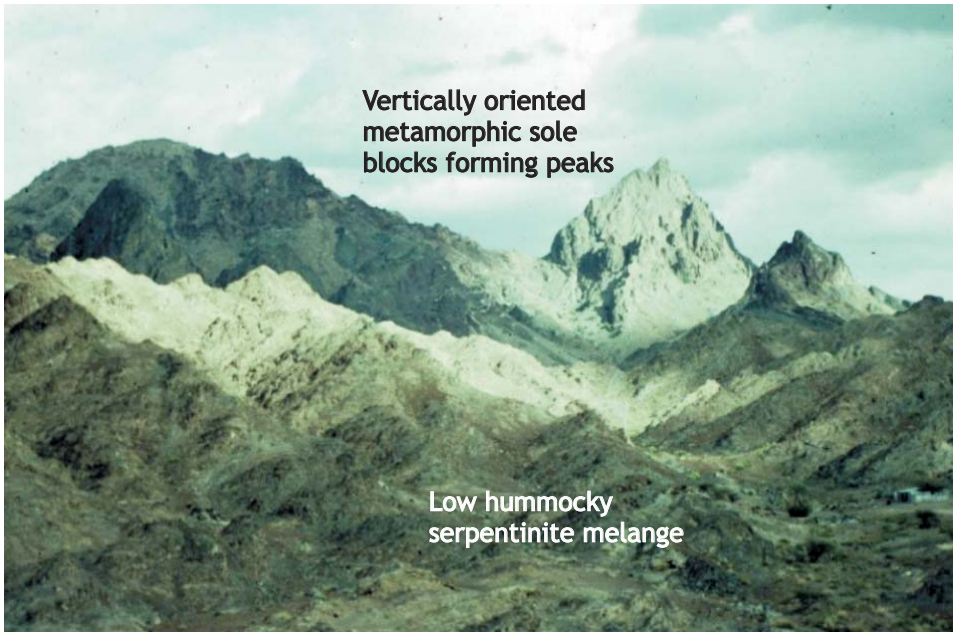


Figure 3.12 The metamorphic sole in the Asjudi area consists of amphibolites and greenschists with the original structural sequence broken up by strong shearing associated with emplacement. A thick mélange zone containing large, generally subvertically oriented blocks of amphibolite and greenschist sole components encased within a low relief serpentinite matrix marks the base of the ophiolite and few primary structural features or relationships have been preserved.

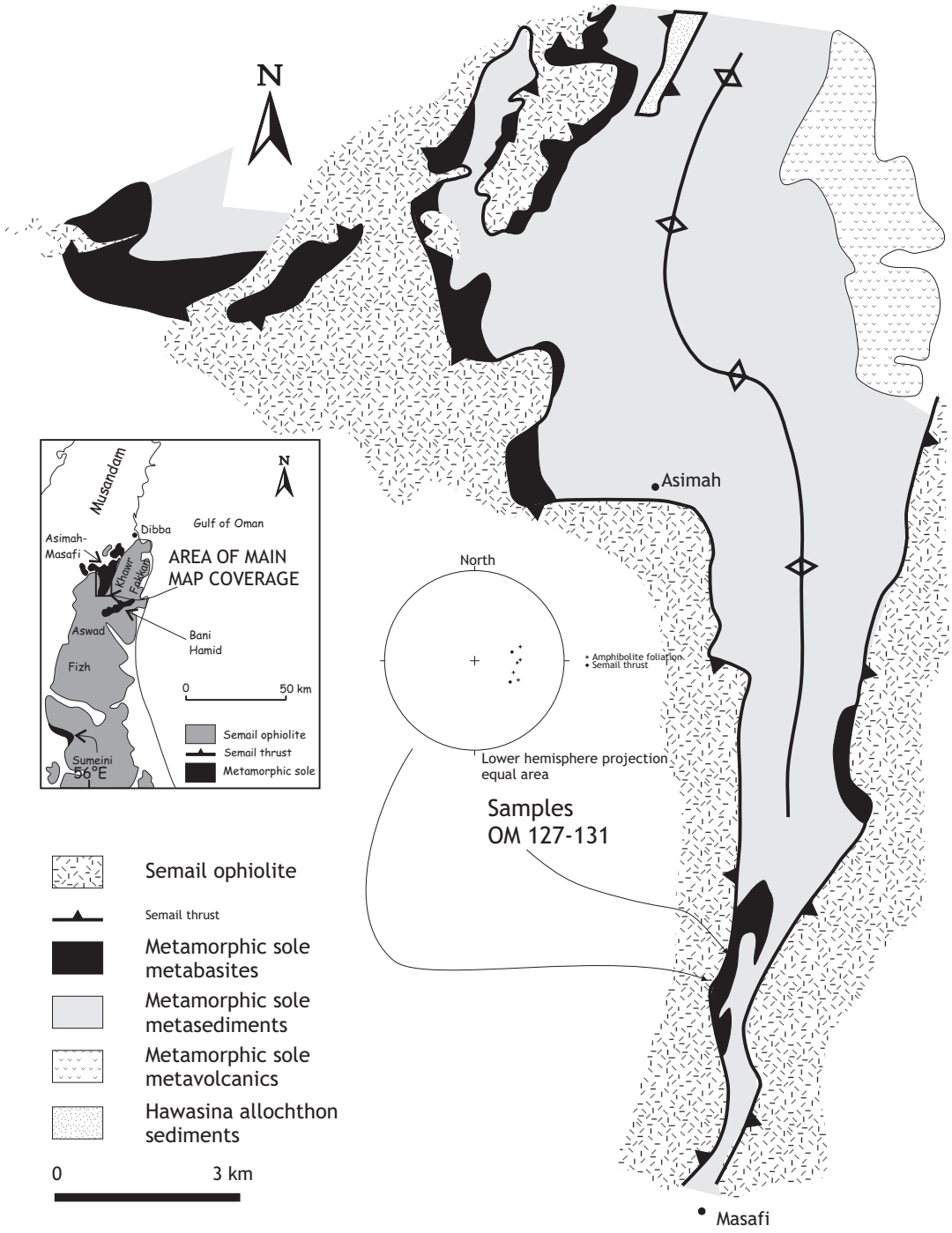


Figure 3.13 Geological sketch map of the Asimah-Masafi metamorphic sole section of the northern Oman/United Arab Emirates area, showing the locations of the samples described in the text, and structural data from the sampled outcrops. A section through the area is presented in Searle & Cox (1999). After Gnos (1992).

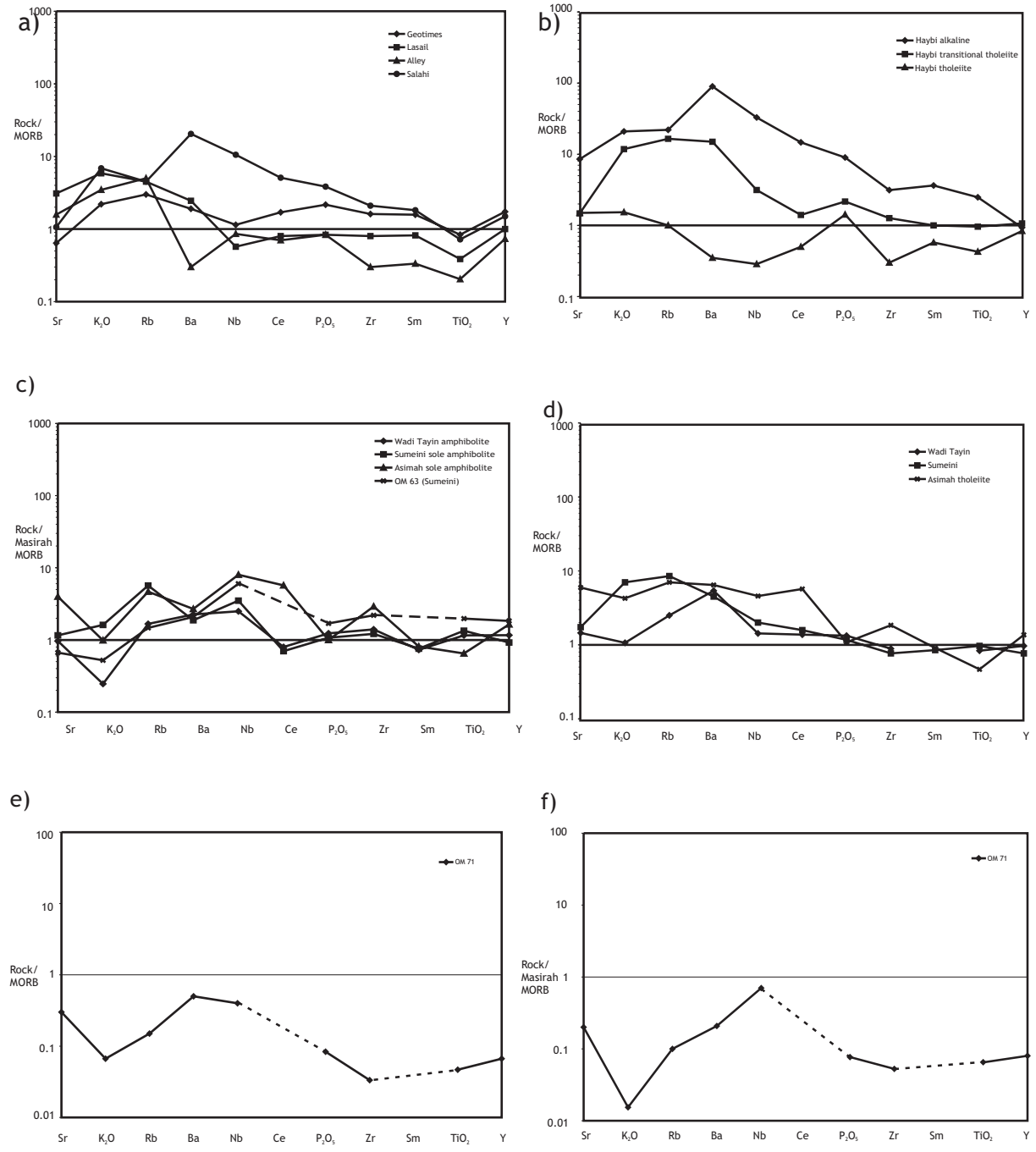
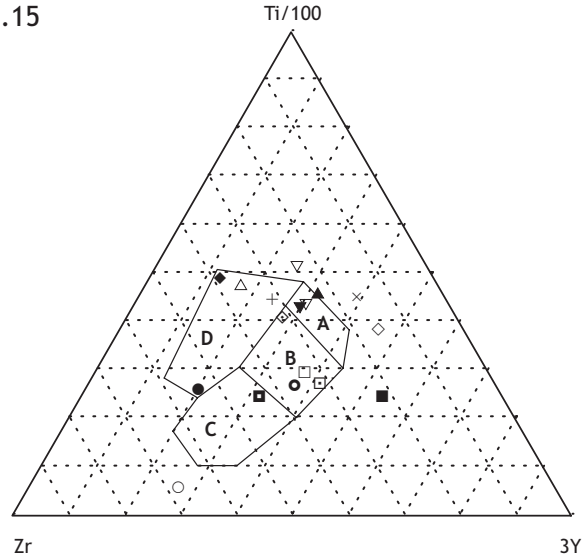


Figure 3.14a-f Spider diagrams for potential protoliths of metamorphic sole two pyroxene and garnet-diopside amphibolites from a variety of locations in the Oman mountains, normalised to a standard MORB (Pearce 1981) and MORB from the neo Tethyan Masirah ophiolite (Meyer et al. 1996). The volcanic units of the Semail ophiolite (a) show an increasing arc component with stratigraphic height (Pearce et al. 1981), measured by an increasing LILE concentration which is larger than that exhibited by the metamorphic sole amphibolites. Volcanic material from the Haybi sequence shows a similar trend with increasing structural height (Searle & Malpas 1980). Partial melt extraction during prograde metamorphism to produce tonalitic melts from the metamorphic sole amphibolites (Searle & Malpas 1982) is reflected in their low LILE concentrations. New analysis (c, d) shows sole metabasalt samples from Asimah, Wadi Tayin and Sumeini all have similar flat profiles that appears to correlate most closely with neo Tethyan MORB, like the ~145-150 Ma Masirah crust. Sample OM 71, a two pyroxene sole (?) granulite from Asjudi, is strongly depleted in all elements relative to MORB and Masirah crust (e, f) which may be a result of increased elemental mobility at temperatures of >900°C. This evidence suggests also that the boulder is not derived from the ophiolite cumulate sequence, which should have higher HFSE concentrations than MORB.

Figure 3.15

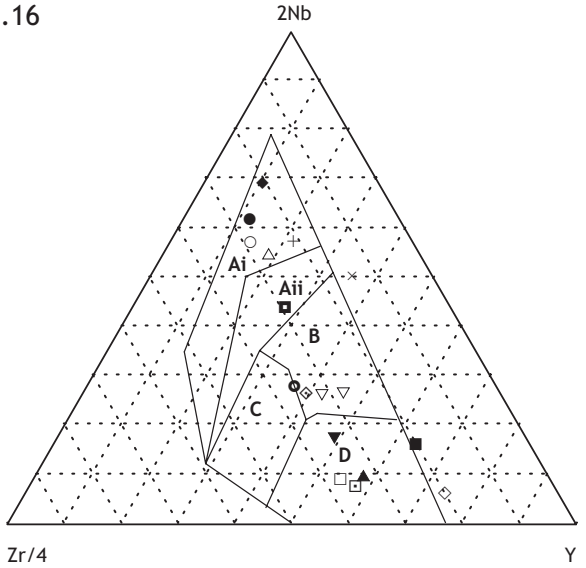


◆ Haybi volcanics (alkaline)
◇ Haybi volcanics (tholeiite)
◈ Haybi volcanics (transitional)
△ Masirah alkaline volcanoes
▲ Masirah MORB unit
■ Semail Alley unit
□ Semail Geotimes unit
⊡ Semail Lasail unit
◘ Semail Salahi unit
▽ Sumeini sole
▼ Wadi Tayin sole
+ Ruwi mélange
● Asimah sole (alkaline)
○ Asimah sole (carbonatite)
⊙ Asimah sole (tholeiite)
× OM 71 (Asjudi)

A Island arc tholeiites
B MORB, calc alkaline basalts & island arc tholeiites
C Calc alkaline basalts
D Within plate basalts

After Pearce & Cann (1973)

Figure 3.16

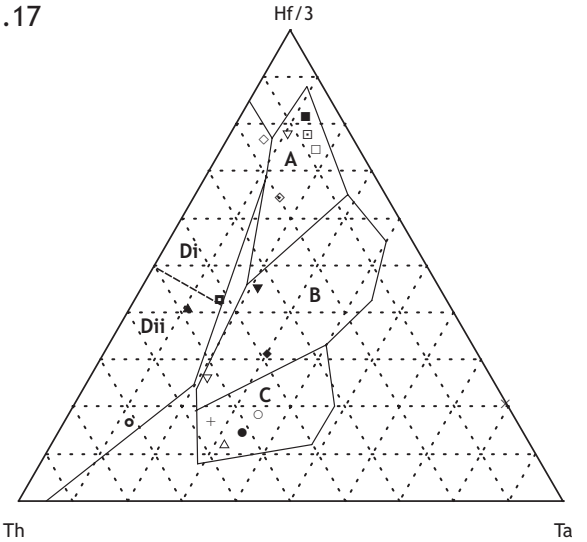


◆ Haybi volcanics (alkaline)
◇ Haybi volcanics (tholeiite)
◈ Haybi volcanics (transitional)
△ Masirah alkaline volcanoes
▲ Masirah MORB unit
■ Semail Alley unit
□ Semail Geotimes unit
⊡ Semail Lasail unit
◘ Semail Salahi unit
▽ Sumeini sole
▼ Wadi Tayin sole
+ Ruwi mélange
● Asimah sole (alkaline)
○ Asimah sole (carbonatite)
⊙ Asimah sole (tholeiite)
× OM 71 (Asjudi)

Ai Within plate alkali basalts
Aii Within plate alkali & tholeiitic basalts
B E type MORB
C Within plate tholeiites & volcanics arc basalts
D N type MORB & volcanics arc basalts

After Meschede (1986)

Figure 3.17



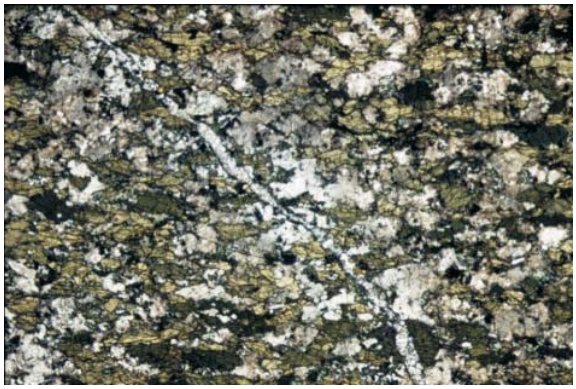
◆ Haybi volcanics (alkaline)
◇ Haybi volcanics (tholeiite)
◈ Haybi volcanics (transitional)
△ Masirah alkaline volcanoes
▲ Masirah MORB unit
■ Semail Alley unit
□ Semail Geotimes unit
⊡ Semail Lasail unit
◘ Semail Salahi unit
▽ Sumeini sole
▼ Wadi Tayin sole
+ Ruwi mélange
● Asimah sole (alkaline)
○ Asimah sole (carbonatite)
⊙ Asimah sole (tholeiite)
× OM 71 (Asjudi)

A N type MORB
B E type MORB, within plate tholeiites
C Alkaline within plate basalts
Di Island arc tholeiites
Dii Calc alkaline arc tholeiites

After Wood (1980)

Figure 3.15-17 Basalt tectonic discrimination diagrams for potential metamorphic sole amphibolite protoliths. The analysed Sumeini, Asimah, Haybi and Wadi Tayin sole amphibolites are typically classified as E/N MORB or IATs, distinct from the ophiolite units, and correlate more closely with Masirah MORB crust than with the ophiolite volcanic units. The two pyroxene granulite from Asjudi (OM 71) does not give a consistent result, but also corresponds better to the sole material rather than the ophiolite. Data from table 3.1, Searle & Malpas (1980), Zeigler et al. (1991) and Meyer et al. (1996). Ta obtained from the ratio Ta:Nb = 1:16, and Hf from a Hf:Zr ration of 1:39.

Figure 3.18a-f Photomicrographs demonstrating the mineralogy and petrography of the key metamorphic sole units described in the text. FOV (base of photo) in all figures is ~7 mm.



a)

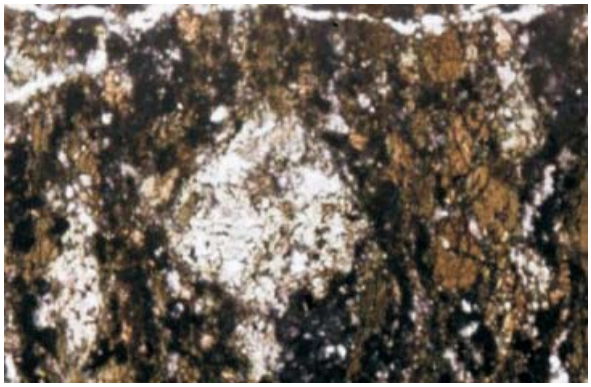


b)

a) Hornblende, altered plagioclase and diopside form the matrix of a typical garnet bearing high grade sole metabasite. Retrogression to greenschist facies assemblages is demonstrated by the presence of veins of prehnite. b) Garnet poikiloblast from the same rock, with inclusions of diopside, hornblende and rare quartz.



c)

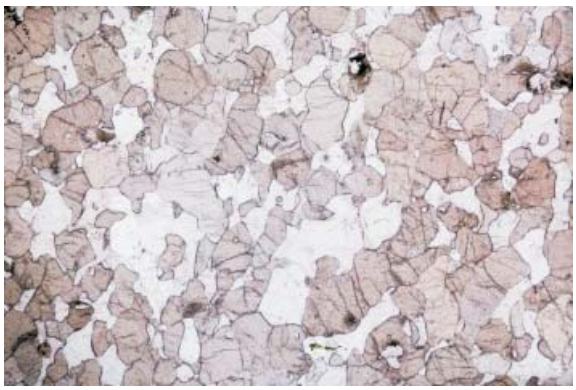


d)

c) Diopside-Ca rich garnet bearing metacarbonate intercalated within high grade metabasites, Sumeini. d) Alteration of highly sheared and dismembered sole outcrops at Al Ajal has resulted in the pseudomorphing of a garnet poikiloblast by chlorite and magnetite.



e)



f)

e) Rare, strongly deformed and protomylonitic garnet-hornblende metapelite from the Asimah sole. f) Fresh sole (?) granulite (brownish enstatite, greenish diopside and Ca plagioclase) with a granoblastic texture found as a wadi boulder (OM 71) in the Asjudi area.

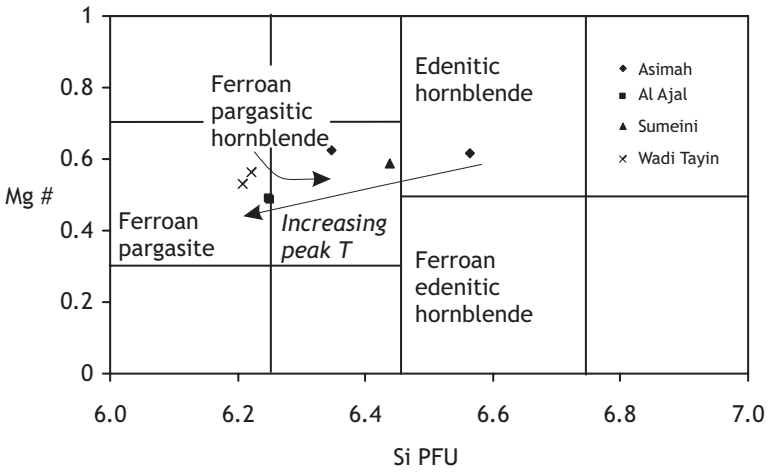


Figure 3.19 Compositional variation of metabasic sole amphiboles with peak metamorphic temperature for a number of sole localities beneath the Semail ophiolite. Analysed amphiboles exhibit a progression from edenitic hornblende to ferroan pargasite with increasing temperature over a range of ~100°C.

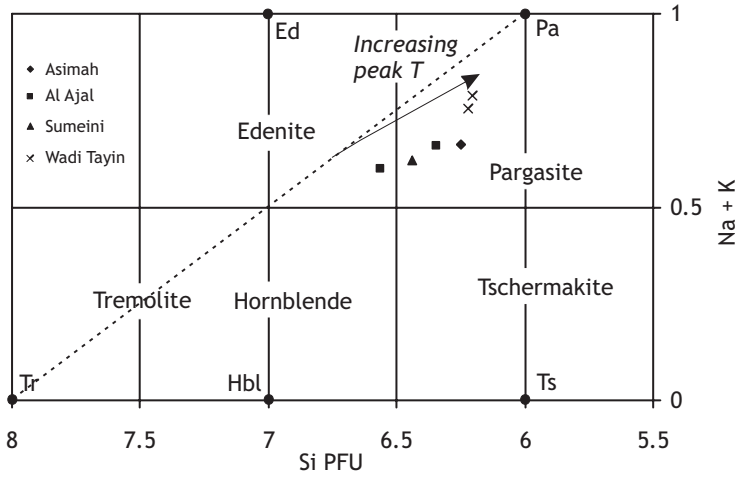


Figure 3.20 Compositional variation of metabasic sole amphiboles with peak metamorphic temperature for a number of sole localities beneath the Semail ophiolite. Amphiboles exhibit a linear progression from edenitic hornblende to ferroan pargasite with increasing T, parallel to the tremolite-pargasite join, equivalent to $Na^{VI}Al^{IV}Al_2 = KMgSi_2$ exchanges.

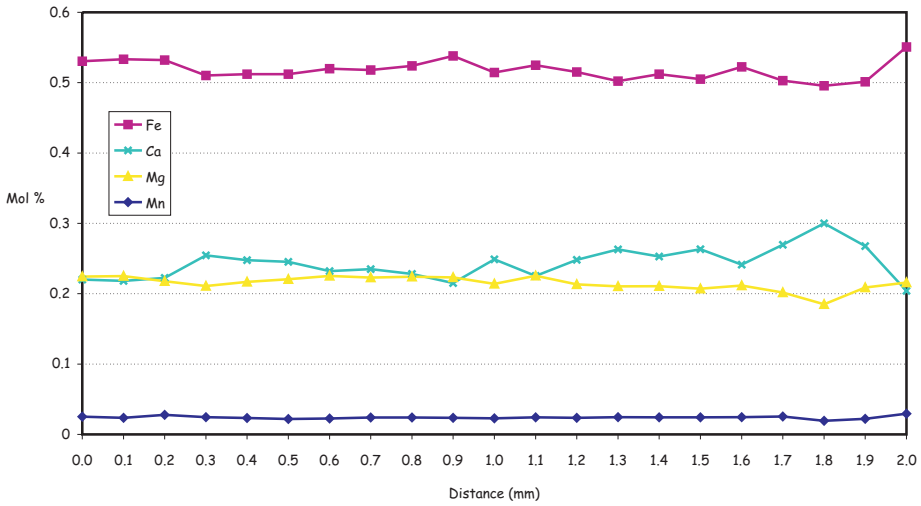


Figure 3.21 Unzoned profile across a ~2 mm sized euhedral garnet poikiloblast from sample OM 61, a garnet-diopside amphibolite from the Sumeini metamorphic sole locality.

Figure 3.22-25 Mineral chemistry of the equilibrium phases of Asimah sole pelite sample OM 131 used in the selection of microprobe analyses for the determination of end member activites in THERMOCALC.

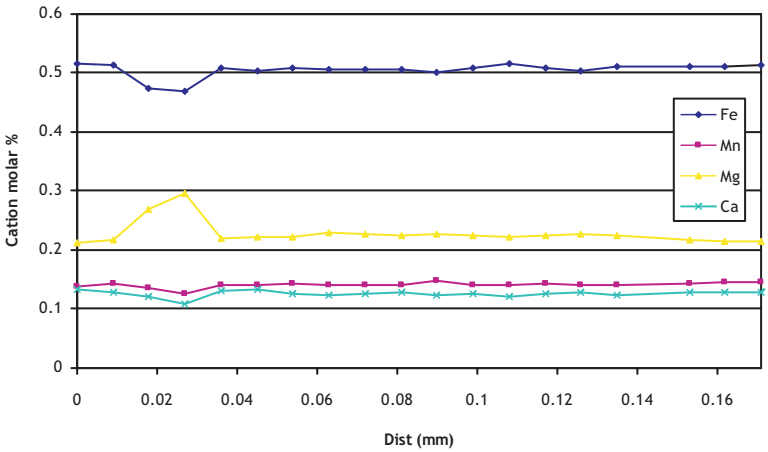


Figure 3.22 Unzoned garnet profile with a typical composition of $Alm_{0.5}Prp_{0.21}Sps_{0.15}Grs_{0.14}$. An average composition was used for PT analysis.

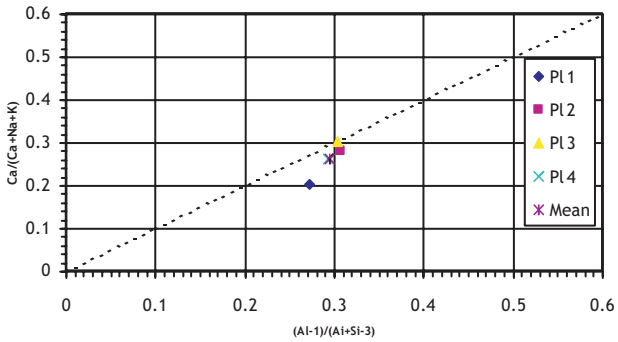


Figure 3.23 Plagioclase mineral chemistry and stoichiometry. Near stoichiometric relationships and little variation between and within individual grains allowed an overall mean to be used for PT analysis.

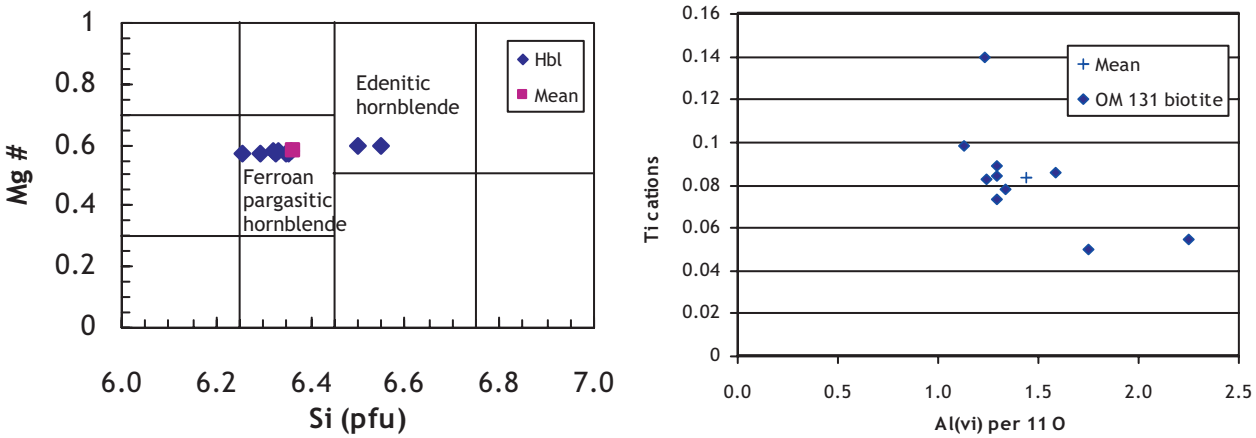


Figure 3.24 Blue green amphibole mineral chemistry of unzoned largely ferroan pargastic hornblende grains. Figure 3.25 Biotite mineral chemistry; an average value, excluding outliers, was used for PT analysis.

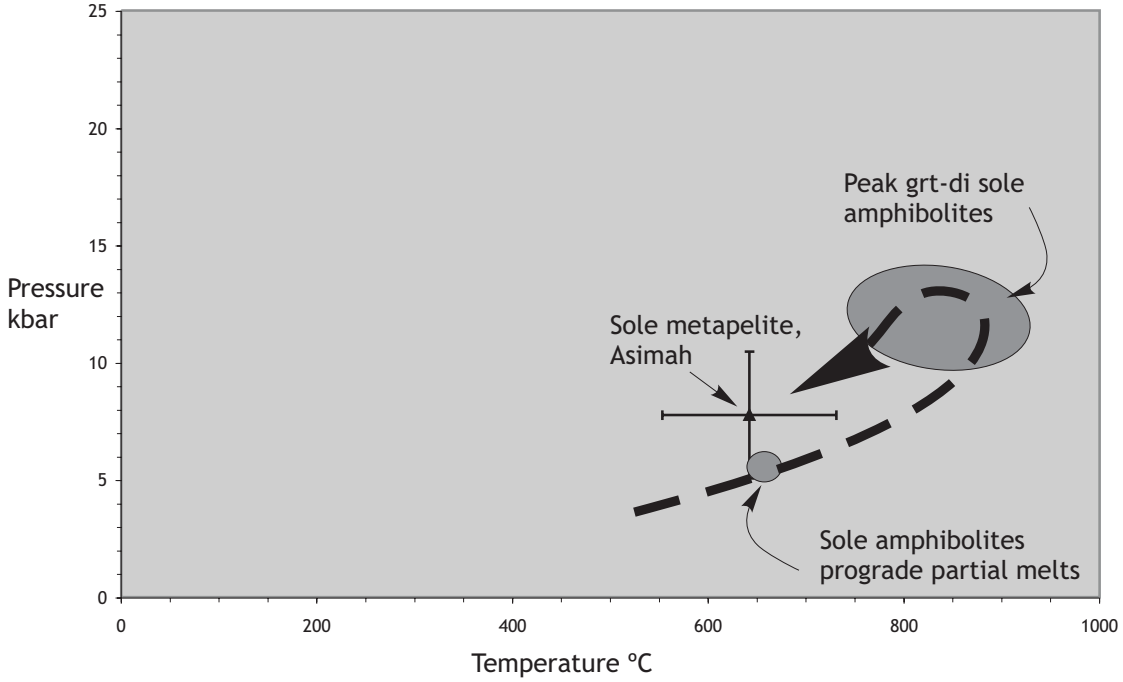


Figure 3.26 Pressure temperature time evolution of the Semail ophiolite metamorphic sole using new PT determinations from this study in conjunction with petrographic and structural evidence. The inferred sole anti clockwise PT evolution and peak temperatures of 840 ± 70ºC exhibits a similar anticlockwise form to that demanded by thermomechanical modelling of subduction zone conditions (Hacker 1990, 1991) and is consistent with a high geotherm environment derived from the heat of the overlying young and hot Semail ophiolite during intra oceanic subduction. $^{40}Ar/^{39}Ar$ (hornblende) ages from the metamorphic sole peak assemblages range from 95.1 to 93.4 Ma (Hacker et al. 1996) which overlap the crystallisation ages of the ophiolite crustal sequence, which range from 97.3 to 93.5 ± 0.25 Ma. This implies that intra-oceanic subduction to depths of at least 40 km beneath the Semail ophiolite was occurring simultaneously with the crystallisation of the ophiolite mantle sequence.

CHAPTER FOUR : SAIH HATAT HIGH PRESSURE TERRANE



Falconer training young Gyr falcons,
Ra’s Dadnah beach

the sole section. However, structural analysis of the Sumeini and Wadi Tayin sole sections has demonstrated the presence of sole folding and imbrication that is difficult to quantify. The metamorphic sole of the Semail ophiolite is a polyphase shear zone (Alleman & Peters 1972; Searle & Malpas 1980, 1982; Gnos 1998) in which inverted temperature and pressure gradients are generated by the juxtaposition of material progressively accreted to the subduction zone hanging wall at different times and under different metamorphic conditions, and preserved by the rapid emplacement process and cooling from the subducting material in the footwall.

Sole exhumation rates, estimated using new PT determinations in conjunction with existing metamorphic sole cooling rates, appear to have reached ~12.5 mm yr^{-1} in the first 1 Ma after the metamorphic peak, before declining to ~4 mm yr^{-1} integrated over the first 5 Ma after the metamorphic peak. Similar peak and mean values have been reported for the exhumation of other recent ophiolite complexes.

CHAPTER FOUR : SAIH HATAT HIGH PRESSURE TERRANE

4.1 INTRODUCTION

At least two distinct subophiolitic metamorphic events have been documented and recognised as part of the Semail ophiolite subduction-obduction event. In addition to the characteristic high temperature sub ophiolite metamorphic sole described in *Chapter Three*, the most internal part of the Saih Hatat window (figure 4.1) exhibits a more extensive regional high pressure (HP) metamorphism (Goffé et al. 1988; El-Shazly & Coleman 1990; El-Shazly et al. 1990). Blueschist facies rocks were first described by Lippard (1983), and eclogite facies material by LeMetour et al. (1986).

An extensive body of work on the HP metamorphism of northern Saih Hatat has been generated in the last fifteen years. Goffé et al. (1988) proposed an anticlockwise path for the Saih Hatat region, based on the presence of (pseudomorphic) chloritoid inclusions in carpholite, and the absence of lawsonite inclusions in lower grade metapelitic rocks of the 'Muscat nappes'. El-Shazly et al. (1990) however proposed a clockwise PT evolution peaking at >10.2 kbar for the As Sifah terrane. Regional structural mapping by Searle et al. (1994) demonstrated the link between the PT conditions of metamorphism and the complex structural history of the region and new eclogite thermobarometry implied a clockwise PT history peaking at 23 $\pm$ 2.5 kbar and 540 $\pm$ 75°C. Modelling of cracking of garnets with quartz inclusions (Wendt et al. 1993) supported similar peak pressures of >20 kbar for the As Sifah area.

The temporal relationship between the formation of the HP and HT terranes is key to any understanding of the ophiolite obduction and emplacement process. The exact timing of this HP event is the major unresolved issue in the obduction and emplacement history of the Semail ophiolite. The present distribution and outcrop of the contrasting HP and HT terranes along the Oman mountains belt may be related in part to Tertiary deformational events such as the formation of the Musandam culmination and the unroofing of the Saih Hatat window.

In this chapter, new and detailed structural mapping (Enclosures 1-3, figure 4.8) and analysis of critical sections of the Saih Hatat terrane, including the Ruwi mélange, the structurally complex Wadi Mayh and Wadi Adai sections through the terrane, and the highest grade (eclogite facies) terrane component, the As Sifah unit. The analysis of macro and microscopic kinematic indicators, fold vergence and facing directions and textural petrography, is coupled with stereographic analysis of fold axes, lineations and foliations, microstructural evidence, new PT determinations from the As Sifah eclogites, and comparative studies of other HP terranes. A coherent exhumation model (presented in *Chapter Seven*) will be constructed

for the generation, exhumation and preservation of the HP rocks exposed in the northern part of the Saih Hatat window.

4.2 GEOLOGICAL SETTING OF SAIH HATAT

The structural and stratigraphic framework of Saih Hatat was initially defined by Glennie et al. (1974). Although the basic structural elements of the window were described, no mention was made of the HP terrane or assemblages. The French BRGM group remapped the area at a scale of 1:100,000 (LeMetour et al. 1986). In addition, the structural and metamorphic history of the Saih Hatat window and the 'Muscat nappes' was first described and analysed in some detail by Michard et al. (1984, 1989) and Goffé et al. (1988).

The Saih Hatat window (figure 4.1) has eroded through all the allochthonous units of the Oman mountains, forming a gently dipping anticlinal dome in the Mesozoic shelf carbonate sequence with a wavelength of 70 km. The Semail ophiolite crops out around the margins of the window, although upper crustal units are not exposed onshore in NE Saih Hatat (Bailey 1981). The ophiolite is intermittently underlain by the metamorphic sole, well seen at Wadi Tayin. Beneath this lie a series of progressively more proximal allochthons ranging from the pelagic cherts and turbidites of the Hawasina complex, through the trench fill mélange of the Haybi complex to the Sumeini carbonate slope units. All were emplaced on to a stable Permian to Cretaceous carbonate platform at least 1.5 km thick, consisting of Permian (Saiq formation), Triassic (Mahil formation) Jurassic (Sahtan formation) and Cretaceous (Kahmah and Wasia formations) limestones and dolomites. Minor volcanic and volcaniclastic units are common, particularly towards the base of the sequence.

Exposed in the core of Saih Hatat are low grade Proterozoic and Palaeozoic basement rocks, dominated by a 3 km thick sequence of Ordovician sand and siltstones, the Amdeh Group (Lovelock et al. 1981). All folding and cleavages in these units, of Hercynian age (Glennie et al. 1974), is truncated by a clear unconformity at the base of the shelf carbonate units above. Southern and central Saih Hatat presents a typical, relatively undeformed and low grade section through the entire allochthon. Stable conditions on the Arabian continental margin continued until rapid subsidence beneath the advancing ophiolite caused the collapse of the shelf and its replacement by a flexural foreland basin, the olistostromal infill of which forms the Muti formation, dated as Campanian-Coniacian (Robertson 1987a,b).

In contrast, the northern margins of Saih Hatat consist of a regionally extensive HP belt, characterised by a tectonically thickened and strongly deformed shelf carbonate sequence. These units are structurally and stratigraphically poorly constrained (due to the absence of stratigraphic markers within the shelf carbonate sequence), show abundant thrusting (often out

of sequence), mylonitisation and large scale folding, and a number of north dipping shear zones (Searle et al. 1994). The overlying ophiolite consists of ~5 km of typically serpentinised harzburgites, and has a distinctive subophiolitic metamorphic sequence, with thick carpholite, kaolinite and pyrophyllite bearing metasediments cropping out between Ruwi and Yiti, first described by Goffé et al. (1988).

The highest grade rocks occur around the coastal village of As Sifah (enclosure 1) to the SE of Muscat, and consist of eclogite facies meta basaltic flows and sills and carbonate rich sediments. A lower age limit on the timing of the various tectonometamorphic events discernable in northern Saih Hatat is given by the Maastrichtian-Palaeocene age of the neoautochthonous reefal limestones that unconformably overlie the HP terrane.

4.3 STRUCTURE AND STRATIGRAPHY OF NORTHERN SAIH HATAT

A general structural and location map of the Saih Hatat region of the NE Oman mountains is shown in enclosure 1. Previous work in the area has defined numerous tectonometamorphic units, based on mineral assemblages in metasediments (Goffé et al. 1988) and metabasites (El-Shazly & Coleman 1990; El-Shazly et al. 1990). Searle et al. (1994) addressed the structural controls on the present outcrop pattern of the region and defined more precisely the structural features that post dated the main metamorphic events and therefore governed their subsequent distribution. The structural units described below in order of increasing grade are basically those of Goffé et al. (1988), as modified by Searle et al. (1994).

4.3.1 Ruwi mélange

The Ruwi mélange is a unique structural unit with a characteristic lithology and paragenesis that is restricted to a small area on the NW margin of the Saih Hatat window. It was initially assigned by Glennie et al. (1974) and Robertson (1987a) to the Santonian (83.5-89 Ma) Muti formation of the Aruma Group, which is found throughout the region but is metamorphosed only in the Ruwi area. The Muti formation represents a syn-depositional foreland basin deposit, derived from both the advancing ophiolite to the north east and the collapsing shelf carbonate sequence to the south and west (Robertson 1987a).

The structural relations of the Ruwi unit are controversial. The unit is clearly juxtaposed against a variety of lithologies, including unmetamorphosed Hawasina cherts, serpentinites and pillow basalts of the Haybi complex to the north, close to Darsayt,

neoautochthonous Maastrichtian-Palaeocene limestones to the west, and Jurassic shelf carbonates of the Kahmah and Sahtan units to the south. A new geological map of the Ruwi area presented here (enclosure 2) shows the boundaries between the mélange and these units thus:

1. Hawasina & Haybi complexes: these bedded cherts, pillow basalts and serpentinite blocks appear to be thrust over the mélange units (El-Shazly 1994).
2. Neoautochthonous Maastrichtian-Tertiary limestones: these are clearly unconformable. The age of the lower limestones, ~70 Ma, is an upper limit on the age of the metamorphism of the mélange. This study (enclosure 2) has identified a double unconformity, with two small outcrops a soft sandstone unit, apparently unfossiliferous and dipping to the east, resting unconformably on top of the Hawasina units. This sandstone is loosely consolidated, and consists of mixed carbonate, serpentinite and chert grains. In addition, it contains angular blocks of the basal units of the Maastrichtian-Tertiary limestones, and thus postdates the Maastrichtian. The occurrence of cross stratification structures suggests the presence of channels in a shallow marine environment.
3. Shelf carbonates: these are separated from the mélange by a major north dipping fault, originally compressional but reactivated as an extensional fault during the development of the Saih Hatat window (Searle et al. 1994). In addition, to the NW of Hamriya, the mélange is overlaid by a klippe of shelf material which exhibits a large scale NNE verging sub-horizontal fold (figure 4.4) interpreted as a gravity collapse fold (Hanna 1990). Similar reasoning may account for the folding of the Maastrichtian-Tertiary limestones visible around Qurum and Ra's al Hamra to the NW, the axial trends of which are normal to the structural trend of northern Saih Hatat.

The Ruwi mélange differs substantially from other subophiolitic metamorphic sole localities in terms of thickness, structure and PT conditions of formation. The presence of metapelitic index minerals such as carpholite and lawsonite clearly imply a lower temperature regime not seen in the typical greenschist-amphibolite 'classic' sole outcrops (Searle & Malpas 1980; Ghent & Stout 1981; *Chapter Three*). Previous PT estimates have produced variable results ranging between >7-8 kbar, <280°C (Goffé et al. 1988) and 3-6 kbar, 250-300°C (El-Shazly 1994), and have been contentious (Vidal & Theye 1996).

New detailed mapping (enclosure 2) has demonstrated that the Ruwi mélange has a minimum thickness of 400-500 m and a clear internal stratigraphy, rather than a macroscopic mélange structure as previously described (El-Shazly 1994). The appearance of lateral

discontinuity within units of the mélange is largely due to oblique down cutting by the north dipping normal fault described above, although the porphyroblastic lawsonite schist unit in particular is laterally discontinuous, and lensoidal. This may reflect protolithic compositional variations (enclosure 2).

The dominant unit within the mélange is a fine grained (typically 50-75 μm) pale grey quartz-chlorite-white mica schist, with abundant matrix rutile. The schistosity is defined by chlorite and white mica, and foliation surfaces carry a clear NNE-SSW oriented mineral stretching lineation. The majority of the metabasaltic blocks characteristic of this mélange are to be found within this unit and contain index minerals including lawsonite and pumpellyite and are similar to those described by El-Shazly (1994). This mica schist is underlain by a patchily outcropping pink to grey schist containing carpholite-chlorite-illite-quartz in which the carpholite is found as characteristic pink 'bow-tie' porphyroblasts up to 5 mm in size and first noted by Goffé et al. (1988)

Also abundant, and found overlying the quartz mica schist, is a fine grained grey green schist with porphyroblastic blue lawsonite grains up to 10 mm in size (figure 4.7). A typical assemblage is lawsonite-chlorite-quartz-calcite-hematite. This unit is not as laterally coherent as the others described and tends towards a more lensoidal morphology, a feature that probably reflects primary sedimentological conditions. This unit is overlaid by a succession of thin, largely carbonate units each 30-50 m thick. They are variable in grain size, with fine grained banded marbles and limestones, and very fine grained slaty marls. These units outcrop only in the Al Wadi al-Kabir / Hamriya area of the Ruwi hills.

The base of the mélange is not seen, but is assumed to be in tectonic contact (a thrust reactivated as a major north dipping extensional fault) with the underlying carbonate shelf units of northern Saih Hatat. The neoautochthonous Maastrichtian-Tertiary limestone sequence unconformably overlies the mélange in the west. Internal deformation of the mélange units is relatively minor, with few apparent large faults. However folding and smaller scale deformational structures are widespread. The mélange units are folded into a series of open folds, with a wavelength of ~2 km and an amplitude of ~500 m, the axes of which plunge about 20° to the NE (figure 4.5, enclosure 2).

The presence of a polyphase deformation is clear from the analysis of small scale fold structures, which contain an axial planar cleavage (typically dipping steeply to the SSW, as well as the occurrence of widespread kink bands (figure 4.6), an extensional crenulation cleavage in the mélange unit, and a locally developed crenulation cleavage. A NNE-SSW mineral stretching lineation on foliation surfaces is ubiquitous. The following deformational history is a new synthesis of the structural history of the Ruwi mélange and can account for all the observed structural evidence observed.

The first major fabric forming event (D_1) is defined by the orientation of phyllosilicate laths and quartz rods in schists (S_1). The mineral stretching lineation observed is parallel to

the assumed allochthon transport direction and is defined by tabular porphyroblastic phases such as lawsonite and carpholite. This event is assumed to have been synchronous with the peak of the metamorphism since blueschist facies phases grew parallel to it, and may have operated continuously during the formation and exhumation of the mélange unit.

D_2 is represented by a set of small amplitude upright open folds with sub vertical fold axial planes and axial traces trending N-S. Locally associated with these folds is a steeply dipping axial planar cleavage (S_2) forming microfolds in S_1. A later phase of deformation is characterised by kink banding, the asymmetry of which suggests a top to the NNE-ENE sense of shearing (figure 4.6). Minor NE verging ductile asymmetrical folding, the fold axial planes of which dip gently to the SW, is common in the upper limestone unit, and may be related to the late extension of the terrane during exhumation.

Identification of the protolith material for the Ruwi mélange can provide a key constraint on the age of the Saih Hatat HP event. If derived from the Santonian (83.5-89 Ma) Muti formation rather than the Haybi complex from which the 'classic' ophiolite sole is formed, the Ruwi HP event has an upper age limit of ~89 Ma rather than the ~94 Ma age of the metamorphic sole. The only published $^{40}Ar/^{39}Ar$ age of the Ruwi mélange of 80.2 ± 0.8 Ma (El-Shazly & Lanphere 1992) is consistent with this interpretation. However, the validity of such dates, which have formed the crux of at least one model of the HP metamorphism of the region (El-Shazly & Lanphere 1992), are questionable due to the possibility of contamination by excess Ar (Searle et al. 1994; Hacker et al. 1996), and Searle & Cox (1999) ascribed the mélange to the Haybi complex.

4.3.2 Wadi Adai – Wadi Mayh – Al Khuryan unit

A geological map and structural data for this unit is presented in figure 4.8. Wadi Adai trends roughly normal to the regional strike of the para-autochthonous carbonate units of the Saiq and Mahil formations, which form the bulk of the outcrop. The northern half of the wadi has a simple structure very similar to that observed in the Yiti-Khawr Yiti section of Wadi Mayh (enclosure 3). Shelf carbonates of the Sahtan, Mahil and upper Saiq formations dip uniformly N-NE at 30-50°, with open upright folds (fold axial planes oriented typically 40-190), repeated by two large scale north dipping thrusts and juxtaposed with lenses of serpentinised peridotite (McMiller et al. 1999). These units were assigned to the blueschist facies by Goffé et al. (1988).

The structurally lower units exposed in Wadi Adai comprise a thick carbonate sequence, with subordinate massive and volcaniclastic metabasic units (with a crossite-epidote blueschist facies assemblage, with abundant matrix pumpellyite, locally retrogressed to an albite-

chlorite-actinolite schist) and a quartz-phengite-plagioclase rich schist, interpreted as a Permian siliceous metatuffite by LeMetour et al. (1986) but ascribed to the Amdeh quartzite by McMiller et al. (1999). Again the units dip relatively uniformly north, but the outcrop pattern is less linear, with large scale E-W trending fold axes suggesting N-S compression, probably associated with the initial compression caused by the emplacement of the allochthon. Furthermore, the competency contrasts between the carbonates, basaltic units and tuffs would have promoted folding rather than the more homogeneous ductile response to deformation observed in the carbonate rich units.

The restoration of the Wadi Adai section is possible to a degree, and such an exercise can produce an estimate of the shortening accomplished during deformation. Such a figure is only a minimum, due both to the still poorly constrained stratigraphic control within the rather homogeneous recrystallised carbonates of the Permian Saiq and Triassic Mahil formations, and the degree of ductile folding and deformation, which is compounded by the plastic nature of carbonate under strain. The calculated figure of ~22% reflects the comparatively undeformed nature of the Wadi Adai section compared with the other analysed sections.

Wadi Mayh presents a complete structural and stratigraphic section through the sub-ophiolitic allochthon and autochthon from Hercynian basement metasedimentary units to neoautochthonous Maastrichtian-Tertiary limestones. The complexity of the structures observed, and the stratigraphic uncertainty of the lithologies present in the complexly deformed gorge section (ascribed to the pre-Permian by Glennie et al. 1974; Bailey 1981; Hanna 1990 and Mann & Hanna 1990, but to the Permian Saiq Formation by LeMetour et al. 1986) increases generally from NE to SW with structural depth within the Wadi Adai – Wadi Mayh – Al Khuryan unit, from simply deformed and stacked shelf carbonate units in the NE to complex mylonitic limestones of uncertain age and structural position in the SW gorge section (figure 4.11 and 12). This study presents a new structural and stratigraphic map of Wadi Mayh (enclosure 3) that represents a continuation of the description and interpretation of the structural development of northern Saih Hatat described in Searle et al. (1994).

Around Khawr Yiti (enclosure 3), neoautochthonous Tertiary bioclastic reefal limestones, with a distinctive yellow colour and an abundant fauna, unconformably overlie the grey and yellow recrystallised dolomites of the Triassic Mahil formation, which have been assigned to the blueschist facies by Goffé et al. (1988) and show evidence of early SW directed thrusting (figure 4.13). The units are separated by an unconformity surface that dips to the north at a relatively uniform 30°.

Beneath the unconformity a small thrust slice belonging to the Haybi complex is imbricated, comprising a lower unit of a weakly bedded mélange unit characterised by a reddish silty matrix containing abundant fragments of a grey-green homogeneous chert. This is in thrust contact with a small sheet of amphibolite metamorphic sole material, which is itself in thrust contact with the overlying Mahil formation.

The Yenkit and Al Khuryan shear zones, as defined by Searle et al. (1994), are well exposed and are characterised by north dipping shear bands in mylonitic limestones and minor metapelites, with isoclinal minor folds that consistently face to the SSW. Fold axial planes dip to the north, except in the Al Khuryan shear zone where synclinal folding of the shear surface has occurred.

Structurally below this, spectacular cliffs of (?) Permian silty grey-brown-black dolomitic limestones with more massive coarse grained yellow to white-pink limestones and intercalated transitional blueschist-greenschist facies metabasaltic horizons (characterised by the assemblage crossite-actinolite-epidote-albite-chlorite) form major south facing recumbent folds, with SSW dipping axial planes.

These units are repeated by two north dipping thrusts and overlie a sequence of similar variable carbonates, with subordinate greenschist units, which are again attributable to the Permian Saiq Formation. Further large scale thrusting and folding is evident forming a tightly recumbent south facing nappe. Minor folding visible within mylonitic carbonate units of the lower limb of this sequence verges consistently to the NNE-NE.

The Hulw shear zone (Enclosure 1) was first characterised by Searle et al. (1994) and dips to the NNW at about 30° and outcrops in Wadi Mayh to the north of the village of Rija. It juxtaposes the overlying low grade greenschist-blueschist facies carbonate-metabasalt sequence of the Saiq Formation from the higher grade blueschist-eclogite facies and lithologically and structurally distinct quartz-phengite and calcite-quartz-phengite schists of the underlying 'Rija culmination' and As Sifah unit to the east.

The peak PT regime of this unit is poorly constrained due to the absence of metabasic units within it, but occurs in a similar structural position to the garnet-glaucophane blueschist bearing sequence of the Diqdah unit (defined by Michard et al. 1994) around As Sifah (Enclosure 1). As in the Wadi Hulw outcrops, the north dipping shear zone, with older Palaeozoic units structurally beneath Permian units, suggests a late extensional geometry.

The protoliths of the Rija carbonate and quartzose schists may, by analogy with the As Sifah block, have been the Permian Saiq Formation and the Ordovician Amdeh quartzite respectively. The schists of the Rija culmination clearly show a more complex microstructural history than the overlying units and are characterised by a kinematic history very similar to that described by Searle et al. (1994) from analogous calcite-phengite-quartz schists overlying the metabasic eclogites at As Sifah.

S_1 is defined by phengite and the preferred orientation of quartz and calcite grains. A D_2 event folded this fabric into small scale tight to isoclinal asymmetric folds that verge consistently to the NE (figure 4.18b). Variably spaced shear bands define D_3 in both calcareous schists and quartz-phengite schists, and form an extensional shear band fabric, consisting of a

pre-existing schistosity and discrete, anastomosing shear bands (figure 4.18a). The latter exhibit a top down to the NE extensional sense of motion.

This microstructural history is very similar to that observed in the calcareous schists of As Sifah, and the close correlation between lithology and structure of the Rija and As Sifah units is consistent with a coeval metamorphic and structural history. However, minor thrusting, with a bimodal NNE-SSW transport direction (and hence clearly parallel to the overall allochthon transport direction) is common in the schists of the Rija culmination and has not been reported from As Sifah. These thrusts are clearly post D_2 and cut the asymmetric fold set but their age relative to the later (D_3) extensional crenulation cleavage has not been constrained from existing fieldwork.

4.3.3 Wadi Hulw unit

The Hulw unit crops out to the south and east of the above described lithologies and now appears to be at a similar structural level to the As Sifah and Rija units, although no eclogite facies assemblages are seen (or preserved?) in the Wadi Hulw area. Dominant lithologies in the Wadi Hulw area are dolomitic calc schists and micaeous quartzose schists originally assigned to the pre–Permian and derived from the Hijam Group and Amdeh Group respectively (Glennie et al. 1974; Lovelock et al. 1981; Bailey 1981), although stratigraphic control is poor. Existing PT estimates for the area suggest that the rocks of this unit exhibit a similar transitional greenschist-blueschist facies assemblage to the lithologically similar Yiti and Wadi Mayh-Al Khuryan units, peaking at 360-420°C and 7 ± 1 kbar (Goffé et al. 1988; El-Shazly et al. 1990; Searle et al. 1994).

The Hulw unit is separated from the As Sifah unit by a sequence of lower grade Saiq (?) formation carbonates containing Permian fossils (LeMetour et al. 1986) and characterised by a different deformational regime which are separated from the underlying higher grade separated by a major, arcuate, west dipping extensional detachment (Enclosure 1). The unit is dominated by large scale nappe structures and sheath folds in dolomitic limestones, white quartzose schists and extensive massive and schistose metabasic sills and flows. Metabasites are characterised by transitional blueschist-greenschist facies assemblages differing only from those found in the overlying ‘nappes’ by their greater degree of retrogression.

The southern limit of this unit is a north verging back thrust where Palaeozoic, low grade Amdeh quartzites overlie the rocks of the Hulw unit, and in general the metamorphic grade to the south of this boundary is inferred to decline rapidly (Lovelock et al. 1981; Goffé et al. 1988). Section restoration and balancing in the Wadi Hulw area could only produce a minimum shortening figure for, for the reasons already outlined. The calculated figure of ~75%

however emphasises the considerable deformation experienced during the creation and exhumation of this HP terrane.

4.3.4 As Sifah unit

The deepest structural units exposed in the Saih Hatat regional HP terrane occur in the east of the region, reflecting the overall westward dipping foliation of northern Saih Hatat, and reach eclogite facies conditions. Eclogites were first described and characterised by LeMetour et al. (1986) and exhibit peak conditions of 23 ± 2.5 kbar at 540 ± 75°C (Searle et al. 1994), although El-Shazly et al. (1997) proposed a lower peak pressure of 12-15 kbar, based on metapelite phase relations.

The remote coast around the village of As Sifah (Enclosure 1) exhibits massive outcrops of metabasic eclogite (sodic clinopyroxene-garnet-phengite-glaucophane-rutile-quartz), occurring as megaboudins up to 500 m in length (figure 4.15), as well as smaller lenses and thin layers within a variety of metasedimentary material, dominated by calcite-phengite-quartz schists (figure 4.14). The eclogitic protoliths remain unconfirmed but are assumed to be derived from basaltic units within the Permian Saiq formation, and the underlying quartzose schists from the Amdeh quartzite (LeMetour et al. 1986).

The first petrographic evidence for HP metamorphism in the As Sifah unit has been described from the latter quartzose schists. Wendt et al. (1993) described radial cracks around α-quartz inclusions in Fe rich garnet porphyroblasts and attributed them to the dilation of the quartz inclusions at low P during retrogression rather than the inversion of coesite to quartz.

The upper boundary of the As Sifah block has been widely taken as a low angle (~35°) detachment, clearly visible in the mountains above As Sifah (figure 4.14). Field mapping by Searle et al. (1994) identified this large scale shear boundary zone to the eclogite zone, the presence of which was confirmed by this study (Enclosure 1; Searle & Cox 1999). The lower grade homogeneous dolomitic limestones of the Wadi Mayh-Al Khuryan unit that overlie the rocks of the As Sifah unit have a basal banded calc-mylonite marking the detachment surface.

The internal structure of the As Sifah unit is complex (Enclosure 1) and is dominated by a number of high amplitude, low wavelength ENE-NE verging asymmetric isoclinal folds with a later generation of E-W trending isoclinal folds which were initially described by El-Shazly et al. (1990). New structural data collected during this study is summarised in figure 4.20. The structurally lower eclogite host schists to the east form a gently dipping anticlinal dome, with the majority of the eclogitic megaboudin outcrops exposed in its core. The degree of shortening and deformation implied by the observed structures in the section is high, although difficult to estimate due to the clearly ductile nature of the deformation.

The major detachment that forms the upper contact of the As Sifah unit dips to the west, typically at 35-40°. It defines a clear metamorphic break: the overlying dolomitic limestones of the Wadi Adai–Wadi Mayh–Al Khuryan unit have been estimated as culminating at ~9 kbar (Goffé et al. 1988; Vidal et al. 1992) and the underlying blueschist units estimated as reaching a peak pressure of 14-15 kbar by Michard et al. (1994) and Searle et al. (1994). This corresponds to the omission of ~25 km of crustal section, equivalent to a detachment surface-parallel displacement of ~40 km. Another structural discontinuity has been proposed (Searle et al. 1994) between the structurally lower, gently folded anticlinal dome that contains the calcite-phengite-quartz schists and the metabasic eclogites (metamorphic zone A of El-Shazly et al. 1990), and the structurally higher isoclinally folded blueschists and quartz ± garnet schists (Diqdah unit of Michard et al. 1994; metamorphic zone B of El-Shazly et al. 1990). No clear detachment surface was discovered in the field, but the contrast in structural style, dominant lithology and peak pressure between the units is suggestive of a tectonic contact.

However, the discovery during this study of fresh unaltered eclogite (sodic clinopyroxene-garnet-phengite-glaucophane-rutile-quartz), occurring as thin layers, intimately interbanded with Fe rich blueschist metapelites (phengite-quartz-epidote-albite-garnet-glaucophane) and quartz-phengite-garnet schists within the upper Diqdah unit (figure 4.19b) above Wadi As Sifah suggests the entire As Sifah unit peaked at eclogite facies.

A number of explanations may account for this observation: the adjacent Fe rich blueschist pelites and the metabasic eclogite may be co-facial, or preferential eclogitisation of metabasic horizons may have occurred due to fluid influx or the partitioning of deformation. Preferential retrogression between the largely unaltered, fresh eclogite and Fe metapelite is demonstrated by the presence in the latter of actinolite-chlorite pseudomorphs after glaucophane (figure 4.16a) and transfolial epidote porphyroblasts, while retrogression in the metabasite is limited to the alteration of garnet to chlorite-magnetite aggregates. However, the fine interlaying of the contrasting lithologies suggests that the primary control on assemblage was protolith composition. $^{18}O/^{16}O$ isotopic studies by El-Shazly et al. (1997) support this conclusion.

The structural history of the eclogitic As Sifah unit is complex. Field relations clearly demonstrate the existence of two major fabric forms events (D_1 and D_3), separated by a set of NNW-NE verging asymmetrical folds (D_2), which deform the regional D_1 schistosity, defined by HP mineral phases such as phengite and omphacite, and compositional banding. A crenulation cleavage is also patchily developed in some metabasic units, although only D_1 and D_2 are apparent in the metabasites. These units exhibit a variable degree of retrogression to greenschist facies assemblages. Crossite, epidote and albite are the dominant matrix minerals with chlorite and hematite pseudomorphs after garnet, and rims of actinolite amphibole occurring around glaucophane porphyroblasts.

The calcareous schists that form the bulk of the As Sifah unit show a widespread and well developed third fabric first noted by (Searle et al. 1994), defining a more spaced D_3 foliation, most clearly developed in the thick sequence of calcareous schists between the eclogite outcrops and the overlying postulated detachment (figure 4.18a and 19). Anastomosing shear bands form extensional shear band fabrics, similar to but distinct from S-C tectonites (Lister & Snoke 1984), in which the original schistosity surfaces (D_1 foliation planes) are disrupted by discrete later shear bands, forming an extensional crenulation cleavage which exhibits a top down to the NNE sense of shear. This is consistent with the movement sense on the overlying detachments, and implies the exhumation of the eclogite material, at least in part, by a process of crustal thinning by extension. The infilling of these late shear bands by greenschist facies phases such as chlorite implies that they formed under greenschist facies conditions.

Microstructural analysis of the As Sifah units has been reported by Searle et al. (1994) and demonstrates the two stage pre and post D_2 growth of zoned blue amphibole porphyroblasts in eclogite facies metabasites: the former with paler rims, and the latter with darker, more Fe rich rims. When close to extinction, these porphyroblasts exhibit 'ghosts' of relict matrix textures that serve to further differentiate the growth phases. The pre D_2 blasts show a clear relict basaltic texture consisting of randomly oriented laths (plagioclase?) whereas the post D_2 blasts show a coarse foliated (phengite?) texture. The latest structural-metamorphic event discernable at As Sifah is a minor extensional phase, represented by ubiquitous quartz-hematite ± calcite veins that trend consistently (figure 4.20a) NNW-SSE, produce greenschist facies (albite-epidote-actinolite) rich 'haloes' in the host mafic units, and imply extension normal to this (SSW-NNE), which suggests that these greenschist facies vein assemblages are related to the ubiquitous mineral stretching lineation found throughout the Saih Hatat terrane.

4.4 THERMOBAROMETRY IN THE AS SIFAH UNIT

PT estimates in eclogite facies material from the As Sifah area were poorly constrained until Searle et al. (1994) made use of the equilibrium

$$py + 2\ grs = 6\ di + 3\ Al_2Mg_{-1}Si_{-1}\ (\text{in phengite})$$

(Waters & Martin 1993), calibrated using the self consistent thermodynamic dataset of Holland & Powell (1990) and calculated using ECBAR96, a DOS program using the above geobarometer in conjunction with the Powell (1985) garnet-clinopyroxene geothermometer.

ECBAR96 employs a Monte-Carlo error-propagation technique to estimate the uncertainty on the PT estimate and to investigate the contribution of each mineral end member activity term to the overall result. With this technique, peak conditions of ~23 kbar and 540°C were estimated for the structurally lowest mafic eclogites in the As Sifah area. El-Shazly et al. (1997) used metapelitic phase relationships in conjunction with bulk geochemistry to suggest a peak pressure of ~15 kbar for the As Sifah unit.

The new results presented in table 4.1 have been obtained from some distance (~300 m) structurally above the coastal eclogite exposures and demonstrate the likelihood that the entire As Sifah unit was metamorphosed under the same eclogite facies conditions of ~20 kbar. The co-facial origin of the contrasting eclogite and blueschist facies assemblages in the As Sifah unit is also shown by the similar PT results obtained for these two assemblages, sampled from the same outcrop (figure 4.19b).

Table 4.1 As Sifah unit peak PT conditions calculated using THERMOCALC and ECBAR.

Sample	JC 122	ASB 1
Facies	Eclogite	Eclogite
Rock type	Metavolcaniclastic	Fe rich pelite
Peak assemblage	Omp-grt-phe-gln	Grt-gln-qtz-phe
Temperature °C		
Krogh (1988) garnet-clinopyroxene	377	
Ai (1994) garnet-clinopyroxene	373	
Ellis & Green (1979) garnet-clinopyroxene	468	
Powell (1985) garnet-clinopyroxene	442	
Pressure		
Rim garnet, ECBAR 96 (Waters & Martin 1993)	21.0 ± 1.5 kbar	
THERMOCALC v2.75 Holland & Powell (1998) Average PT mode		20.0 ± 1.7 kbar 467 ± 28°C

4.5 AGE OF HIGH PRESSURE METAMORPHISM IN NORTHERN SAIH HATAT

The exact timing of the Saih Hatat HP event is the major unresolved issue in the obduction and emplacement history of the Semail ophiolite, despite the publication of numerous geochronological studies of the terrane (Lippard 1983; Montigy et al. 1988; El-Shazly & Lanphere 1992; Searle et al. 1994; McMiller et al. 1999). The dating of the Saih Hatat HP

metamorphic event(s) remains controversial, with several models proposed, some of which require at least two phases of continental subduction and the presence of previously unknown Tethyan microplates (eg El-Shazly & Lanphere 1992), to account for the wide range (130-80 Ma) of $^{40}Ar/^{39}Ar$ and K/Ar ages published. No age determinations using other systems, such as U-Pb (monazite, titanite) or Sm-Nd/Lu-Hf (garnet) have been successfully employed.

Recent evidence (Hacker et al. 1996) has dismissed much of the existing data as unreliable due to the presence of excess lattice Ar in analysed phengite and glaucophane grains, producing discordant or disturbed profiles. Estimates of the Ar closure temperature in white micas vary between 350-450°C, well below the accepted peak temperature of ~550°C in the As Sifah eclogites (Searle et al. 1994; El-Shazly et al. 1997) and therefore none of the published ages can be interpreted as crystallisation ages. The only plateau yielding muscovite $^{40}Ar/^{39}Ar$ spectrum obtained from the entire Saih Hatat HP terrane, from the As Sifah eclogites, gave an age of 96 ± 2 Ma (Searle et al. 1994). This may be contrasted with a mean $^{40}Ar/^{39}Ar$ age of 93.5 ± 0.1 Ma for HT sole metamorphism in the adjacent Wadi Tayin area (Hacker et al. 1996). In the northern mountains, the mean age of sole metamorphism is 94.9 ± 0.2 Ma.

This suggests that the HP metamorphism was roughly coeval with the formation of the ophiolite and the metamorphic sole, and that the HP event was synchronous with the HT metamorphism characteristic of the sole, and was not due to earlier (~130-110 Ma) continental subduction (El-Shazly & Coleman 1990; El-Shazly & Lanphere 1992) or coeval with the final emplacement of the ophiolite onto the Arabian passive margin at ~80 Ma (El-Shazly & Lanphere 1992; Michard et al. 1994).

McMiller et al. (1998) used new $^{40}Ar/^{39}Ar$ data, which ranged in age widely from 130-75 Ma, only to conclude that there was a series of cooling events, possibly at depth, within the subducted continental margin in the 95-82 Ma period, followed by further deformation at low structural depths synchronous with the subaerial erosion of the overlying ophiolite at ~70 Ma. Material from the As Sifah units yielded unreliable cooling ages ranging from ~119-82 Ma. Hacker (1999, pers. comm.) has been unable to produce satisfactory $^{40}Ar/^{39}Ar$ plateau ages from the As Sifah eclogites.

None the less, in the absence of conflicting data, the only $^{40}Ar/^{39}Ar$ age (80.2 ± 0.8 Ma; El-Shazly & Lanphere 1992) for the Ruwi mélange suggests that (a distinct?) HP metamorphism was occurring at the same time as the ophiolite was emplaced onto the continental margin and the low grade HP material at least may not be part of the normal subophiolitic sole that has undergone a HP event. Furthermore, petrographic evidence from the limited metamorphic sole outcrops preserved at the base of the Muttrah ophiolite (Rabu 1987; Gnos 1993), in the form of crossite rims to hornblende, suggests that the development of HP assemblages *post dated the peak of sole metamorphism* in northern Saih Hatat. Whether this HP overprint assemblage was coeval with the eclogite facies metamorphism or later, lower grade HP

assemblages, exposed in the Ruwi mélange and with Santonian (83.5-89 Ma) protoliths (Searle et al. 1994), is unresolved.

4.6 BRIEF REVIEW OF UHPM AND THE EXHUMATION OF HP MATERIAL

The term *ultra high pressure metamorphism* (UHPM) is generally taken to refer to the processes that produce metamorphic assemblages characterised by the presence of the high pressure SiO_2 polymorph coesite, which requires a formation pressure of ~28 kbar (equivalent to burial to ~100 km) at ~700°C. Although coesite and diamond have long been recognised in mantle derived kimberlite material, meteorites and impact craters, they have only recently been described from demonstrably crustal material. Such material is found in globally distributed collisional zones of varying age and morphology, which suggests that the subduction and subsequent exhumation of continental rocks from mantle depths is not uncommon. Although the Saih Hatat terrane does not exhibit in its assemblages the coesite that characterises UHPM, the controversies and issues surrounding the formation, preservation and exhumation of global examples of extreme HP metamorphism of crustal material are of considerable relevance to the Saih Hatat terrane and these issues are summarised here.

Chopin (1984) first described coesite in crustal rocks, as inclusions in pyrope mega blasts, from a quartzite forming part of the Dora Maira massif of the western Italian Alps. Subsequently, coesite has been confirmed in the Western Gneiss Region of the Norwegian Caledonides (Smith 1984), various localities in the former USSR, and most extensively from the Dabie Shan range of central China (Okay et al. 1989; Wang et al. 1989).

A comparative overview of Saih Hatat and other known occurrences of UHPM material is presented in table 4.2. Initial work characterising and describing the petrographic, geochemical, structural, and regional affinities of UHPM rocks has been supplemented by more recent work on the exhumation of these terranes. Models based on both theoretical analysis (Platt 1987, 1993) and field observation based techniques (Andersen & Jamviet 1990; Avigad 1992; Okay & Sengor 1992; Searle et al. 1994) have been presented.

There are a number of clear similarities between globally distributed UHPM terranes, both in physical details and in problems and controversies relating to their interpretation. The spatial extent and volume of such terranes is often difficult to delineate, due to generally extensive retrogression and overprinting of the peak assemblage (the grade of which can vary from granulite through amphibolite to greenschist). Apparent contrasts in grade between intimately juxtaposed metabasic units, which seem to better preserve UHPM assemblages, and metapelitic or felsic units which may only contain microscopic relics of their former

assemblage, are widespread within many terranes and have been controversial in the generation of exhumation models for UHP terranes.

Until the discovery of armoured relics of UHP phases within metapelitic or granitic 'country rock' gneisses (eg Chopin 1984), it was widely believed that the metabasic eclogites, which characteristically occur as boudins within felsic or metasedimentary gneisses, or as blocks within a serpentinite mélange, were tectonically emplaced. However, the recognition of UHP assemblages and textures in these country rocks has led to the search for alternative exhumation mechanisms for entire terranes, rather than for small discrete metabasic blocks. Furthermore, the very highly deformed nature of such rocks implicit in their preservation often precludes any accurate estimate of the thickness of the terrane.

Table 4.2 Features of the Saih Hatat HP terrane and other well described global examples.

	Saih Hatat, NE Oman	Western Gneiss Region, Norway	Dabieshan, China	Dora Maira massif, Western Alps	Kokchetav, Russia	Bohemian massif, Europe
Protolith age	Permian continental shelf limestones, dolomites and basaltic sills	Proterozoic gneisses (1600 Ma- 1800 Ma)	Archean to Proterozoic gneisses	Permian (Variscian) sediments (350-300 Ma)	Archean to Proterozoic gneisses (1800 Ma- 2600 Ma)	550-600 Ma Cadomian?
Regional UHPM assemblages	cal-phe-qtz; omp-grt-gln-phe; gln-grt-qtz-phe-ab	grt-cpx-kfs-ky-pl-qtz	pl-qtz-hbl-bt-phe-kfs-grt	ab-kfs-phe-bt-qtz-grt	pl-qtz-hbl-bt-grt-phe	Variable
Age of UHPM	96 ± 2 Ma ($^{40}Ar/^{39}Ar$), 89.3 ± 1.5 Ma (K-Ar ms cooling age) (Searle et al. 94)	437-33 Ma (K-Ar cooling age)	218 Ma (U-Pb)	Controversial; ~100Ma ($^{40}Ar/^{39}Ar$), ~39Ma (U-Pb)	530 Ma (U-Pb, Sm-Nd)	350-400 Ma
Peak UHPM PT conditions	23 ± 2.5 kbar 540 ± 75°C	32 ± 5 kbar 800 ± 100°C	28 kbar 690 ± 90°C	37 kbar 800°C	40 kbar 1000°C	13-20 kbar 650-880°C
Tectonic event	Subduction-obduction during emplacement of Semail ophiolite onto Arabian passive margin	Caledonian orogeny; continental collision between Europe and America	Collision of Sino-Korean craton with Yangtze craton	Alpine orogeny; collision between Europe and Apulian microcontinent	Caledonian orogeny, collision of Kokchetav massif with central Kazakhstan	Variscian orogeny collision of Laurasia with Gondwana 320-400 Ma
Exhumation timescales	Approximate duration 25 Ma @ ~3.5 mm yr^{-1}	Approximate duration 80 Ma @ 1.4 mm yr^{-1}	Approximate duration 100 Ma @ 1.3 mm yr^{-1}	Approximate duration 40 Ma @ 2.5 mm yr^{-1}	Approximate duration 72 Ma @ 1.8 mm yr^{-1}	Approximate duration 100 Ma @ 1.4 mm yr^{-1}
Extent of terrane	30 x 20 km (3×10^3 km^3)	350 x 150 km (2.1×10^6 km^3)	450 x 100 km (4.5×10^6 km^3)	200 x 75 km (6×10^5 km^3)	300 x 150 km (1.8×10^6 km^3)	100 x 50 km (3×10^3 km^3)

The PT conditions of formation implied by UHP mineral assemblages are both extreme and unusual; thermobarometry indicates typical temperatures of ~700°C at 100 km in UHP terranes, compared with 1000°C at a similar depth under a normal crustal geotherm (Pollack & Chapman 1977). Such depressed lithospheric isotherms are characteristic of subduction zones. The preservation of such low temperatures during exhumation is more problematic, with the majority of thermal models (eg England & Richardson 1977) suggesting that exhumation must be accompanied by a degree of heating, which should replace the eclogite assemblages with granulite facies minerals.

Buoyancy contrasts and hydrodynamically driven return flow have only a limited role in the exhumation of large packages of crustal material from depths greater than 20 km (Platt 1987). Such models may however be valuable in smaller terranes such as northern Saih Hatat, particularly considering the occurrence of high ρ eclogite metabasites as megaboudins within low viscosity, low ρ carbonate rich country rock. Numerous authors have suggested alternative exhumation models, which generally fall into three distinct categories:

1. Models emphasising intracontinental thrusting, combined with later erosion (Avigad 1992; Okay & Sengor 1992).
2. Models emphasising orogenic collapse, accompanied by low angle extensional faulting (Andersen & Jamtviet 1990).
3. Models emphasising initial continental subduction and rapid extensional exhumation to mid crustal depths, followed by slower erosion (Searle et al. 1994; Michard et al. 1994; Chemenda et al. 1996; Gregory et al. 1998).

Postulated formative and exhumation models for the Saih Hatat terrane are shown in figures 4.21-23. It is possible to conclude from the described UHPM terranes and the invoked preservation mechanisms that:

1. UHPM protoliths tend to be supracrustal.
2. UHPM rocks form in a collisional tectonic environment by rapid subduction.
3. Low geothermal gradients define the PT regime of UHPM assemblages, and exhumation rates must exceed rates of thermal equilibration for UHPM assemblages to be preserved.
4. Possible driving mechanisms of the subduction regime necessary to produce UHPM conditions include the presence of a thickened lithospheric mantle, slab pull forces, or the eclogitisation of crustal roots.

5. The density of UHPM material is a fundamental control on exhumation processes and rates and is controlled by deformation and composition (a function of P, T, fluid volume and compositional rheological variations).
6. The widespread occurrence of structures such as low angle extensional faulting, the excision of thick sections of crust and the presence of complex folding and ductile shearing in many UHPM terranes suggests a common exhumation mechanism.

The HP rocks of northern Saih Hatat are particularly important in contributing to the understanding of the mechanisms that exhume crustal material from depths of ~100 km. Northern Saih Hatat is characterised by a wide area of well exposed intermediate crustal levels and detailed structural mapping (Searle et al. 1994; this study) has demonstrated the presence of boundary faults and shear zones, which are poorly preserved in other UHPM terranes. Large scale structures in the northern Saih Hatat HP terrane mirror those in other well described UHPM terranes and include distinct metamorphic breaks, the presence of low angle extensional faulting, and large scale ductile shear zones.

4.7 DISCUSSION

The northern part of the Saih Hatat window, NE Oman, is characterised by an incomplete HP metamorphic profile through an exhumed portion of Arabian continental crust, which was subducted to depths of ~80 km during the obduction of the Semail ophiolite in the late Cretaceous. New structural mapping and analysis demonstrates some similarities in structural style and metamorphic regime between Saih Hatat and classic continent-continent HP terranes such as the western Alps and Sino-Korean collision zones. The Saih Hatat terrane is unique in preserving the record of continental subduction beneath an obducting ophiolite. Eclogite barometry in the As Sifah region of the southern Oman mountains has demonstrated the subduction of the Arabian continental passive margin to depths of ~80 km beneath the Semail ophiolite (Searle et al. 1994).

A new synthesis of all the available structural, geochronological and metamorphic data, from this study and from published work, is used to produce a model to account for the formation, exhumation and present day occurrence of HP rocks in the Saih Hatat window. This is proposed to have occurred in two distinct stages, with a rapid initial exhumation due to relative extension in the subduction zone hanging wall and driven by buoyancy contrasts, followed by a slower erosion and crustal extension dominated phase.

Structural mapping in the northern part of the window has shown that tectonometamorphic units, characterised by distinct metamorphic mineral assemblages and

structural styles, are bounded by diffuse extensional shear zones or discrete detachments that can be shown to have juxtaposed during exhumation material originally separated by up to 50 km of original crust. The structures within individual tectonometamorphic units are truncated by the detachments and predate final exhumation.

The Saih Hatat HP terrane comprises two major structural levels, the As Sifah-Wadi Hulw-Rija unit, and the Wadi Adai-Wadi Mayh-Al Khuryan unit, separated by a major, largely west dipping ductile extensional detachment with some evidence of late brittle motion in the development of minor mélanges. Each structural domain is characterised by a distinct metamorphic assemblage and structural evolution, and the contemporary distribution of the two structural domains is controlled by interference between an early N-S trending, E verging and a later NW-SE trending folds (Enclosure 1).

The As Sifah, Wadi Hulw and Rija units have been tentatively linked together in the enclosed map and section (Enclosure 1) and ascribed to the same structural unit on the basis of their very similar lithological units and proportions, and, in the As Sifah and Rija outcrops at least, apparently very similar microstructural development. This assessment is a departure from the structural model of Searle et al. (1994) and Searle & Cox (1999), which suffers from a distinct geometrical space problem, and instead leans towards the model of McMiller et al. (1999). While the apparent absence of earlier higher grade assemblages in the metabasites in the lower Wadi Hulw area (Enclosure 1), and some structural observations, remain antithetic to this interpretation, there is some evidence for the presence of earlier higher grade assemblages in the Wadi Hulw metabasites (Goffé et al. 1988) and it is possible that the two units, while representing the same structural units, did peak at different depths and have been repeated and (apparently) juxtaposed by some deeper, westerly directed detachment that remains unexposed.

The higher grade, structurally lower As Sifah-Wadi Hulw-Rija unit reached peak metamorphic conditions of ~20 kbar and ~500°C in metabasic, metavolcaniclastic, semi-pelitic and carbonate material derived from the Palaeozoic Amdeh quartzites and Permian Saiq formation shelf carbonates of the Arabian continental margin, and form co-facial intercalated eclogite-blueschist units (El-Shazly et al. 1997). Metabasic material in the Wadi Hulw and Rija areas does not preserve eclogite facies assemblages but this may be a result of the pervasive retrogression in these areas rather than an indication of substantially lower peak conditions (Searle et al. 1994; McMiller et al. 1999) in structurally equivalent units, and Goffé et al. (1988) noted the presence of pseudomorphs after garnet in metabasites of the Wadi Hulw area. Metabasic boudins up to ~1 km in extent in the As Sifah area preserve eclogite facies assemblage metamorphic fabrics (S_1) oriented E-W and crenulated by asymmetric isoclinal folds (S_2) that verge northwards and parallel major nappes in the As Sifah unit (figure 4.16c, enclosure 1). Major ductile extension, largely partitioned into the carbonate schist of the As Sifah and Rija units, forms D_3 extensional shear band fabrics (Searle et al. 1994; figure 4.18a)

with shear bands composed of greenschist facies assemblages that indicate top down to the NE relative extension.

A later D_4 event is represented by greenschist facies assemblage in filled veins implying NNE-SSW extension, parallel to, and possibly synchronous with, the development of widespread mineral stretching lineations in all assemblages. The similarity in PT estimates (~7 kbar, 550°C) for the post peak greenschist facies events in the As Sifah and Wadi Hulw areas (Searle et al. 1994) suggests that these domains equilibrated at similar structural level during their exhumation at least.

The lower grade, structurally higher Wadi Adai-Wadi Mayh-Al Khuryan unit reached peak metamorphic conditions of ~7-8 kbar and ~300°C (Goffé et al. 1988; Vidal et al. 1992) in largely metabasic and metacarbonate material derived largely from the Saiq formation and other Mesozoic carbonate shelf sequence components of the Arabian continental margin. At high structural levels, these units are characterized by generally north dipping ductile shear zones with a top to the south sense of shear, well seen in upper Wadis Mayh, Hulw and Adai which truncate major recumbent folds (figure 4.10). At lower structural levels, as in the Wadi Mayh gorge, intense mylonitisation, sheath folding and out of sequence thrusting in recrystallised carbonates (figure 4.11 and 12) are common.

The Ruwi mélange may represent the result of a later stage in the evolution of the Saih Hatat HP terrane, and has a $^{40}Ar/^{39}Ar$ cooling age of 80.2 ± 0.8 Ma (El-Shazly & Lanphere 1992) which is substantially lower than the best estimate of the eclogite facies metamorphism of 96 ± 2 Ma (Searle et al. 1994) but similar to estimates of the age of nappe formation in the Wadi Adai-Wadi Mayh-Al Khuryan unit, which has similar peak conditions (McMiller et al. 1999). Initially correlated with the Santonian (83.5-89 Ma) Muti formation, a syn-depositional foreland basin deposit of the Aruma Group, by Glennie et al. (1974) and Robertson (1987a), the mélange was more recently ascribed to the Haybi trench fill mélange sequence by Searle & Cox (1999). The mélange units are folded into a series of open folds, with a wavelength of ~2 km and an amplitude of ~500 m, the axes of which plunge about 20° to the NE (figure 4.5a).

The first major fabric forming event (D_1) is defined by the orientation of phyllosilicate laths and quartz rods in schists (S_1). The NNE-SSW oriented mineral stretching lineation, defined by lawsonite and carpholite, is assumed to have been synchronous with the peak of the greenschist-blueschist facies metamorphism. Small amplitude upright open folds with sub vertical fold axial planes and axial traces trending N-S define D_2. Locally associated with these folds is a steeply dipping axial planar cleavage (S_2) forming microfolds in S_1. A later phase of deformation is characterised by kink banding, the asymmetry of which suggests a top to the NNE sense of shearing.

Intra-oceanic subduction resulted in the formation of the ophiolite metamorphic sole at ~94-95 Ma (Hacker et al. 1996), characterised by higher temperatures and lower pressures of metamorphism, and the generation of granitoid melts at the subduction front whereas, to the

south, the subduction of a continental promontory (Searle et al. 1994; Hacker & Gnos 1997) led to higher pressures and lower temperatures of metamorphism at the same time as the formation of the metamorphic sole. These two processes, involving distinct source materials and different tectonometamorphic regimes, cannot have occurred together in a single subduction zone and hence it is proposed that there were two coeval NE dipping subduction zones during the mid-late Cretaceous in the Oman area: an intra-oceanic subduction zone, along which the metamorphic sole formed and the ophiolite was initially obducted, and a more proximal, deeper subduction zone in which the Arabian passive margin carbonate shelf and basement was subducted to, and exhumed from, a depth of ~80 km. Both Searle et al. (1994) and Hacker & Gnos (1997) suggest that the margin of the Arabian continent may have been irregular, with the Saih Hatat terrane protoliths forming a promontory.

4.7.1 Exhumation rates and mechanisms

It is proposed that a combination of initial deep level thrusting followed by later high level tectonic thinning, facilitated by extensional faulting, is the most likely mechanism of HP rock exhumation in northern Saih Hatat. The new structural and petrographic material presented in this chapter, coupled with existing geochronological data, has shown that exhumation of the As Sifah units was accompanied by top to the NE (relative) extension, with the development of major recumbent nappe structures that truncate earlier fabrics formed under peak conditions.

Estimation of the exhumation rates of the As Sifah eclogites and other components of the Saih Hatat HP terrane are key to any model of the tectonometamorphic evolution of the terrane, and can be used to constrain a PTt path for the As Sifah unit of the terrane (figure 4.24). A minimum age of exhumation is constrained by the onlap of ~68 Ma Maastrichtian neoautochthonous limestones onto the blueschist facies components of the terrane (Goffé et al. 1988). While the following calculations utilise imprecise $^{40}Ar/^{39}Ar$ geochronological data, they can at least give an estimate of the range of exhumations rates and therefore perhaps processes undergone by the Saih Hatat HP terrane.

While the PT conditions and age of the eclogite facies metamorphic peak are relatively well constrained at 23 ± 2.5 kbar, 540 ± 75°C (equivalent to an average crustal geotherm of ~7°C km^{-1}) and 96 ± 2 Ma respectively (Searle et al. 1994), the exhumation path is less well known in time and space. Searle et al. (1994) used THERMOCALC and its associated self consistent thermodynamic dataset (Holland & Powell 1998) to infer a post peak greenschist facies retrogressive assemblage at 6.5 ± 1.5 kbar, 550 ± 100°C in the As Sifah eclogites, implying near isothermal decompression during initial exhumation.

However, the age of this greenschist facies overprint of the HP assemblage is unclear. Nonetheless, the widespread occurrence of a similar retrograde assemblage throughout the amphibolite-granulite facies sub ophiolitic metamorphic material of the Semail ophiolite allochthon suggests that a correlation between existing greenschist event age constraints of 91.2 ± 0.5 Ma (Gnos & Peters 1993), and to a *maximum* of 93.7 ± 0.8 Ma in the Wadi Tayin area (Hacker et al. 1996) may be appropriate.

Fission track dating of the As Sifah eclogites further imply that the eclogites did not cool below ~210°C until 68 ± 2 Ma, although the lower grade Ruwi mélange had cooled to ~210°C by 80 ± 8 Ma (Saddiqi et al 1995). If the crustal geotherm by this time had increased from a value of ~7°C km^{-1} at the peak of metamorphism towards a more 'normal' value of ~15°C km^{-1} by the Maastrichtian due to thermal relaxation, then a temperature of ~210°C implies a pressure of ~3.5 kbar.

This data can be used to calculate an exhumation rate between the metamorphic peak at 96 ± 2 Ma and inferred attainment of greenschist facies conditions (at ~91 Ma) of ~12.5 mm yr^{-1} assuming a crustal density of 2.75 g cm^{-3}. If this exhumation was accommodated along the extensional detachment that juxtaposes eclogites against lower grade material at an angle of ~40°, then motion along this detachment occurred at ~20 mm yr^{-1}. Subsequently, between ~91 and 68 Ma, an exhumation rate of ~0.5 mm yr^{-1} is implied, using the same crustal density and assuming attainment, by thermal relaxation, of a near normal crustal geotherm of ~15°C km^{-1} by 68 Ma.

Alternatively, McMiller et al. (1999) reported new data that suggest greenschist facies white mica, associated with chlorite, albite and epidote in retrogressed mafic schists from As Sifah, had cooling ages of 79-82 Ma, equivalent to a lower exhumation rate for the As Sifah units of ~3.75 mm yr^{-1} between 96 and ~80 Ma. Since Searle et al. (1994) noted that the greenschist facies retrogression of the As Sifah units formed at a similar temperature to the HP assemblage, the McMiller et al. (1998) data used here cannot be interpreted as marking the age of the greenschist facies assemblage development, and the calculated figure of ~3.75 mm yr^{-1} should be regarded as a minimum. The ophiolite metamorphic sole, in contrast, was exhumed at a similar peak rate (*Chapter Three*) but at a lower average rate of 3.5-4.5 mm yr^{-1} (Gnos 1998) integrated over the same period.

4.7.2 Post tectonic evolution

The post tectonic evolution of the Saih Hatat terrane may be defined as its post Maastrichtian, post ophiolite emplacement evolution. Carbonate sedimentation in the Oman area continued from the Maastrichtian until the Miocene, when extensive regional deformation

began (Glennie et al. 1974; Searle et al. 1983). The regional extent and consistency of orientation of the structures between the major windows of Saih Hatat and Jebel Akhdar suggest they formed coevally during the post-Eocene period. In northern Saih Hatat, neoautochthonous carbonates in the Ra's Al Hamra area (Enclosure 1) exhibit gentle upright folding trending N-S, normal to the strike of the Saih Hatat culmination.

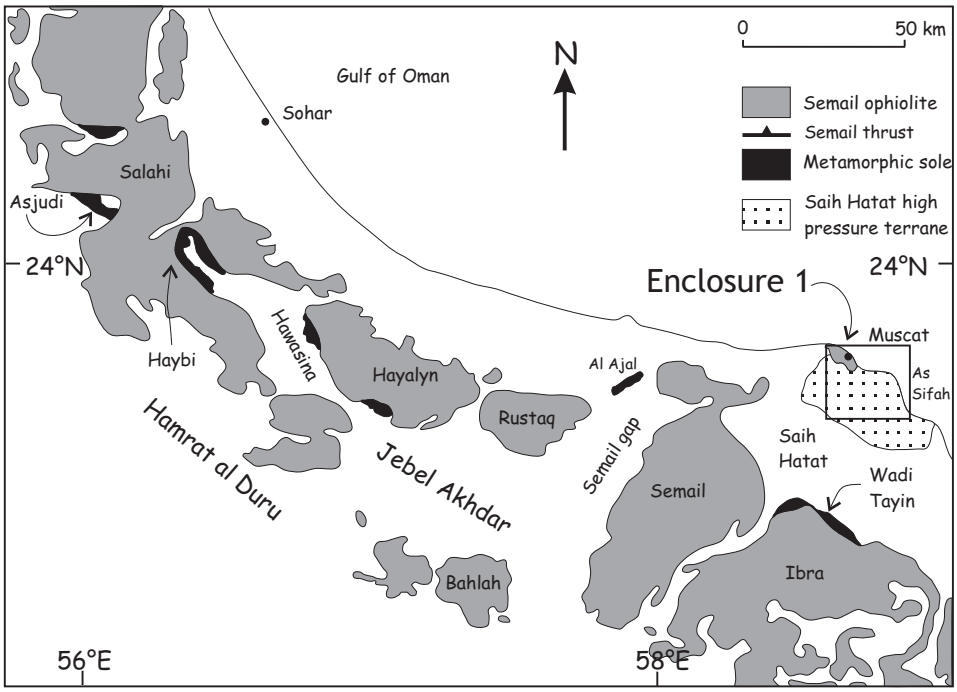


Figure 4.1 Geological sketch of the SE Oman mountains showing the extent and position of the Saih Hatat high pressure metamorphic terrane beneath the Semail ophiolite. A detailed geological map of

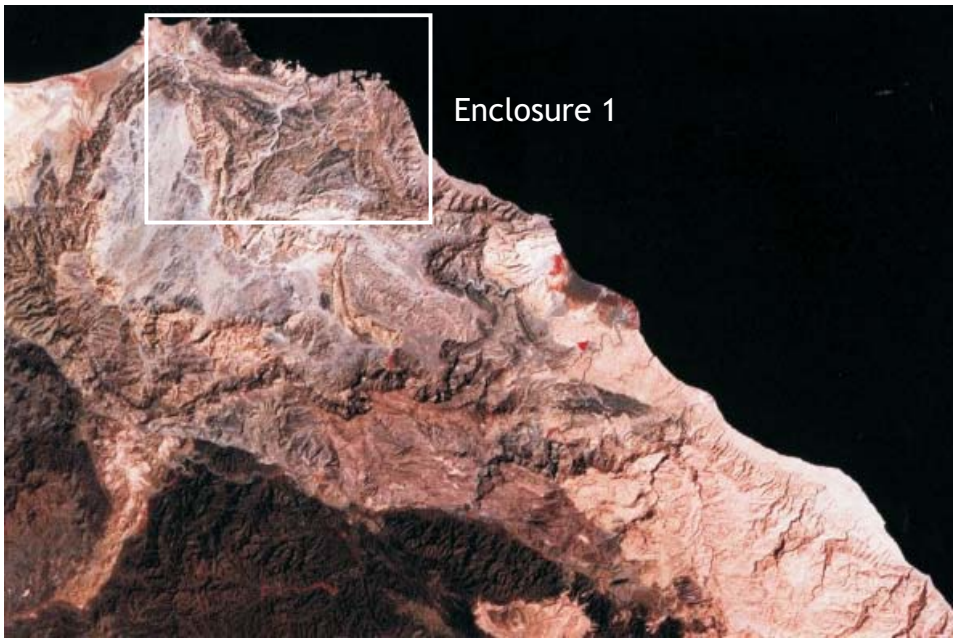


Figure 4.2 Landsat image of the Saih Hatat area of the SE Oman mountains and the Gulf of Oman, with north at the top. The SW part of the image shows the dark, serpentinised harzburgites of the Ibra and Semail blocks of the ophiolite mantle sequence. The small outcrop of ophiolite around Muscat on the Gulf of Oman is the Muscat-Mutrah ophiolite. The SE part of the image, around Quryat, is covered by pale yellow carbonates of the Maastrichtian-Tertiary neoautochthonous cover sequence. The margin of the Saih Hatat window consists in the W and S of largely low grade and weakly deformed Mesozoic shelf carbonates which in the NE, adjacent to the coast, are complexly deformed and metamorphosed at eclogite facies conditions of >20 kbar (Searle et al. 1994). The low relief core of the Saih Hatat window comprises a thick sequence of weakly deformed, greenschist facies Palaeozoic



Figure 4.3 Aerial view, centred over Ruwi and looking SE, of the highest grade (blueschist-eclogite facies) and structurally deepest parts of the Saih Hatat high pressure terrane. The prominent NW-SE ridge is a late normal fault, shown on the map of the Ruwi mélange (enclosure 2), downthrowing to the NW and separating the dark Muscat ophiolite (left, NW) and its neoautochthonous Maastrichtian-Palaeocene shallow marine carbonate cover from the greenschist-blueschist facies (Goffé et al. 1988) Mesozoic shelf sequence carbonates of the Wadi Adai-Wadi Mayh-Al Khuryan unit of the Saih Hatat terrane (right, SE). Wadi Mayh is visible in the centre of the image, draining into the Gulf of Oman at Khawr Yiti. Beyond Wadi Mayh lies the Wadi Hulw and As Sifah unit of the terrane which is characterised by more common metabasic material whose grade culminates at eclogite facies at As

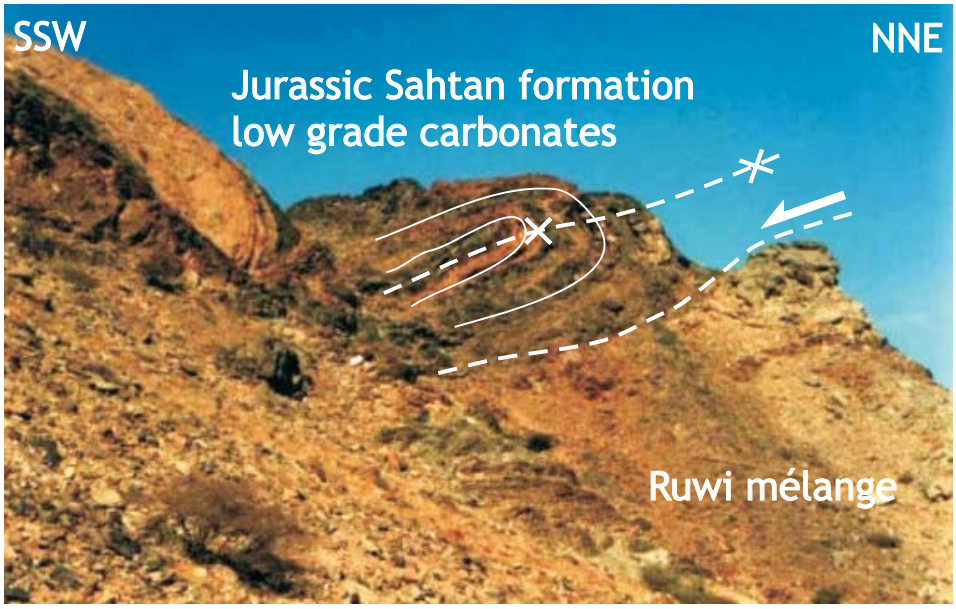


Figure 4.4 View of major NNE vergent recumbent syncline within a klippe of low grade Jurassic (Sahtan formation) carbonates, which are separated from the structurally lower Ruwi mélange by a low angle extensional fault (see enclosure 2). The Ruwi mélange consists of largely metapelitic material forming gentle upright NE plunging folds and contains index minerals including carpholite

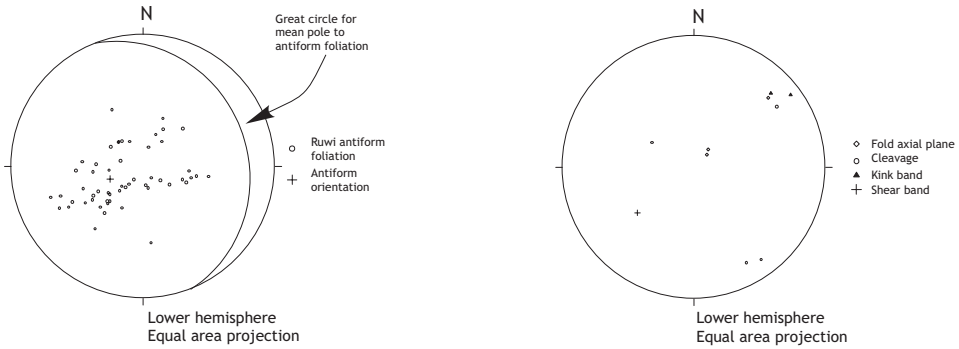


Figure 4.5 a) Stereonet showing the variation of S_1 fabrics around the shallow plunging, upright, major NE oriented Ruwi mélange structures. See enclosure 1. b) Stereonet showing the orientation

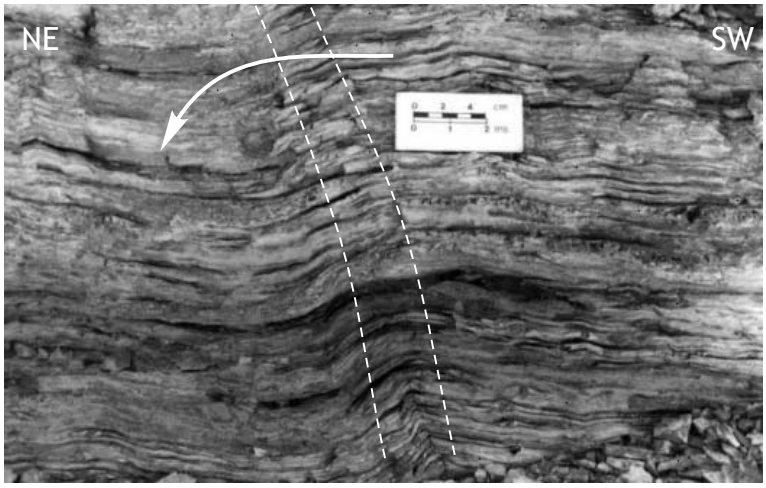


Figure 4.6 Kink band, showing top to the NE shear sense, in lawsonite schists of the Ruwi mélange.

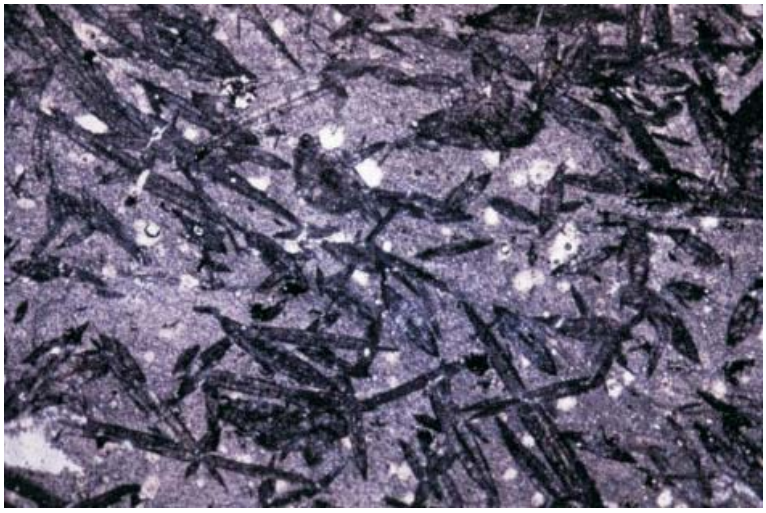


Figure 4.7 Thin section view of the lawsonite bearing schist shown in figure 4.6. Porphyroblasts of lawsonite are aligned to form a NNE-SSW mineral stretching lineation that postdates the development

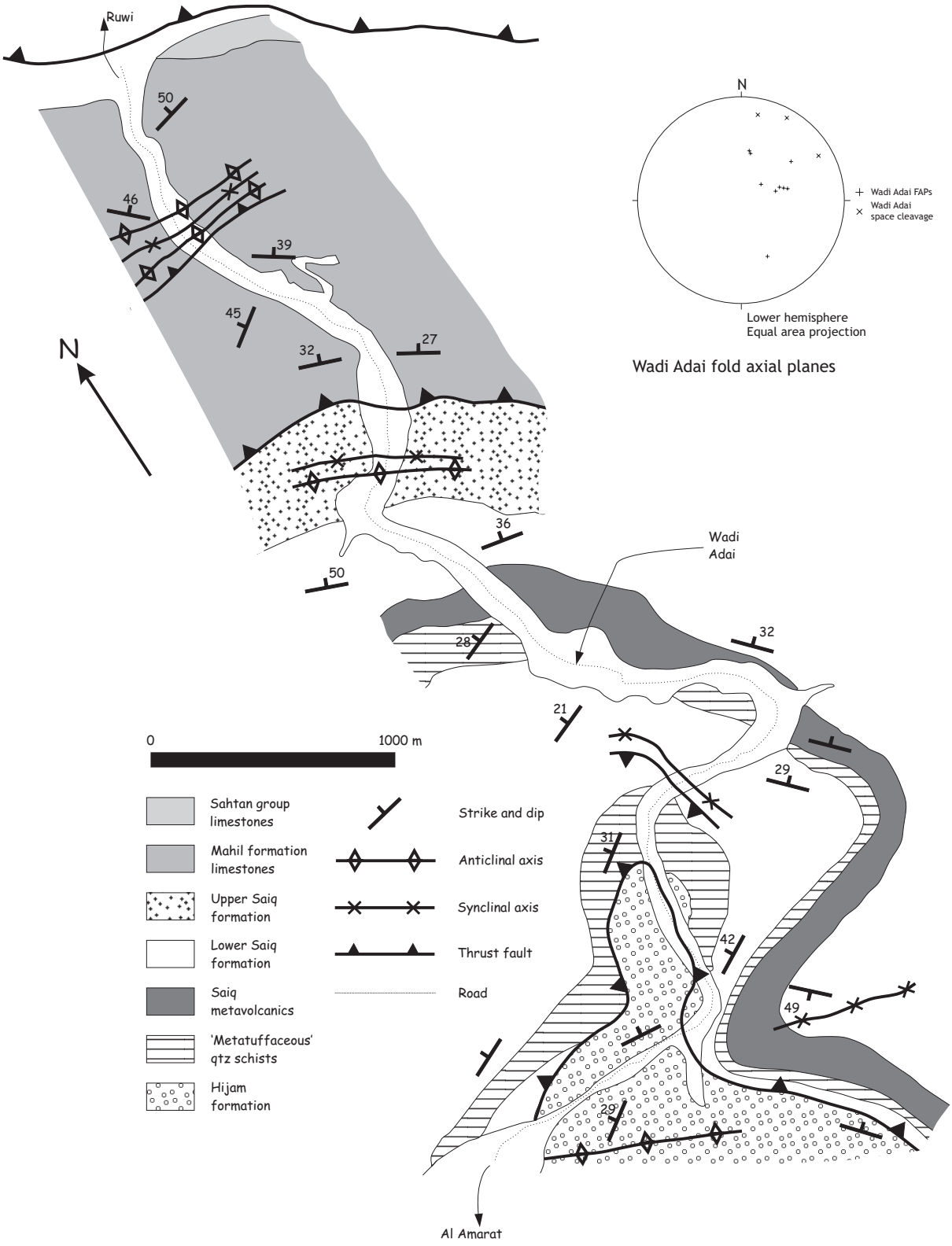


Figure 4.8 Geological sketch map and structural data for the Wadi Adai section through the Saih Hatat high pressure terrane. The location of this map area is shown on enclosure 1, and a cross section is shown in figure 4.9. Similar structural levels are exposed in the northern part of Wadi Mayh (see enclosure 3).

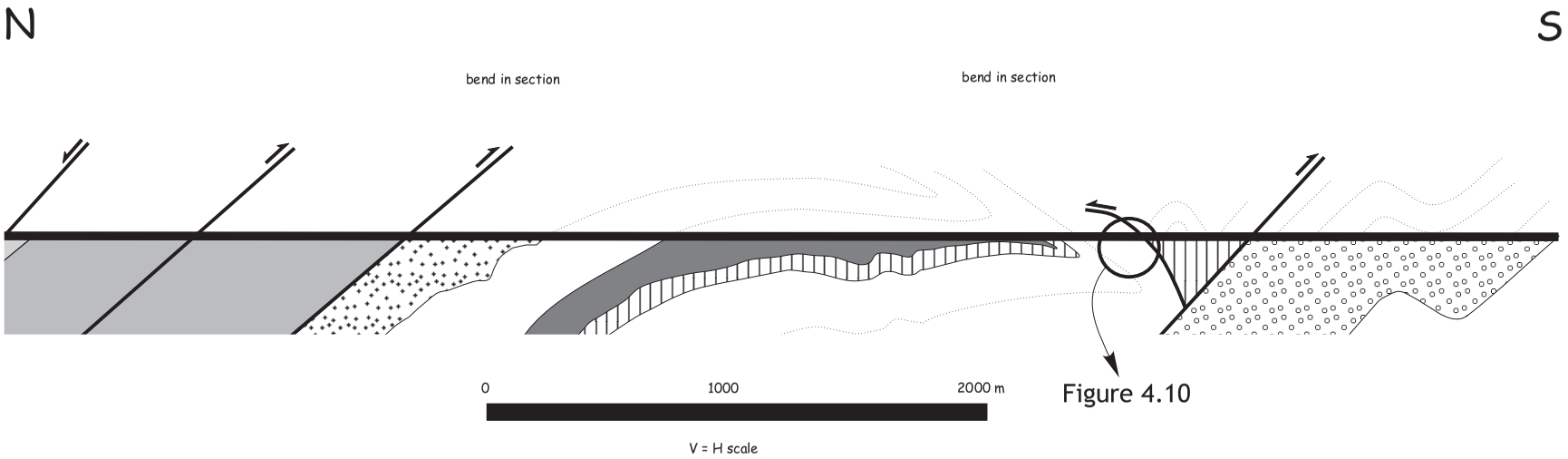


Figure 4.9 Section through the Saih Hatat high pressure terrane in the Wadi Adai area. See figure 4.8 for legend and line of section. Compare with the northern part of Wadi Mayh, which exhibits the same structural units ~20 km along strike.

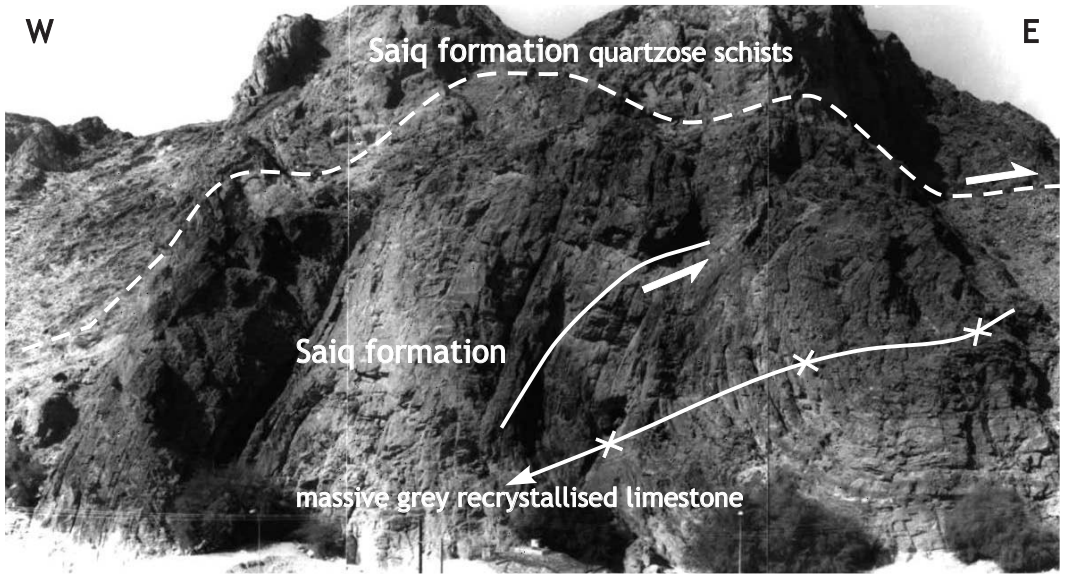


Figure 4.10 Recumbent syncline with SW plunging axial trace in massively bedded, recrystallised limestones of the Permian Saiq formation, Wadi Adai. Note also the overturned minor thrusts within the limestones. NE directed back thrusting has placed quartzose schists, ascribed to the Permian by LeMetour et al. (1990) but more likely derived from the Palaeozoic Amdeh quartzites, over Permian carbonates. See figure 4.9 for photo location; 5 m telegraph pole for scale.

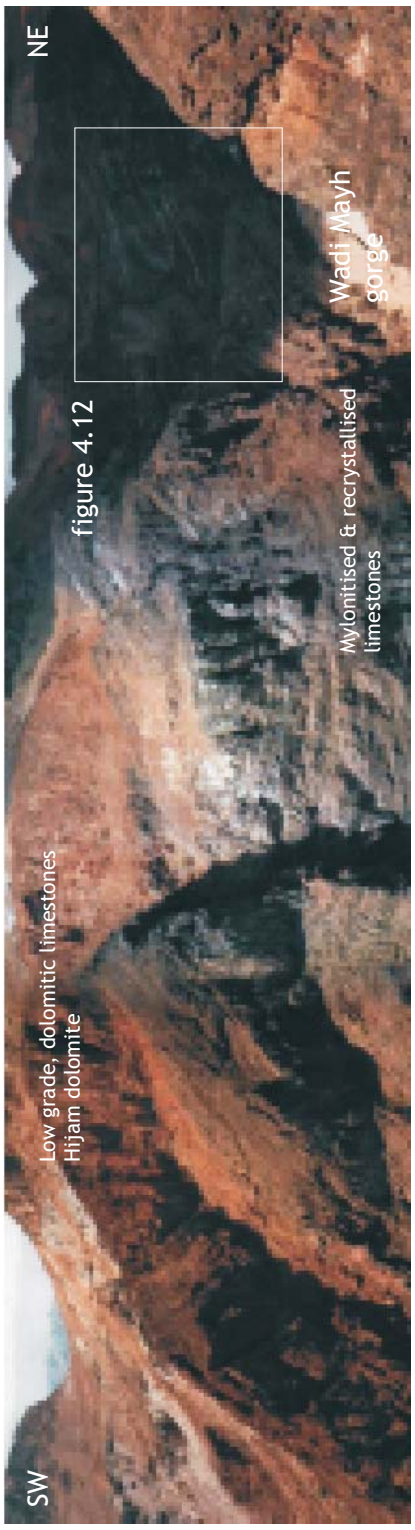




Figure 4.12. View looking NE from the base of the gorge and showing large scale recumbent folds and out of sequence thrusting in mylonitic (?) Permian Saiq formation carbonates. See enclosure 3 for an interpretation of the structures.



Figure 4.13. Small scale (~10 m), SW directed duplex complex in greenschist-blueschist facies (Goffé et al. 1988) Triassic Mahil limestones, northern Wadi Mayh. This SW directed structure is parallel to the allochthon emplacement direction and predates the widespread NE directed, exhumation related structures seen in the Saih Hatat terrane.

Figure 4.11 Panorama of the gorge section of Wadi Mayh, looking NW and showing reddish dolomitic limestones of the Hijam formation thrust NE over mylonitic and heavily deformed and thrusted carbonates of the (?) Permian Saiq formation which represent the structurally lowest and most deformed parts of the greenschist-blueschist (Goffé et al. 1988) facies Wadi Adai-Wadi Mayh-Al Khuryan unit. See figure 4.12 for detailed view of the structurally lower carbonates of the gorge, and enclosure 3 for an interpretation of the structures. Height of gorge is ~ 150 m.



Figure 4.14 View looking SW from the road above Wadi As Sifah, from the top of the As Sifah dome (see section accompanying enclosure 1) looking structurally up section within the As Sifah unit and towards the lower grade material of the overlying Wadi Adai-Wadi Mayh-Al Khuryan unit. The low hills in the middle distance consist of eclogite facies (>20 kbar) metabasic and volcaniclastic (dark) material, with carbonate and semipelitic schists (pale) forming an isoclinally folded sequence that flattens to the east to form the As Sifah dome. The break of slope at the top of the background scarp marks the detachment surface separating the lower grade material of the Wadi Adai-Wadi Mayh-Al Khuryan unit.

Figure 4.15-16 Field relations and petrography of eclogite facies pelitic to metavolcanoclastic units of the Saih Hatat high pressure terrane. Field of view for all photomicrographs is ~7 mm.





Figure 4.15 Megaboudin (outcrop along beach is ~200 m) of metabasic to metavolcanoclastic eclogite entrained within ductile carbonate-quartz schists, north of As Sifah. Figure 4.16a Retrogressed metapelitic blueschist cofacial with the metabasic eclogites, with porphyroblasts of epidote and albite overgrowing a peak phengite-garnet-glaucophane (pseudomorphed by chlorite and actinolite) fabric.



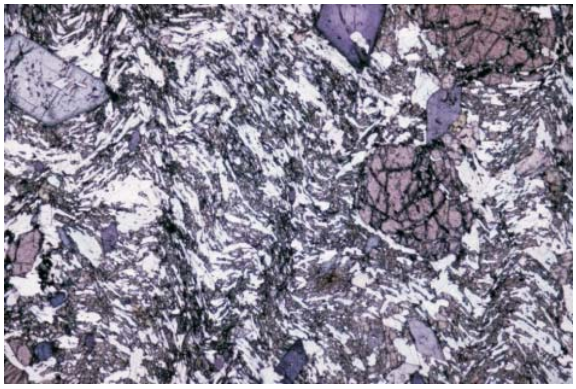
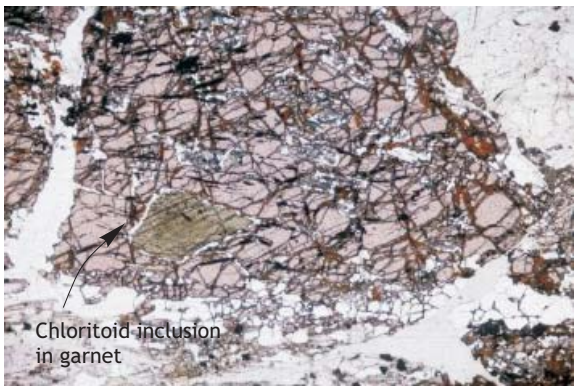


Figure 4.16b Metavolcanoclastic eclogite from Wadi As Sifah, showing E-W oriented omphacite-phengite-garnet fabric overgrown by glaucophane, parallel to NNE-SSW regional stretching lineation. Section parallel to schistosity. 4.16c section normal to foliation, showing microfolding of the schistosity, parallel to NE verging macrofolds in the As Sifah unit.



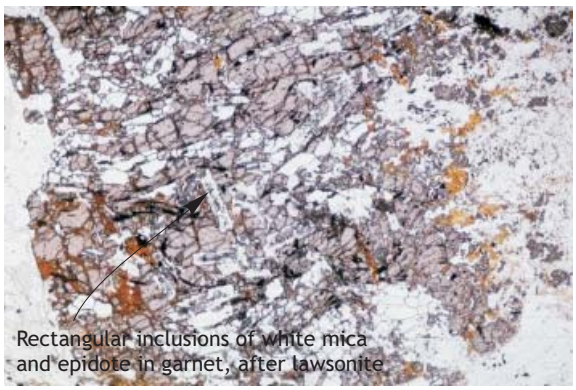


Figure 4.16d Fe rich metapelite cofacial with, but structurally higher within the As Sifah than the eclogites shown above. Preserved within Fe garnet poikiloblasts are prograde relicts of chloritoid. 4.16e epidote-white mica pseudomorphs after lawsonite (Searle et al. 1994), showing the clockwise nature of the PTt path followed by the As Sifah unit.

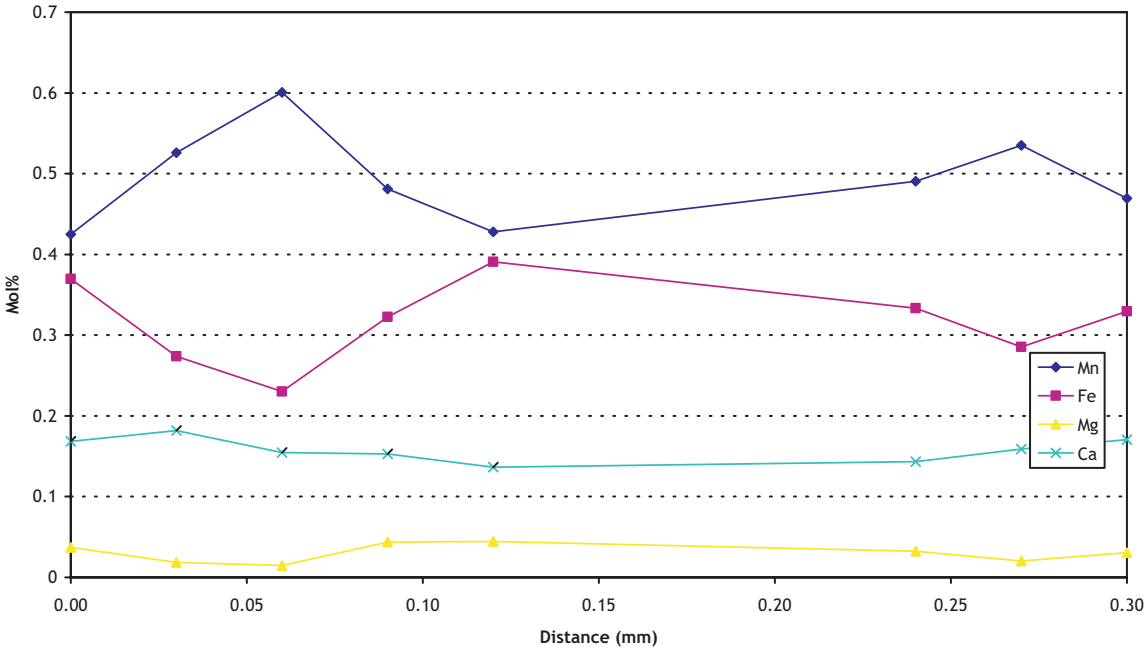
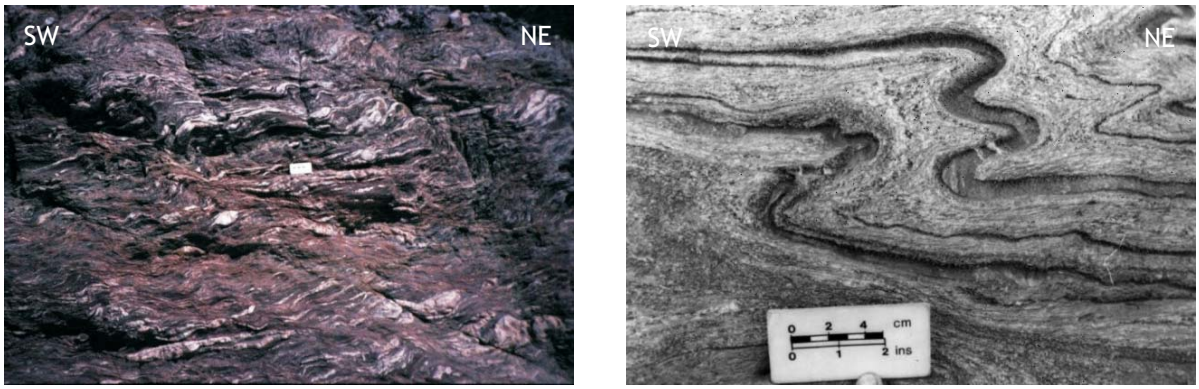


Figure 4.17 Garnet profile from sample JC 122, a metavolcanoclastic eclogite from above As Sifah village and structurally ~300 m above the major eclogite megaboudins exposed along the Gulf of Oman coast. This sample records similar peak conditions of ~470°C and 21.0 ± 1.5 kbar (table 4.1), and Mn-Fe garnet grains exhibit cation zoning profiles as shown, characterised by low but constant (unzoned) Ca and Mg contents, and Fe and Mn contents that respectively rise and fall from the core to the rim of the garnet grain, suggesting the presence of retrograde diffusional zonation.

Figure 4.18 Kinematic indicators of exhumation related deformation within the structurally lowest (As Sifah) unit of the Saih Hatat terrane, exposed in the Rija culmination and the As Sifah dome.



a) Extensional shear band fabrics and fold asymmetry in carbonate-phengite-quartz schists of the eclogite facies As Sifah dome, indicating *relative* top down to the NE extension that postdates the attainment of eclogite facies conditions (Searle et al. 1994). The shear bands are largely composed of greenschist facies minerals. b) NE vergence in asymmetric minor folds within similar quartz-phengite-carbonate schists of the Rija culmination, Wadi Mayh.

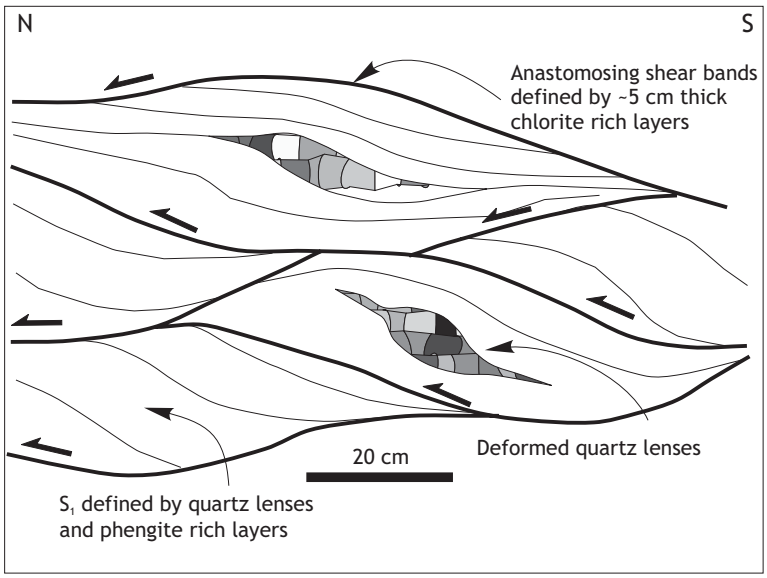


Figure 4.19a Sketch showing macrostructural extensional shear band fabrics in blueschist-eclogite facies carbonate schists of the As Sifah unit. Quartz lenses exhibit a top to the N shear sense and the phengite layer defined foliation of the calc schists is deformed into N verging asymmetric folds which are enveloped and truncated by chlorite rich top to the N shear bands which probably grew under greenschist facies conditions.

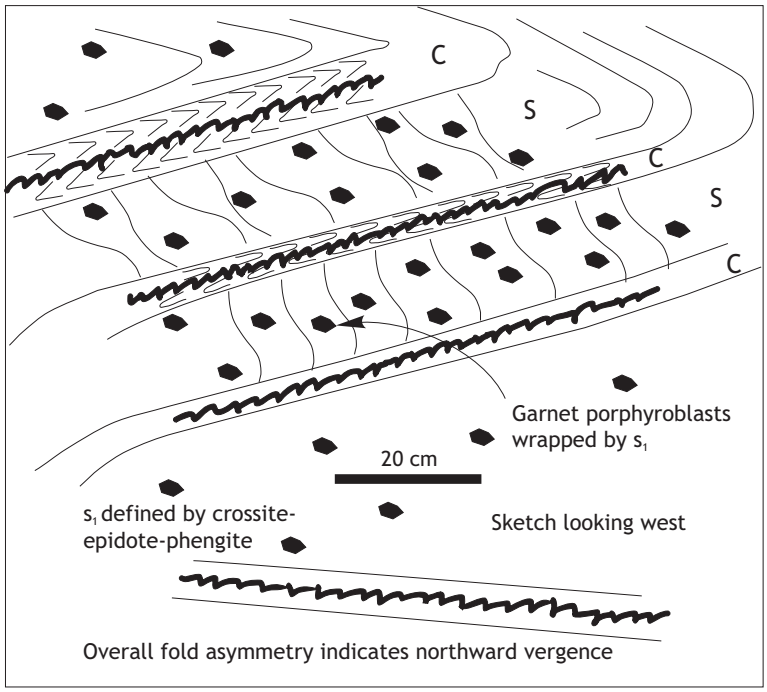
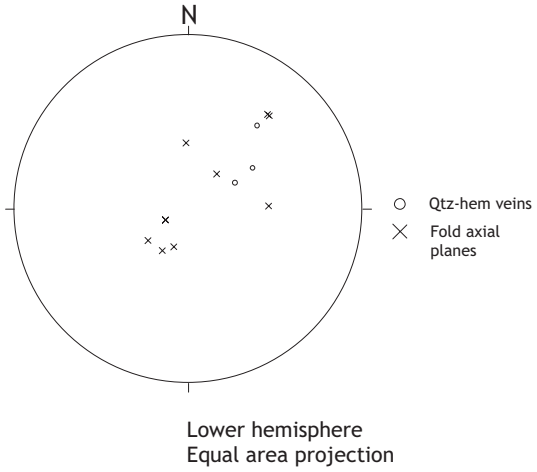
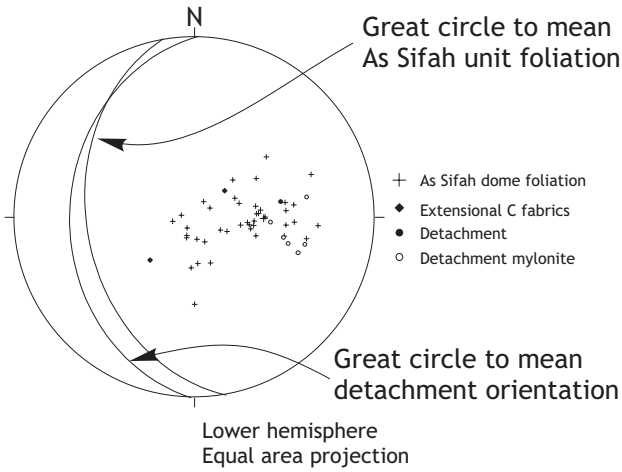


Figure 4.19b Sketch showing outcrop relationships within intimately intercalated and co-facial (El-Shazly et al. 1997) phengite bearing eclogites, garnet-glaucophane-epidote semi-pelites and quartz-phengite-garnet schists. Both eclogite and semi-pelite have similar calculated PT conditions (see table 4.1) of ~20 kbar. Overall fold asymmetry indicates NE directed vergence, and the shear planes have crenulated microfolds with the hinges formed from polygonal phengite and the limbs of crossite.

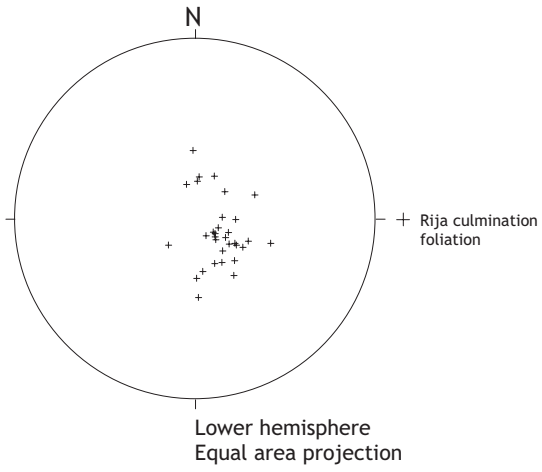
Figure 4.20a-f Structural data for the structurally equivalent As Sifah, Wadi Hulw and Rija areas of the Saih Hatat terrane. Orientation data for the NNE-SSW mineral stretching lineation is taken from all structural levels of the terrane.



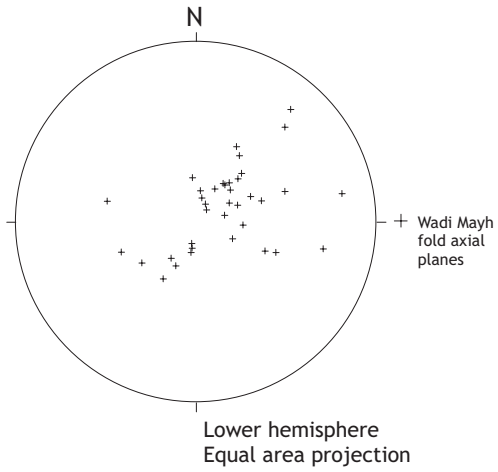
a) As Sifah unit fold axial planes and vein sets.



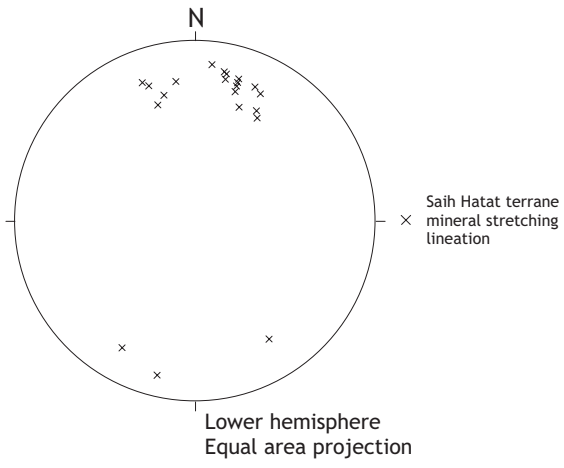
b) As Sifah unit foliation



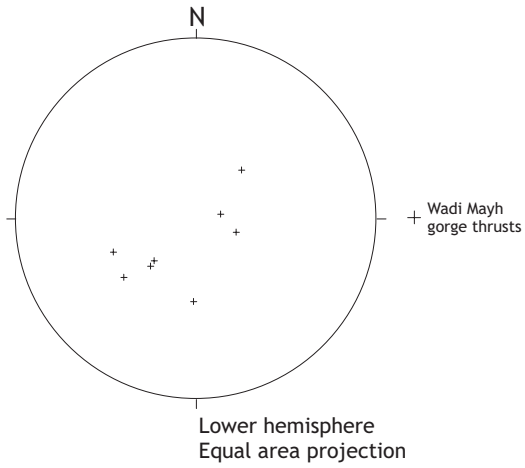
c) Rija culmination foliation



d) Wadi Mayh fold axial planes



e) Saih Hatat mineral stretching lineation



f) Thrusts within Wadi Mayh gorge (Wadi Adai-Wadi Mayh-Al Khuryan unit)

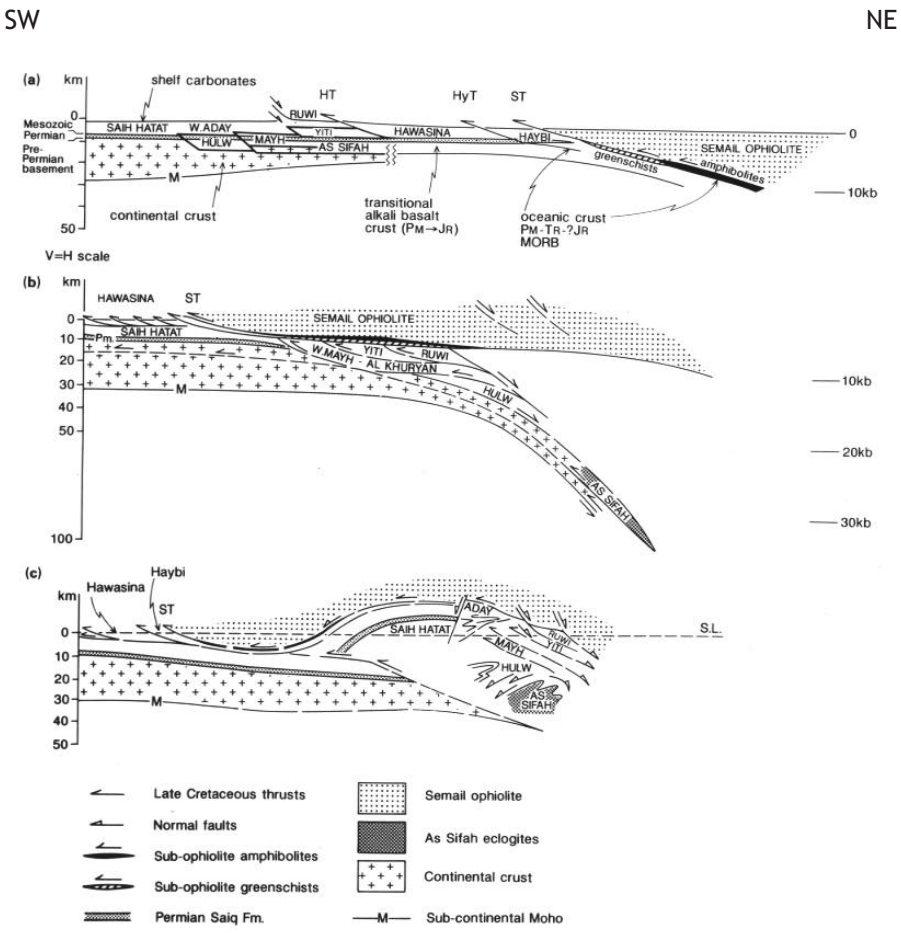


Figure 4.21 'Twin subduction zone' model for the formation, preservation and exhumation of the Saih Hatat HP terrane, from Searle et al. (1994). This model postulates a contemporaneous formation of the ophiolite metamorphic sole and the Saih Hatat HP terrane by subduction of the Arabian continental margin (at a promontory) in a deeper NE directed subduction zone beneath the thrust

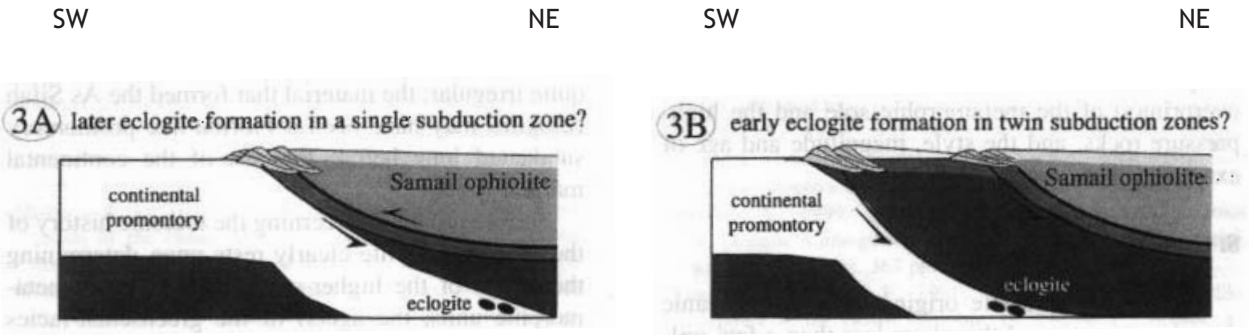


Figure 4.22 Alternative models for the formation of the Saih Hatat HP terrane from Hacker & Gnos (1997). Two contrasting tectonic configurations are postulated depending on the interpretation of the ambiguous age data for the Saih Hatat HP terrane presented in the literature (see discussion in text). The second of the models, in which the ophiolite sole and the eclogites are assumed to have formed contemporaneously, is very similar to the Searle et al. (1994) model shown in figure 4.21.

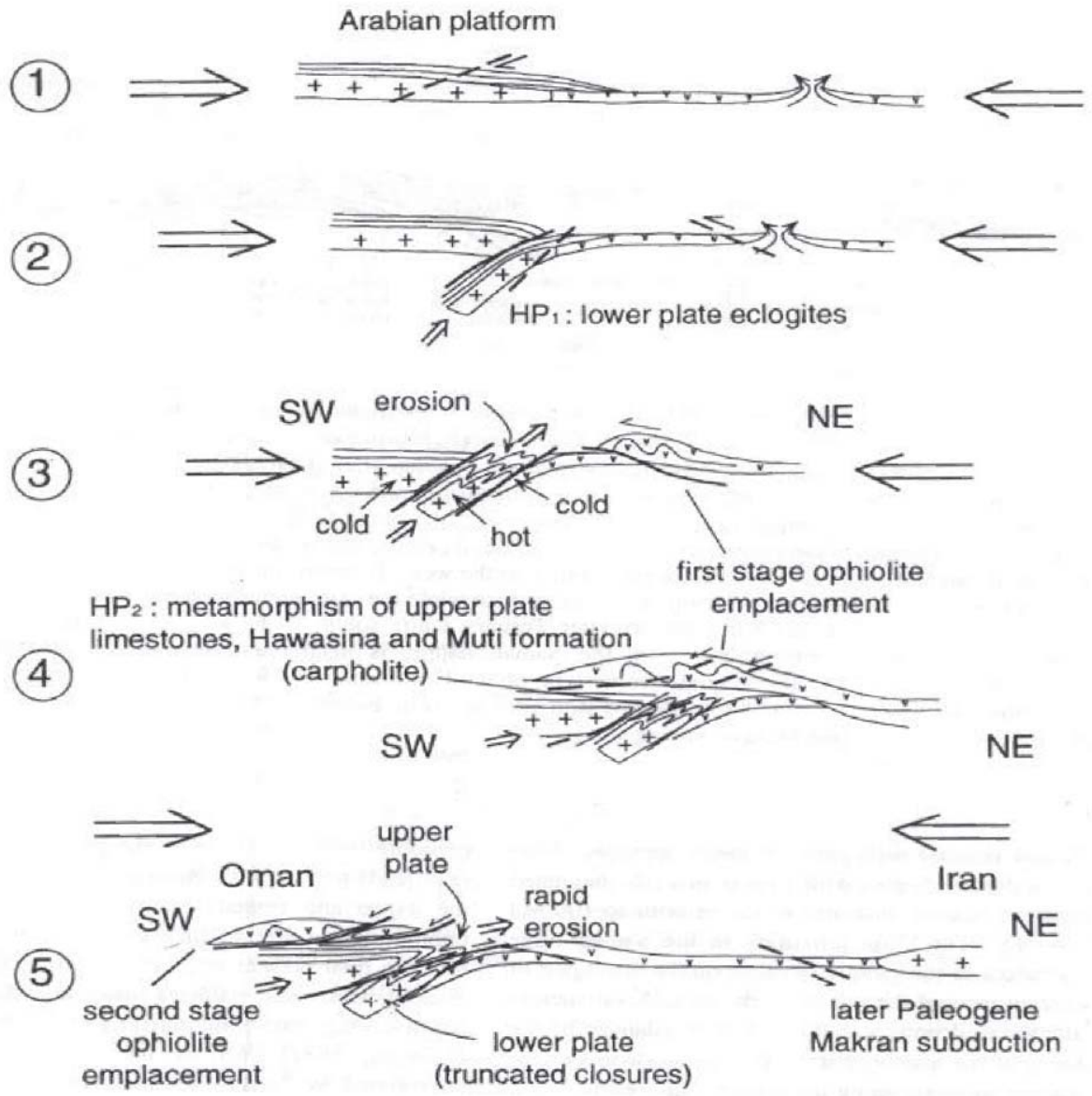


Figure 4.23 Model for the formation and tectonometamorphic evolution of the Saih Hatat high pressure terrane from Gregory et al. (1998). The model requires the Saih Hatat terrane to have formed prior to the Semail ophiolite metamorphic sole derived from intraoceanic thrusting. However, the best age determination (Hacker & Gnos 1997) of the eclogites at As Sifah is 96 ± 2 Ma ($^{40}Ar/^{39}Ar$; Searle et al. 1994) which is almost contemporaneous with the 93.5 ± 0.1 Ma age of the Wadi Tayin metamorphic sole amphibolites and overlaps the formation age of the Semail ophiolite crust (Tilton et al. 1981). If the Ruwi mélange metabasaltic blocks were derived from the metamorphic sole amphibolites of the Haybi complex, as suggested by Searle & Cox (1999), then the sole metamorphism must have *preceded* the Ruwi HP event, which has an $^{40}Ar/^{39}Ar$ age of 80.2 ± 0.8 Ma (El-Shazly & Lanphere 1992). Petrographic evidence from the limited metamorphic sole outcrops preserved at the base of the Muttrah ophiolite in NE Saih Hatat (Rabu 1987; Gnos 1993), in the form of crossitic overgrowths of hornblende, also suggests that the development of HP assemblages postdated the peak of sole metamorphism. However, what remains controversial, due to the questionable accuracy of the Ar geochronology, is whether the Saih Hatat HP metamorphism occurred in a single event at ~95 Ma, or whether there was a later, lower grade HP event also.

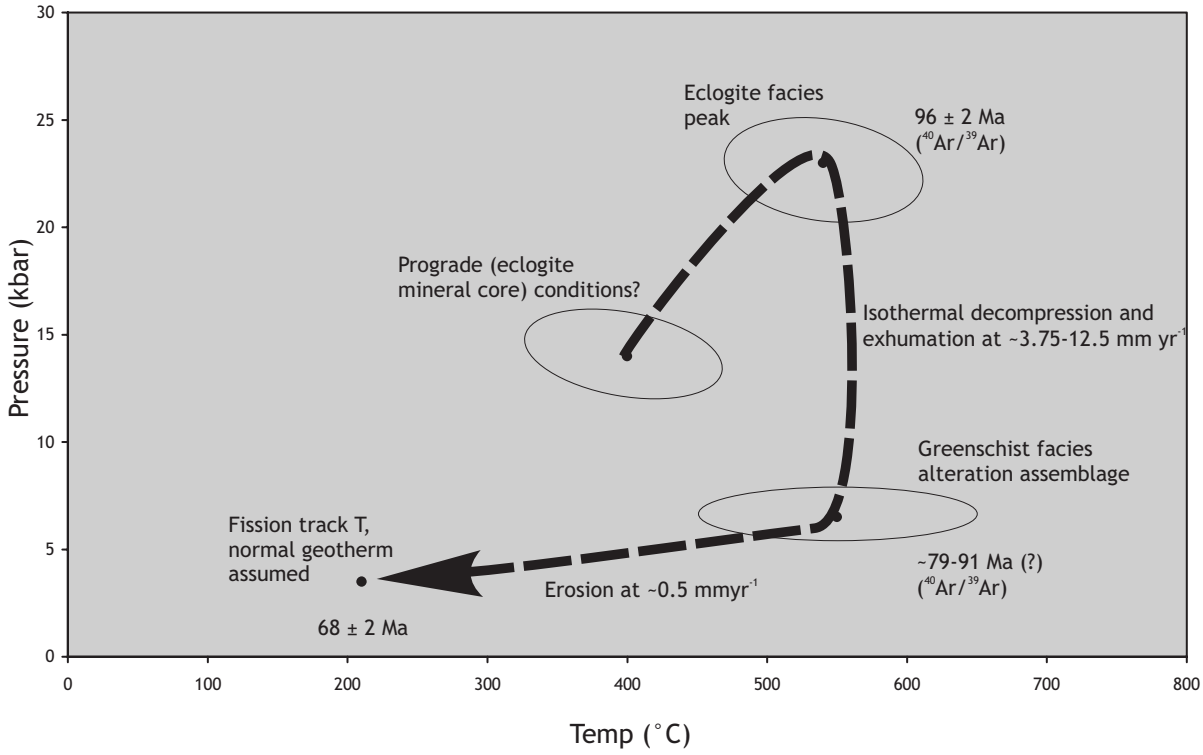


Figure 4.24 PT evolution of the highest grade parts of the Saih Hatat terrane, the As Sifah unit, showing the proposed clockwise PT path, exhumation rates calculated from associated geochronology and inferred tectonic processes. Data from this study, Searle et al. (1994), Saddiqi et al. (1995), and McMiller et al. (1999). See text for discussion of thermobarometric data and techniques, the validity of the geochronology of the As Sifah and other Saih Hatat terrane components, and assumptions used in the calculation of exhumation rates.

CHAPTER FIVE : BANI HAMID METAMORPHIC SOLE TERRANE



Late afternoon light over the
Hajar oasis, Bani Hamid

CHAPTER FIVE : BANI HAMID METAMORPHIC SOLE TERRANE

5.1 INTRODUCTION

A structurally and petrographically distinct metamorphic sole terrane is found beneath the Semail ophiolite in the Bani Hamid area of the eastern United Arab Emirates (figure 5.1). The Bani Hamid terrane is bounded by the villages of Hajar and Shis to the east and Bulaydah in Wadi Ham to the west (figure 5.2) and is characterised by an extensive (~15 km^2), well exposed, though rather inaccessible, high grade metamorphic terrane (figure 5.3) comprising material distinct from the 'classic' subophiolitic metamorphic sole described in *Chapter Three* in terms of thickness, grade, structural positional with respect to the Semail ophiolite, and petrography.

The Bani Hamid sequence has been the subject of little detailed research but was described by Alleman & Peters (1972) and Searle (1980) in reconnaissance studies, while subsequent work by Stössel & Zeigler (1985), Bucher & Kurz (1991) and Gnos (1992) concentrated on the mineral chemistry of a variety of rare, often Mn rich phases (eg Gnos et al. 1996) within Bani Hamid granulite assemblages. The structural and metamorphic evolution of the terrane has been addressed in part by Gnos & Kurz (1994) and Gnos & Nicolas (1996), while the genetic relationship between the Bani Hamid granulites and the leucogranitoid intrusions of the overlying Khawr Fakkan ophiolite block has been explored by Cox et al. (1999).

An outcrop width of ~2 km of subophiolitic metamorphic rocks is observed in the Bani Hamid terrane, and the uniformly SE dipping sequence is bounded at the top (SE side) by the Semail thrust (figure 5.4), and at the base (NW) by a later out-of-sequence thrust, the Bani Hamid thrust (figure 5.5; Searle & Cox 1999). Average dips of 35-45° to the SE suggest a typical thickness of ~1 km of amphibolite to granulite grade rocks.

The presence of abundant enstatite-cordierite-sillimanite-spinel ± sapphirine quartzites, alkaline and Ti rich mafic granulites and calc silicate (metacarbonatite) assemblages in the Semail ophiolite metamorphic sole is unique to Bani Hamid and these assemblages have been described by Bucher & Kurz (1991), Gnos (1992), Gnos & Kurz (1994) and Searle & Cox (1999). The rocks all exhibit upper amphibolite to granulite facies assemblages, and the steep inverted metamorphic gradient seen in the classic metamorphic sole is absent. Lower grade, greenschist facies, material is also entirely absent. Rare partial melt segregations (figure 5.7-8), petrographically distinct from the leucogranitic dykes common in the mantle sequence of the adjacent, overlying Khawr Fakkan ophiolite block (*Chapter Six*),

have been described from mafic granulites (enstatite-diopside-hornblende ± plagioclase) in the Bani Hamid sequence (Searle 1980).

The contrasts in tectonic position, metamorphic assemblages, protoliths, and apparent grade between the Bani Hamid terrane and the adjacent Asimah and other similar 'classic' subophiolitic metamorphic sole outcrops, make a study of the metamorphic evolution of this unique terrane vital to a clear understanding of both the subduction-obduction related and post emplacement tectonics of the Semail ophiolite allochthon.

5.2 TECTONICS OF GRANULITE FACIES METAMORPHISM

Presented here is a brief review of the tectonic occurrences, morphology, origin and PT histories of a variety of granulite facies metamorphic terranes to place the Bani Hamid terrane in its tectonic context.

5.2.1 Tectonic settings of granulite facies metamorphism

Granulite facies metamorphic material is found as often regionally extensive terranes in a variety of typical occurrences, including, in order of decreasing extent:

1. As extensive 'crystalline basement' terranes of Archean and Proterozoic age in major cratons, often associated with extensive synmetamorphic magmatism. The Lewisian complex of NW Scotland is an example.
2. As the rare culmination of dry prograde metasedimentary sequences in young collisional orogens: the high Himalayan and Karakoram metamorphic complexes, although characterised by wet partial melting and migmatisation in the upper amphibolite facies, may arguably have reached granulite facies conditions.
3. Accreted to the base of obducted ophiolite complexes as (rare) metabasic and metasedimentary metamorphic sole components. The sole of the St Anthony complex, Newfoundland (Jamieson 1986) is the type locality.
4. As the products of rare, deep seated contact metamorphism of sedimentary sequences; the Courtland complex of New York is an example.

Granulite facies terranes are diverse, as the above list of examples shows, but are typically characterised by largely anhydrous mineral assemblages as a result of the high metamorphic peak temperatures of >800°C, a polyphase deformational history dominated by ductile fabrics, the intimate juxtaposition of metasedimentary and metaigneous material, and Archean or Proterozoic ages. More recent (Palaeozoic to Mesozoic) granulite facies material is largely restricted to the exhumed bases of large obducted island arc complexes such as the Chilas and Jijal complexes of the Kohistan arc, and more rarely to the culmination of metamorphism in young orogenic belts such as the Himalaya, or as deep seated contact aureoles.

The Bani Hamid terrane clearly fits rather poorly into this conceptual framework but none the less, there are a number of genetic and metamorphic parallels between the more common tectonic expressions of granulite facies material and the distinctive type of subophiolitic metamorphism that the Bani Hamid terrane represents and consideration of some of these petrogenetic analogies will elucidate processes apparent in the Bani Hamid terrane.

PTt histories in granulite facies material (Harley 1989) are usually described solely in terms of post peak paths, derived from retrogressive coronae, symplectites and assemblages since prograde assemblages (porphyroblast inclusion suites are widely used to constrain early PT histories in metamorphic terranes) of granulites are rarely preserved. Post peak paths may be divided into two contrasting styles: ITD or *isothermal decompression*, and IBC or *isobaric cooling*, leading to several tectonic models of formation for terranes with different petrological and tectonic characteristics.

By the late 1970s it was widely accepted that prograde metamorphic rocks in orogenic belts typically experienced a clockwise PTt path culminating in granulite facies conditions and associated partial melting and generation of migmatites and anatectic granitoids. The major tectonic environment for which *Isothermal decompression paths* have been deduced is a convergent orogenic setting where deep exhumation after thickening, associated with warm crust or prolonged thermal relaxation (England & Richardson 1977), occurs, such as in the Himalaya (high Himalayan and Karakoram metamorphic complexes), where ITD type exhumation paths for upper amphibolite to granulite facies migmatitic terranes have recently been described (Searle et al. 1999).

Ellis (1980) first described an anticlockwise or *isobaric cooling* PTt path from an Antarctic granulite terrane (Napier Complex, Enderby Land) that was regarded as being the result of an unusual tectonic and metamorphic history. However, many more globally distributed examples of *isobaric cooling* PTt paths were subsequently noted, and a variety of models, all proposed for Archean to Proterozoic terranes where tectonometamorphic constraints suggested that magmatic accretion had played an important role in crustal thickening and heat advection, have been suggested to account for this type of PT evolution and may encompass:

1. Cooling at deep structural levels of collision zones characterised by thickened crust (material left at depth after orogenic collapse; Ellis 1987).
2. After metamorphism in zones of extensional thinning (eg Basin & Range province; Sandiford & Powell 1986).
3. Magmatic accretion and heating (with 'anticlockwise' PT path), postulated for a variety of tectonic regimes, including magmatic heating in Cordilleran-type continental margins (Bohlen 1987, 1991); magmatic heating in a back-arc region, immediately following convergence of previously-thinned crust (Waters 1990); heating in extensional continental settings with lithospheric delamination, or the heating and convergence of attenuated crust above a mantle plume.
4. Heating of cold subducted material accreted to the hot base of a subduction zone hanging wall, as in the formation of a subophiolitic metamorphic sole (Jamieson 1986; Searle & Cox 1999).

Isobaric cooling paths therefore more commonly characterise granulite facies terranes in which peak conditions were achieved in continental lithosphere of a more stable configuration than the collisional orogenic terranes characterised by *Isothermal decompression paths*. In contrast, the tectonic setting of the Bani Hamid granulite facies event occurred in a collisional, supra-subduction zone environment (Searle & Cox 1999) in which the main heat source for the sole metamorphism was the residual heat of the young, hot, overthrust Semail ophiolite mantle wedge.

5.2.2 UHT metamorphism: definitions and principles

The term *ultra high temperature metamorphism* (UHTM), as defined by Harley (1998), refers to granulite facies metamorphic rocks equilibrated at peak temperatures of 900-1100°C at pressures of 7-13 kbar. Key mineralogical phases indicative of UHT metamorphism in pelites and quartzites include sapphirine, aluminous orthopyroxene (8-12% Al_2O_3), garnet, cordierite, aluminous spinel and quartz. Quartzose assemblages from the Bani Hamid terrane include most of these key phases and thus the terrane may be regarded as potentially the first recognized sub ophiolitic UHT metamorphic terrane.

In metabasic material, the amphibolite to granulite prograde transition is defined by dehydration reactions producing pyroxene from amphibole, leading to largely anhydrous two pyroxene assemblages (eg Yardley 1989). Garnet is entirely absent from metabasic gneisses

from the Bani Hamid terrane, in contrast to the highest grade parts of the 'classic' metamorphic sole. However, the abundance and distribution of garnet in granulite facies metabasites of the Semail ophiolite sole appears to have been controlled largely by lateral and vertical protolith compositional changes (*Chapter Three*; Gnos 1998) and it may be that the protoliths of the Bani Hamid metabasites did not contain sufficient Ca or exhibit high enough Fe/Mg ratios to produce garnet, despite the similarity in peak conditions between the two contrasting assemblages. The high f_{O_2} values implied by the ore mineral assemblages seen in the Bani Hamid terrane (Gnos & Peters 1995) also favour the presence of orthopyroxene over garnet.

In quartzose and semi-pelitic material, characteristic granulite facies phases may include cordierite, phlogopite, spinel, orthopyroxene, diopside and sapphirine, all of which are present in semi-pelitic assemblages from the Bani Hamid terrane. Sapphirine was first reported from the Bani Hamid terrane by Gnos & Kurz (1994). The dominance of anhydrous phases again emphasises the high temperatures characteristic of such assemblages – hydrated phases are generally found solely in retrograde assemblages.

Defining the onset of granulite facies conditions in calc silicate and metacarbonate systems is more complex, since the role of bulk and fluid compositions is critical in determining the appearance of minerals characteristic of high grade calc silicate and metacarbonate assemblages. Phases such as scapolite, diopside, wollastonite, forsterite and other, more uncommon calc silicate minerals are widespread in the calc silicate and metacarbonate assemblages of the Bani Hamid terrane.

5.2.3 Formation and preservation of granulite facies terranes

The origin of granulite facies conditions in metamorphic terranes has been controversial. The wide variety of tectonic environments in which granulite terranes are found has been demonstrated, and the diversity of granulite facies assemblages commonly present in granulite terranes presents many different petrological problems. The most fundamental and widespread petrological issue is that typical granulites, both felsic and mafic, have assemblages that require $P_{H_2O} << P_{total}$ for stability, and debate has centred around how these low P_{H_2O} values have been achieved in such a wide variety of tectonic contexts. There are three distinguishable end member models:

1. The extraction of H_2O during prograde granulite facies melting and metamorphism from intergranular fluid and hydrous phases, and subsequent partitioning into

(granitic) melts, which may be removed and emplaced at higher structural levels, leaving an anhydrous granulite restite.

Fyfe (1973) suggested that granulites could be regarded as restites after removal of relatively large amounts (>20%) of partial melt based on a study of the Lewisian Complex. Furthermore, Thompson (1982) demonstrated that dehydration melting (vapour absent incongruent melting) of prograde metasedimentary assemblages containing hydrous phases (eg muscovite, biotite, hornblende) had an important role in the generation of the migmatites and leucogranites commonly associated with granulite facies metamorphism in the exposed cores of orogenic belts. More recent studies have however emphasised the likely low (<20%) degrees of partial melting common in migmatitic granulite terranes (Waters 1988). This mechanism may have considerable application to the Bani Hamid terrane, since the intimate juxtaposition of the Bani Hamid terrane and the leucogranitic intrusions of the overlying Khawr Fakkan ophiolite block have led to tectonic models that firmly link the genesis of the granitoids to the Bani Hamid granulites (Searle & Cox 1999; Cox et al. 1999; *Chapter Six*).

2. CO_2 rich vapour from an external source flushing through the protoliths during prograde metamorphism, driving dehydration reactions to produce largely anhydrous assemblages while diluting or flushing out the resulting H_2O rich fluids.

The recognition that a number of globally distributed high grade metamorphic terranes were characterised by a transition from H_2O rich fluid inclusion suites to CO_2 rich suites at the amphibolite to granulite boundary, as well as the associated phenomenon of 'arrested charnockitisation', led to the hypothesis that CO_2 rich fluidisation was responsible for the development of some granulite facies assemblages (eg Hansen et al. 1984). The abundance of carbonate rich material in the Bani Hamid terrane and the recognition of carbonatites in the adjacent Asimah sole (Zeigler et al. 1990), coupled with the presence of CO_2 rich fluid inclusion suites in Bani Hamid granulites (Gnos & Kurz 1994) suggests that CO_2 rich fluids, perhaps derived from these sources, may also have played a role in the development of granulite facies assemblages in Bani Hamid.

3. In certain terranes granulite protoliths may have already been characterised by largely anhydrous assemblages (for example, H_2O undersaturated igneous rocks and associated dehydrated emplacement related metamorphic aureoles) so that subsequent high grade metamorphic events did not require an unusual tectonic or metamorphic regime to generate anhydrous granulite facies assemblages.

The type location for this model of granulite formation is the Adirondack Highlands of the east USA, where much of the terrane comprises metabasic pyroxene-bearing igneous protoliths and associated high-grade thermal aureoles, subsequently metamorphosed to give Grenvillian age (~1000 Ma) granulite-facies assemblages (Lamb & Valley 1984). The recognition of H_2O undersaturated alkaline ultramafic igneous sills within the Bani Hamid sequence (Searle 1980; Cox et al. 1999), correlated with similar sills within the Hawasina and Haybi allochthons of the Oman mountains (Searle 1984) and Asimah metamorphic sole (Zeigler et al. 1990,1991; Cox et al. 1999) means that this mechanism may also be of limited application to the formation of granulite facies assemblages in the Bani Hamid terrane.

The three end members models described are not mutually exclusive and all may have played a role in the generally complex petrogenetic evolution of specific granulite facies terranes. The anecdotal and limited experimental evidence outlined above certainly indicates a potential role for all three mechanisms in the generation of components of the Bani Hamid terrane. Other commonly noted features of granulite terrains relevant to the discrimination of formative models for granulite assemblages in the Bani Hamid area include:

1. LILE depletion: regarded as a major issue in terranes such as the Lewisian (Fyfe 1977), and ascribed either to melt extraction or to deep-seated fluid metasomatism. It is now accepted that the Lewisian complex is atypical, and exceptionally depleted in LILE, whereas many other tectonically similar granulite terrains exhibit a less marked depletion. None the less the tectonically distinct, quartzose gneisses of the Bani Hamid terrane have the low LILE abundances and structurally adjacent leucogranitic intrusions consistent with the extraction of granitic melts (Cox et al. 1999).
2. CO_2-rich fluid inclusions: a classic study in southern Norway established that a change from H_2O-rich to CO_2 rich fluid inclusions coincided with the regional orthopyroxene isograd (Touret 1977). Limited evidence from the fluid inclusion suite of the Bani Hamid granulites indicates the presence of CO_2 rich fluids in quartzites (Gnos & Kurz 1994).
3. 'Arrested charnockitisation': a phenomenon first described from south India (Hansen et al. 1984) and Sri Lanka, where granulite facies (charnockite) assemblages are found in vein like arrays superimposed over amphibolite facies gneisses in acid to intermediate rocks. These features have subsequently been described, albeit more sparsely distributed, from a variety of other terranes and have been attributed to CO_2 streaming. Although alternative mechanisms may have contributed to the development of arrested charnockitisation, the phenomenon none the less demonstrates that the amphibolite to granulite transition may not depend entirely on PT conditions.

The tectonic origin of the Bani Hamid metamorphic terrane and indeed the rest of the Semail ophiolite metamorphic sole is widely ascribed (Searle & Malpas 1980; Ghent & Stout 1981; Stössel & Zeigler 1985; Bucher & Kurz 1991; Gnos 1992; Searle & Cox 1999; Cox et al. 1999) to the mechanism outlined above: the progressive metamorphism of oceanic and continental rise material subducted beneath the young and hot Semail ophiolite wedge and accreted to the base of the subduction zone hanging wall, culminating in granulite facies conditions and the removal of leucogranitic melts by anatexis (*Chapter Six*).

Geochemical analysis of Bani Hamid granulites, in conjunction with associated anatectic leucogranitoids (Cox et al. 1999; *Chapter Six*) has demonstrated the loss of LILE from quartzose gneisses of the terrane and the similarity in Sr isotopic abundances in both postulated sources and melts, showing that the largely anhydrous nature of the Bani Hamid granulites, particularly with respect to the amphibole rich metabasites of the 'classic' sole outcrops (*Chapter Three*), may be due in part at least to the more widespread extraction of LILE and volatile rich material to form leucogranitic melts which intrude up into the Khawr Fakkan block mantle sequence.

However, the abundance of carbonate material in the Bani Hamid terrane, coupled with evidence suggesting the presence of CO_2 rich fluid inclusion suites, described by Gnos & Kurz (1994), is compatible with the absence of amphibolite facies material in the terrane being a (partial) result of CO_2 streaming. A more detailed study of the fluid inclusion compositions and distributions throughout the Bani Hamid terrane would be required to establish the contribution of this mechanism to the generation of granulite facies conditions in the Bani Hamid terrane.

5.3 FIELD RELATIONSHIPS, PETROGRAPHY AND MINERAL CHEMISTRY

5.3.1 Calc silicate rocks and marbles

Perhaps the most spectacular lithologies to be found in the Bani Hamid area, both in terms of petrology and field relationships, are the calc silicate mineral bearing and marble units. In the western part of the area, around Bulaydah (figure 5.1), the calc silicates have a limited outcrop and tend to occur as pods, lenses, or thin continuous layers up to 5 m thick intercalated within the more abundant metabasites and quartzites, particularly the former. However, in the eastern part of the Bani Hamid area, around Wadi Shis, calc silicate rocks are the dominant lithology and they exhibit spectacular ptygmatic folding on all scales (figure

5.10), as well as euhedral porphyroblasts of garnet and pyroxene up to 50 cm in size (figure 5.9). Unlike the quartzites and amphibolites, which generally have a foliation defined by mineral preferred orientations, the calc silicate mineral bearing units have ptygmatic folds defined by compositional and modal variations (figure 5.10). Two distinct calc silicate and carbonate bearing assemblages are found in the Bani Hamid terrane:

1. Marbles *senso stricto*, with dominant calcite and subordinate dolomite and Fe-Mg bearing phases, derived from sedimentary protoliths (figure 5.9,10).
2. Calc silicate rocks, with rare carbonates, dominated by Fe-Mg-Ca silicates including andradite, diopside, epidote, wollastonite and anorthite. The frequent association of these more mafic parageneses with ultramafic assemblages including glimmerites, suggests that they may be correlated with low grade carbonatites exposed in the adjacent Asimah terrane (figure 5.11).

Metasedimentary carbonate rich material is less abundant than the more varied calc silicate units and is restricted to lenses and thin layers within metabasic gneisses, well seen in upper Wadi Limarit, in a similar manner to carbonate units in the highest grade parts of the classic metamorphic sole.

Typical marble assemblages include: calcite-diopside-K-feldspar-titanite; calcite-wollastonite-scapolite-garnet-K-feldspar and calcite-chondrodite-quartz-K-feldspar-diopside. Carbonate material often exhibits post peak coronae and reaction rim textures that can be used to deduce components of the post peak PT path of the samples.

The calc silicate mineral bearing units can form thicker continuous sequences, well seen just below the Semail thrust in lower Wadi Shis, and thus have similar field relationships to those described from the metacarbonatite sheet of the Asimah terrane by Zeigler et al. (1990,1991). Typical calc-silicate mineral bearing assemblages include: grossular-wollastonite-diopside-scapolite-K-feldspar; diopside-grossular-wollastonite-spinel; merwinite-clinozoisite-titanite-K-feldspar-calcite; grossular-epidote-diopside-idocrase-K-feldspar-titanite.

5.3.2 Quartzites

The Bani Hamid terrane is dominated by granoblastic to mylonitic quartzofeldspathic gneisses (figure 5.1, 5.8), which in part retain granulite facies index minerals often used as indicators of UHT conditions, as defined by Harley (1998) such as enstatite, diopside, spinel and cordierite ± sapphirine. The latter phase was first noted from the Bani Hamid terrane by

Gnos (1992) and Gnos & Kurz (1994). More unusual Mn rich units contain the assemblage johannsenite-piemontite-rhodochrosite. These quartzose lithologies are heterogeneous, both laterally and vertically, with variable degrees of schistosity and grain size; compositional layering is manifested by thin monomineralic spinel and pyroxene layers.

The quartzose lithologies are commonest close to the thrust surfaces that bound the Bani Hamid area, particularly the NW bounding (Bani Hamid) thrust. There are systematic variations in the grain size, degree of metamorphic segregation, and strength of the mylonitic fabric of the quartzites, depending on their distance from the Bani Hamid thrust. In addition, fluid metasomatism, derived from overthrust harzburgites, has altered the primary metamorphic mineralogy, and the marginal quartzites contain retrogressive phases including uralitic amphiboles, epidote group minerals and abundant phyllosilicates.

The quartzites in the core of the thrust sheet tend to be intercalated with amphibolites and calc silicate rocks. They have a less well defined fabric, weaker compositional layering, and more modal feldspar and cordierite, the latter with inclusions of matted fibrolitic sillimanite. Also, distinctive pinkish piemontite, johannsenite and other Mn rich phase bearing quartzites are more common, and these Mn rich lithologies have been taken as evidence for an ultimately oceanic protolith for the Bani Hamid precursors (Gnos et al. 1996).

Quartzites from the Bani Hamid terrane appear to fall into two distinct end member parageneses, each with distinct geochemistry and assemblages (figure 5.17-20, table 5.1 and 5.2) – Mn and Al rich 'metasedimentary' gneisses (figure 5.12e) and Mg rich, garnet and diopside bearing quartzites (figure 5.12f) that exhibit assemblages and trace element distribution patterns (figure 5.17-20) compatible with a silicified basaltic or volcaniclastic protolith, as suggested by Gnos & Kurz (1994).

Quartz is dominant and may form up to 90% by volume of some quartzites and frequently imparts a blue to grey colour that alters to a rusty red-brown. A wide range of deformational textures are observed, from largely undeformed and near granoblastic fabrics to the development of sutured subgrains, to wholly recrystallised ribbon textures in mylonitic quartzites.

Orthopyroxene is common in quartzose gneisses from the Bani Hamid terrane. A typical enstatitic composition is $Mg_{1.62}Mn_{0.16}Al^{(vi)}_{0.11}Fe_{0.08}Al_{0.03}Fe^{3+}_{0.02}[Si_{1.83}Al^{(iv)}_{0.17}]O_6$, ($X_{Mg}$ = 0.8) with an Al_2O_3 content of ~7 wt% which produces a pronounced yellow colour (figure 5.12e). The high Al_2O_3 content is suggestive of UHT conditions and the high MnO content is compatible with an oceanic pelagic (metachert) sedimentary protolith.

Cordierite is present in many of the blue-grey enstatite-spinel bearing quartzites of the Bani Hamid area and has a typical composition of ~$Mg_{1.90}Fe_{0.07}Mn_{0.03}Si_5Al_4O_{18}$ (X_{Mg} = 0.95). It occurs as subhedral grains up to ~5 mm in size with characteristic marginal pinitic alteration

and forms up to ~10% of the quartzites by volume. The minimal Na content is compatible with a largely anhydrous nature (Vry et al. 1990).

Diopside is colourless to pale green with a typical composition in (?) silicified metabasalts of $Ca_{0.92}Mg_{0.73}Mn_{0.12}Fe^{3+}_{0.10}Na_{0.09}Al^{(vi)}_{0.03}Fe_{0.02}[Si_{1.94}Al]_{0.06}O_6$) and frequently occurs as aggregates in association with granditic garnet and plagioclase in granoblastic coarse grained quartzites and has a typical grain size of ~1-2 mm (figure 5.12f).

Garnet commonly occurs associated with diopside and plagioclase in silicified metabasalts (figure 5.12f) and has a typical andraditic, unzoned composition of $(Ca_{2.93}Mn_{0.05}Mg_{0.01}Fe^{2+}_{0.01})(Fe^{3+}_{1.48}Al^{(iv)}_{0.37}Ti_{0.15})[Si_{2.96}Al_{0.04}]O_{12}$.

Plagioclase in metavolcaniclastic assemblages occurs as fresh, unaltered, almost pure anorthite (~An_{99}) and as rare, largely altered, slightly less calcic (~An_{85}) augen like grains in metasedimentary granulites.

The commonest oxide phase observed is magnetite forming grains up to ~1 mm in size, which may contain up to ~10% hercynite, and forms almost monomineralic layers parallel to lithological banding in quartzose gneisses. Subordinate ilmenite and spinel are also observed and contain up to ~10% ZnO according to Gnos & Kurz (1994).

5.3.3 Metabasites and ultramafic sills

Metabasic assemblages form a subordinate component of the Bani Hamid terrane (figure 5.13), in contrast to the classic metamorphic sole outcrops of the Oman mountains, where metabasic amphibolites form the bulk of the highest grade parts of the sole. Rare partial melt segregations (figure 5.7), petrographically distinct from the leucogranitic dykes of the structurally overlying Khawr Fakkan ophiolite block, but similar to analogous partial melt veins in the upper mafic parts of the classic sole outcrops (*Chapter Three*) were first described from mafic granulites (enstatite-diopside-hornblende ± plagioclase) in the Bani Hamid sequence (Searle 1980).

Alkali and Ti rich mafic granulite sills (figure 5.6), with ultramafic xenoliths (figure 5.12d) within metacarbonatite calc silicate bearing granulites of the Bani Hamid terrane may be correlated with similar alkalic metavolcanics units described from the Asimah terrane by Zeigler et al. (1990, 1991). A wide range of assemblages, from true two pyroxene alkali rich mafic granulites (figure 5.12c) to hornblende-plagioclase amphibolites are found in the Bani Hamid sequence. This diversity of mafic assemblages contrasts strongly with the more homogeneous classic sole mafic units and possible reasons for the contrast will be addressed in **5.5**.

The amphibolite lithologies are dark brown to black, medium grained, well foliated rocks with a typical granulite grade assemblage characterised by the presence of amphibole as well as clinopyroxene (colourless to pale green diopside, typically $Mg_{0.85}Ca_{0.72}Fe_{0.12}Al^{(vi)}_{0.11}Na_{0.09}Fe^{3+}_{0.11}[Si_{1.85}Al_{0.15}]O_6$) and less abundantly, enstatite (typically $Mg_{1.58}Fe_{0.29}Fe^{3+}_{0.06}Al^{(vi)}_{0.02}Ca_{0.02}Mn_{0.02}Na_{0.01}[Si_{1.92}Al^{(iv)}_{0.08}]O_6$).

However, modal variations are large, perhaps reflecting protolith heterogeneity, and subsequent alteration to epidote amphibolite grade assemblages is common, with brown-green pargasitic amphiboles rimming diopside. There is a distinct variation in mineral chemistry and modal proportions between the core and marginal amphibolite units. The former have limited modal clinopyroxene, andesine and hastingitic amphibole; the latter have more abundant diopside, labradoritic plagioclase, and pargasitic amphibole. Apatite, ilmenite and magnetite, with rutile and titanite are common accessory phases and can be of rock forming abundance in ultramafic (glimmerites) xenoliths (figure 5.12d).

Throughout the Bani Hamid area, stromatic (foliation parallel) leucocratic partial melt pods and lenses up to 20 cm in size are found in the amphibolites; a typical tonalitic assemblage includes coarse grained andesine, quartz and biotite (figure 5.7). The presence of such evidence of melting can provide a key prograde constraint on the PTt path and metamorphic temperature obtained for the terrane.

Typical metabasite assemblages from the Bani Hamid terrane include true two pyroxene granulites and amphibolites: diopside-enstatite-K-feldspar-labradorite-magnetite-titanite; diopside-enstatite-pargasitic hornblende-labradorite-magnetite-titanite, diopside-hastingitic hornblende-andesine-apatite-magnetite and hornblende-andesine-epidote-biotite-spinel. Garnet is entirely absent from metabasic assemblages in the Bani Hamid terrane.

5.4 TECTONOSTRATIGRAPHY AND STRUCTURE

A geological map and cross section of the Bani Hamid metamorphic sole terrane is presented in figures 5.13 and 5.14, which supplement the reconnaissance mapping studies of Stössel & Zeigler (1985) and Bucher & Kurz (1991). Further structural details are shown in the metamorphic profiles seen in figures 5.15 and 5.16. The remoteness, high altitude and severe relief of the terrain in the Bani Hamid area made the detailed collection of structural data difficult, and the high strain rates suggested by the mylonitic nature of (particularly) quartzose components of the sole, adjacent to the Bani Hamid thrust, make the presence and certainly the clear identification and characterisation of large scale brittle structures very difficult.

An outcrop width of ~2 km (figure 5.1) of subophiolitic metamorphic rocks is observed in the Bani Hamid terrane. The uniformly SE dipping sequence is bounded at the top (SE side)

by the Semail thrust, and at the base (NW side) by a later out of sequence thrust (Searle & Cox 1999) which is here termed the Bani Hamid thrust. Typical foliation and lithological unit boundary dips of 35-45° to the SE indicate an apparent structural thickness of ~1 km of granulite facies metamorphic sole rocks.

The unusual structural position of the Bani Hamid terrane, apparently intercalated within the ophiolite mantle sequence, is due to the thrust repetition of the entire ophiolite in the Khawr Fakkan block (Searle & Cox 1999; Cox et al. 1999). Evidence for this out of sequence thrusting is implicit in a number of key tectonic field observations, some new, and some pre-existing, from the Bani Hamid terrane and the surrounding mantle sequence:

1. Low T mylonitisation fabrics and assemblages overprinting granulite fabrics in Bani Hamid quartzites restricted to assemblages found adjacent to the structurally lower bounding thrust surface formed at temperatures as low as 300°C (Gnos & Kurz 1994).
2. Landsat images (Gnos et al. 1991) show a clear contrast between the mantle sequence to the east and west of Bani Hamid in terms of the extent of harzburgite serpentinisation, suggesting that different structural levels are exposed. Harzburgites structurally above and to the SE of the metamorphic terrane are more strongly altered. Since increasing levels of mantle sequence serpentinisation are widely accepted to be found at lower structural levels in the ophiolite due to the influx of basally derived fluids in serpentinisation (Chen & Pallister 1981), this observation indicates that the mantle sequence to the SE of Bani Hamid was originally at a structurally lower level than the harzburgites to the NW of Bani Hamid.
3. Leucogranitoid intrusions are restricted to the eastward, structurally higher mantle sequence harzburgites of the Khawr Fakkan block, from which they are derived (Gnos & Nicolas 1996; Cox et al. 1999) and are absent structurally beneath (to the NW) of the Bani Hamid terrane.
4. The banded ultramafic unit of the ophiolite mantle sequence (Searle & Malpas 1980) is entirely absent along the NW boundary thrust of the Bani Hamid terrane, which suggests that the out of sequence Bani Hamid thrusting event occurred at low temperatures compared to the thrusting that bounds the terrane to the SE, where the banded ultramafic unit is better, albeit weakly, developed.

These lines of evidence all support the hypothesis that the Bani Hamid granulites attained their present structural position relative to the Semail ophiolite by post peak metamorphic (re) thrusting along the Bani Hamid thrust rather than being incorporated into the

mantle sequence by a complex tectonic rearrangement, such as that of a pull apart transform basin as suggested by Gnos & Nicolas (1996).

The out of sequence, break back thrust that exhumed the Bani Hamid terrane and repeated the ophiolite mantle sequence in the Khawr Fakkan block is here termed the Bani Hamid thrust (figure 5.5). The timing of thrusting that exhumed the Bani Hamid terrane is not well known, although Gnos & Kurz (1994) estimated that motion on the Bani Hamid thrust continued at temperatures as low as 300°C. This figure can be used in conjunction with existing data on the rate of cooling in the Semail ophiolite metamorphic sole, coupled with Bani Hamid peak metamorphism conditions and ages, to obtain a time of motion along the Bani Hamid thrust.

Hacker et al. (1996) used $^{40}Ar/^{39}Ar$ amphibole geochronology to estimate metamorphic sole cooling rates of ~200°C Ma^{-1} before 93.5 Ma, ~90°C Ma^{-1} between 93.5 Ma and 92.6 Ma and ~20°C Ma^{-1} until biotite closure at 89.2 Ma, and obtained a $^{40}Ar/^{39}Ar$ hornblende age of 95.3 $\pm$ 0.5 Ma (recalculated from Gnos & Peters 1993) for the Bani Hamid granulite facies event. Peak conditions in the Bani Hamid terrane are assumed to be ~850°C. This data suggests that the Bani Hamid metamorphic sole had cooled to ~300°C by ~94 Ma and places a lower age constraint on the motion along the Bani Hamid thrust.

The lower structural levels of the Bani Hamid terrane, exposed in the NW, adjacent to the Bani Hamid thrust, are dominated by metabasic granulites and quartzofeldspathic gneisses. Calc silicates bearing rocks (both metasedimentary and metaigneous) are more common towards the top of the sequence, adjacent to the Semail thrust. The dominant schistosity in the Bani Hamid granulites is sub-parallel both to lithological and compositional banding and to the Semail and Bani Hamid thrusts. Minor parasitic folds generally close to the NW (figure 5.15 and 5.16) and the repetition of lithological units along well exposed and accessible wadi sections has facilitated the recognition of major, large amplitude, NW verging isoclinal folds (figure 5.14) within the sequence. Lower grade metamorphic material may be preserved at depth in the unexposed cores of these folds.

The boundary thrust surfaces, both the structurally higher (original) Semail thrust and the structurally lower and later out of sequence thrust, cut obliquely through the metamorphic sole, exposing different assemblages and structural levels along strike. Both thrusts however parallel the layering of the banded ultramafic unit (Searle & Malpas 1980) in the ophiolite mantle sequence structurally above the Semail thrust. The section through the Bani Hamid terrane (figure 5.14) demonstrates the presence of large amplitude isoclinal NW facing folds that thicken the metamorphic sole sequence to an estimated structural thickness of ~1 km, although the true thickness of the sequence may be ~500 m, which is similar to the best preserved and thickest classic sole sequences in the Oman mountains (eg Sumeini).

5.5 GRANULITE PROTOLITHS AND SOURCE MATERIALS

The Bani Hamid terrane has a variety of components that occur in different proportions and at different grades to the classic metamorphic sole of the Asimah terrane. None the less, the different rock units of the Asimah terrane, comprising metavolcanic amphibolites and lower grade metasediments (both quartzose and carbonate rich) and carbonatites, are very similar to those described from Bani Hamid, both in terms of internal architecture and relative abundance.

For example, alkali and Ti rich mafic granulite sills (containing ultramafic xenoliths, including glimmerites, figure 5.12d) within metacarbonatite units of the Bani Hamid terrane may be correlated with similar alkalic metavolcanics described from the Asimah terrane by Zeigler et al. (1991) and it is therefore likely that the Asimah (greenschist-amphibolite facies) and Bani Hamid (granulite facies) sole terranes represent the variably metamorphosed equivalents of the unmetamorphosed Permo-Triassic and Jurassic Haybi volcanic material observed beneath the Semail ophiolite in the Oman mountains that were first noted by Searle (1980, 1984). Rare metasedimentary material, both restitic garnet-biotite aggregates and unassimilated banded quartzose enclaves, has been observed in leucogranitic intrusions in the ophiolite mantle sequence structurally above the Bani Hamid terrane by Cox et al. (1999) and the presence of these enclaves suggests the structurally underlying Bani Hamid terrane as a potential source for the granitoids.

5.5.1 Trace element geochemistry

Gnos (1992) and Bucher & Kurz (1991) provided XRF analyses of Bani Hamid quartzose granulites that can be used both to characterise the sources of these rocks, and to compare them with other metamorphic sole sediments of lower grade in the adjacent Asimah terrane. Structural and tectonic constraints demand that the Bani Hamid terrane has the same protoliths, at least in part, to the Asimah terrane (Zeigler et al. 1990, 1991), where greenschist facies quartzose sediments (psammitic to phyllitic) occur intimately associated with silicified metabasalts and volcaniclastic, tuffaceous units (Bucher & Kurz 1991).

The XRF analyses of Bani Hamid quartzose gneisses presented by Gnos (1992) and Bucher & Kurz (1991) are summarised in table 5.1 and 5.2 and clearly form a bimodal population. New analyses of these contrasting quartzite populations show clear differences are evident between the major and trace element concentrations of the two contrasting assemblages, with 'silicified basaltic' or metavolcaniclastic/volcanogenic sedimentary quartzites characterised by SiO_2 < 70%, FeO/Fe_2O_3, MgO and CaO all >5%, Cr >100 ppm, Ni >100

SiO_2	TiO_2	Al_2O_3	Fe_2O_3	FeO	MnO	MgO	CaO	Na_2O	K_20	P_2O_5	H_20 etc	Total
Metasediments												
77.08	0.29	12.05	1.08	1.46	0.08	1.32	5.10	1.79	0.24	0.10	0.48	101.07
77.73	0.62	9.53	4.82	1.22	0.16	2.58	0.17	0.11	1.78	0.04	2.32	101.08
82.92	0.38	0.24	4.94	0.02	9.74	2.11	0.27	0.00	0.00	0.07	0.73	101.42
86.68	0.40	5.91	1.97	0.26	0.03	0.55	0.51	0.77	2.47	0.02	0.59	100.16
93.54	0.18	2.24	1.88	0.24	0.03	0.66	0.22	0.13	0.34	0.03	0.63	100.12
95.59	0.16	1.10	0.52	0.85	0.02	1.14	0.23	0.00	0.06	0.02	0.73	100.42
89.53	0.14	0.84	0.91	0.82	0.12	2.77	4.45	0.00	0.05	0.10	0.23	99.96
86.59	0.70	5.79	4.53	0.52	0.05	2.31	0.05	0.01	0.02	0.01	1.95	102.53
79.68	0.72	9.01	6.09	0.82	0.20	2.91	0.48	0.00	0.09	0.01	0.98	100.99
80.46	0.70	7.57	5.33	1.12	0.07	2.78	0.26	0.00	0.11	0.00	2.37	100.77
87.20	0.31	1.56	1.47	1.50	0.10	4.39	2.79	0.00	0.04	0.12	0.72	100.20
93.44	0.19	1.37	1.08	1.14	0.07	2.11	1.69	0.00	0.22	0.04	0.51	101.86
94.88	0.12	0.35	0.87	0.65	0.06	1.73	3.07	0.00	0.00	0.04	0.23	102.00
90.77	0.39	2.31	3.77	0.33	0.18	1.60	0.12	0.00	0.14	0.07	1.02	100.70
86.79	0.11	1.99	0.71	1.75	0.05	2.01	4.74	0.02	1.44	0.15	0.08	99.84
84.35	0.72	6.56	4.78	0.94	0.13	2.17	0.30	0.00	0.03	0.01	0.67	100.66
77.58	0.39	0.24	0.56	2.10	0.09	2.54	14.82	0.00	0.00	0.16	1.16	99.64
86.17	0.38	4.04	2.67	0.93	0.66	2.10	2.31	0.17	0.41	0.06	0.91	100.79
Metabasites												
55.94	0.22	1.38	3.62	5.19	0.45	9.3	17.8	0.29	0.04	0.1	5.5	99.83
76.13	0.69	6.76	2.97	3.98	0.27	4.87	2.31	0	0.08	0.03	2.59	100.68
79.1	0.73	5.82	4.82	2.34	0.24	4.75	2.48	0.06	0.07	0.06	1.07	101.54
61.04	1.03	8.57	5.77	4.05	0.27	12.26	5.83	0.14	0.07	0.12	0.76	99.91
70.95	1.37	8.14	7.2	3.71	0.29	4.89	3	0.11	0.03	0.01	0.47	100.17
47.08	2.93	17.35	13.68	1.52	0.23	4.15	1.01	1.63	9.28	0.06	1.32	100.24
54.49	0.76	7.57	5.87	5.36	0.37	18.11	7.31	0	0.03	0.06	1.07	101
63.53	1.10	7.94	6.28	3.74	0.30	8.33	5.68	0.32	1.37	0.06	1.83	100.48

Table 5.1 Major element analyses of Bani Hamid quartzose granulites, from Bucher & Kurz (1991). The mean for each proposed protolith type is shown in the last row.

Sc	V	Cr	Co	Ni	Cu	Zn	Ga	Rb	Sr	Y	Zr	Nb	Ba	La	Ce	Nd	Pb	Th	U
Metasediments																			
4	62	0	24	14	9	45	17	15	239	17	72	10	28	0	0	0	5	19	20
0	147	77	0	57	13	85	13	63	53	11	115	9	237	0	0	0	2	23	0
13	9	29	53	71	654	68	8	15	16	32	90	14	26	45	26	9	0	34	27
4	34	11	22	15	0	22	11	67	84	19	133	15	388	15	0	0	8	21	18
13	5	6	38	39	0	19	8	24	32	15	47	16	0	0	0	0	8	17	15
7	52	14	31	25	6	31	7	9	9	13	19	7	0	0	0	0	7	15	15
10	14	23	37	42	6	43	7	9	11	26	36	7	0	0	0	0	0	16	17
0	81	63	0	45	8	33	8	6	8	3	20	5	11	0	0	0	1	14	0
8	43	65	22	51	0	95	21	23	58	20	91	20	0	21	0	0	9	33	28
4	63	63	29	63	0	75	17	18	20	17	49	19	0	24	0	0	9	32	25
15	25	79	36	80	0	46	7	11	13	21	32	10	0	0	0	0	0	16	14
10	39	20	32	43	14	47	9	14	22	20	37	12	1	0	0	0	11	24	18
6	11	8	40	26	0	25	7	9	10	18	24	12	0	0	0	0	8	22	20
6	0	16	25	46	0	46	10	16	10	15	23	10	0	1	0	0	6	22	20
8	46	18	31	23	0	49	6	33	33	18	33	8	63	0	0	0	0	17	14
7	78	55	57	58	0	58	16	14	37	13	51	12	0	22	0	0	0	19	17
6	24	24	20	31	0	58	0	11	22	28	34	18	0	0	5	17	0	24	20
7	43	34	29	43	42	50	10	21	40	18	53	12	44	8	2	2	4	22	17
Metabasites																			
47	72	254	16	214	0	97	0	8	17	11	26	7	27	0	0	0	0	0	8
22	138	236	46	165	11	100	15	15	61	18	55	14	17	41	27	30	0	25	20
21	81	210	37	171	0	94	15	14	82	21	49	16	5	22	0	11	0	30	28
25	119	596	49	511	93	113	15	15	134	29	48	13	8	35	32	11	0	24	20
27	250	156	51	121	0	141	19	14	151	20	69	18	23	69	30	10	0	25	20
44	0	117	35	126	0	291	27	179	115	22	199	51	481	129	67	10	15	13	18
40	110	1023	64	845	7	153	15	13	91	33	43	13	16	35	67	55	0	28	24
32	110	370	43	308	16	141	15	37	93	22	70	19	82	47	32	18	2	21	20

Table 5.2 Trace element analyses of Bani Hamid quartzose granulites, from Bucher & Kurz (1991).

ppm and Sc >25 ppm (figures 5.17-20). Without structural controls on the distribution of the Bucher & Kurz (1991) samples compared in this manner, it has not been possible to clearly distinguish the quartzose parageneses on the geological map of the Bani Hamid terrane presented in figure 5.1.

5.5.2 Isotope geochemistry

New Rb-Sr and Sm-Nd isotopic data for a representative sample of granulite facies quartzofeldspathic and metabasic gneisses from the Bani Hamid metamorphic terrane was presented as part of this study by Cox et al. (1999) and is shown in table 5.3. The quartzofeldspathic and calc silicate bearing gneisses have ε_{Nd} and ε_{Sr} values that range from –2.3 to –6.5 and 52 to 76 respectively.

The Asimah and Bani Hamid granulite facies metavolcanics represent the metamorphic equivalents of the Haybi volcanic units (Zeigler et al. 1990, 1991; Cox et al. 1999). The Bani Hamid examples analysed exhibit a wide range of ε_{Nd} and ε_{Sr} values from 1.7 to 5.8 and –7 to 17 respectively (table 5.3). This may be expected from a diverse volcanic sequence, interpreted by Searle (1980) and Zeigler et al. (1990, 1991) as evolving compositionally over time from a heterogeneous source. All however have lower ε_{Nd} values and higher ε_{Sr} values than the Semail ophiolite volcanic sequence. The positive ε_{Sr} values obtained suggest the subducted volcanic material represented by the Bani Hamid granulites was variably altered by interaction with seawater. McCulloch et al. (1981) estimated seawater locally to have had a ε_{Sr} value of ~30 during the Cenomanian (~95 Ma). The LILE enriched, subducted metabasalts have values approaching this figure.

The similarity in Nd and Sr isotopic characteristics between the Khawr Fakkan block leucogranites (*Chapter Six*) and the majority of the analysed Bani Hamid metasediments also suggests they may be closely related. LILE covariation modelling is compatible with the leucogranites being the products of the vapour absent melting of the Bani Hamid granulites, and the minimum melt type nature of the leucogranites will be demonstrated. Briqueu et al. (1991) also established that the granitoids of the Ra's Dadnah composite sill have Pb isotopic compositions inherited from the quartzose metasedimentary components of the Bani Hamid granulites. The analysed calc silicate bearing gneiss has a similar range of ε_{Sr} and ε_{Nd} values to the Asimah carbonatites analysed by Zeigler et al. (1991) although the analysed 'metavolcaniclastic' and 'metasedimentary' quartzites, JC 92 and JC 95 respectively, are not clearly distinguishable in terms of ε_{Sr} and ε_{Nd} values.

Sample	Rock Unit	Sm (ppm)	Nd (ppm)	$^{147}Sm/^{144}Nd$	$^{143}Nd/^{144}Nd$	$\varepsilon_{Nd(90Ma)}$	Rb (ppm)	Sr (ppm)	$^{87}Rb/^{86}Sr$	$^{87}Sr/^{86}Sr$	$^{87}Sr/^{86}Sr_{i\ (90Ma)}$	$\varepsilon_{Sr(90Ma)}$
	Bani Hamid Granulites											
OM 132	*Alkali feldspar-phlogopite-enstatite*	5.57	21.85	0.154	0.512702 ± 6	1.7	2.33	313.99	0.021	0.703959 ± 9	0.703932	-6.6
OM 135	*diopside-spinel granulite gneisses*	2.33	6.29	0.224	0.512953 ± 6	5.8	6.24	119.04	0.152	0.705771 ± 8	0.705577	16.8
JC 92	*Quartz-diopside-andradite gneiss*	1.42	4.34	0.198	0.512315 ± 6	-6.3	0.17	5.60	0.089	0.709847 ± 18	0.709734	75.8
JC 94	*Calc-silicate gneiss*	1.88	9.54	0.119	0.512476 ± 5	-2.3	6.76	200.39	0.098	0.708143 ± 8	0.708018	51.4
JC 95	*Quartz-phlogopite-cordierite gneiss*	0.05	0.24	0.117	0.512256 ± 25	-6.5	0.98	3.66	0.773	0.709059 ± 11	0.708071	52.2
	Normal Metamorphic Sole, Sumeini											
OM 65	*Garnet-diopside amphibolite*	4.11	13.62	0.182	0.512862 ± 5	4.5	8.47	163.72	0.150	0.705608 ± 8	0.705417	14.5

Table 5.3 Rb-Sr and Sm-Nd isotopic data from a representative suite of granulite facies metamorphic sole rocks from the Bani Hamid and classic (Sumeini) sole outcrops (*see Chapter Three*). See text for discussion.

5.5.3 Structural constraints

New field mapping (figure 5.1, 5.13 and 5.14) as part of this study has clearly demonstrated the processes behind the exhumation of the Bani Hamid terrane, and the similarities in lithological proportions and stratigraphic thickness between the Bani Hamid and Asimah metamorphic terranes. The new recognition of metacarbonatites and ultramafic xenoliths in the Bani Hamid area equivalent to those described from the 'metavolcanic sheet' of the Asimah area by Bucher & Kurz (1991) and Zeigler et al. (1990, 1991) strongly supports the suggestion of Searle & Cox (1999) and Cox et al. (1999) that the Bani Hamid terrane is derived from the same source as the lower grade Asimah terrane. Zeigler et al. (1990, 1991) showed that the Asimah sole metamorphic units formed from the LILE enriched, metabasaltic extrusive volcanic rocks and arc derived sediments subducted beneath the ophiolite and preserved unmetamorphosed in the Haybi complex

5.6 PT EVOLUTION OF BANI HAMID

5.6.1 Existing data

Existing estimates of peak metamorphic temperatures in the Bani Hamid terrane have been largely derived from exchange thermometry in two pyroxene bearing metabasites and quartzites, while pressures have been estimated utilising experimental data on the stability of wet and dry cordierite in the MAS system (Newton 1992). Estimated peak conditions of equilibration of the Bani Hamid terrane are 800 $\pm$ 50^{o}C and 6.5-9 kbar (Gnos 1992; Gnos & Kurz 1994), while coronae and symplectites in garnet-diopside-scapolite-plagioclase $\pm$ wollastonite calc silicate rocks are consistent with an anticlockwise PT evolution (Searle & Cox 1999).

An empirical estimate of the pressure conditions attained by the Bani Hamid terrane is suggested by metabasic assemblages such as the absence of orthopyroxene in metabasaltic clinopyroxene bearing plagioclase amphibolites, as well as the coexistence of quartz with diopside and garnet in metabasites. Both assemblages are restricted to high (>10 kbar) pressure granulites (Yardley 1989), a conclusion that conflicts with the existing estimates of Bani Hamid peak pressures (Gnos 1992).

5.6.2 Comparison with classic sole

Peak conditions in the 'classic' metamorphic sole of the adjacent Asimah terrane are 840 ± 70°C and 11.6 ± 1.6 kbar (THERMOCALC average PT mode) and 840-870°C and 11.8-13.9 kbar using conventional thermobarometry (*Chapter Three*), calculated for garnet diopside amphibolites immediately below the Semail thrust.

These values are very similar to peak temperatures and pressures calculated in the Bani Hamid terrane, a result which precludes any tectonic model for its origin that differs radically for those proposed for the classic sole (eg Gnos & Nicolas 1996). Tonalitic melts derived from garnet-diopside amphibolites of the classic sole typically formed at 656 ± 17 °C and 5.6 ± 0.6 kbar during prograde metamorphism, very similar to petrographically identical partial melt pods from the Bani Hamid terrane. These partial melts may have preserved their conditions of melting and not equilibrated at the ~850°C peak conditions of the Bani Hamid terrane due to freezing as a result of flushing by CO_2 rich fluids after their formation.

The unique features of the Bani Hamid terrane include the absence of the steep inverted metamorphic profile associated with the classic metamorphic sole. The Bani Hamid terrane does none the less exhibit a significant range in peak pressures, which vary from 14.7 ± 2.8 kbar (OM 135, metabasite) to 10.5 ± 1.1 kbar (JC 107, metasedimentary quartzite) at consistent peak temperatures of ~850°C over an apparent structural thickness of ~100 m.

Samples JC 107 and OM 135 occur at similar structural levels but on different limbs within the same fold; OM 135 occurs at most ~100 m structurally higher which demonstrates at least the presence of an apparent inverted pressure gradient within the Bani Hamid terrane, as in the classic sole sequences described in *Chapter Three*.

An apparent pressure gradient of ~4 MPa m^{-1}, assuming structural coherence in this sole section, is indicated by these estimates although the large errors and lack of coherence between the two contrasting assemblages makes the estimate rather imprecise. Average inverted sole gradients of ~2°C m^{-1} and ~3.7 MPa m^{-1} were reported from the adjacent Asimah classic sole sequence in *Chapter Three*. Gnos (1998) calculated similar figures of ~1°C m^{-1} and ~0.3-2 MPa m^{-1} for the Asimah sole using data from Bucher (1990).

5.6.3 Thermobarometry issues in UHT terranes

The applicability of Fe-Mg thermometers to UHT terranes is problematic in that cation exchange thermometers tend to record peak conditions no higher than 850°C due to post peak diffusional exchange and closure effects. Different calibrations of the garnet-clinopyroxene

thermometer have been shown to be best applied to a variety of different tectonic situations, dependent on mineral chemistry parameters (Harley 1998).

Another key feature of many UHT terranes of relevance to the Bani Hamid sequence is the stability of spinel in quartzose assemblages characterised by the absence of garnet. The quartzites sampled for this study (eg JC 107) contain abundant Fe-Ti oxides, normally magnetite and ilmenite with up to ~10% ZnO and ~2% MnO according to Gnos & Kurz (1994) and associated with high Al_2O_3 (~6-8%) enstatite and Mg cordierite. The distribution of minor components (Fe^{3+}, Zn, Cr and Mn) between phases and overall oxidation conditions, measured by f_{O_2}, controls the stability fields of phases in the FMAS system (eg Hensen 1986; Harley 1998) in such a manner as to cause stability inversions.

For example, the high oxidation states of many of the components of the Bani Hamid quartzose granulites, a result of high f_{O_2} values of 10^{-9}-10^{-11} during the granulite facies event (Gnos & Peters 1995), causes the assemblage quartz + sapphirine to migrate to lower temperatures and demonstrates that the presence of sapphirine in quartzites from the Bani Hamid terrane cannot necessarily be used to infer true UHT (>900°C) conditions (Harley 1998).

5.6.4 New PT determinations

New PT determinations for the various components of the Bani Hamid terrane have been calculated, using new microprobe analyses in conjunction with existing petrogenetic grids derived from experimental data, and the self consistent thermodynamic dataset of Holland & Powell (1998) utilised in the DOS program THERMOCALC v2.75.

Metabasites from Bani Hamid have typical peak measured PT conditions of 864 ± 15 °C and 14.7 ± 2.8 kbar (OM 135: enstatite-diopside-plagioclase-phlogopite), using THERMOCALC in average PT mode and the Brey & Kohler (1990) orthopyroxene-clinopyroxene Fe-Mg exchange thermometer. The small errors quoted for the peak temperatures contrast with the larger errors in pressure estimates from THERMOCALC in average PT mode.

Peak pressures have proved more difficult to estimate in typical metabasic assemblages, using either THERMOCALC or conventional thermobarometry. This is largely due to the absence of garnet in all metabasic assemblages from the Bani Hamid terrane and the frequent absence of diopside in amphibolite hornblende-plagioclase-quartz assemblages.

Table 5.4 Mineral analyses from sample OM 135 used in THERMOCALC PT determinations.

Mineral	Enstatite	Plagioclase	Diopside	Phlogopite
SiO_2	54.59	59.52	37.78	35.93
TiO_2	0.04	0.00	0.34	0.72
Al_2O_3	2.32	24.13	20.99	18.96
Cr_2O_3	0.00	0.00	0.00	0.00
Fe_2O_3	2.78	0.29	0.98	2.20
MnO	10.02	0.00	23.16	11.21
FeO	0.63	0.00	6.44	0.29
MgO	29.93	0.00	5.50	12.03
CaO	0.58	5.16	4.68	0.18
Na_2O	0.18	7.22	0.00	0.23
K_2O	0.00	1.09	0.00	4.89
Total	101.07	97.41	99.87	86.65
Oxygens	6	8	12	11
Si	1.918	2.717	2.976	2.822
Ti	0.001	0.000	0.020	0.043
Al	0.096	1.299	1.949	1.756
Cr	0.000	0.000	0.000	0.000
Fe^3	0.074	0.010	0.058	0.130
Fe^2	0.294	0.000	1.526	0.736
Mn	0.019	0.000	0.430	0.019
Mg	1.567	0.000	0.646	1.408
Ca	0.022	0.252	0.395	0.015
Na	0.012	0.639	0.000	0.035
K	0.000	0.064	0.000	0.491
Sum	4.003	4.980	8.000	7.455

Table 5.5 THERMOCALC PT results from sample OM 135, Bani Hamid

Location	Bani Hamid
Sample	OM 135
Rock type	Metabasite
Peak assemblage	en-di-phl-pl-spl
Average opx-cpx temp	864
Independent reactions	6
Best fit av PT result	838 ± 286°C 14.7 ± 2.8 kbar
Independent opx-cpx exchange T (Brey & Kohler 1990)	864°C
Corr	0.527
Fit	1.61
a_{H_2O}	All values
End members excluded	-

Tonalitic to monzodioritic partial melt pods and lenses with the assemblage plagioclase-hornblende-quartz-biotite-K-feldspar derived from similar metabasic granulites from Wadi Shis (figure 5.1) formed at 673 ± 17 °C and 5.6 ± 0.6 kbar (table 5.6), during the prograde evolution of the Bani Hamid terrane and can be used in conjunction with post peak petrographic textures to deduce the PT evolution of the Bani Hamid metamorphic sole (figure 5.25).

Table 5.6 Estimated crystallisation conditions for a prograde amphibolite partial melt, Bani Hamid.

Location	Bani Hamid
Sample	JC 50
PT stage	Prograde melting
Rock type	Tonalite partial melt
Assemblage	Pl-qtz-hbl-bt-kfs
Hbl-Pl temperature (Holland & Blundy 1994)	673 ± 17°C
Al in hbl pressure (Anderson 1995)	5.6 ± 0.6 kbar

Similar pressures and temperatures were obtained from analogous tonalitic partial melt veins in garnet-diopside amphibolites from the Sumeini classic sole terrane.

Calc silicate rock and marble PT conditions are not as readily obtained using either conventional thermobarometry or THERMOCALC as conditions in quartzose or metabasic assemblages, and even the estimation of peak temperatures using Fe-Mg exchange thermometry produces unrealistic results (table 5.8) in Ca rich garnet bearing assemblages due to the non ideal mixing nature of the Ca-Mg substitution pair at high Ca# values in granditic garnet compositions. However, THERMOCALC has been used to derive petrogenetic grids in the CASV system (Harley & Buick 1992; Fitzsimons & Harley 1994; Harley et al. 1994) to qualitatively constrain PT conditions in calc silicate bearing granulites and it will be qualitatively demonstrated below than the PT conditions implied for the Bani Hamid calc silicate rocks using these techniques are consistent with those derived independently for other assemblages.

Quartzites from Bani Hamid have peak measured PT conditions ranging from 860 ± 100°C and 12.9 ± 2.0 kbar (JC 90; andradite-diopside-quartz-plagioclase; metabasic protolith) to ~850°C and 10.5 ± 1.1 kbar (JC 107; enstatite-cordierite-spinel-quartz; metasedimentary protolith). Mineral analyses from JC 107 used in THERMOCALC PT analysis are shown in table 5.7.

The absence of significant alkalis (Na & K) in the cordierites analysed suggests that they were largely anhydrous (Vry 1990) although it may equally indicate that the protoliths were

depleted in the LILE by the extraction of leucogranitic partial melts. The upper pressure limit of stability of anhydrous Mg cordierite is up to ~10 kbar (Newton 1972) although more recent experimental and theoretical evidence (eg Hensen 1986) supports the earlier conclusions of Hensen & Green (1973) in which cordierite was stable up to pressures of ~11 kbar.

Table 5.7 Mineral analyses from sample JC 107 used in THERMOCALC PT determinations.

Mineral	Enstatite	Cordierite	Spinel
SiO_2	52.87	49.83	0
TiO_2	0.07	0.01	4.05
Al_2O_3	7.03	34.83	1
Cr_2O_3	0.00	0	0
Fe_2O_3	0.80	0.1	58.36
MnO	2.86	0.37	31.11
FeO	5.43	0.84	1.86
MgO	31.50	12.89	0.7
CaO	0.18	0.02	0
Na_2O	0.27	0.16	0
K_2O	0.00	0.11	0
Total	101.01	99.16	97.09
Oxygens	6.00	18	4
Si	1.828	4.932	0
Ti	0.002	0.001	0.119
Al	0.286	4.064	0.046
Cr	0.000	0	0
Fe^3	0.021	0.008	1.716
Fe^2	0.083	0.03	1.017
Mn	0.159	0.07	0.062
Mg	1.623	1.901	0.041
Ca	0.007	0.002	0
Na	0.018	0.031	0
K	0.000	0.014	0
Sum	4.026	11.054	3

Table 5.8 Results of Bani Hamid quartzite garnet-clinopyroxene exchange thermometry.

Sample	JC 59	JC 105	JC 92	JC 90
Powell (1985) grt-cpx	1090	1067	862	1095
Ellis & Green (1979) grt-cpx	1087	1065	867	1087
Krogh (1988) grt-cpx	429	838	294	498
Ai (1994) grt-cpx	832	829	557	860

Table 5.9 Estimated peak PT conditions of Bani Hamid quartzites.

Location	Bani Hamid	Bani Hamid
Sample	JC 107	JC 90
PT stage	Peak	Peak
Rock type	Metasediment	Silicified basalt (?)
Assemblage	Qtz-En-Crd-Spl	Qtz-Grt-Di-Pl
Best Grt-Cpx exchange temperature (Ai 1994)	-	860°C
Pressure (THERMOCALC Av P mode)	10.5 ± 1.1 kbar (850°C ref temp)	12.9 ± 2.0 kbar (850°C ref temp)

5.6.5 Microstructural evidence

Microstructurally the mafic and calc silicate bearing granulites tend to be granoblastic in texture (figure 5.12a-d). Deformation tends to be partitioned into quartzose assemblages, which generally exhibit a more subidiomorphic to protomylonitic texture. Calc silicate and carbonate assemblages, particularly metasedimentary marbles, in the Bani Hamid terrane commonly exhibit coronae and other reaction textures that can be used to characterise components of the (post peak) PTt evolution of the terrane. The distinction between calc silicate and carbonate assemblages has already been noted in terms of assemblage, texture and protoliths and the distinction extends to the presence of coronae and reaction rims in metasedimentary marble assemblages only. Reaction volumes are however very small, with coronae and reaction rim phases having peak modal proportions of at most ~5% (figure 5.21-23).

Sample JC 98 contains the prograde assemblage cal-K feldspar-diopside-wollastonite-titanite, with the latter phases occurring as sub idiomorphic porphyroblasts in a matrix of calcite (figure 5.21). Thin monomineralic reaction rims of quartz are found around wollastonite grains in contact with matrix calcite (figure 5.22), and similarly grossular-andradite garnet reaction rims surrounding K feldspar in contact with matrix calcite (figure 5.22). These two textures imply the following (partial) reactions respectively:

- wol + cal = qtz
- kfs + cal = grt

Sample JC 109 contains the prograde assemblage calcite-K feldspar-diopside-andraditic garnet-epidote-titanite-quartz, with the Fe-Mg silicate phases occurring as sub idiomorphic

porphyroblasts in a matrix of calcite (figure 5.21-23) and was sampled in lower Wadi Shis, immediately adjacent (within a stratigraphic distance of ~50 m; see figure 5.16) to the Semail thrust. Quartz is found only in thin reaction rims and was identified by microprobe analysis. Thin monomineralic reaction rims of quartz are found around garnet grains in contact with matrix calcite, and similarly garnet reaction rims surrounding diopside in contact with matrix calcite. These two textures imply the following (partial) reactions respectively:

- grt + cal = qtz
- di + cal = grt

The Bani Hamid marbles may all be represented in the CASV (CaO-Al_2O_3-SiO_2-CO_2) system, with other minor phases present including MgO, K_2O, Na_2O, TiO_2, FeO and Fe_2O_3. The presence of garnet ± quartz rims and symplectites around peak phases in granulite facies calc silicate rocks, modelled in the CASV system, has been ascribed to post peak H_20 rich fluid flushing (Warren et al. 1987) but in some cases was also associated with isothermal decompression. However, this interpretation was based on the T-x_{CO_2} grid of Ellis (1978) which is shown in figure 5.24 and on a purely empirical basis, assigned positive $dT/d\,x_{CO_2}$ orientations for the granulite facies conditions garnet-quartz producing CASV decarbonation reactions, for which no direct experimental evidence exists.

Characterisation of the PTt conditions that produce coronae and reactions rims or symplectites in granulite facies calc silicate rocks in the simplified model system CASV has more recently been attempted using THERMOCALC by Harley & Buick (1992), Fitzsimons & Harley (1994) and Harley et al. (1994), based on the Holland & Powell (1990) dataset. Unusual negative dT/da_{CO_2} and dT/dx_{CO_2} slopes were assigned to these CASV decarbonation reactions, in contrast to the Ellis (1978) T-x_{CO_2} grid, which can therefore be interpreted as representing cooling below 780-850°C or H_2O rich fluid infiltration under low to moderate (~0.4) a_{CO_2} conditions at >6 kbar, a set of conditions that match well those independently inferred for the Bani Hamid terrane in this and other studies (Bucher & Kurz 1991; Gnos 1992; Gnos & Kurz 1994).

Non CASV components introduce multivariance into CASV reactions, causing CASV univariant reactions to become composition dependent bands in PT-a_{CO_2} space (Fitzsimons & Harley 1994) and therefore somewhat reducing the precision of any PT conditions inferred from textural and petrogenetic criteria. However, the presence of the clinopyroxene diopside in the samples (typically $Ca_{0.96}Mg_{0.51}Fe_{0.21}Fe^{3+}_{0.18}Al_{0.06}Na_{0.05}Ti_{0.02}Mn_{0.01}[Si_{1.78}Al_{0.22}O_6]$ in JC 98) means that the enlarged system CMASV, and the role of the clinopyroxene Ca Tschermak end member in the formation of garnet from diopside must be considered. Harley et al. (1994) ascribe the

development of garnet ± quartz rims around diopside to (FM)CASV system multivariant decarbonation reactions involving the essenite ($CaFeAlSiO_6$) component of clinopyroxene.

Independent estimates of the fluid compositions prevalent within the Bani Hamid terrane during the metamorphic peak have been obtained by Gnos & Kurz (1994). Using fluid inclusion analysis, in conjunction with the experimental data on cordierite compositions obtained by Vry (1990), a 'CO_2 rich' fluid composition was indicated. However, THERMOCALC results on sample JC 107 (enstatite-cordierite quartzite; table 5.9) in this study proved most precise using a H_2O activity of ~0.75, and the textural criteria outlined above from Bani Hamid calc silicate bearing granulites are consistent with a fairly low CO_2 activity during the post peak evolution of the terrane. Furthermore, the assemblage wollastonite-scapolite has also been noted from the lower Wadi Shis area, and such an assemblage is indicative of high x_{H_2O} and low x_{CO_2} conditions (Warren et al. 1987).

Since JC 109 was sampled close to JC 107, adjacent to the Semail thrust (figure 5.16), along which extensive H_2O fluidisation during ophiolite obduction has been widely demonstrated (Chen & Pallister 1981; Zeigler et al. 1991; Cox et al. 1999), it is possible that fluid compositions were locally externally buffered by fluidisation along the Semail thrust. The patchy development of coronae despite the abundance of calc silicate bearing assemblages in the Bani Hamid terrane may indicate that coronae formation was largely controlled on a local scale by the intermittent infiltration of H_2O rich fluids along the Semail thrust plane. However, cooling of the calc silicate bearing granulites, by the underplating of cold subducted material to the base of the Semail thrust hanging wall, may have also facilitated cooling of the granulites.

5.6.6 PT profiles through Bani Hamid

The arguments outlined in **3.2** concerning the value and interpretation of structural or metamorphic profiles through the structurally poorly constrained polyphase ductile shear zone that the Semail ophiolite metamorphic sole represents are especially pertinent to the highly deformed and rethrusted Bani Hamid terrane. The absence of a clear temperature profile through the ~1 km thick sequence was first noted by Gnos & Kurz (1994) and implies the thickening and disruption of the original architecture of the outcrop by repetition of the originally highest grade sole material, and structural profiles through the western and eastern sectors of the Bani Hamid terrane (figure 5.15 and 5.16) indicate the presence of both large amplitude isoclinal folding and imbricate thrusting within the terrane.

5.7 AGE OF BANI HAMID METAMORPHISM

The age of the Bani Hamid granulite facies sequence relative to the adjacent Asimah sole terrane is unclear and no accurate (U-Pb) dating of the peak of granulite facies metamorphism exists in the literature. A $^{40}Ar/^{39}Ar$ hornblende age of 95.3 ± 0.5 Ma (Hacker et al 1996; recalculated from Gnos & Peters 1993) from a Bani Hamid metabasic granulite overlaps the mean hornblende age of 94.9 ± 0.2 Ma for the amphibolite facies metamorphism in the Asimah area (Hacker et al. 1996) and suggests the Bani Hamid granulites formed at a similar time to the highest grade, amphibolite-granulite facies, components of the classic metamorphic sole.

Given that the Bani Hamid peak temperature conditions were ~850°C, that the best estimate of the attainment of hornblende $^{40}Ar/^{39}Ar$ system closure in the Bani Hamid terrane is 95.3 ± 0.5 Ma (Hacker et al. 1996), the closure temperature of hornblende in the $^{40}Ar/^{39}Ar$ system is ~550°C, and assuming a metamorphic sole cooling rates of ~200°C Ma^{-1} before 93.5 Ma (Hacker et al. 1996) an age of ~96.3-97.3 Ma is indicated for the Bani Hamid metamorphic peak. Similar calculations for the adjacent Asimah terrane garnet-diopside sole amphibolites yield an indistinguishable peak metamorphic age of ~96.4 Ma and imply that the two distinct sole terrane were formed at the same time.

Gnos & Peters (1993) used the K/Ar system to constrain the timing of the greenschist event age seen overprinting granulite facies assemblages in the Bani Hamid terrane to 91.2 ± 0.5 Ma (actinolitic overgrowth of hornblende in metabasic granulite). Since the rethrusting event that exhumed the Bani Hamid terrane along the Bani Hamid thrust is characterised by the presence of greenschist facies assemblages in quartzose mylonites along the thrust surface which formed at temperatures as low as 300°C (Gnos & Kurz 1994), it is possible that the two greenschist assemblages were formed during the same event soon after the formation of the granulites themselves.

5.8 SUMMARY

New field mapping indicates that the heavily imbricated Bani Hamid granulite facies metamorphic sole sequence was exhumed along a major out of sequence thrust (the Bani Hamid thrust) that repeats the entire ophiolite mantle sequence (Searle & Cox 1999). Recognition of this repetition of the mantle sequence means that more complex models accounting for the presence of the arc-trench complex derived material within the ophiolite mantle sequence can be discarded (eg the transform fault pull apart basin model proposed by Gnos & Nicolas 1996).

The age of the Bani Hamid terrane is imperfectly constrained but the limited existing data suggests the granulites formed synchronously with material of similar grade from the adjacent Asimah classic sole terrane. Neither is the timing of the late thrusting and repetition of the Khawr Fakkan block of the ophiolite along the Bani Hamid thrust well constrained although the extrapolation of existing metamorphic sole cooling rates to the Bani Hamid terrane suggests an age of ~94 Ma, which is similar to the age of the greenschist facies overprint (91.2 ± 0.5 Ma; Gnos & Peters 1993) seen throughout the Bani Hamid terrane. Further movement along the Bani Hamid thrust, related to the early Tertiary exhumation of the adjacent Musandam culmination along the Hagab thrust (Searle 1985), is entirely possible also.

The likely equivalence of the Bani Hamid and Asimah terranes (Searle & Cox 1999; Cox et al. 1999) in terms of protolithic material (the Haybi complex), peak metamorphic conditions, and age implies that Permo-Triassic to Jurassic transitional oceanic crustal material and associated sediments were subducting NE beneath the obducting Semail ophiolite. Furthermore, the presence of the Haybi complex beneath the entire Semail ophiolite may imply the presence of granulite facies metamorphic material at depth throughout the ophiolite belt that has only locally been exhumed in the Bani Hamid area. Reasons for the clear compositional and modal differences in the internal stratigraphy of the Bani Hamid terrane compared to the 'classic sole' are therefore attributable to palaeogeographical variations along strike during the subduction-obduction event that emplaced the Semail ophiolite.

New PT determinations from a variety of lithologies from different structural positions within the terrane demonstrate the absence of a strong temperature gradient within the Bani Hamid sole sequence. However, the restoration of isoclinally folded sequences within the terrane demonstrates the presence of an apparent inverted pressure gradient in the terrane. Typical peak conditions recorded within the terrane are 850 ± 50°C and 13.5 ± 2 kbar. Recorded pressures appear to be slightly higher in metabasic granulites, and the highest temperatures are recorded in the metacarbonatites, some of which exhibit temperatures of over 1200°C that may represent relict igneous crystallisation temperatures. However, Fe-Mg exchange thermometry is unreliable when applied to Ca/Fe^{3+} rich garnets due to the non ideal mixing nature of the Ca-Mg substitution pair at high Ca# values in granditic garnet compositions. It is notable (table 5.8) that the more recent calibrations (eg Ai 1994) of the garnet-clinopyroxene thermometer produce more realistic results with such garnet compositions due to their use of more refined empirical garnet cation mixing models.

The inferred sole anti clockwise PT evolution and peak conditions attained by the Bani Hamid terrane are very similar to those of the 'classic' sole of the ophiolite (cf figure 3.26, *Chapter Three*) and are consistent with formation of the Bani Hamid sole terrane in a similar high geotherm environment derived from the heat of the overlying young and hot Semail ophiolite during intra oceanic subduction.

Metasedimentary carbonates from the terrane frequently exhibit coronae and reaction rims around porphyroblast phases, and comparison of the implied reactions with reactions derived both experimentally and from THERMOCALC in the CASV system suggests that the formation of garnet coronae to peak CASV phases is attributable to either cooling below 780-850°C or H_2O fluid influx under conditions of relatively low a_{CO_2} at pressures greater than 6 kbar. Independent assessments of local fluid compositions and local tectonic considerations are most consistent with coronae formation being driven by both processes, although the limited occurrence of coronae and their proximity to the Semail thrust suggest that local external fluid buffering by H_2O rich fluid infiltration along the Semail thrust may have been the more dominant factor.

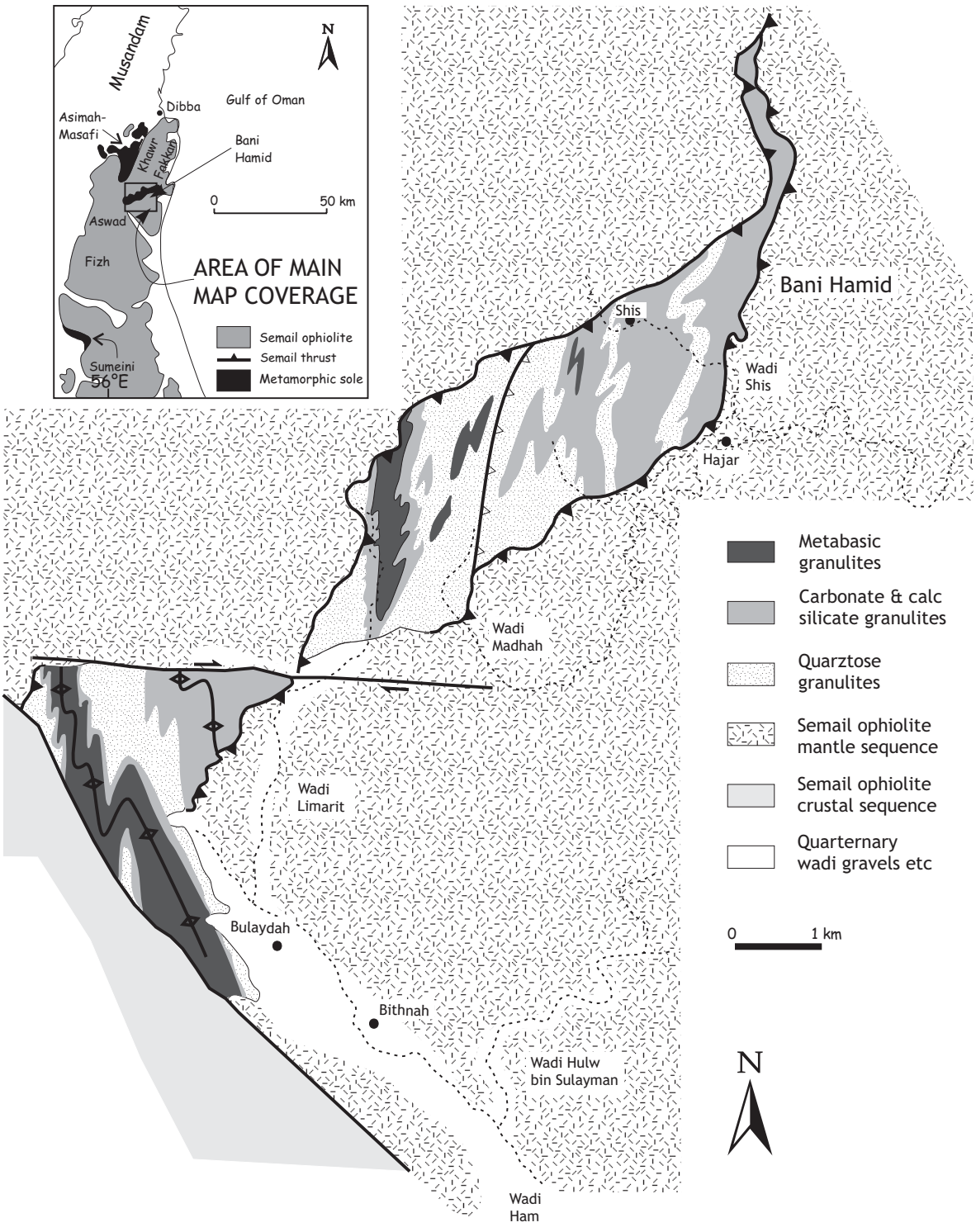


Figure 5.1 Location and geology of the Bani Hamid metamorphic sole terrane. Map drawn from field observations during January 1997 and January 1998 and based on 1:20,000 colour aerial photography courtesy of the Directorate General of Petroleum and Minerals, Muscat, Oman. The Bani Hamid area is largely within the United Arab Emirates, although the Omani enclave of Madhah to the east extends as far west as the Wadi Shis area of eastern Bani Hamid in a poorly defined manner. The ophiolite block to the east of the Tertiary Wadi Ham fault is the Khawr Fakkan block, and to the east, the Aswad block. After Searle (1980); Stossel & Zeigler (1985); Bucher & Kurz (1991) and Gnos (1992). Structural elements of the Bani Hamid terrane geology are summarised in figure 5.13 and a new cross section through the entire terrane is presented in figure 5.14. The location of more detailed metamorphic profiles through the terrane is shown in figures 5.15 and 5.16.

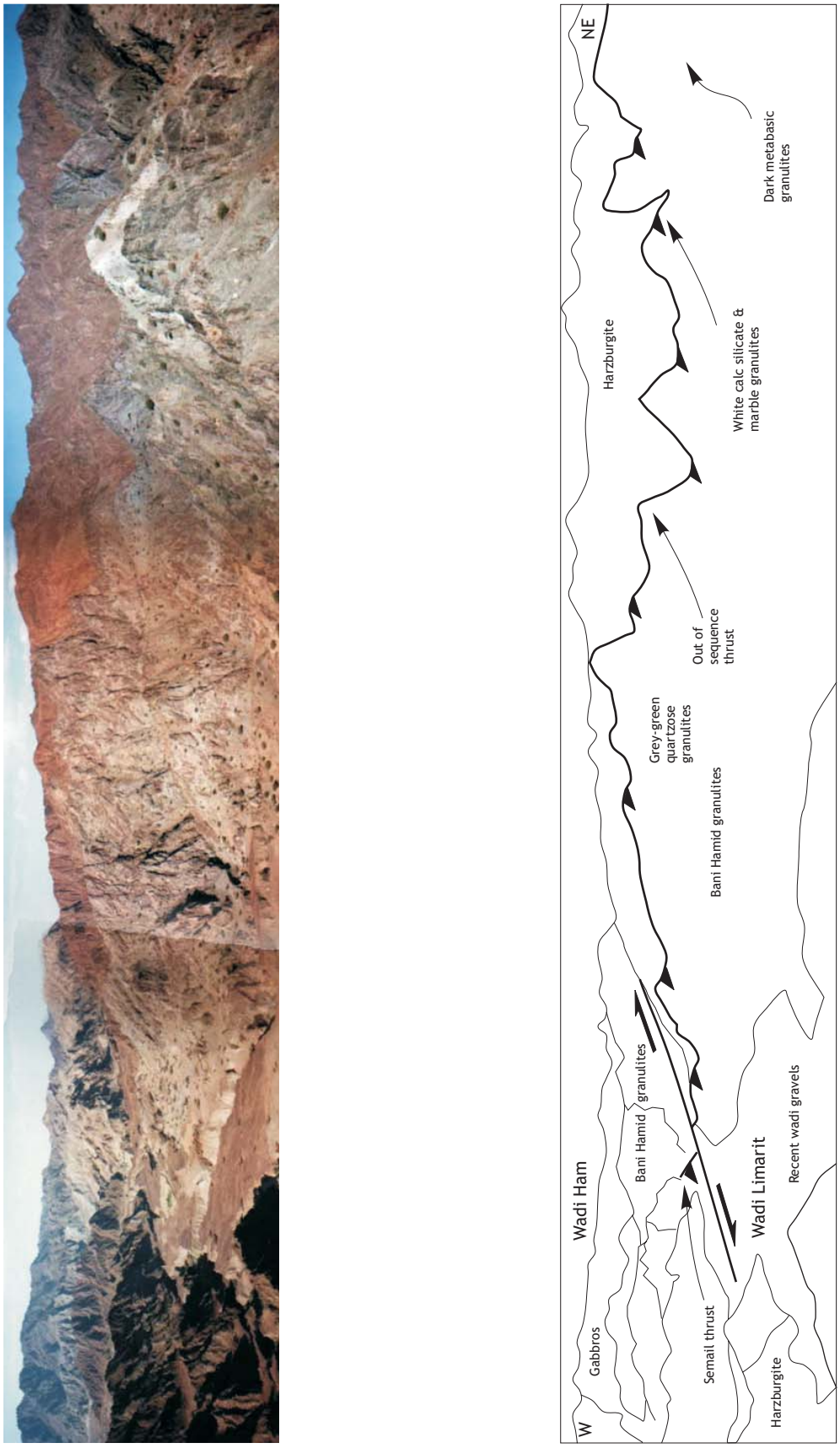


Figure 5.2 Field relationships of the Bani Hamid granulite facies high pressure metamorphic sole terrane and surrounding ophiolite as seen from the peaks above Wadi Limarit in the eastern part of the terrane (figure 5.1). In the far distance, the major Tertiary Wadi Ham fault can be seen which separates the eastern (rethrusted) Khawr Fakkan ophiolite block with its associated leucogranitic intrusions (*Chapter Six*) from the Aswad block.

Field views of the Bani Hamid granulite facies metamorphic sole terrane.



Figure 5.3 View of the Bani Hamid granulite facies metamorphic sole terrane, looking east from Wadi Limarit. The uniformly SE dipping different sole components are readily distinguished: dark metabasic granulites, blue-grey quartzose granulites and pale metacarbonates and calc silicate rocks. Brown harzburgites of the Khawr Fakkan ophiolite block occur in the foreground.



Figure 5.4 The Semail thrust, dipping SE at ~40° and separating wollastonite-scapolite marbles from serpentinised harzburgites of the Khawr Fakkan block of the ophiolite, seen at the junction of Wadi Hajar and Wadi Shis in eastern Bani Hamid.

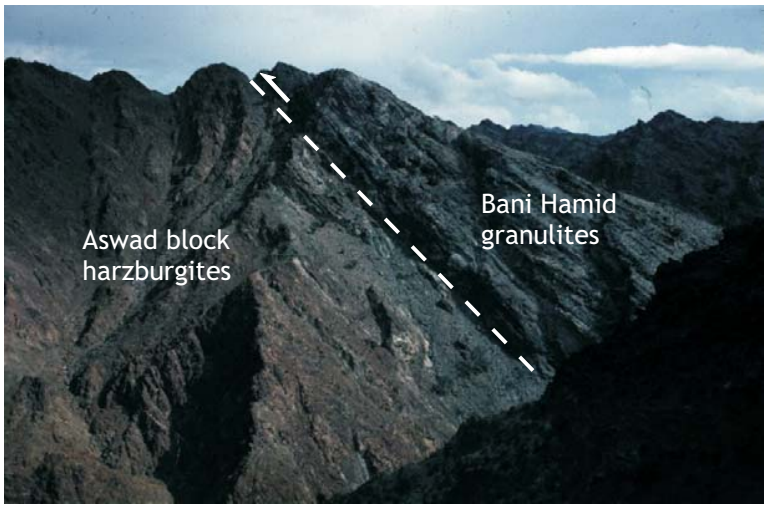


Figure 5.5 The Bani Hamid out of sequence thrust, dipping SE at ~50° and separating quartzose granulites from serpentinised harzburgites of the Khawr Fakkan block of the ophiolite, seen from upper Wadi Limarit.

Some key field relationships within the Bani Hamid terrane that help to identify protoliths and elucidate tectonic processes.



Figure 5.6 Contact between banded enstatite-cordierite bearing metasedimentary quartzose gneisses and diopside-enstatite-phlogopite ultramafic gneiss, Wadi Shis. The sharp linear contact and the presence of xenoliths of quartzose material aligned with their long axes parallel to the contact suggests that the ultramafic unit was originally a sill within a sedimentary sequence and most probably represents a component of the mid Triassic (~220 Ma; Hacker et al. 1996) suite of ultramafic sills that intrude the Hawasina and Haybi sediments (Searle 1984). Image is ~3 m across.



Figure 5.7 Transfolial tonalitic (plagioclase-hornblende-biotite) partial melt vein in hornblende-plagioclase-biotite-diopside metabasic gneiss, lower Wadi Hajar.



Figure 5.8 Similar transfolial tonalitic (plagioclase-hornblende-biotite) partial melt vein truncating foliation in diopside-hornblende retrogressed mylonitic quartzose gneiss, Wadi Shis.

Field relationships and appearance of the contrasting metasedimentary and metacarbonatite marbles and calc silicates of the Bani Hamid terrane.

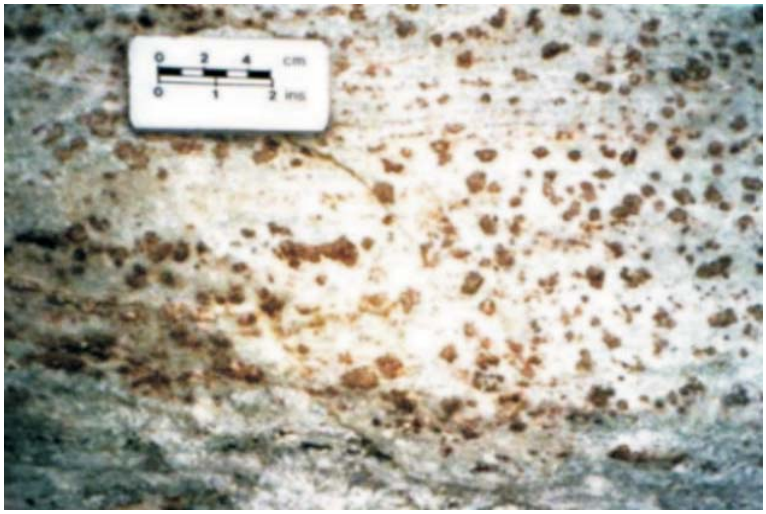


Figure 5.9 Metasedimentary marble stream boulder, upper Wadi Shis, showing euhedral zoned granditic garnet porphyroblasts up to ~10 mm in size.

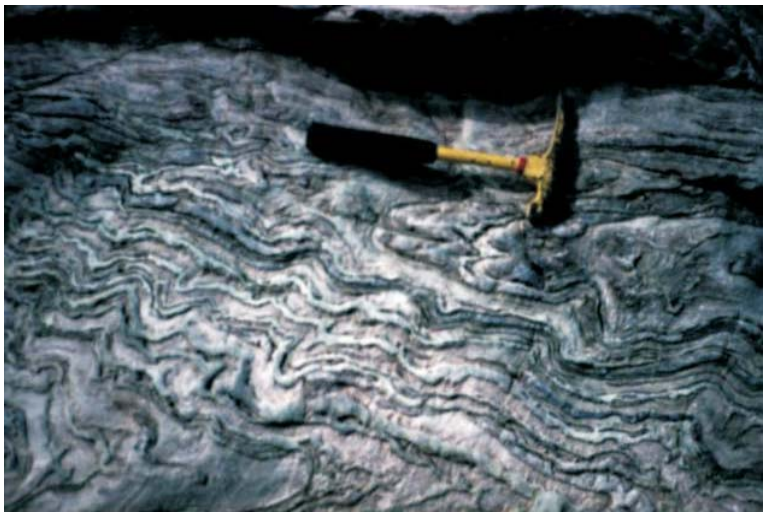


Figure 5.10 Ptygmatic folding in metasedimentary marbles, Wadi Shis, with folding picked out by compositional and (?) metamorphic transfer layers.

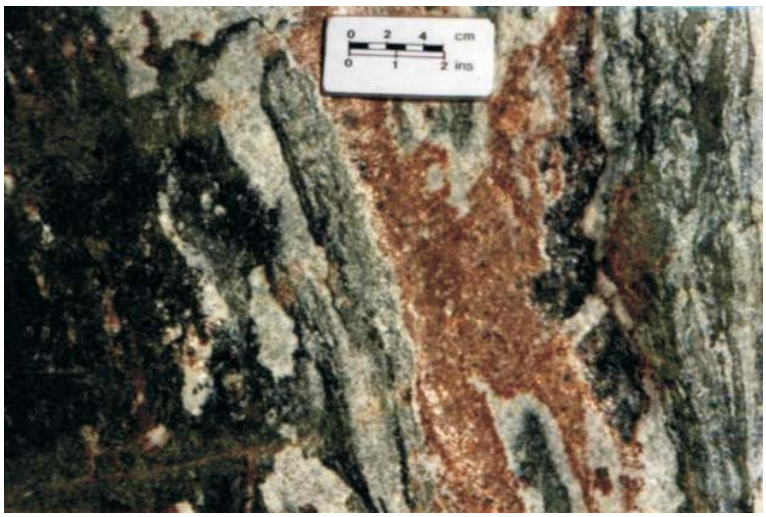
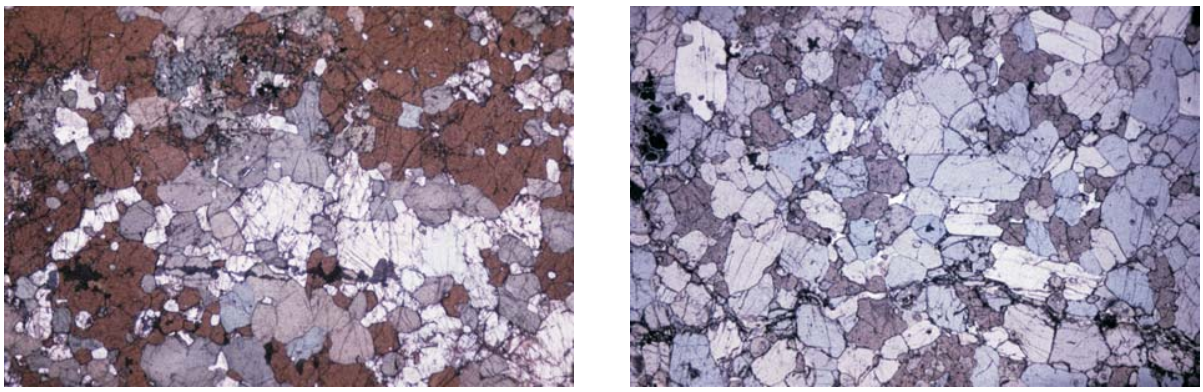
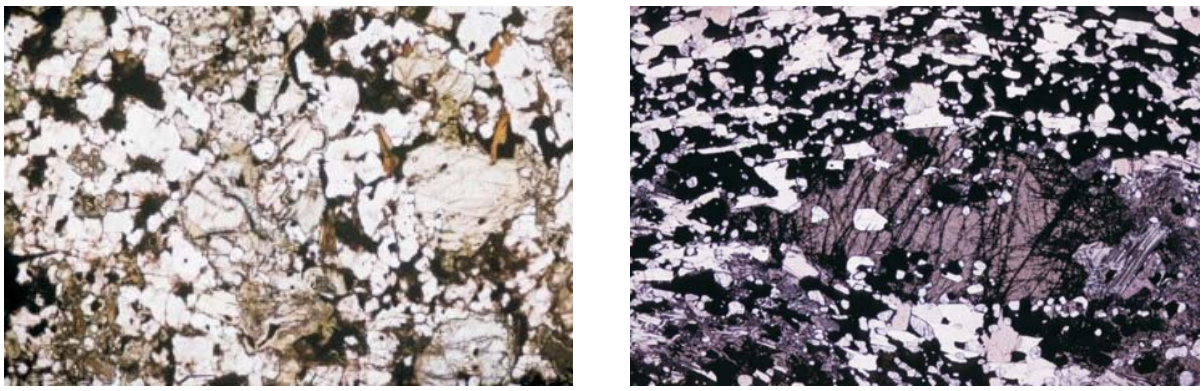


Figure 5.11 Mineralogy of massive calc silicate unit adjacent to the Semail thrust at the top of the Bani Hamid sequence, lower Wadi Shis, showing green diopside, red-brown andraditic garnet, white wollastonite and dark grey scapolite. Compare with thin sections in figure 5.12.

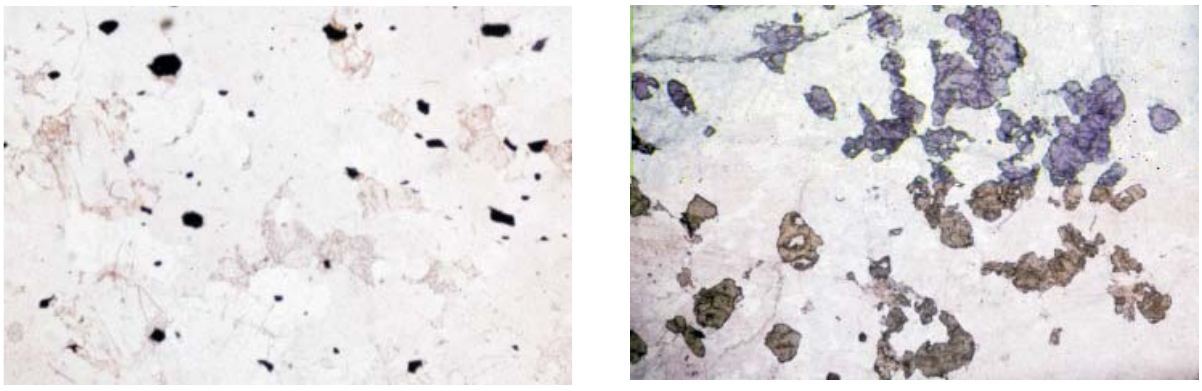
Figure 5.12 Petrography of the major components of the Bani Hamid granulite terrane. Field of view for all thin sections is ~7 mm.



a) Metacarbonatite (?) calc silicate gneiss with coarse grained granoblastic texture and brown granditic garnet, greenish diopside and colourless scapolite. b) Similar calc silicate gneiss with wollastonite rather than scapolite.



c) Coarse grained meta alkali basalt with yellowish enstatite, diopside, plagioclase, phlogopite and some microcline. d) Occurring as nodules and lenses within metacarbonatites and alkali basalts in the Bani Hamid terrane are ultramafic xenoliths such as this apatite-phlogopite-magnetite glimmerite which contains occasional porphyroblasts of strongly pleochroic clinopyroxene.



e,f) Much of the quartzose material of the Bani Hamid terrane is strongly retrogressed and mylonitised due to low temperature recrystallisation associated with exhumation along the out of sequence thrust that forms the northern boundary of the terrane. These examples however are from structurally higher in the sequence and show the contrasting assemblages in metasedimentary and (?) silicified basaltic or volcanogenic material. A metachert (e) exhibits Al_2O_3 rich (~7.5%) Mn enstatite, Mn cordierite and Mn/Zn spinel (Gnos & Kurz 1994). A silicified basaltic quartzite contains diopside and Ca garnet.

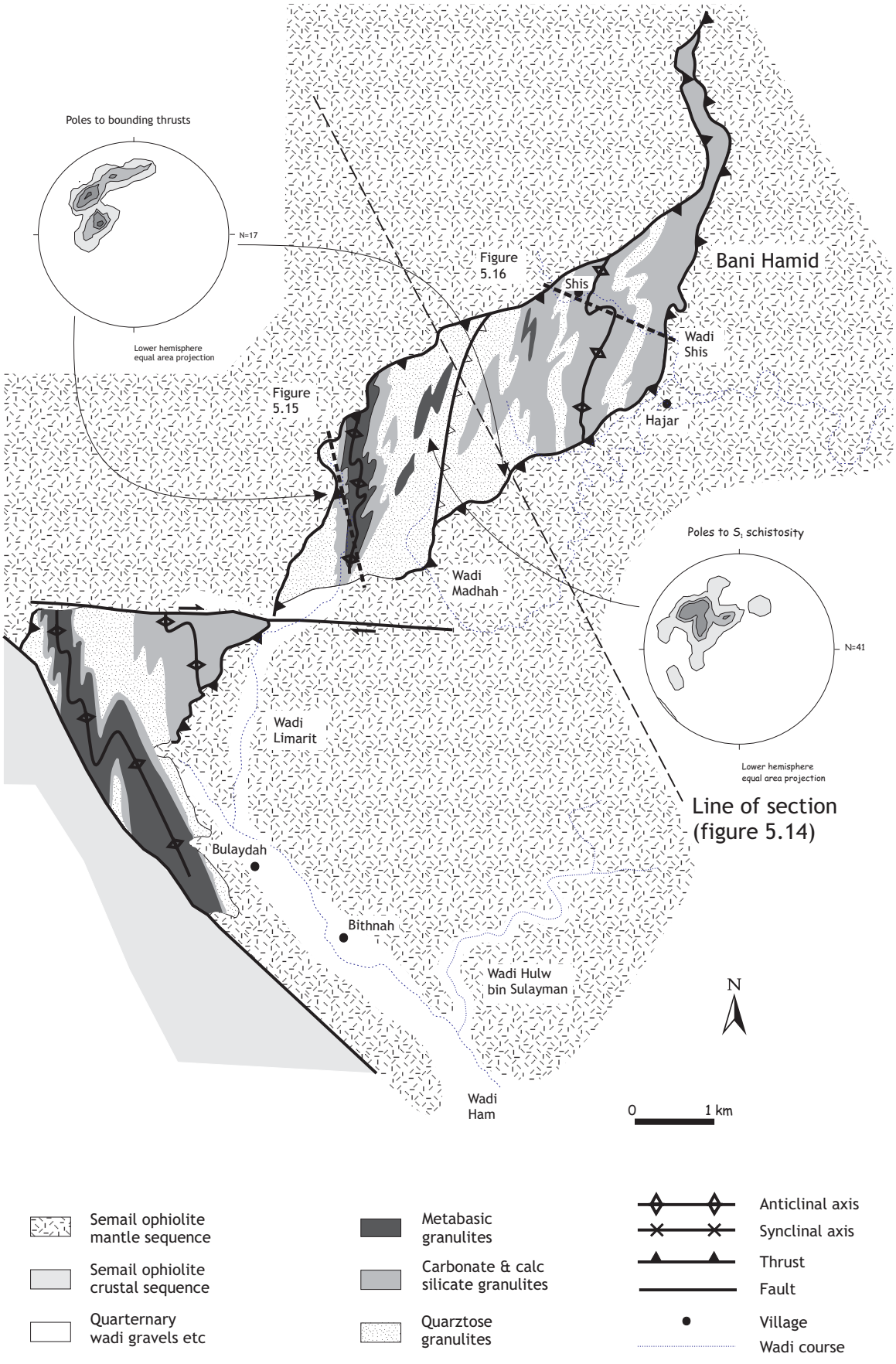


Figure 5.13 Structure and petrography of the Bani Hamid metamorphic terrane, showing the line of section (figure 5.14), location of the metamorphic sample profiles shown in figure 5.16 and 16, as well as the structural disposition of the Semail and Bani Hamid thrusts.

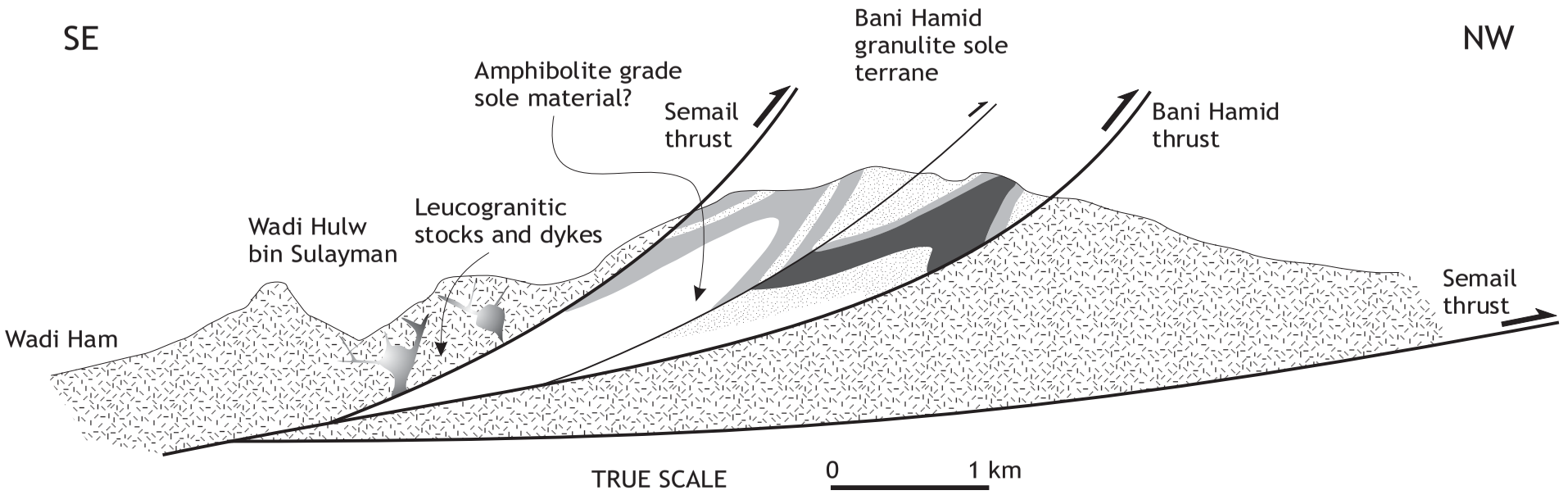


Figure 5.14 Section through the Bani Hamid granulite facies metamorphc sole terrane. The granulite facies metamorphic sole is here ~1.25 km thick but has been thickened by NW verging isoclinal folding and imbricated by minor thrusting. It is possible that lower grade sole material is present in the core of the folded sequence below present erosion levels. Granitoid intrusions in the Khawr Fakkan ophiolite block in the Wadi Hulw bin Sulayman area, structurally above the Bani Hamid terrane, are discussed in *Chapter Six*. See figure 5.13 for key and line of section.

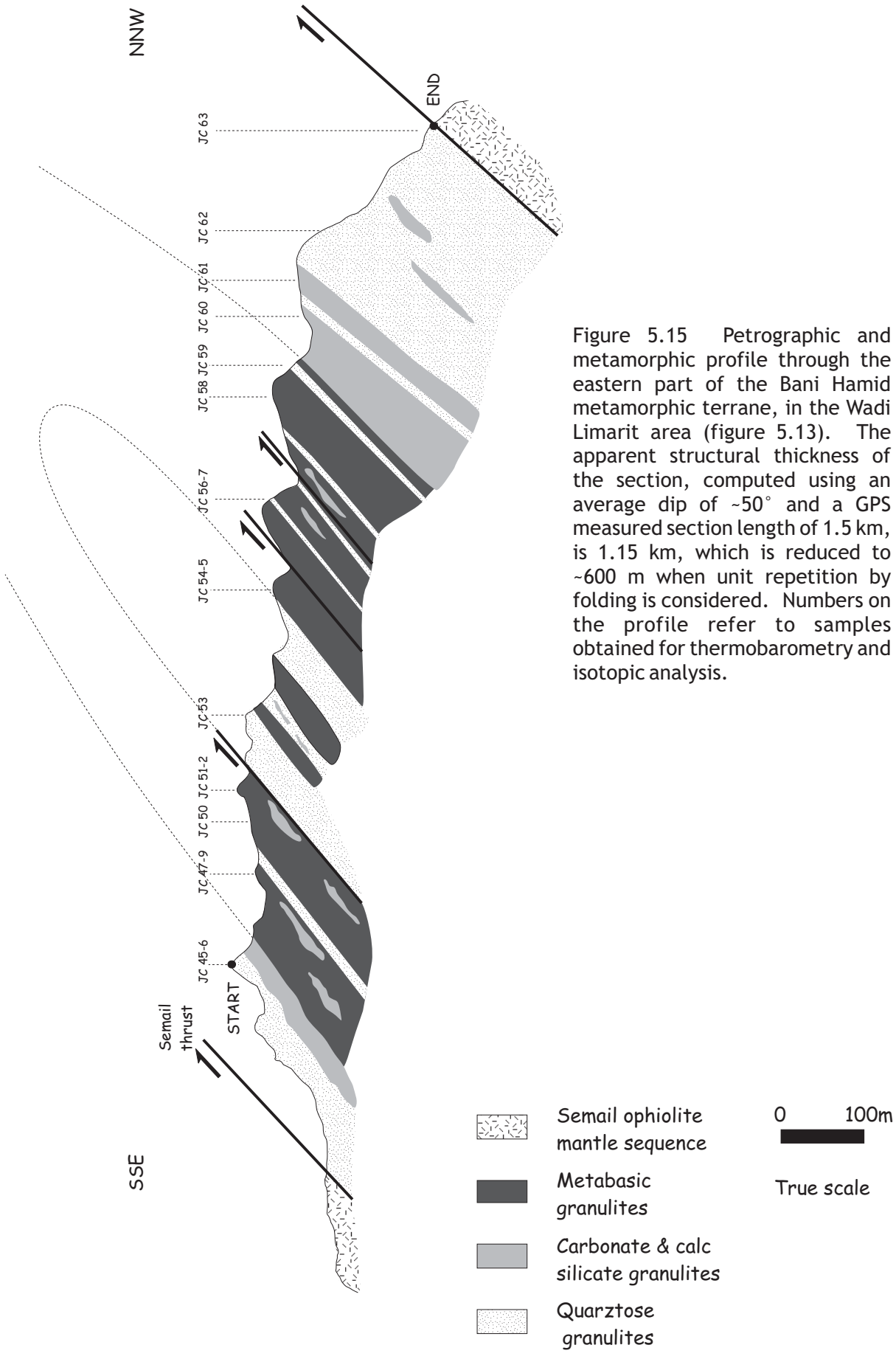


Figure 5.15 Petrographic and metamorphic profile through the eastern part of the Bani Hamid metamorphic terrane, in the Wadi Limarit area (figure 5.13). The apparent structural thickness of the section, computed using an average dip of ~50° and a GPS measured section length of 1.5 km, is 1.15 km, which is reduced to ~600 m when unit repetition by folding is considered. Numbers on the profile refer to samples obtained for thermobarometry and isotopic analysis.

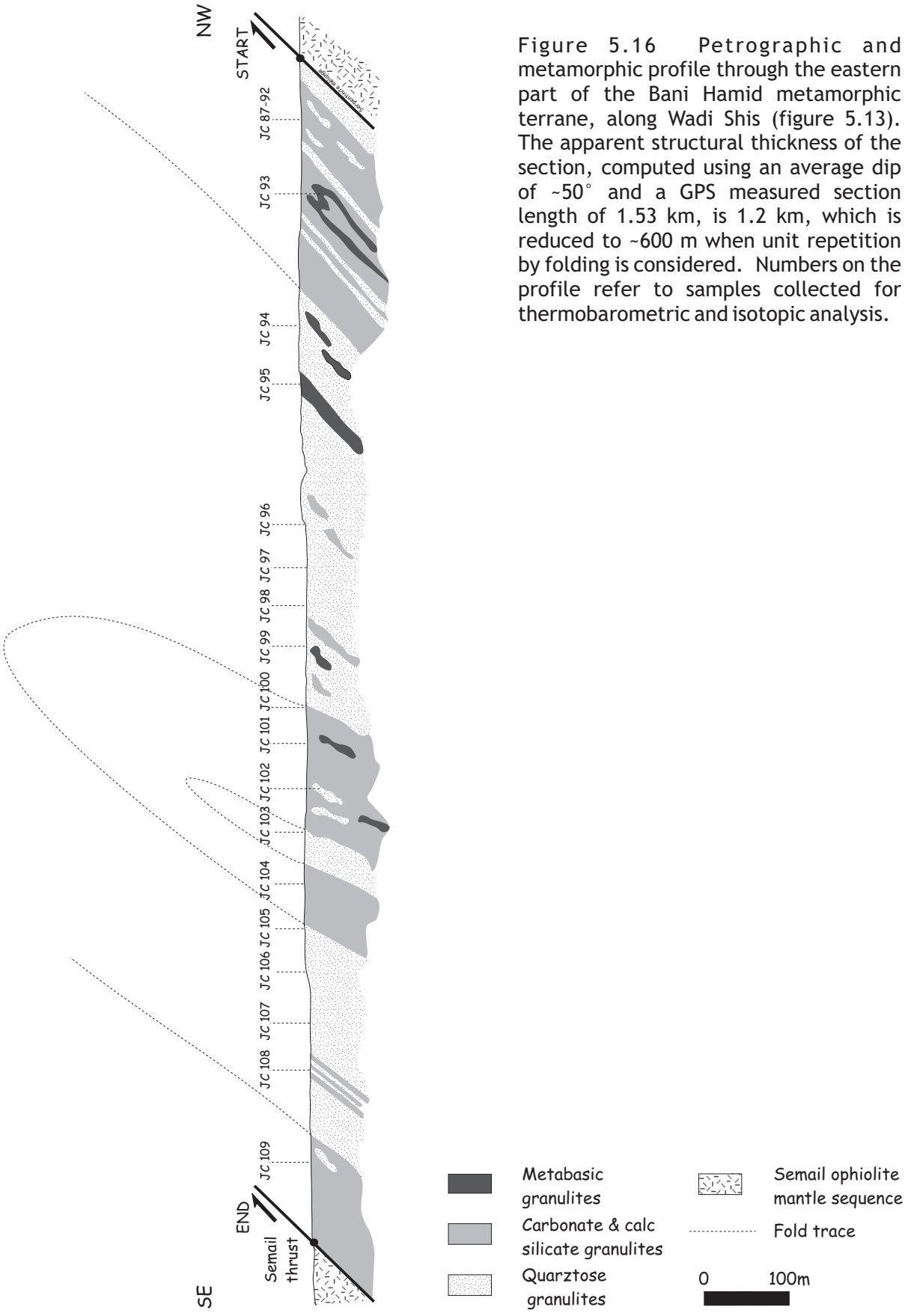
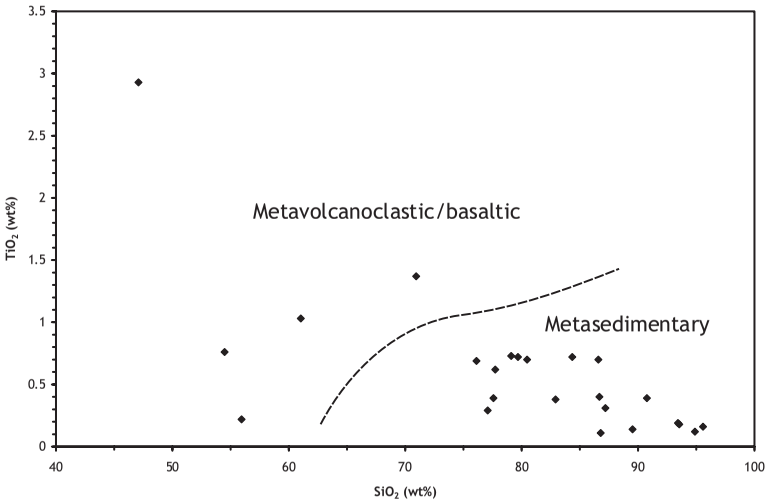


Figure 5.16 Petrographic and metamorphic profile through the eastern part of the Bani Hamid metamorphic terrane, along Wadi Shis (figure 5.13). The apparent structural thickness of the section, computed using an average dip of ~50° and a GPS measured section length of 1.53 km, is 1.2 km, which is reduced to ~600 m when unit repetition by folding is considered. Numbers on the profile refer to samples collected for thermobarometric and isotopic analysis.



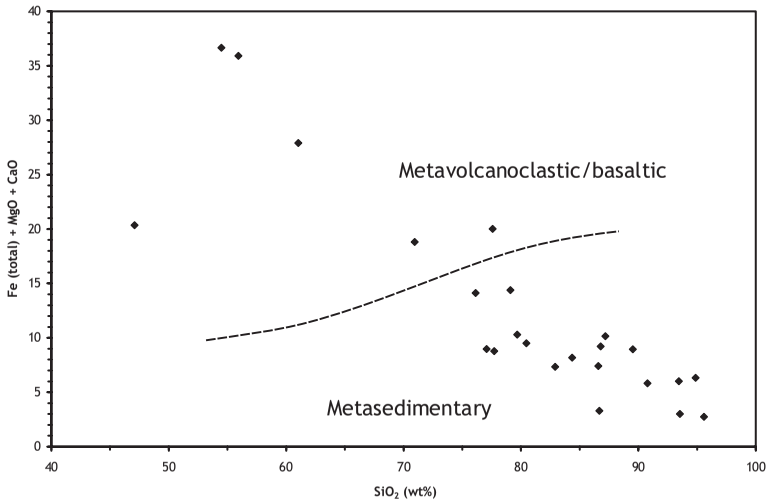
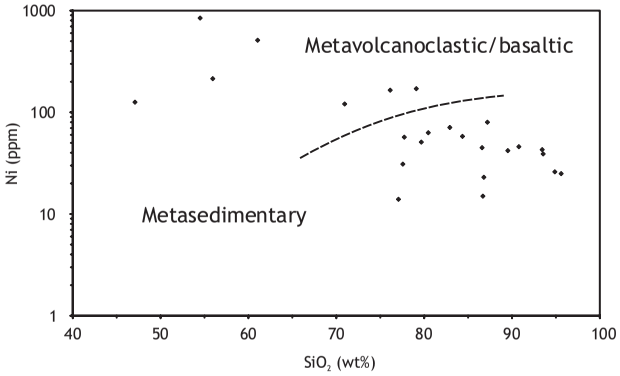
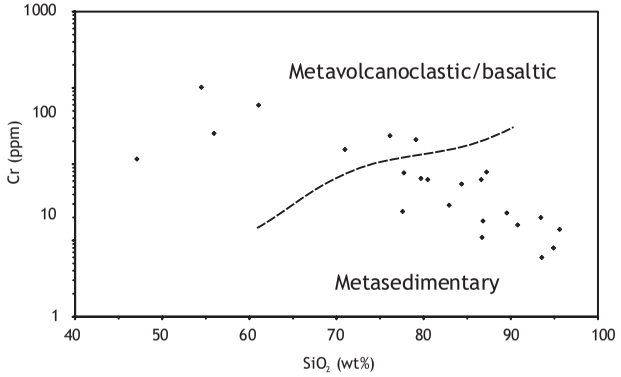


Figure 5.17a,b TiO_2 and total mafic ($FeO + Fe_2O_3 + MgO + CaO$) Harker plots for Bani Hamid quartzose granulites showing the clear compositional contrasts between the metabasaltic or volcanoclastic and metasedimentary gneisses.





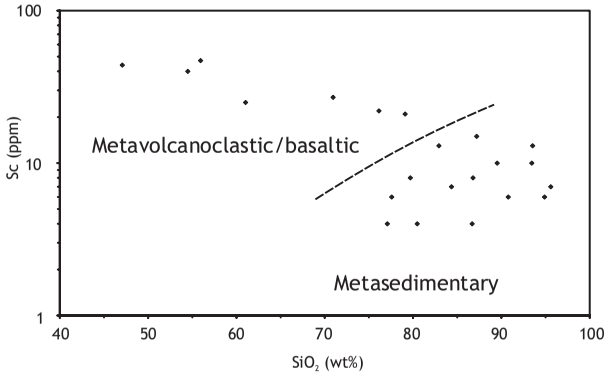


Figure 5.18a-c Logarithmic trace element Harker plots for Bani Hamid quartzose granulites. The trace elements Sc, Cr and Ni are preferentially partitioned into mafic minerals and have higher concentrations in metamorphic rocks derived from mafic precursors.

Spider diagrams illustrating the contrasts between the metasedimentary and volcaniclastic or silicified basalt quartzose gneisses in the Bani Hamid terrane. Normalising data for ORG and MORB from Pearce et al. (1984) and Pearce (1983) respectively. Bani Hamid quartzose granulite analyses are shown in table 5.1 and 5.2 and are from Bucher & Kurz (1991), and Khawr Fakkan block leucogranite analysis from Cox et al. (1999).

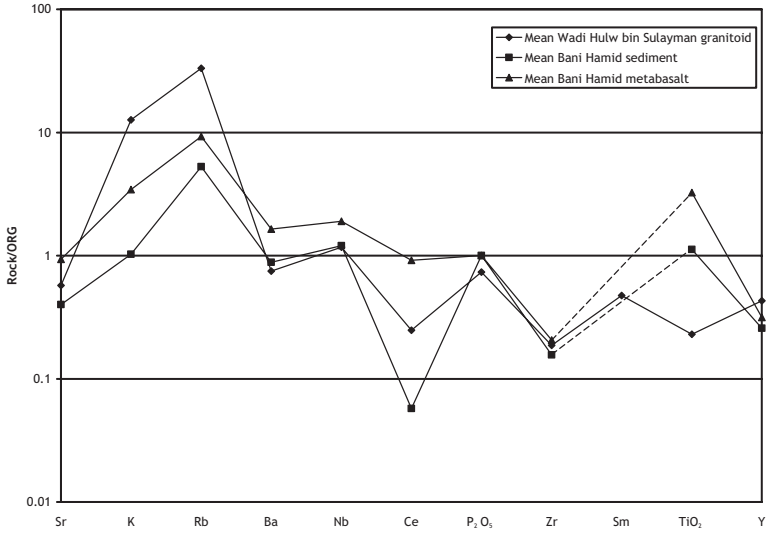


Figure 5.19 ORG normalised spider diagrams illustrating the contrasts between the metasedimentary and volcaniclastic or silicified basalt quartzose gneisses in the Bani Hamid terrane. A leucogranite from Wadi Hulw bin Sulayman, intruding mantle sequence harzburgites immediately above the Bani Hamid terrane is shown for comparison and the clear genetic relationship between the Bani Hamid granulites and these anatectic melts is suggested by the close correlation in trace element concentrations and will be demonstrated in *Chapter Six*. The Bani Hamid quartzose granulites all exhibit LILE enrichment and are distinguished only by the TiO_2 enrichment and Ce (LREE) depletion shown by the non sedimentary analyses.

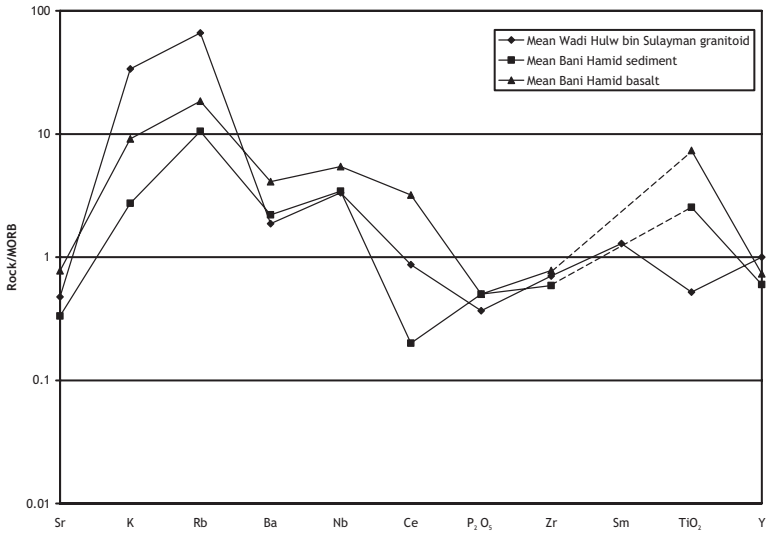


Figure 5.20 MORB normalised spider diagrams illustrating the contrasts between the metasedimentary and volcaniclastic or silicified basalt quartzose gneisses in the Bani Hamid terrane. The Bani Hamid granulites and anatectic melts have similar patterns and are characterised by strong enrichment relative to MORB.

Figure 5.21-23 Coronae around porphyroblasts in metasedimentary carbonate granulite sample JC 108. Field of view in all photomicrographs is ~7 mm.

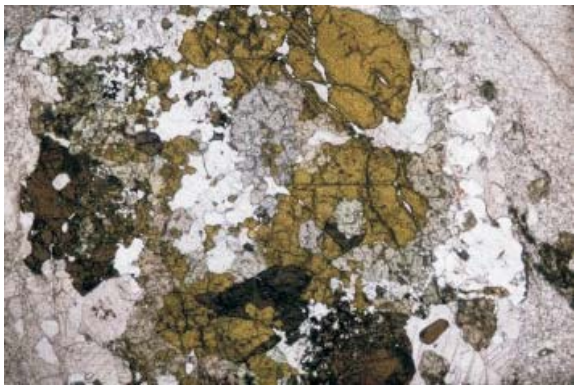


Figure 5.21 Aggregate of epidote, titanite, andraditic garnet and diopside in metasedimentary carbonate sample JC 108.



Figure 5.22 Quartz rimming andraditic garnet in contact with matrix calcite, implying the partial reaction garnet + calcite ➡ quartz.



Figure 5.23 Granditic garnet (more Ca rich than andraditic garnet porphyroblasts in the sample) rimming diopside again in contact with matrix calcite, suggesting the partial reaction diopside + calcite ➡ garnet. See text for discussion.

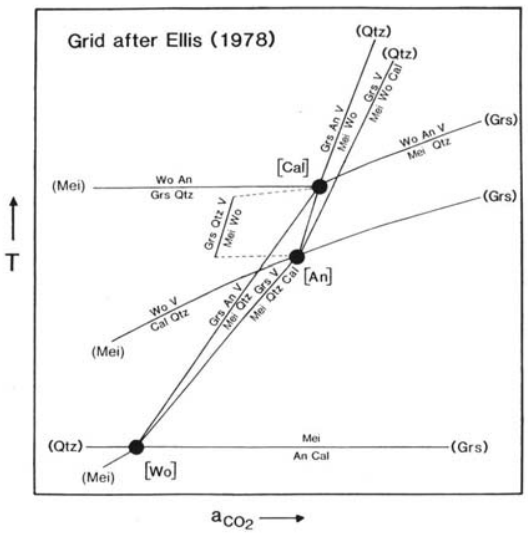


Figure 5.24 Isobaric T-a_{CO2} grid, from Fitzsimons & Harley 1994) and after Ellis (1978), for the calc silicate granulite facies phases grossular, meionite (scapolite), calcite, quartz, anorthite, wollastonite and CO_2 in the system CASV. In this grid, the garnet and quartz coronae producing decarbonation reactions (for which there is still no experimental data) such as (An, Qtz) and (An, Cal) are assigned positive dT/da_{CO2} slopes, an interpretation which implies that these reaction would proceed with heating or H_2O influx. The recent treatments of Fitzsimons & Harley (1994) and Harley et al. (1994), based on the internally consistent thermodynamic dataset of Holland & Powell (1990), give these reactions negative slopes in T-a_{CO2} space and the reactions are therefore ascribed to cooling or H_2O influx. See text for further discussion.

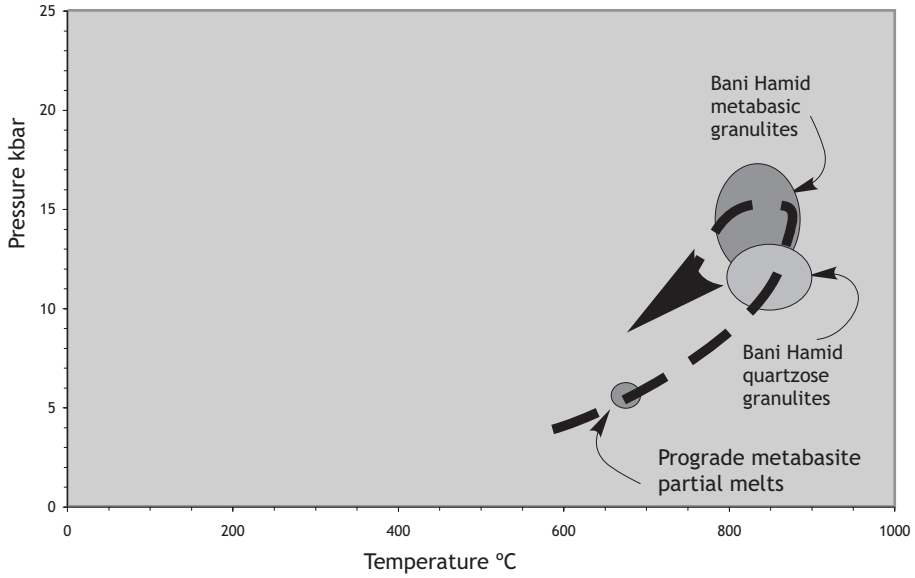


Figure 5.25 Pressure temperature time evolution of the Bani Hamid metamorphic sole using new PT determinations from this study. Error ellipses shown derived from THERMOCALC in average PT mode. The inferred sole anti clockwise PT evolution and peak conditions attained by the Bani Hamid terrane are very similar to those of the 'classic' sole of the ophiolite (cf figure 3.26, *Chapter Three*) and are consistent with formation of the Bani Hamid sole terrane in a similar high geotherm environment derived from the heat of the overlying young and hot Semail ophiolite during intra oceanic subduction. The similarity in PTt paths for the Bani Hamid and 'classic' sole terranes supports the inference that they both formed in a similar subduction zone hanging wall environment and the Bani Hamid terrane was subsequently emplaced at its present structural level by late out of sequence thrusting. The age of the Bani Hamid terrane, especially relative to the classic sole as seen in the adjacent Asimah area, is not clear. A K/Ar hornblende age of 95.3 ± 0.5 Ma has been reported from a Bani Hamid metabasic granulite (Gnos & Peters 1993).

CHAPTER SIX : MELT GENERATION BENEATH THE SEMAIL OPHIOLITE



Even on a summer afternoon, the wadi pools of the Sultanate are cool

CHAPTER SIX : MELT GENERATION BENEATH THE SEMAIL OPHIOLITE

6.1 INTRODUCTION

Leucogranitic material is rare in oceanic crust and leucocratic trondhjemites or plagiogranites present in oceanic crust represent the products of extreme fractionation of basaltic parent magmas and comprise << 0.5% of the Semail ophiolite crustal sequence. Plagiogranites consist mainly of plagioclase and quartz with minimal K_2O or mafic minerals (Pedersen & Malpas 1984). Leucogranitic material, such as that seen at the base of the Semail ophiolite in the Khawr Fakkan and Hayalyn blocks, has only rarely been reported from ophiolitic terranes (Abbotts 1978; Pearce 1989; Ahmed 1991; Pedersen & Dunning 1997; Peters & Kamber 1994).

Cordierite-andalusite-biotite bearing granites and other granitoid intrusions in the mantle sequence of the Khawr Fakkan block of the Semail ophiolite in the eastern UAE have been variously interpreted; proposed petrogenetic models have invoked extreme crystal fractionation in the ophiolite late intrusive series, or (at least in part), partial melting of the metamorphic sole at the base of the ophiolite (Peters & Kamber 1994; Gnos & Nicolas 1996). Potassium bearing granitoids in the Masirah ophiolite of SE Oman were ascribed to deep mantle fractionation processes on the basis of Nd and Pb isotopic compositions by Frei & Nagler (1994). Briqueu et al. (1991) concluded that dykes at Ra's Dadnah in the UAE formed from melting during obduction of the metabasalts and metasediments of the ophiolite metamorphic sole. Rare potassium bearing leucogranitoid intrusions in the mantle sequence of the Hayalyn block of the ophiolite in the central Oman mountains (Browning 1982; Lippard et al. 1986) were analysed by Pearce (1989) who concluded that they were derived by melting of subducted Arabian margin sediments (Hawasina and Haybi complexes) thrust under the ophiolite.

6.1.1 Definition of 'leucogranite'

Leucogranites are holocrystalline, plutonic to hypabyssal leucocratic granitic rocks characterised by the presence of aluminous minerals like muscovite, biotite, cordierite, garnet, and aluminosilicate polymorphs. They can form extensive bodies resulting from the prograde anatexis of metasedimentary sequences in continental collisional settings like the Himalaya (eg LeFort et al. 1987). Such granitoid melts can be produced by a wide variety of mechanisms and from a wide range of source materials. It is generally recognised however that the generation of the majority of peraluminous granitoid bodies has involved the anatexis of sedimentary

material (Miller 1985). Generation by the vapour absent partial melting of high grade metapelitic, muscovite rich source materials during continent-continent collision is now widely accepted as the major petrogenetic mechanism for granites of this type (Patiño Douce & Harris 1998).

6.1.2 Leucogranitic material in other ophiolite complexes

Leucogranitic material within the ultramafic mantle sequence of ophiolite complexes has rarely been reported, but none the less appears to be a widespread phenomenon in ophiolite complexes of variable age, tectonic origin and state of preservation. The consistent presence of minor amounts of similar leucogranitoid material in comparable structural positions within a range of ophiolite complexes suggests a common petrogenetic and tectonic origin. Pearce (1989) provides a thorough review of occurrences from the Lizard (ophiolite) complex, Cornwall and the Guevgueli complex, Greece, as well as the Semail ophiolite, and proposed, on the basis of their structural position within ophiolite complexes and the geochemistry of these leucogranitoids, that they formed as subduction-obduction related anatectic melts, rather than being mantle derived melts. Leucogranitic peraluminous pegmatoid dykes are present in the base of the Kohistan arc in the western Himalaya and have been interpreted as being derived from the under thrust Indian continental margin (Treloar et al. 1990). Pedersen & Dunning (1997) demonstrated that leucogranitoid plutons at the base of Karmoy island arc ophiolite in the Norwegian Caledonides were derived in part by the anatexis of sedimentary material subducted beneath the obducting arc ophiolite.

6.1.3 Distribution, recognition and tectonic discrimination of leucogranitoids

Barbarin (1996) recognised two contrasting types of peraluminous anatectic melts: minimum melt leucogranitoids, characterised by the presence of primary muscovite, and biotite rich monzogranitoids, characterised by the presence of cordierite and accessory aluminium silicates. The characteristic phases of such melts may be related by equilibria such as:

$$Kfs + Grt + Crd + H_2O = Ms + Bt + Qtz$$

The inference that high water activity favours the production of muscovite bearing granitoids leads to the conclusion that muscovite bearing granitoids are characteristic of highly tectonised zones. Shearing in such zones facilitates partial melting (by the provision of fluid

flow channels) and produces often deformed and pegmatitic muscovite-bearing melts that have low vertical mobility and remain close to their sources. In contrast, cordierite bearing granitoids can be produced without the addition of externally derived H_2O in less deformed tectonic environments. These contrasting examples demonstrate that variations in the physical conditions of partial melting, as well as source heterogeneity, can control the mineralogy and tectonic distribution of granitoid melts.

A complementary petrogenetic scheme for collisional granitoids, proposed by Harris et al. (1986), differentiates between muscovite bearing, syn-collisional leucogranitoids produced directly by the anatexis of metasediments, and post-collisional granitoids, formed from LILE enriched mantle melts, and characterised by the presence of magmatic cordierite with enclaves and xenoliths of mafic material.

6.2 DISTRIBUTION AND EXTENT OF LEUCOGRANITES IN THE SEMAIL OPHIOLITE

A few minor granitic bodies intrude the upper part of the Semail ophiolite mantle sequence in the Hayalyn block in the central Oman mountains (Browning 1982; Lippard et al. 1986; Pearce 1989) although pegmatoid leucogranitic dykes appear to be restricted to the northernmost part of the Semail ophiolite in the Khawr Fakkan block in the UAE (figure 6.1a), where they locally form ~5-10% volume of the mantle sequence country rock (figure 6.2a-f). While these two sampled areas contain the densest concentrations of granitoid intrusions in the ophiolite, granitoids appear to be widely, albeit sparsely, distributed throughout the mantle sequence of the entire ophiolite complex.

6.3 FIELD RELATIONSHIPS

Granitoid intrusions are widespread in the Khawr Fakkan area (figure 6.1a) and occur as irregular and often anastomosing dykes or lenses up 100 m in length and 5 m in width, or as small (<<1 km^3) stocks (Peters & Kamber 1994; Gnos & Nicolas 1996; Searle & Cox 1999) intruding tectonised serpentinised harzburgites and cumulate gabbros of the upper mantle and lower crustal sequences. They clearly postdate mantle fabrics in the harzburgites and igneous layering in ultramafic cumulates and consistently occur in a similar structural position around the mantle transition zone.

The dykes exhibit a range of features, summarised in a ‘composite’ dyke sketch (figure 6.4), that clearly demonstrate their intrusive nature, such as the development of actinolitic

altered country rock margins, and the truncation of mantle sequence igneous fabrics. The dykes are often intruded along existing shear zones. Many dykes exhibit a multistage history with margin parallel zonation (Peters & Kamber 1994). From field relations this can be ascribed both to *in situ* differentiation (eg the presence of garnet-tourmaline and muscovite leucogranite veins and segregations within biotite granites) and to the exploitation of the same melt channels by discrete melt pulses. Xenoliths are common in all dyke localities. Most are of wall rock mantle sequence material, as well as cogenetic granitic material in larger composite dykes. Rare metasedimentary material, both restitic garnet-biotite aggregates and unassimilated banded quartzitic enclaves, has been observed in leucogranitic dykes in Wadi Hulw bin Sulayman. The presence of these enclaves suggests the adjacent Bani Hamid terrane as a potential source for the granitoids. Deformation and metamorphism of granite dykes to produce gneissic and mylonitic fabrics is widespread, accompanied by low grade metamorphism with the development of albite (replacing K feldspar), prehnite, pumpellyite, chlorite and epidote-clinozoisite. This deformation is most intense in regions of serpentinised country rock.

Granitoid intrusions in the Hayalyn block of the ophiolite in the central mountains (figure 6.1b) occur as thick (~100 m) sills and lenses strung out along NW-SE trending shear zones in the uppermost mantle and lower crustal sequence (figure 6.2f). The sill has a similar morphology and margin parallel zonation to comparable composite sills in the Ra's Dadnah area of the Khawr Fakkan block, ranging from marginal leucogranites to a core of quartz diorite. Contacts between the various sill components, where observed, are sharp and intrusive, suggesting the exploitation of the same melt channels by discrete melt pulses. Abundant xenoliths of mantle sequence material in the sills were observed, although no entrained metasedimentary enclaves were noted, in contrast to the Khawr Fakkan block granitoids.

6.4 MINERALOGY, PETROGRAPHY AND MINERAL CHEMISTRY

6.4.1 Mineralogy and petrography

The sampled granitoids are typically medium to coarse grained, holocrystalline, leucocratic, equigranular and hypabyssal igneous rocks. Intrusions were sampled from a large composite body at Ra's Dadnah, Ra's Dibba and Wadi Hulw bin Sulayman adjacent to the Bani Hamid terrane (figure 6.1a) in the Khawr Fakkan block of the ophiolite (UAE) and in and around Wadi Al Hajar on the NE margin of the Hayalyn block (figure 6.1b) of the ophiolite (Oman). Each locality is dominated by a particular granitoid paragenesis: hornblende-biotite diorites to biotite granites and garnet leucogranites (forming a large composite sill), cordierite-andalusite monzogranites, garnet-tourmaline with biotite-muscovite leucogranites and another large

composite sill respectively. No cross cutting relationships between different leucogranite assemblages were observed. Peters & Kamber (1994) have also described garnet-tourmaline leucogranites intruding the Bani Hamid metamorphic terrane at Bulaydah in Wadi Ham.

In the Ra's Dadnah composite sill, the increase in quartz content from diorites through tonalites to granites is accompanied by an increase in the presence of perthitic alkali feldspar, the replacement of amphibole by biotite and a fall in the Ca content of plagioclase from An_{50} to An_{20}. The presence of a late anhedral generation of albite (An_{5-15}) overgrowing zoned euhedral plagioclase crystals (An_{25-35}) suggests that sub-solidus metasomatic albitisation of potassium feldspars occurred (Briqueu et al. 1991). The marginal leucogranitic components of the Ra's Dadnah composite body contain abundant skeletal, spessartine rich garnet and occasional tourmaline.

At Ra's Dibba (figure 6.1a), a suite of more homogeneous and mesocratic pegmatitic dykes contains abundant cordierite and andalusite with inclusions of staurolite and hercynite (Peters & Kamber 1994), rare biotite and secondary muscovite. The felsic assemblage is restricted to quartz graphically intergrown with a perthitic or rarely anti-perthitic feldspar. Grain sizes in these pegmatitic granitoids can reach 30 cm.

In Wadi Hulw bin Sulayman (figure 6.1a) granitoid intrusions are common, with fine grained, homogeneous and often mylonitised biotite granites predominating and exhibiting a genetic relationship with enclosed pegmatitic segregations of garnet-tourmaline bearing, leucogranitic material.

Granitoid intrusions in the Hayalyn block of the ophiolite have a simple mineralogy, with an absence of the peraluminous minerals that characterise the Khawr Fakkan block granitoids. The major granitoid intrusion, exposed in Wadi Al Hajar, forms a thick (~100 m) sill or sheet intruded into a shear zone separating mantle sequence harzburgites from crustal sequence cumulate gabbros. This body has a very similar morphology to the Ra's Dadnah composite sill, with margin parallel zonation defining a core of quartz diorite, marginal foliated leucogranites and intermediate tonalites and granodiorites.

The leucogranites exhibit a protomylonitic texture, with ribbon quartz layers displaying sutured subgrains defining the fabric and wrapped around augen of heavily altered plagioclase (An_{25}) and less altered orthoclase. Mafic minerals are almost entirely absent, with chloritised biotite having a modal abundance of ~2%. Intermediate tonalites and granodiorites contain variable (up to ~15%) proportions of chloritised biotite and green hornblende amphibole, and exhibit a fall in the modal proportions of quartz and alkali feldspar and an increase in the Ca content of plagioclase to ~An_{40} (core) to An_{30} (rim) relative to the leucogranites.

6.4.2 Mineral chemistry

Quartz is ubiquitous in the dyke suite, commonly reaching a modal proportion of 60% in the more leucocratic granitoids. Grain size, and crystal morphology are variable depending on rock type and the degree of deformation, although quartz is always clear and unaltered. Grain size varies from ~0.2 mm in the finer grained granodiorites, particularly those with a strong fabric, to 2-3 mm in the pegmatitic biotite granites. Crystal morphology is invariably anhedral, although the majority of the dykes exhibit a degree of deformation, which is initially expressed by the development of undulose extinction and deformational twins. At higher strain rates, the quartz takes on a ribbon texture, and most grains have an aspect ratio >1, a preferred c axis orientation, and granoblastic subgrains, with complete extinction and mutually sutured grain boundaries. The most deformed examples show the formation of aggregates of small, granoblastic neomorphic quartz grains at boundaries.

Plagioclase is shows a consistent variation in composition and modal proportion, varying from An_{40} in quartz diorites to An_{20-10} in leucogranites. Intermediate compositions contain oligoclase, typically An_{25}. Grain size is variable from 0.5 mm up to 3-4 mm in the pegmatitic samples, and grain morphology is subhedral to euhedral, with a characteristic lath shape often developed. Feldspar is generally heavily altered, with the development of turbid clay minerals, sericite, and veins of clinozoisite and epidote. Feldspars exhibit brittle deformation: porphyroclastic augen textures are developed in the most deformed, gneissose dykes. The multiple twin planes of many grains are clearly kinked.

Alkali feldspar is rare in the more mafic dyke compositions, but is abundant in leucogranites and cordierite monzogranitoids occurring as microperthitic microcline, characterised by cross-hatch twinning, and trains of small lensoidal blebs of plagioclase. In addition, graphic intergrowths of alkali feldspar and quartz are commonly observed. Grains tend to be subhedral, with reasonably well developed grain boundaries and a grain size varying between 2 and 4 mm. As with the calcic feldspar, alteration to clayey aggregates and sericite is ubiquitous.

Biotite is relatively uncommon although this is more due to subsequent alteration than igneous mineralogy. It is most obvious in the biotite leucogranitic pegmatites observed as marginal zones within multistage dykes. Here biotite forms large euhedral books up to 10 mm by 5 mm, with a greenish colour. In diorites, tonalites and granodiorites, biotite occurs as subhedral grains, typically 0.5-1 mm in size, with a brownish yellow pleochroic scheme. In the more deformed rocks, biotite is segregated into thin discrete layers that define the rock fabric, and many individual laths are frequently kinked, with sweeping extinction. Alteration of the biotite to colourless or green chlorite is pervasive and characteristic of hydrothermal metamorphism.

Garnet is widespread in the Khawr Fakkan block granitoids but absent in the Hayalyn block sill components, occurring as aggregates and monomineralic layers of fine grained, granular, pink-red coloured grains associated with tourmaline and muscovite. Grains are typically 1-2 mm in size, unzoned and euhedral though mostly skeletal in form, with a typical composition of $Sps_{0.55}Alm_{0.38}Prp_{0.04}Grs_{0.03}$. Inclusions of quartz are common.

Andalusite is a minor component of monzogranitic to leucogranitic dykes in the Ra's Dibba and Wadi Zikt areas of the Khawr Fakkan block, forming pink crystals up to ~20 cm in size in extreme pegmatoid examples. In thin section, andalusite is subidiomorphic and exhibits pink Fe_2O_3 rich pleochroic cores. Marginal alteration to mica aggregates is common.

Cordierite is common in monzogranitic to leucogranitic dykes in the Ra's Dibba and Wadi Zikt areas and has a typical composition of $Fe_{1.33}Mg_{0.49}Mn_{0.17}Si_5Al_4O_{18}$; the high Mn contents may reflect derivation from Mn rich pelagic cherts metamorphosed to form the ophiolite metamorphic sole. It forms large euhedral grains up to 5 mm in size that exhibit cyclical twinning and pinitic alteration along cracks and around grain margins. The contrast in composition between the Mn cordierite found in the Ra's Dibba granitoids and the Mg cordierite prevalent in the adjacent Bani Hamid metamorphic sole (typically $Mg_{1.90}Fe_{0.07}Mn_{0.03}Si_5Al_4O_{18}$) suggests the granitoid grains are not xenocrystal in origin.

Oxides (largely *magnetite*) are rare in the predominantly leucocratic dykes, but are found in the more intermediate, melanocratic quartz diorites and tonalites. They occur as ~0.5 mm sized euhedral granular grains which are widely distributed as accessories but are spatially associated with amphibole and biotite grains.

Tourmaline is a common accessory in the leucogranitic dykes sampled, and is visible in outcrop as black acicular grains, up to 10 mm in length. In section, tourmaline exhibits brown-yellow zoned pleochroism and a euhedral trigonal form.

Other minerals encountered include a blue-green edenitic *hornblende* typical of calc-silicate intermediate rocks, forming up to 20% by volume of the quartz diorites and tonalites. Common accessories, occurring widely in volumes of up ~1%, are euhedral, wedge shaped *titanite* grains and *apatite*, which is commonly found as inclusions in epidote group minerals and feldspars.

6.4.3 Metamorphic assemblage and distribution

The granitoids of the Ra's Dadnah and Hayalyn areas exhibit a distinctive metamorphic assemblage, which appears to be most strongly developed in areas strongly sheared and serpentinised mantle sequence material. These minerals are ubiquitous and include epidote,

clinozoisite, pumpellyite, chlorite (often after primary igneous biotite), and prehnite, which is generally restricted to veins.

Chlorite is widely observed in granitoid assemblages as a product of alteration and metamorphism and is found intergrown with, and replacing, primary igneous biotite. Growth is frequently mimetic after biotite, and habit and grain size mirrors that of biotite. Chlorite is also widely distributed in veins, where it is associated with epidote group minerals, pumpellyite and prehnite.

Epidote group minerals are again abundant, and in most occurrences can be ascribed to metamorphic growth, although in some sections this is not clear and the crystal form and distribution suggests a primary, igneous origin. *Clinozoisite* is widely distributed as medium grained subhedral aggregates, often as veins or patches within plagioclase, but also as neomorphic aggregates in the matrix of the granitoids. *Epidote* also occurs as isolated, small (~0.5 mm) euhedral granular grains distributed throughout garnet leucogranites. This occurrence is more consistent with an igneous source. In addition, epidote group minerals form the bulk of wholly saussaritised plagioclase rich aplites.

Pumpellyite, a index mineral in the prehnite-pumpellyite facies, is found in tonalitic, granodioritic and leucogranitic members of the dyke suite, and forms small radial or felted aggregates of acicular grains up to ~0.1 mm long, associated with chlorite, which may be colourless, or exhibit a weak blue-green pleochroism.

Prehnite is also an index mineral in the prehnite-pumpellyite facies. It is widely distributed across the dyke suite but less abundantly than pumpellyite. Prehnite occurs as small, colourless, moderate relief subhedral grains in the matrix of the dykes, associated with pumpellyite and chlorite. The most common occurrence however is in thin veins of one apparent generation, which may be up to 10 mm in width. These veins are consistently oriented normal to the fabric of the more deformed members of the dyke suite.

Such metamorphic assemblages are characteristic of the prehnite-pumpellylite facies, associated with hydrothermal fluidisation and PT conditions of ~300°C and ~1-2 kbar (Yardley 1989), equivalent to depths of ~5-7 km. The mantle sequence country rocks exhibit a similar degree of metamorphism, characterised by extensive serpentinisation. The granitoid sills of the Hayalyn block are not as strongly metamorphosed as the similar Ra's Dadnah composite sill components although primary feldspars are largely altered to aggregates of zoisite and white mica, and biotite is mostly replaced by mimetic chlorite. Veining by prehnite is restricted to the deformed marginal leucogranites. None the less, they occupy a similar structural and tectonic position to the Ra's Dadnah sill and have also been emplaced in a locally deformed and sheared part of the ophiolite mantle sequence.

6.5 MAJOR AND TRACE ELEMENT GEOCHEMISTRY

6.5.1 Analytical techniques

All the analytical data presented in this chapter is the result of work carried out at the Department of Geology at the University of Bergen, Norway, under the guidance of Rolf Pedersen, and also in part by John Watson at the Open University. Major and trace elements analyses were determined by X-ray fluorescence (XRF) spectrometry (Philips PW 1404, Bergen; ARL 8420+, OU) using glass beads and pressed-powder pellets respectively, with an accuracy of 1% for major elements and $\pm$ 10 ppm for trace elements. The typical quoted XRF detection limits are from Potts (1987). % FeO was determined from total Fe (as Fe^{3+}) by standard titration methods. See appendix B for details.

6.5.2 Major and trace element rock classification

Major and trace element XRF analyses for a range of Khawr Fakkan and Hayalyn ophiolite block granitoids and their mineral assemblages and CIPW norms are presented in tables 6.1, 6.2, 6.3 and 6.4. A variety of techniques are commonly used to represent geochemical variations in granitic rock types. Major element classification diagrams such as that devised by Streckeisen (1976) can be used to classify igneous rocks on the basis of mineral modal proportions and demonstrate that the analysed granitoids fall in the granodiorite, tonalite and granite fields (figure 6.6).

Harker diagrams present various major element variations plotted relative to SiO_2 and with the exception of sample OM 77 all the studied granitoids occupy a narrow range in SiO_2 content of 72-76%. Within individual suites (such as the Ra's Dadnah composite sill) the observed linear inverse correlations between Si contents and Al, Fe and Mg content (figure 6.8) may be indicative of *in situ* fractional crystallisation of feldspars and biotite. Field and petrographic evidence is generally consistent with this interpretation. However, such linear correlations are controversial and other mechanisms invoked to account for them include the progressive incorporation of restitic phases (Chappell & White 1992) or multi-stage partial melting (Holtz & Barbey 1991). All may be true in specific instances, and field evidence (the presence of garnet-biotite restitic enclaves within dykes) compatible with the restite unmixing model has been observed. The components of the Ra's Dadnah sill also exhibit very low (typically <0.25%) K_2O contents (figure 6.8) due to metasomatic replacement of potassium feldspar by albite (Briqueu et al. 1991). The Nd-Sr isotopic signature of these dyke components

distinguishes them from typical oceanic plagiogranites, as does their position within the ophiolite stratigraphy. Samples from Ra's Dibba are similarly affected, which may account for the high $^{87}Sr/^{86}Sr$ ratios and normative sodium metasilicate of these dykes.

The relationship between melt geochemistry and magmatic differentiation varies among the dyke suites, although these relationships have been distorted somewhat by subsequent metasomatism (figure 6.7a,b). The andalusite-cordierite monzogranitoids of Ra's Dibba exhibit a small increase in peraluminous character with differentiation (figure 6.7b). Similar trends are observed in cordierite bearing granitoids from the Hercynides and Himalaya (eg LeFort et al. 1987). The intermediate and granodioritic components of the Ra's Dadnah composite sill show a slight decrease in peraluminous character with differentiation. In contrast, the leucogranitic components of the sill exhibit a large variation in [A/CNK] although values increase strongly with differentiation, as do those of the Wadi Hulw bin Sulayman biotite granites and garnet-tourmaline and muscovite-biotite leucogranites. Similar trends have been observed in two mica leucogranitic bodies such as the Manaslu granite of the Nepal Himalaya (LeFort et al. 1987).

The trace element data (figure 6.9a-d) for the granitoid dykes have been normalised to a standard ocean ridge granite (ORG) that represents a pure crystal fractionate of mantle origin (Pearce et al. 1984). Each distinct dyke paragenesis is represented separately for ease of comparison. Each dyke dataset occupies a relatively narrow range for most plotted elements although there are differences among individual dyke assemblages. The Wadi Hulw bin Sulayman leucogranites exhibit the strong LILE enrichment, negative Ba anomaly (probably due to the fractional crystallisation of biotite and potassium feldspar) and low HFSE (Zr, Sm, Y) abundances characteristic of syn-collisional granitoids. Their trace element patterns are consistent with derivation from the partial melting of a sedimentary protolith and are similar to those of Himalayan type syn-collisional granites derived from metasedimentary material (figure 6.9). The Ra's Dibba monzogranitoids also have trace element distributions that closely match typical syn-collisional type leucogranitoids. In contrast, the Semail ophiolite trondhjemite and metamorphic sole leucotonalitic amphibolite partial melt show flat patterns close to that of the hypothetical normalising plagiogranite. This is to be expected as both these rocks were ultimately derived from a wholly mantle source.

The Ra's Dadnah composite body is found at a higher structural level than the other described granitoids, in the mantle transition zone, and all samples exhibit flat trace element patterns. Metasomatic leaching of LILE from these outcrops has been described by Briqueu et al. (1991) and may account for the low recorded LILE concentrations, while the slightly increased HFSE concentrations compared with the other analysed granitoids may reflect mixing between 'sedimentary' and 'mantle' type sources. The leucogranitic components of the Ra's Dadnah composite body have a pronounced negative Ba anomaly, likely to be caused by the

fractional crystallisation of biotite and potassium feldspar. The positive Nb anomaly again may reflect the presence of a mantle source in the petrogenesis of this body.

6.5.3 Tectonic discrimination diagrams

Discriminant analysis requires a sample suite from which linear functions of measured variables that allow clear sample discrimination can be calculated. Most commonly, the ratio of two immobile trace elements, highly fractionated relative to each other by some well constrained, tectonically controlled magmatic process, is used. Ternary plots are often employed and provide more powerful discriminant potential. Although there is some theoretical basis for the geochemical rationale behind most commonly used diagrams, they can rarely provide unequivocal results, and must be applied with caution, considering factors like the effects of rock alteration and element mobility, the nature of sample populations and crystal fractionation processes. Tectonomagmatic discrimination techniques were first applied to rocks of granitic composition by Pearce et al. (1984), and discrimination diagrams based on plots of Rb-Y-Nb are here used.

The alteration independent Nb-Y diagram (figure 6.10) of Pearce et al. (1984) is effective at discriminating between tectonic environments in granitoid material. The majority of the analysed granites lie in the volcanic arc/syn-collisional granite field, although those intruded at higher structural levels within the ophiolite mantle sequence (Ra's Dibba and Ra's Dadnah) cluster in the within-plate granite field. Peraluminous granites can, however, inherit widely varying compositions depending on petrogenetic conditions and source component compositions. The fact that some of the analyses extend into the within plate granite field is consistent with a mantle source component in the petrogenesis of these melts. The analysed dykes are clearly distinct from the Semail ophiolite trondhjemite dataset.

6.5.4 Characterisation of anatectic processes using LILE covariation

The trends defined by major and trace element concentrations of leucogranitic melts, particularly when compared with potential source compositions, can be used to characterise the extent and nature of partial melting processes in leucogranite source regions (Inger & Harris 1993). More recently, they have been used in conjunction with experimental petrology (Patiño Douce & Harris 1998) to show the close relationships between Himalayan leucogranites and their sources, commonly high grade metapelites. Partial melting in such regimes is dominated by the dehydration melting of metasediments without the addition of a fluid phase.

The influence of such a phase on the degree of partial melting, restite mineralogy, and the trace element geochemistry (particularly the LILE Sr, Rb and Ba) of melts can be used to characterise the melting and tectonic regimes that govern the petrogenesis of such leucogranites.

LILE (Sr, Rb and Ba) covariation is an important tool in the analysis of granitic melt evolution, since they are partitioned into major granitoid phases like plagioclase, alkali feldspar and biotite. The Wadi Hulw bin Sulayman granitoids have higher (~10-100) Rb/Sr ratios than the Ra's Dadnah suites, which have typical values of ~0.01-0.1 (figure 6.16). Inger & Harris (1993) have argued that such differences may be attributed to different melt processes, with high Rb/Sr ratios resulting from dehydration melting, and lower values, coupled with higher Ba concentrations, resulting from H_2O fluxed melting, which produces a higher proportion of restitic alkali feldspar. Since the ophiolite in the Ra's Dadnah area is heavily deformed and sheared, these lines of weakness in the country rock may have facilitated the input of excess fluid into melts emplaced locally. It is inferred that the Wadi Hulw bin Sulayman granitoids were generated by dehydration melting, with minimal added fluid, whereas the Ra's Dadnah suites may have been influenced by excess fluid added to melts emplaced into a sheared part of the ophiolite thrust sheet. However post emplacement LILE leaching makes these conclusions equivocal.

Linear trends of Rb/Sr against Sr and Ba (figure 6.16a-c) suggest that intra-suite variation is largely a result of fractional crystallisation of biotite and alkali feldspar from a melt source corresponding to the average composition of the underlying Bani Hamid quartzose granulites. The Wadi Hulw bin Sulayman and Ra's Dibba suite trends match the calculated vapour absent partial melting of muscovite trend, resulting in the crystallisation of alkali feldspar. Post emplacement metasomatism of the Ra's Dadnah body makes any such interpretation uncertain. The components of the Hayalyn block granitoid intrusion exhibit a trend consistent with an origin by the fractional crystallisation of biotite.

6.6 Rb-Sr AND Sm-Nd ISOTOPE GEOCHEMISTRY

6.6.1 Analytical techniques

Rb-Sr and Sm-Nd isotopes were measured at the University of Bergen on a Finnigan MAT 262 RPQ mass-spectrometer. The chemical processing was carried out in a clean-room environment with HEPA filtered air supply and positive pressure, and the reagents were purified in two bottle Teflon stills. Samples were dissolved in a mixture of HF and HNO_3. Sr

and Rb were separated by specific extraction chromatography using the method described by Pin et al. (1994). Sr was loaded on a double filament and analysed in static mode. Repeated measurements of the NBS 987 Sr standard at the time of this study yielded an average of 0.710252 ± 19 (2σ) (n = 30); the accepted value is 0.710240.

REE were separated by specific extraction chromatography using the method described by Pin et al. (1994). Sm and Nd were subsequently separated using a modified version of the method described by Richard et al. (1976). Sm and Nd were loaded on a double filament and analysed in static and dynamic mode respectively. Nd isotopic ratios were corrected for mass fractionation using a $^{146}Nd/^{144}Nd$ ratio of 0.7219. Sm and Nd concentrations were determined using a mixed $^{150}Nd/^{149}Sm$ spike. Repeated measurements of the Johnson and Matthey Nd^{203} oxide (batch #S819093A) yielded an average $^{143}Nd/^{144}Nd$ ratio of 0.511120 ± 10 (2σ) (n = 17).

6.6.2 Summary of analytical data

The Ra's Dibba andalusite-cordierite bearing monzogranitoid pegmatites exhibit the highest ε_{Nd} values (typically –1.0) and the most mantle like initial $^{87}Sr/^{86}Sr$ ratios (~0.706). In contrast, the Wadi Hulw bin Sulayman garnet tourmaline leucogranites exhibit the low ε_{Nd} values (-6.0) and high initial $^{87}Sr/^{86}Sr$ ratios (ε_{Sr} values of 70-80) characteristic of pure metasedimentary melt leucogranites. However, these values are not comparable with Himalayan leucogranites, which have typical ε_{Nd} values of -15 to -20 and ε_{Sr} values of 600-800 (eg Inger & Harris 1993). This may reflect a more quartzofeldspathic component in the source region of the Semail leucogranites compared with the metapelitic sources of the Himalayan leucogranites. The complete dataset plots in the 'enriched' (+ve ε_{Sr}, -ve ε_{Nd}) quadrant on a ε_{Sr} versus ε_{Nd} diagram (figure 6.17a,b), indicating derivation from a relatively old, LREE enriched (low Sm/Nd), high Rb/Sr source typical of continental crust. The Hayalyn block granitoids form a more homogeneous suite with a narrow range in ε_{Nd} values ranging from –5 to –6 and ε_{Sr} values of ~25 to ~70 (table 6.5), which again are characteristic of material derived from a continental rather than an oceanic source. All samples were taken from a single major composite sill and in a similar manner to the Ra's Dadnah composite sill, the most mafic intrusive components have a more 'continental' (+ve ε_{Sr}, -ve ε_{Nd}) Nd-Sr signature than the leucogranitic components.

6.6.3 Comparison with oceanic plagiogranites

Plagiogranites (Malpas 1979; Pedersen & Malpas 1984) represent the final products of the fractional crystallisation of the basaltic melts that make up the crustal sequence of the

oceanic crust. The negative ε_{Nd} values and intermediate to high initial $^{87}Sr/^{86}Sr$ ratios of the analysed granitoids contrast strongly with the published data on the Semail ophiolite plagiogranites, which have typical hydrothermal metamorphism enriched MORB like ε_{Sr} and ε_{Nd} values of ~10-30 and ~7-8 respectively (McCulloch et al. 1981).

6.6.4 Granitoid sources and protoliths: mixing modelling and identification of end members

The Khawr Fakkan block granitoid intrusion dataset defines a hyperbolic array in ε_{Sr} and ε_{Nd} space consistent with an origin by the mixing of two distinct source components - a LILE enriched mantle component and a 'continental' sedimentary component.

Possible continental end member components involved in the generation of the granitoid dyke suite are Tethyan crustal material subducted beneath the ophiolite (represented by the Haybi complex and metamorphic sole) and the Arabian basement of the passive margin. Numerous arguments suggest that melting of the Arabian basement was unlikely. Estimates indicate that the ophiolite formed as much as 400-500 km offshore (Lippard et al. 1986; Béchennec et al. 1988), and that the ophiolite was not obducted onto the continental margin until ~78 Ma (Hacker et al. 1996). By this time the ophiolite would not have contained enough residual heat to cause anatexis in the under thrust margin. The Sm-Nd isochron age of the Ra's Dadnah body is ~20 Ma older than the continental margin obduction age and therefore precludes melting of the Arabian margin at ~99 Ma. Briqueu et al. (1991) noted that the influence of the Sr rich carbonates of the passive margin would also greatly alter the isotopic characteristics of the granitoids. In the southern Oman mountains, regional HP metamorphism in the crust has been ascribed to the subduction of the leading edge of the Arabian continental margin to depths of ~80 km beneath the ophiolite (Searle et al. 1994).

Rb-Sr and Sm-Nd isotopic data for granulite facies quartzofeldspathic gneisses from the Bani Hamid metamorphic terrane is presented in table 6.6. The juxtaposition of the highest grades of sub-ophiolitic metamorphism seen in the Oman mountains and the high density of granitoid intrusions in Wadi Hulw bin Sulayman (figure 6.1) suggests a genetic relationship between the two lithologies. The Wadi Hulw bin Sulayman leucogranites have trace element patterns that are very similar to typical Himalayan leucogranites. The similarity in Nd and Sr isotopic characteristics between the Wadi Hulw bin Sulayman leucogranites and the majority of the analysed Bani Hamid metasediments also suggests they may be closely related.

LILE covariation modelling is compatible with the leucogranites being the products of the vapour absent melting of the Bani Hamid granulites (figure 6.16), and the minimum melt type nature of the leucogranites (figure 6.15) has been demonstrated. Briqueu et al. (1991)

demonstrated that the granitoids of the Ra's Dadnah composite sill have Pb isotopic compositions inherited from the Bani Hamid granulites. The Wadi Hulw bin Sulayman leucogranites and their inferred metasedimentary protoliths in the Bani Hamid terrane can be used to represent the continental end member in mixing calculations. The end member used in the mixing model calculations is sample OM 124 (table 6.6).

Possible depleted mantle end member components involved in the generation of the granitoid dyke suite are oceanic or volcaniclastic sediments subducted beneath the ophiolite and the LILE and volatile enriched harzburgitic mantle wedge above the subduction zone. Acceptance of the SSZ origin of the ophiolite precludes the possibility of material identical to the preserved ophiolitic crustal sequence lavas being subducted beneath the ophiolite (Searle & Cox 1999).

Subducted crustal material is represented by the unmetamorphosed Permo-Triassic to Jurassic tholeiitic to alkaline volcanics and associated volcaniclastic sediments found in the sub-ophiolitic Haybi complex (Searle 1980) and its subducted greenschist to granulite facies metamorphic equivalents, the Asimah and Bani Hamid metamorphic sole terranes (c et al. 1991; Cox et al 1999). No Nd-Sr isotopic data are available for the volcanics of the Haybi complex, but Zeigler et al. (1991) present analyses of the Asimah tholeiitic and alkaline metavolcanic suite.

New Rb-Sr and Sm-Nd analyses of granulite facies alkalic and tholeiitic units from the Bani Hamid and Sumeini metamorphic sole localities are presented in table 6.6. All Nd-Sr isotopic data relevant to the petrogenesis of the Khawr Fakkan block granitoids are presented in figure 6.17a.

It is proposed that the LILE and volatile enriched mantle wedge above the intra-oceanic subduction zone that obducted the Semail ophiolite is preserved as the basal mantle sequence serpentinised harzburgites of the Khawr Fakkan block. Lanphere et al. (1981) and Zeigler et al. (1991) report basal mantle sequence harzburgite analyses that have positive ε_{Sr} values and differ greatly from the analyses reported by McCulloch et al. (1981).

Chen & Pallister (1981) and Briqueu et al. (1991) have reported Pb isotopic data for Semail ophiolite mantle sequence harzburgites and the ophiolite metamorphic sole. Chen & Pallister (1981) analysed hydrothermal galena and serpentinised harzburgite from the basal mantle sequence in the Ibra area of the southern Oman mountains and concluded that both contained continentally derived Pb. Briqueu et al. (1991) demonstrated that these mantle sequence analyses had a similar Pb isotopic composition to granulite facies sedimentary material from the Bani Hamid terrane, and concluded that devolatilisation of the Bani Hamid granulites may have induced melting and metasomatism of the overlying mantle wedge.

It is proposed that the LILE enrichment implicit in these analyses is attributable to the prograde devolatilisation of sediments subducted beneath the hot ophiolite or to contamination

of the mantle wedge by ascending granitic melts. Fluids circulating at the base of the mantle wedge caused perhaps some or all of the widespread mantle sequence serpentinisation. Mixing calculations, using typical harzburgite compositions (1.1 ppm Sr, 0.035 ppm Nd: Lanphere et al. 1981; McCulloch et al. 1981) and the leucogranites of Wadi Hulw bin Sulayman as end members, however rule out the possibility of major mantle wedge mixing as a genetic mechanism. This mixing model requires granites formed by melting of the continental end member to have assimilated 100 times as much harzburgite to obtain the isotopic signature of the Ra's Dadnah composite dyke. This mechanism must therefore be discarded.

The metamorphic equivalents of the Haybi volcanics, represented by the Bani Hamid and Asimah terrane metavolcanics, have a wide range of ε_{Nd} and ε_{Sr} values. This may be expected from a diverse volcanic sequence, evolving compositionally over time, from a heterogeneous source (Searle 1980; Zeigler et al. 1991). All have lower ε_{Nd} values and higher ε_{Sr} values than the Semail ophiolite (figure 6.17). This suggests the subducted basaltic material was altered by interaction with seawater. McCulloch et al. (1981) estimated seawater locally to have had a ε_{Sr} value of ~30. The LILE enriched, subducted metabasalts have values approaching this figure.

Mixing calculations using such a subducted metabasalt suggest the Ra's Dibba monzogranitoids contain ~65% of the basaltic end member, components of the Ra's Dadnah composite dyke between 30 and 50%, and the Wadi Hulw bin Sulayman dykes less than 5%. The components of the Hayalyn block composite sill sampled have a similar range in end member mixing components to the Ra's Dadnah sill.

The observed hyperbolic trend of granitoid intrusions analysed in this study can be accounted for by mixing between the immediate precursors of the Wadi Hulw bin Sulayman peraluminous leucogranitoids (the quartzofeldspathic components of the Bani Hamid metamorphic terrane) and LILE enriched, metabasaltic extrusive units or derived arc sediments subducted beneath the ophiolite. These units are preserved unmetamorphosed in the Haybi complex and at greenschist (Asimah) and granulite (Bani Hamid) facies in the metamorphic sole. The basaltic metamorphic sole end member component used in mixing calculations has the composition: 200 ppm Sr, 7 ppm Nd, $^{147}Sm/^{144}Nd = 0.194$, $\varepsilon_{Nd} = 5.05$, $\varepsilon_{Sr} = 26$ (Zeigler et al. 1991).

6.6.5 Sm-Nd isotope systematics

Mixing relationships between the two chosen mixing end members are shown in figure 6.17b. The curvature of the mixing line in figure 6.17b is controlled only by the Nd/Sr ratios of the end members. It matches the observed hyperbolic array of the analysed granitoids well,

suggesting that mixing between LILE enriched metabasaltic material and Bani Hamid granulite derived melts can explain the observed hyperbolic array.

However, Sm-Nd isotope systematics indicate that the source relationships may be more complex since there is a considerable spread of data on a Sm-Nd isochron diagram (figure 6.18a,b). For example, the granites may have formed by the mixing of melts derived from two contrasting subducted components, or from mixed sedimentary material (quartzofeldspathic and volcaniclastic). In the latter case, the observed two component mixing would have a pre-magmatic source.

Pure mixing components should lie on a straight line between the mantle and metasedimentary sources on figure 6.18a,b and, although individual dyke domains do define linear trends, they do not lie on the modelled mixing line. However, a linear array would only be expected if the granitoid melts had assimilated mantle material or mixed with such melts. If the mixing was pre-magmatic, any linear relationship between the melts and the source components would be altered by subsequent anatexis and fractional crystallisation.

Partial melts from such a source should plot at lower Sm/Nd ratios with the degree of displacement from the mixing line dependent on the degree of melting and source partition coefficients. These initial compositions could subsequently be modified by fractional crystallisation processes, which would produce arrays with variable Sm/Nd ratios but near constant ε_{Nd}. There is abundant field evidence of fractional crystallisation processes. The Wadi Hulw bin Sulayman leucogranites may have formed by the fractional crystallisation of alkali feldspar from a minimum melt derived directly from the quartzofeldspathic granulites of the Bani Hamid terrane. The fact that the continental end member is not intersected by the granitoid trends on figure 6.18b is consistent with source mixing (Pedersen & Dunning 1997).

6.6.6 Isotopic disequilibrium in the Rb-Sr system

Isotopic disequilibrium between melt and restite phases during melt generation will occur when the volume diffusion rates of Rb and Sr between phases which accommodate Rb and Sr (plagioclase and micas) are slower than the rate of melt extraction from the source region. Such studies are increasingly used to constrain rates of melt generation in collisional terranes.

Harris & Ayres (1998) showed that advective heating and rapid melt extraction from source regions are major causes of isotopic disequilibrium between protoliths and melts, and that disequilibrium is facilitated by rapid protolith heating, although the dynamic recrystallisation that accompanies shearing promotes isotopic re-equilibration. Melt processes also influence the relative $^{87}Sr/^{86}Sr$ ratios of restite and melt.

During the vapour absent melting of muscovite, the release of radiogenic Sr from muscovite (which has a high Rb/Sr ratio compared to plagioclase) will cause melts to inherit higher $^{87}Sr/^{86}Sr$ ratios than their source. In contrast, vapour present derived melts contain a greater $^{87}Sr/^{86}Sr$ contribution from plagioclase, which results in minimal disequilibrium between source and melt.

Tectonic models suggest that the Semail ophiolite granitoid dyke suite formed under conditions of advective heating (from the residual heat of the ophiolite) and strong shearing. However, the similarity in initial $^{87}Sr/^{86}Sr$ ratios of the proposed metasedimentary source (~0.709-0.710) and the adjacent Wadi Hulw bin Sulayman leucogranites (up to ~0.710), suggest that significant disequilibrium in the subduction zone Rb-Sr system of the leucogranitic dykes can be discounted, a result consistent with dynamic recrystallisation of the source sediments during shearing in the subduction zone, coupled with melt extraction slower than the ~0.2 Ma threshold for the preservation of Sr isotopic disequilibrium (Harris & Ayres 1998).

6.7 CONDITIONS OF GRANITOID FORMATION BENEATH THE SEMAIL OPHIOLITE

A combination of major and trace element modelling, Sm-Nd and Rb-Sr isotope geochemistry, thermobarometric and Sm-Nd and U-Pb dating techniques have been used to characterise the processes and rates of subduction beneath the Semail ophiolite. From these results, it is clear that granitoid melt formation was occurring at the subduction front at temperatures of ~700°C and pressures of 2-3 kbar.

Table 6.7 Estimates of PT conditions of crystallisation of Semail ophiolite granitoids.

Sample	OM 76	OM 3-5
Location	Ra's Dadnah, UAE	Hayalyn, Oman
Granitoid type	Qtz diorite	Qtz diorite
Temperature		
Holland & Blundy (1994) hbl-pl	724 ± 17°C	702 ± 17°C
Pressure		
Anderson & Smith(1995) Al in hbl	2.75 ± 0.6 kbar	2.0 ± 0.6 kbar

New thermobarometric data, using the hornblende-plagioclase thermometer of Holland & Blundy (1994), in conjunction with the Al in hornblende barometer of Anderson et al. (1995), is summarised in table 6.7 and suggests that the Semail ophiolite granitoids crystallised at temperatures of ~700°C at pressures of between 1.5 and 3.5 kbar. These results are in good agreement with the ternary system modelling summarised in figure 6.15b, and also with the experimental data of Peters & Kamber (1994), who suggested values of 650-675°C at pressures of ~2 kbar, equivalent to depths of ~7-10 km.

6.8 TIMING OF GRANITOID FORMATION

No U-Pb (crystallisation) ages have been determined for the Khawr Fakkan block granitoids (Alleman & Peters 1972; Peters & Gnos 1993; Hacker et al. 1996). The formation of residual harzburgite from the melting event that produced the ophiolite crustal sequence has been estimated to predate crystallisation of the crustal sequence by at most 6 Ma (McCulloch et al. 1981), giving an upper age for granitoid intrusion.

Structural evidence suggests that the crystallisation of the Ra's Dadnah composite granitoid sill post dated the formation of the residual harzburgites of the ophiolite mantle sequence, and must therefore be younger than ~101 Ma – if the accepted mean ophiolite crustal sequence age of ~95 Ma (Tilton et al. 1981) is appropriate for the Khawr Fakkan block area. The peak metamorphism of the Bani Hamid terrane at ~95 Ma (Hacker et al. 1996) is also truncated by components of the dyke suite and is therefore older.

The granitoid dykes were clearly associated with the initial stages of sub-ophiolite metamorphism and ophiolite obduction. The age of the greenschist facies metamorphism of some dykes, if correlated with the similar grade overprint event observed in the adjacent Bani Hamid and normal metamorphic sole sequences, can provide a minimum emplacement age. Gnos & Peters (1993) dated an actinolitic rim of pargasitic hornblende from a Bani Hamid sequence hornblende granulite at 91.2 $\pm$ 0.5 Ma (K-Ar).

6.8.1 Existing cooling ages

Published cooling ages of granitoid material within the Semail ophiolite are restricted to the K-Ar and Ar-Ar systems, and plagiogranitic and leucogranitic granitoid assemblages are not clearly distinguished. Muscovite $^{40}Ar/^{39}Ar$ cooling ages from garnet bearing granitoid dykes in the Khawr Fakkan block average 89.5 $\pm$ 0.4 Ma (Hacker et al. 1996), and ages of Khawr Fakkan block peraluminous granitoids from Gnos & Peters (1993) average 90.4 $\pm$ 0.9 Ma. Searle

(1980) reported a K-Ar biotite cooling age of 85 ± 3 Ma for a leucogranitic dyke from Wadi Sharm, UAE.

6.8.2 Extrapolation of ophiolite cooling rates

K-Ar granitoid cooling ages which, in conjunction with ophiolite cooling rates (~200°C Ma^{-1} between 94.8 Ma and 93.5 Ma; Hacker et al. 1996) and metamorphic sole (~90°C Ma^{-1} between 93.5 Ma and 92.6 Ma and ~20°C Ma^{-1} until biotite closure at 89.2 Ma; Hacker et al. 1996) cooling rates can be used to estimate a crystallisation age of ~93 Ma for the dykes, assuming a solidus temperature of ~650°C at 2.5 kbar for the dykes (Peters & Kamber 1994) and a muscovite closure temperature in the K-Ar system of ~475°C (Hacker et al. 1996).

6.8.3 New U-Pb dating

The first true crystallisation ages for the Semail ophiolites anatectic granitoids are here reported in table 6.8. Samples JC 25 and 36 were taken from a garnet-tourmaline leucogranite dyke at Ra's Dadnah, adjacent to the composite sill dated by Sm-Nd whole rock techniques. Zircons from this intrusion are discordant and yield an upper, regressed discordia intercept age of 105 ± 4 Ma (figure 6.19), with lower concordia intercepts of ~78-84 Ma. Since these lower discordia ages closely agree with the estimated age of ophiolite emplacement onto the Arabian continental margin at ~78 Ma (Hacker et al. 1996), as well as K-Ar biotite cooling ages of similar adjacent Khawr Fakkan block leucogranites (Searle 1980), they are likely to be incorrect.

6.8.4 New Sm-Nd dating

A new Sm-Nd isochron age for the large Ra's Dadnah composite dyke is here presented and represents the first whole isochron age in the Sm-Nd system for Semail ophiolite leucogranitic material (figure 6.20a). Five cogenetic components of this large composite sill range from hornblende diorite to garnet leucogranite and generate an isochron (MSWD = 1.18) with an age of 98.8 ± 9.5 Ma and an initial ε_{Nd} value of –4.31. A new Sm-Nd isochron is also reported for the large composite granitoid sill in Wadi Al Hajar from the Hayalyn block of the ophiolite in Oman (figure 6.20b). Four cogenetic components of this large composite sill range

from hornblende diorite to biotite leucogranite and generate an isochron (MSWD = 0.33) with an age of 93.0 ± 10.0 Ma and an initial ε_{Nd} value of –5.07, very similar to the Ra's Dadnah intrusion.

6.9 SUMMARY

The Khawr Fakkan block (United Arab Emirates) and the Hayalyn block (Oman) of the Semail ophiolite exhibit suites of 10-100 m scale metaluminous to peraluminous granitic intrusions, ranging from cordierite-andalusite-biotite monzogranites to garnet-tourmaline leucogranites, which intrude mantle sequence harzburgites and lower crustal sequence cumulate gabbros. Structural constraints suggest that the subduction of continental sedimentary material beneath the hot proto-ophiolite in an intra-oceanic arc environment led to granulite facies metamorphism at the subduction front and the generation of granitic melts which were emplaced up to the level of the ophiolite Moho.

Major and trace element analyses demonstrate that the leucogranitic dykes of the Khawr Fakkan block of the Semail ophiolite are compositionally similar to crustal melt leucogranites from the Himalaya and other similar collisional environments. The distinction, in terms of geochemistry, mineralogy and structural position, between the analysed dyke suite and the trondhjemites of the ophiolite late intrusive sequence is clear (Browning 1982). They are also distinct from the rare tonalitic partial melt pods observed within amphibolite to granulite facies metabasalts of the ophiolite metamorphic sole (Searle & Malpas 1982).

CIPW normative ternary system diagrams indicate that the granitoid melts found at the lowest structural levels exhibit minimum melt type compositions and were formed by the dehydration melting of muscovite bearing sediments at 3-5 kbar. Independent PT estimates of crystallisation of components of the dyke suite suggest they formed at 2-3.5 kbar. Melts emplaced at higher structural levels formed by H_2O saturated melting.

LILE (Sr, Rb and Ba) covariation modelling show that the structurally lowest granitoids formed by the dehydration melting of the Bani Hamid granulite facies muscovite bearing metasediments. Melts emplaced at higher structural levels underwent a greater degree of partial melting (eg Ra's Dadnah) forming diverse but cogenetic suites (ranging from peraluminous hornblende-biotite diorites to garnet-tourmaline leucogranites) due to the fractional crystallisation of alkali feldspar and biotite.

Initial $^{87}Sr/^{86}Sr$ ratios of analysed dykes vary between 0.713 and 0.706 at initial ε_{Nd} values of between -6.3 and -0.5. The absence of significant Rb-Sr isotopic disequilibrium between the granitoid dyke suite and the subducted source sediments, despite assumed rapid advective heating of the sediments subducted beneath the hot ophiolite, may be due to

subduction zone isotopic homogenisation during melt extraction. Dynamic recrystallisation due to shearing in the subduction zone would have facilitated this process.

Geochemical and isotopic characteristics of the analysed granitic intrusions indicate that the subducted continental material was derived from oceanic trench fill (Haybi complex) sediments, preserved as greenschist to amphibolite (Asimah area) to granulite facies (Bani Hamid area) ophiolitic metamorphic sole terranes. Hybrid granitic melts were derived from pre-magmatic mixing of two contrasting (quartzofeldspathic and basaltic) subduction zone sources. Sr-Nd isotope systematics show that the observed two component mixing reflects pre-magmatic mixing between these contrasting components. The latter source may represent volcaniclastic sediments derived from volcanic islands on the subducting continental margin. The analysed dykes formed by the melting of trench fill Haybi complex material (subsequently metamorphosed to granulite facies) at the subduction front beneath the ophiolite.

It is possible that the granitoid dyke suite represents the highest structural levels of a more extensive zone of granitoid intrusion at the base of the ophiolite mantle sequence, as in the Karmoy ophiolite of SW Norway (Pedersen & Dunning 1997). The status of the Semail ophiolite as an exposed example of SSZ mantle, and the study of the petrogenetic and metamorphic processes related to the generation and emplacement of the ophiolite, may have parallels with processes in similar intra-oceanic arcs observable today. Potassium bearing leucogranitoids found in the Masirah ophiolite (Abbots 1978) have mantle like Pb and Nd isotopic compositions (Nagler & Frei 1994), mineral assemblages and paragenesis distinct from the isotopic composition of the analysed Semail ophiolite granitoids and have a distinct, wholly oceanic, petrogenetic source.

A new Sm-Nd isochron from the Ra's Dadnah composite sill (UAE) gives an age of 98.8 ± 9.5 Ma (MSWD = 1.18), and one from a similar composite sill in the Hayalyn block of the ophiolite (Oman) gives a similar, overlapping, age of 93.0 ± 10.0 Ma (MSWD = 0.33). Both agree within error with the formation age of the ophiolite crust. Structural considerations, published granitoid K-Ar and $^{40}Ar/^{39}Ar$ cooling ages and existing ophiolite age constraints indicate that the dyke suite is younger than ~95 Ma and older than ~91 Ma.

New U-Pb dating of a garnet leucogranite dyke associated with the Ra's Dadnah composite sill gives an age of 105 ± 4 Ma age, which in within error of the Ra's Dadnah composite sill Sm/Nd age, but is ~10 Ma older than other modelling constraints would suggest. Zircon fractions from the dyke are discordant and the regression line and the concordia curve are almost parallel (figure 6.19) at ages of ~100 Ma, which leads to large uncertainties for such young intercept ages.

If this age is correct, it implies that intra-oceanic subduction was occurring beneath the Semail ophiolite in the Khawr Fakkan block area at ~105 Ma, as suggested by Lippard et al. (1986). However, since the intrusions are found around the MTZ, at a fairly high structural position within the ophiolite mantle sequence, the age may suggest that the ophiolite in the

Khawr Fakkan area may be older than the accepted age of ~95 Ma (Tilton et al. 1981). McCulloch et al. (1981) calculated that the ophiolite mantle sequence may have crystallised up to ~6 Ma before the crustal sequence, which when used in conjunction with field structural constraints, is consistent with the ophiolite crustal sequence in this area being formed at ~99 Ma. The accepted Tilton et al. (1981) mean age of ~95 Ma is largely drawn from the SE Oman ophiolite section rather than the UAE area. Equally, the analysed zircons may have been inherited from older subducted material in the Haybi complex. Further investigation of the U-Pb ages of granitoids and the ophiolite crustal sequence is required to clarify the data here presented.

Sample:	OM 79	JC 11	OM 85	JC 25	OM 77	JC 31	JC 33	JC 112	OM 620a	OM 94	OM 91	OM 628	OM 92	F 201	OM 98	OM 124	OM 125	OM 120	OM 119	OM 118	OM 99	Typical XRF detection limits
	Ra's Dadnah leucogranites				*Ra's Dadnah calc alkaline suite*				*Ra's Dibba monzogranitoids*							*Wadi Hulw bin Sulay man leucogranites*					*Wadi Zikt*	
Major Elements (Wt %)																						
SiO_2	75.97	76.10	76.71	76.76	63.63	72.49	74.09	74.47	72.16	72.84	73.54	73.87	74.14	74.21	76.09	74.07	74.59	74.69	74.83	75.21	76.34	0.032
TiO_2	0.03	0.02	0.03	0.02	0.24	0.19	0.15	0.15	0.10	0.20	0.07	0.06	0.12	0.11	0.09	0.08	0.05	0.05	0.07	0.14	0.04	0.001
Al_2O_3	13.64	12.75	12.79	12.93	15.54	14.06	13.07	13.21	12.29	14.58	13.32	12.94	14.01	13.96	13.36	13.19	13.43	13.62	13.18	13.09	13.32	0.078
Fe_2O_3	0.11	0.07	0.03	0.27	1.85	0.47	0.75	0.78	0.37	0.95	0.01	0.02	0.51	0.70	0.27	0.00	0.14	0.31	0.12	0.50	0.02	0.004
FeO	0.36	0.18	0.29	0.29	4.75	0.94	1.44	1.37	0.36	1.22	0.14	0.30	0.76	0.36	0.40	0.32	0.27	0.58	0.34	0.58	0.29	0.004
MnO	0.03	0.00	0.16	0.32	0.13	0.03	0.07	0.05	0.04	0.17	0.00	0.02	0.10	0.09	0.04	0.09	0.41	0.66	0.09	0.10	0.02	0.001
MgO	0.00	0.31	0.00	0.16	2.85	1.01	0.75	0.75	0.03	0.47	0.59	0.40	0.18	0.13	0.09	0.45	0.06	0.05	0.25	0.62	0.20	0.075
CaO	2.01	5.61	1.36	2.47	6.00	5.55	2.54	2.23	0.29	0.32	0.62	2.02	0.24	0.23	0.33	0.93	1.11	0.65	0.97	1.03	1.83	0.012
Na_2O	6.81	3.39	7.82	5.27	2.47	3.14	5.74	4.63	8.61	4.69	8.28	7.56	5.32	4.81	5.24	4.76	4.13	6.02	4.04	3.14	5.40	0.233
K_2O	0.23	0.14	0.23	0.14	0.28	0.09	0.26	1.02	4.11	2.54	2.92	0.82	3.41	3.67	3.31	5.23	4.61	1.87	5.10	4.82	1.64	0.021
P_2O_5	0.02	0.00	0.00	0.00	0.06	0.11	0.08	0.05	0.05	0.06	0.07	0.03	0.04	0.04	0.03	0.03	0.05	0.05	0.05	0.04	0.02	0.031
H_2O etc	0.43	1.33	0.35	1.01	2.19	1.76	0.96	0.95	0.73	1.12	0.58	1.08	0.85	0.92	0.47	0.54	0.83	0.92	0.51	0.36	0.57	-
Total	99.64	99.90	99.77	99.59	99.99	99.84	99.90	99.66	99.14	99.16	100.14	99.12	99.68	99.23	99.72	99.69	99.68	99.47	99.55	99.63	99.69	-
Trace Elements (ppm)																						
S	2300	8700	2300	2400	3100	8500	3100	3400	2200	2200	2300	2400	4200	2200	2200	2300	2600	2400	2400	2500	2500	20
V	5	2	2	2	178	54	43	39	7	2	2	4	2	2	2	12	10	2	10	32	3	2
Cr	2	2	2	2	37	10	14	2	2	2	2	2	2	2	2	2	2	2	2	2	2	2
Co	2	5	2	6	34	12	13	16	2	5	2	2	2	4	2	2	2	2	2	3	2	6
Ni	2	4	4	5	29	23	14	8	2	2	2	2	5	2	2	6	5	2	4	8	2	6
Cu	49	33	37	49	146	48	44	46	39	42	40	41	40	33	40	29	31	38	37	76	35	6
Zn	11	8	10	13	73	19	33	25	11	31	11	11	27	23	14	16	17	26	15	32	12	9
Rb	2	4	1	2	6	1	4	17	46	43	101	13	65	101	38	129	156	111	129	139	27	3
Sr	59	103	35	68	145	206	152	128	12	11	28	190	20	40	3	39	50	13	56	76	168	3
Y	107	13	166	155	25	15	27	23	33	47	8	22	79	69	33	20	28	36	24	46	24	3
Zr	110	76	72	77	64	122	100	99	51	106	22	91	66	64	48	46	62	45	55	89	62	6
Nb	20	12	64	33	9	8	13	14	39	91	12	6	43	45	36	8	8	44	12	15	7	6
Ba	2	2	2	2	44	51	20	74	2	74	70	389	15	29	2	20	51	14	7	85	406	7
La	7	4	11	5	6	2	9	11	14	15	7	7	3	11	7	10	12	8	11	18	7	3
Ce	6	2	34	21	6	120	7	40	2	2	4	13	5	2	6	2	2	2	5	19	7	8
Nd	10	2	16	21	9	40	8	15	6	10	7	10	11	7	7	20	5	14	8	20	8	6

Table 6.1 Major and trace element geochemistry of the analysed Khawr Fakkan block granitoids. Samples F 201, OM 620 and OM 620a are from Peters & Kamber (1994).

Sample:	OM 79	JC 11	OM 85	JC 25	OM 77	JC 31	JC 33	JC 112	OM 620a	OM 94	OM 91	OM 628	OM 92	F 201	OM 98	OM 124	OM 125	OM 120	OM 119	OM 118	OM 99
	Ra's Dadnah leucogranites				*Ra's Dadnah calc alkaline suite*				*Ra's Dibba monzogranitoids*							*Wadi Hulw bin Sulayman leucogranites*					*Wadi Zikt*
CIPW Norms (Wt%)																					
Q	31.88	45.13	29.62	39.90	28.05	40.95	36.73	37.11	24.71	35.22	24.38	25.87	29.70	31.52	31.95	25.23	30.31	30.71	29.76	35.19	34.66
Or	1.36	0.83	1.64	0.83	1.66	0.53	6.06	6.06	23.30	15.00	17.24	4.84	20.13	21.68	19.57	30.91	27.24	10.56	30.02	28.36	9.70
Ab	57.54	28.61	64.43	44.54	20.88	26.51	39.14	39.14	39.24	39.61	51.19	61.94	44.96	40.66	44.28	38.62	34.90	50.83	34.06	26.72	45.64
An	5.96	19.16	0.00	11.21	29.42	23.98	10.74	10.74	0.00	1.58	0.00	0.00	1.20	1.14	1.64	0.00	4.46	2.90	2.83	4.86	7.24
C	0.00	0.00	0.00	0.00	0.38	0.00	0.54	0.54	0.00	3.53	0.00	0.00	1.12	1.66	0.55	0.00	0.00	0.72	0.00	0.90	0.00
Ac	0.00	0.00	0.09	0.00	0.00	0.00	0.00	0.00	1.06	0.00	0.03	0.06	0.00	0.00	0.00	0.00	0.00	0.00	0.00	0.00	0.00
SMS	0.00	0.00	0.54	0.00	0.00	0.00	0.00	0.00	9.98	0.00	3.54	0.68	0.00	0.00	0.00	0.57	0.00	0.00	0.00	0.00	0.00
Di	1.08	2.29	1.46	0.89	0.00	2.28	0.00	0.00	1.27	0.00	2.31	3.19	0.00	0.00	0.00	3.65	0.63	0.00	1.22	0.00	1.41
Wo	1.12	2.44	2.13	0.00	0.00	0.00	0.00	0.00	0.00	0.00	0.00	2.50	0.00	0.00	0.00	0.00	0.00	0.00	0.00	0.00	0.00
Hy	0.00	0.00	0.00	0.81	14.15	2.51	3.58	3.59	0.14	2.51	0.51	0.00	1.40	0.38	0.65	0.57	0.88	2.08	0.63	2.16	0.29
Mt	0.16	0.11	0.00	0.39	2.69	0.68	1.13	1.13	0.00	1.39	0.00	0.00	0.74	1.02	0.39	0.00	0.20	0.44	0.17	0.73	0.03
Il	0.06	0.04	0.06	0.04	0.46	0.36	0.29	0.29	0.19	0.38	0.27	0.11	0.23	0.21	0.17	0.15	0.10	0.10	0.13	0.27	0.08
Ap	0.04	0.00	0.00	0.00	0.12	0.24	0.11	0.11	0.11	0.12	0.67	0.06	0.09	0.09	0.06	0.07	0.11	0.11	0.11	0.09	0.04
Total	99.20	98.61	99.97	98.61	97.81	98.04	98.32	98.71	100.00	99.34	100.14	99.25	99.57	98.36	99.26	99.77	98.83	98.45	98.93	99.28	99.09
Mineralogy (Vol%)																					
Qtz	30	60	45	55	5	40	40	35	25	50	45	50	50	20	60	30	40	25	35	30	35
Kfs	5	5	5	5	-	5	10	10	60	35	40	10	30	40	30	40	30	25	35	40	30
Pl	50	30	40	30	50	35	35	50	-	-	-	30	-	-	-	15	15	35	15	15	25
Bt	-	-	-	-	5	-	10	-	5	-	-	5	-	20	-	5	5	-	5	10	7
Ms	-	-	-	-	-	-	-	-	-	-	-	-	-	-	-	5	5	-	5	5	3
Crd	-	-	-	-	-	-	-	-	-	10	5	5	5	15	5	-	-	-	-	-	-
And	-	-	-	-	-	-	-	-	10	-	10	-	15	5	5	-	-	-	-	-	-
Grt	-	-	5	5	-	-	-	-	-	-	-	-	-	-	-	5	-	10	3	-	-
Tur	-	-	-	2	-	-	-	-	-	-	-	-	-	-	-	-	-	5	2	-	-
Other	Chl: 15	Chl: 5	Chl: 5	Chl: 3	Chl: 10; Hbl: 30	Chl: 20	Chl: 5	Chl: 10	-	Ore: 5	-	-	-	-	-	-	Chl: 5	-	-	-	-

Table 6.2 Modal mineralogy and calculated CIPW norms of the analysed Khawr Fakkan block granitoids.

Sample:	OM 3-1	OM 3-3	OM 3-5	OM 3-7	Typical XRF detection limits (ppm)
Hayalyn block composite sill components					
Major Elements (Wt %)					
SiO_2	77.96	72.84	73.11	75.15	500
TiO_2	0.06	0.24	0.28	0.17	50
Al_2O_3	12.40	12.50	12.32	12.71	500
Fe (total)	0.29	2.52	2.75	1.19	50
MnO	0.01	0.09	0.13	0.06	50
MgO	0.24	2.33	1.89	0.52	300
CaO	2.26	5.92	4.16	1.59	100
Na_2O	4.49	1.23	3.00	2.66	400
K_20	0.54	0.04	0.18	4.63	100
P_2O_5	0.02	0.11	0.11	0.06	100
H_20 etc	0.64	1.34	1.11	0.44	-
Total	98.90	99.17	99.04	99.18	-
Trace Elements (ppm)					
Rb	15.0	0.7	4.8	136.1	2.0
Sr	264.0	208.0	183.0	117.0	2.0
Y	42.3	26.0	20.8	16.8	2.0
Zr	48.0	104.0	82.0	72.0	2.0
Nb	24.0	11.4	9.2	14.9	1.5
Ba	38.0	11.0	41.0	345.0	12.0
Pb	6.0	1.0	7.0	35.0	5.0
Th	20.0	7.0	4.0	8.0	4.0
U	8.0	4.0	3.0	3.0	3.0
Sc	1.0	9.0	8.0	5.0	5.0
V	8.0	74.0	70.0	19.0	5.0
Cr	6.0	61.0	24.0	9.0	4.0
Co	14.0	24.0	19.0	14.0	2.0
Ni	5.0	71.0	51.0	11.0	3.0
Cu	3.0	1.0	83.0	6.0	3.0
Zn	4.0	25.0	38.0	16.0	3.0
Ga	9.0	12.0	11.0	11.0	3.0
Mo	0.0	0.0	0.0	0.0	2.0
As	3.0	3.0	2.0	4.0	5.0
S	85.0	24.0	53.0	29.0	50.0

Sample:	OM 3-1	OM 3-3	OM 3-5	OM 3-7
CIPW Norms (Wt%)				
Q	44.69	48.23	41.97	37.30
Or	3.19	0.24	1.06	27.33
Ab	37.95	10.40	25.36	22.48
An	11.07	28.45	19.61	7.49
C	0.37	-	-	0.58
Ac	-	-	-	-
SMS	-	-	-	-
Di	-	0.15	0.25	-
Wo	-	-	-	-
Hy	0.93	9.18	8.30	2.83
Mt	0.06	0.55	0.60	0.26
Il	0.11	0.46	0.53	0.32
Ap	-	0.24	0.24	0.13
Total	98.37	97.90	97.92	98.72
Mineralogy (Vol%)				
Qtz	60	30	30	45
Kfs	10	-	5	25
Pl	25	50	35	15
Bt	5	10	15	15
Hbl	-	10	15	-
Other	-	-	-	-

Table 6.3. Major and trace element data for components of the Wadi Al Hajar composite granitoid sill, Hayalyn block, Oman.
Table 6.4. CIPW norms and modal abundances of the same samples.

Sample	Rock Unit	Sm (ppm)	Nd (ppm)	$^{147}Sm/^{144}Nd$	$^{143}Nd/^{144}Nd$	$\varepsilon_{Nd(90Ma)}$	Rb (ppm)	Sr (ppm)	$^{87}Rb/^{86}Sr$	$^{87}Sr/^{86}Sr$	$^{87}Sr/^{86}Sr_{i\,(90Ma)}$	$\varepsilon_{Sr(90Ma)}$
Hayalyn block granitoids												
OM 3-1	*Leucogranitoids*	3.80	9.99	0.230	0.512267 ± 7	-4.97	14.49	268.17	0.156	0.706558 ± 9	0.706359	27.9
OM 3-2		2.75	13.86	0.120	0.512266 ± 6	-4.99	28.52	133.49	0.618	0.707243 ± 9	0.706452	29.2
OM 3-3	*Granodiorites*	4.20	18.56	0.137	0.512232 ± 6	-5.67	0.87	216.65	0.012	0.706422 ± 9	0.706408	28.6
OM 3-4		3.83	19.03	0.122	0.512224 ± 6	-5.82	6.01	198.06	0.088	0.706950 ± 9	0.706837	34.7
OM 3-5	*Quartz diorites*	3.47	14.34	0.146	0.512264 ± 5	-5.03	4.08	183.47	0.064	0.707147 ± 9	0.707065	37.9
OM 3-6B		6.23	41.86	0.090	0.512263 ± 7	-5.06	25.70	164.84	0.451	0.707373 ± 9	0.706796	34.1
OM 3-7	*Biotite tonalite*	3.32	14.68	0.137	0.512220 ± 6	-5.89	135.93	121.32	3.244	0.713356 ± 9	0.709208	68.3

Table 6.5 Sm-Nd and Rb-Sr isotope geochemical data for the analysed Hayalyn block granitoids. The notation is taken from DePaolo & Wasserburg (1976a), using UR values for Sr from DePaolo & Wasserburg (1976b), and CHUR values for Nd from Jacobsen & Wasserburg (1984). Decay constants from Steiger & Jager (1977).

Sample	Rock Unit	Sm (ppm)	Nd (ppm)	$^{147}Sm/^{144}Nd$	$^{143}Nd/^{144}Nd$	$\varepsilon_{Nd(90Ma)}$	Rb (ppm)	Sr (ppm)	$^{87}Rb/^{86}Sr$	$^{87}Sr/^{86}Sr$	$^{87}Sr/^{86}Sr_{I\,(90Ma)}$	$\varepsilon_{Sr(90Ma)}$
	Khawr Fakkan block granitoids											
OM 79	*Ra's Dadnah leucogranites*	4.41	10.48	0.255	0.512456 ± 7	-4.2	1.45	58.73	0.071	0.707153 ± 9	0.707062	37.9
OM 85		6.61	15.71	0.254	0.512458 ± 7	-4.2	1.32	34.82	0.110	0.706987 ± 10	0.706847	34.8
JC 25		7.85	20.52	0.231	0.512435 ± 6	-4.4	1.86	68.10	0.079	0.706850 ± 9	0.706749	33.4
OM 77	*Ra's Dadnah calc alkaline suite*	2.34	8.81	0.161	0.512396 ± 6	-4.3	6.43	144.71	0.129	0.707447 ± 10	0.707282	41.0
JC 31		6.51	40.29	0.098	0.512325 ± 6	-5.0	1.32	206.27	0.019	0.707130 ± 9	0.707106	38.5
JC 112		3.23	14.78	0.132	0.512375 ± 8	-4.4	17.04	127.59	0.386	0.707406 ± 9	0.706912	35.7
OM 91	*Ra's Dibba monzogranitoids*	1.43	7.26	0.119	0.512505 ± 6	-1.7	100.84	28.14	10.367	0.719590 ± 9	0.706334	27.5
OM 628		2.17	9.86	0.133	0.512575 ± 6	-0.5	13.16	189.79	0.201	0.706730 ± 9	0.706473	29.5
OM 124	*Wadi Hulw bin Sulayman*	5.80	19.55	0.180	0.512305 ± 6	-6.3	128.54	39.07	9.517	0.722223 ± 9	0.710054	80.4
OM 119	*leucogranites*	2.05	7.65	0.162	0.512313 ± 6	-6.0	129.22	56.16	6.657	0.718358 ± 10	0.709845	77.4
OM 118		4.92	19.93	0.149	0.512315 ± 6	-5.8	139.16	75.85	5.307	0.715961 ± 10	0.709175	67.9
OM 99	*Wadi Zikt granites*	1.83	7.84	0.141	0.512463 ± 6	-2.8	27.41	168.20	0.471	0.707367 ± 9	0.706764	33.6
	Bani Hamid Granulites											
OM 132	*Alkali feldspar-phlogopite-diopside-*	5.57	21.85	0.154	0.512702 ± 6	1.7	2.33	313.99	0.021	0.703959 ± 9	0.703932	-6.6
OM 135	*spinel granulite gneisses*	2.33	6.29	0.224	0.512953 ± 6	5.8	6.24	119.04	0.152	0.705771 ± 8	0.705577	16.8
JC 92	*Quartz-diopside-andradite gneiss*	1.42	4.34	0.198	0.512315 ± 6	-6.3	0.17	5.60	0.089	0.709847 ± 18	0.709734	75.8
JC 94	*Calc-silicate gneiss*	1.88	9.54	0.119	0.512476 ± 5	-2.3	6.76	200.39	0.098	0.708143 ± 8	0.708018	51.4
JC 95	*Quartz-phlogopite-cordierite gneiss*	0.05	0.24	0.117	0.512256 ± 25	-6.5	0.98	3.66	0.773	0.709059 ± 11	0.708071	52.2
	Normal Metamorphic Sole, Sumeini											
OM 65	*Garnet-diopside amphibolite gneiss*	4.11	13.62	0.182	0.512862 ± 5	4.5	8.47	163.72	0.150	0.705608 ± 8	0.705417	14.5

Table 6.6 Sm-Nd and Rb-Sr isotope geochemical data for the analysed Khawr Fakkan block granitoids and Bani Hamid granulites. The notation is taken from DePaolo & Wasserburg (1976a), using UR values for Sr from DePaolo & Wasserburg (1976b), and CHUR values for Nd from Jacobsen & Wasserburg (1984). Decay constants from Steiger & Jager (1977).

FRACTIONS			CONCENTRATIONS		MEASURED		ATOMIC RATIOS								AGE (Ma)	
No.	Properties	Wt.	U (ppm)	Pb (ppm)	Pb (pg)	Pb	Pb	Pb		Pb		Rho		Pb	Pb	Pb
				rad	Total comm						+/-		+/-			
jc36	zircons, unabraded	0.010	4415.1	49.1	44	588	0.0930	0.01084	6	0.0721	7	0.66	0.04825	35	69.5	70.7
jc36	zircons, abraded	0.013	12080.4	146.4	43	2409	0.0515	0.01269	6	0.0841	5	0.93	0.04808	10	81.3	82.0
jc25	zircons, abraded	0.010	7324.1	95.6	52	993	0.0856	0.01304	5	0.0866	6	0.61	0.04820	28	83.5	84.4
jc25	zircons, abraded	0.019	967.3	12.0	5	1090	0.0496	0.01306	6	0.0869	6	0.74	0.04824	24	83.6	84.6

Table 6.8 U-Pb data used in the plotting of figure 6.19.

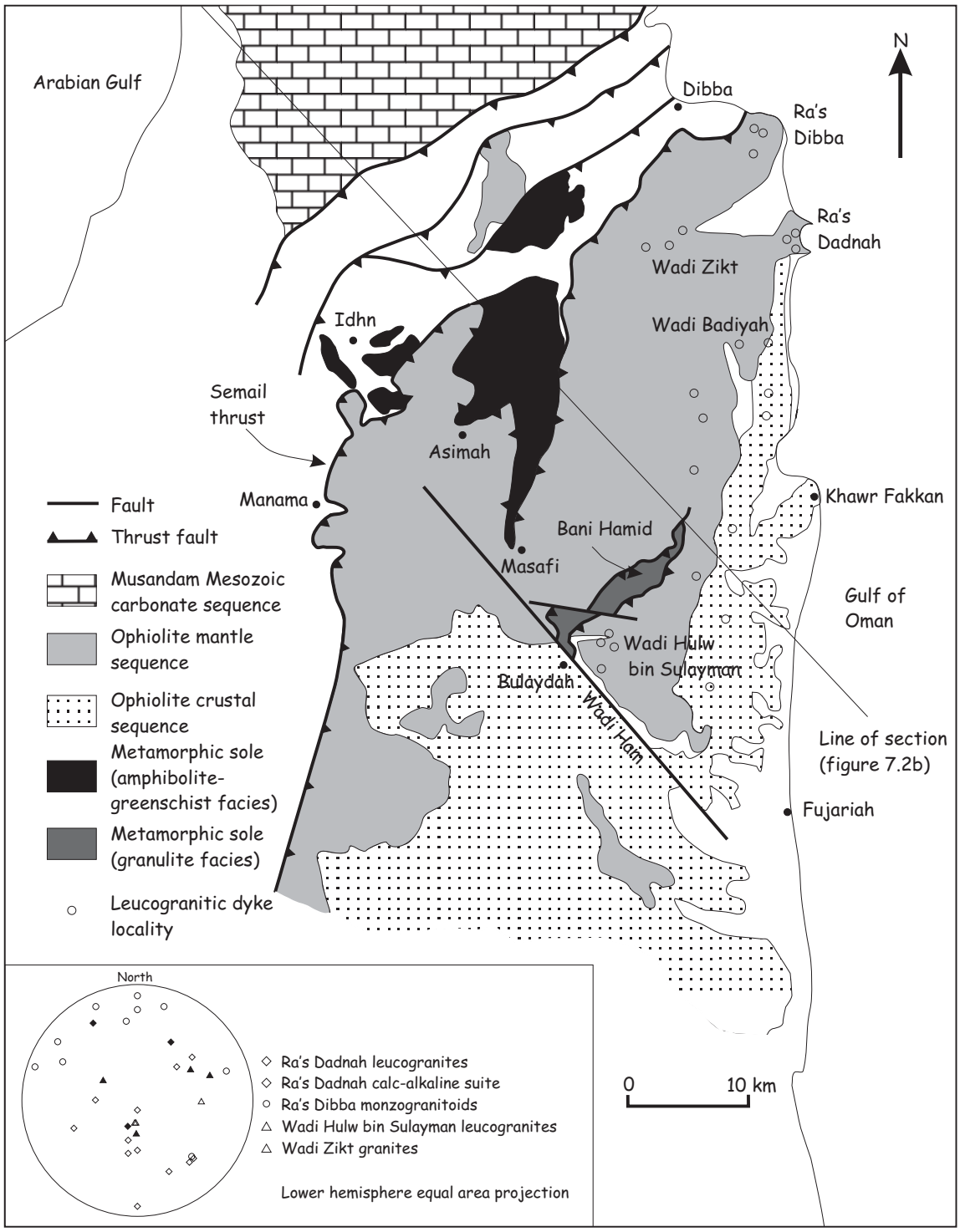


Figure 6.1a Generalised geological map of the Khawr Fakkan block of the Semail ophiolite in the UAE, showing the Bani Hamid granulite metamorphic sole unit, the classic sole localities of the Asimah and Masafi region, and the major granitoid dyke localities referred to in *Chapter Six*. See Figure 2.4a for location within the Semail ophiolite. Inset: stereonet showing the similarity in orientation within individual dyke suites. Some (unsampled) dyke localities from Gnos & Nicolas (1996).

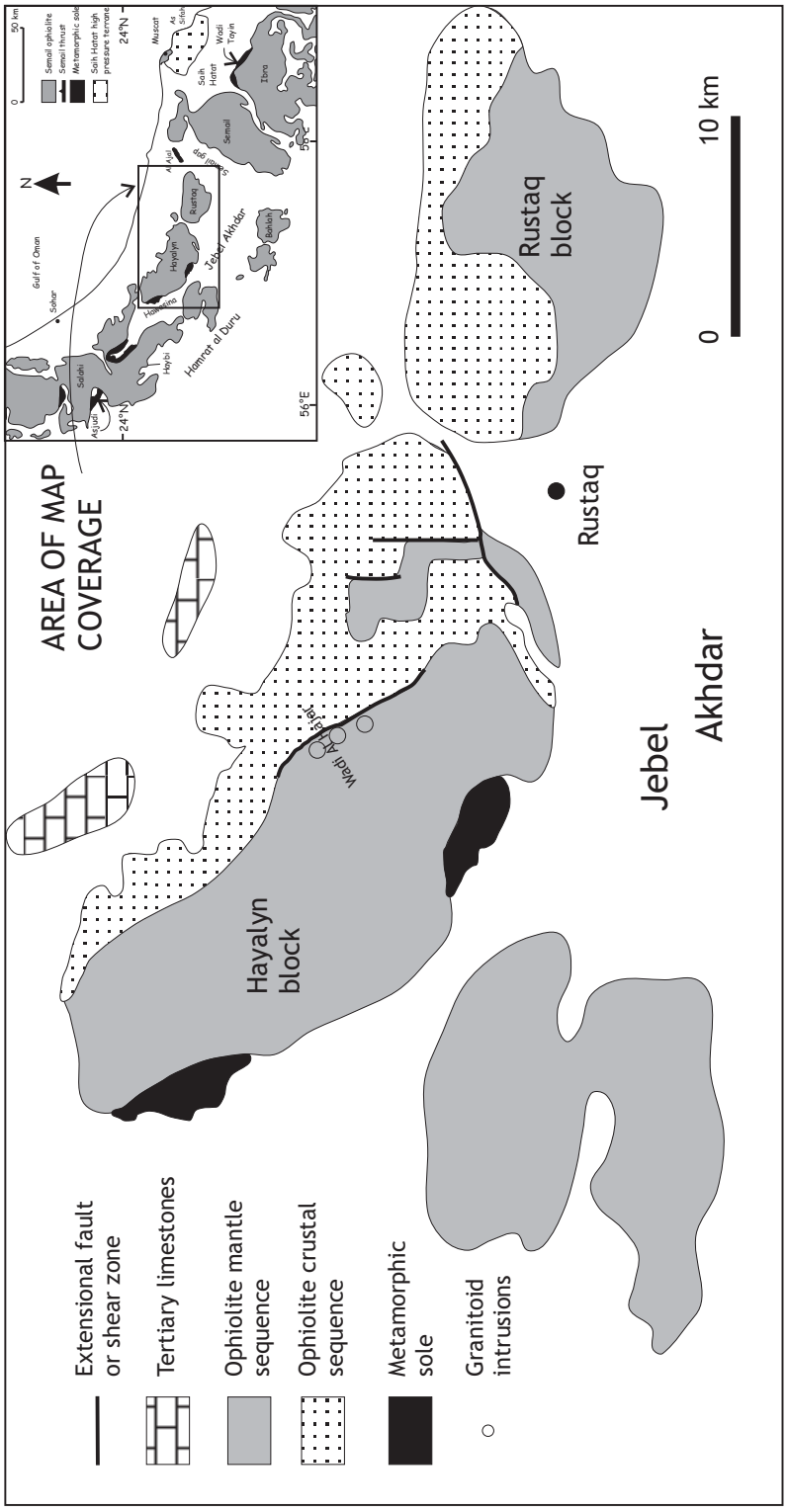


Figure 6.1b Geological sketch map of the Hayalyn block of the Semail ophiolite in the central Oman mountains, after Browning (1982) and Lippard et al. (1986), showing the major granitoid intrusions sampled in this study.

Figure 6.2 Field views of a variety of granitoid intrusion parageneses in the Semail ophiolite.



a



b

a) Large (~75 m thick) composite sill intruding mantle transition zone cumulate peridotites and gabbros, containing a core of quartz diorite and margins of garnet leucogranite. Ra's Dadnah, UAE, looking north. b) Smaller scale dyke and sill networks intruding mantle transition zone units, Ra's Dadnah.



c



d

c) Leucogranitic stock at the base of the Khawr Fakkan block mantle sequence, Bithnah, Wadi Ham. d) Andalusite-cordierite monzogranitic dyke, Zikt. Many similar small scale intrusions can be seen in the brown serpentinised harzburgites of the background ridges.



e



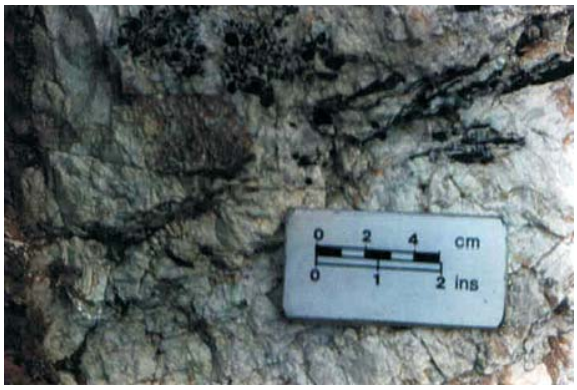
f

e) Large (~100 m thick) composite sill intruding mantle transition zone cumulate peridotites and gabbros along a shear zone, Wadi Al Hajar, Hayalyn, Oman. f) Small tonalitic stock, Wadi Al Hajar.

Figure 6.3a-d The variety of microstructures and mineral assemblages displayed by Semail ophiolite granitoid intrusions.



a



b

a) Pegmatoidal andalusite-tourmaline bearing leuocgranitoid dyke, Wadi Zikt, UAE. b) Pegmatoidal 'sweat' containing spessartine garnet, muscovite and tourmaline enclosed within biotite granite, Bithnah, Wadi Ham.



c



d

c) Granitic mylonite dyke margin, Wadi Hulw bin Sulayman, with a strong foliation defined by biotite and quartz ribbon layers. d) Detail of intrusive sequence in composite sill, Ra's Dadnah.

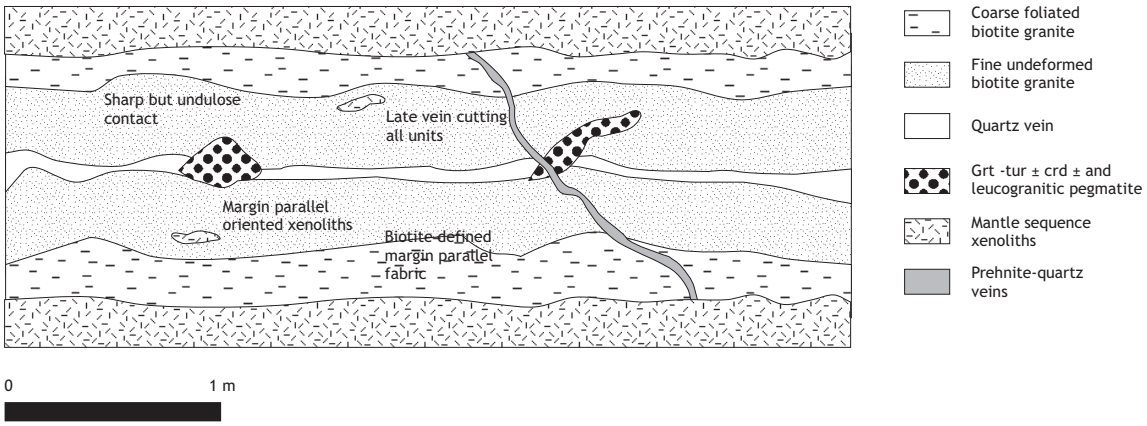
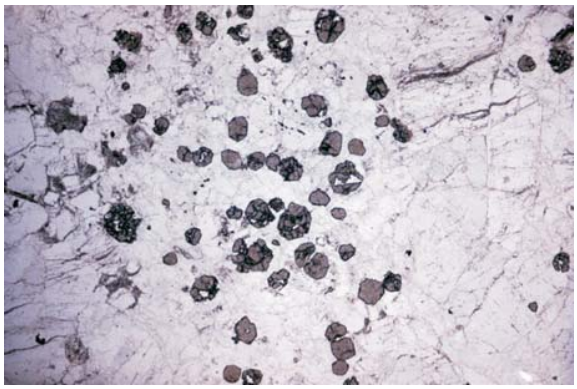
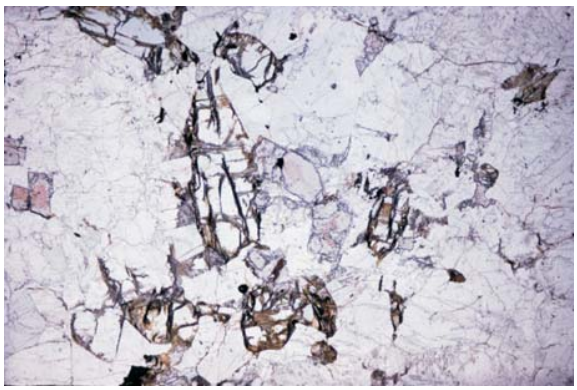


Figure 6.4 Composite diagram to demonstrate the typical petrographic and multigenerational range of granitoid material found in Khawr Fakkan block granitoid intrusions.

Figure 6.5 Photomicrographs of leucogranitoids from the Semail ophiolite, illustrating the variety of mineral assemblages seen. Field of view is ~4 mm.



a) Spessartine rich garnet-tourmaline Himalayan style leucogranite with muscovite (not seen), Wadi Hulw bin Sulayman (figure 6.1a).



b) Cordierite-anadalusite monzogranitic dyke, Ra's Dibba area (figure 6.1a). Cordierite exhibits sector twinning and strong marginal alteration to pinite, while andalusite contains inclusions of staurolite and hercynite (Peters & Kamber 1994), and Fe_2O_3 rich, pink pleochroic cores.



c) Mylonitised biotite granite, Wadi Hulw bin Sulayman (figure 6.1a), with augen of plagioclase (An_{20}) entrained in a foliated matrix of chloritised biotite and recrystallised quartz.

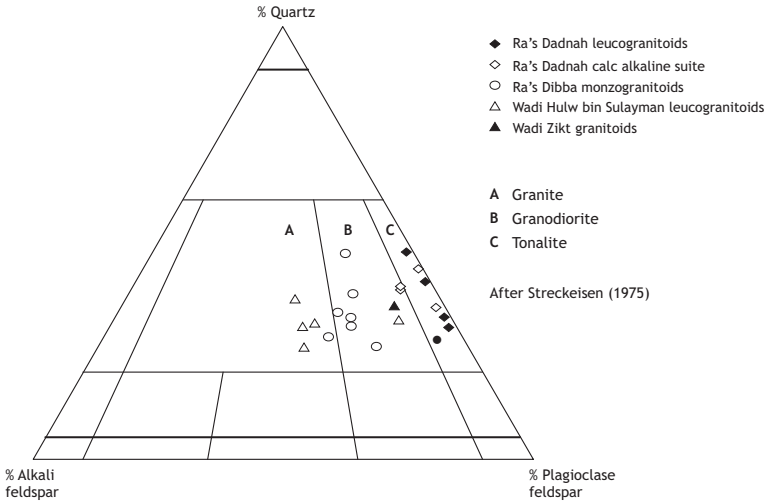


Figure 6.6 Streckenheisen plutonic rock classification diagram. The Semail ophiolite granitoids vary in composition from tonalites to granites.

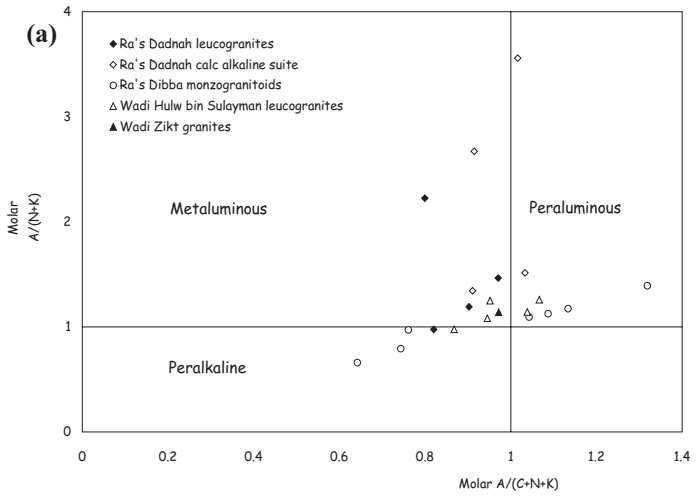


Figure 6.7a Diagram showing distribution of granitoids in [A/NK] and [A/CNK] space. The low (< 0.5%) K_2O contents of some of the Ra's Dadnah samples can be attributed to post emplacement, fluid driven albitisation of potassium feldspar.

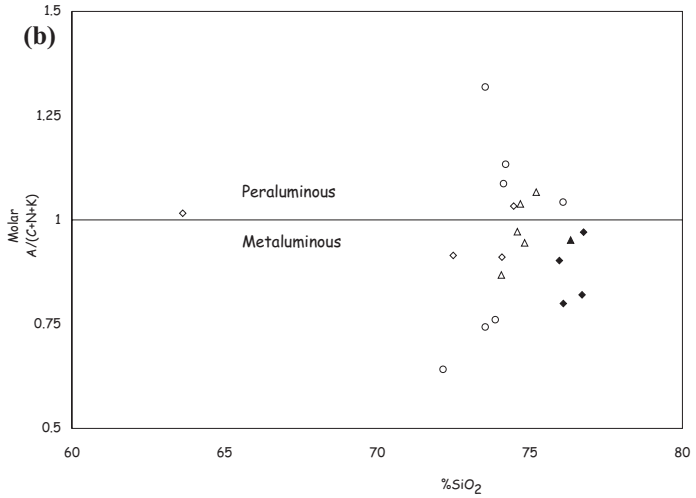


Figure 6.7b Diagram showing the variation of peraluminous character with differentiation, represented by wt % SiO_2. Each mineralogical assemblage exhibits a different trend. See text for discussion.

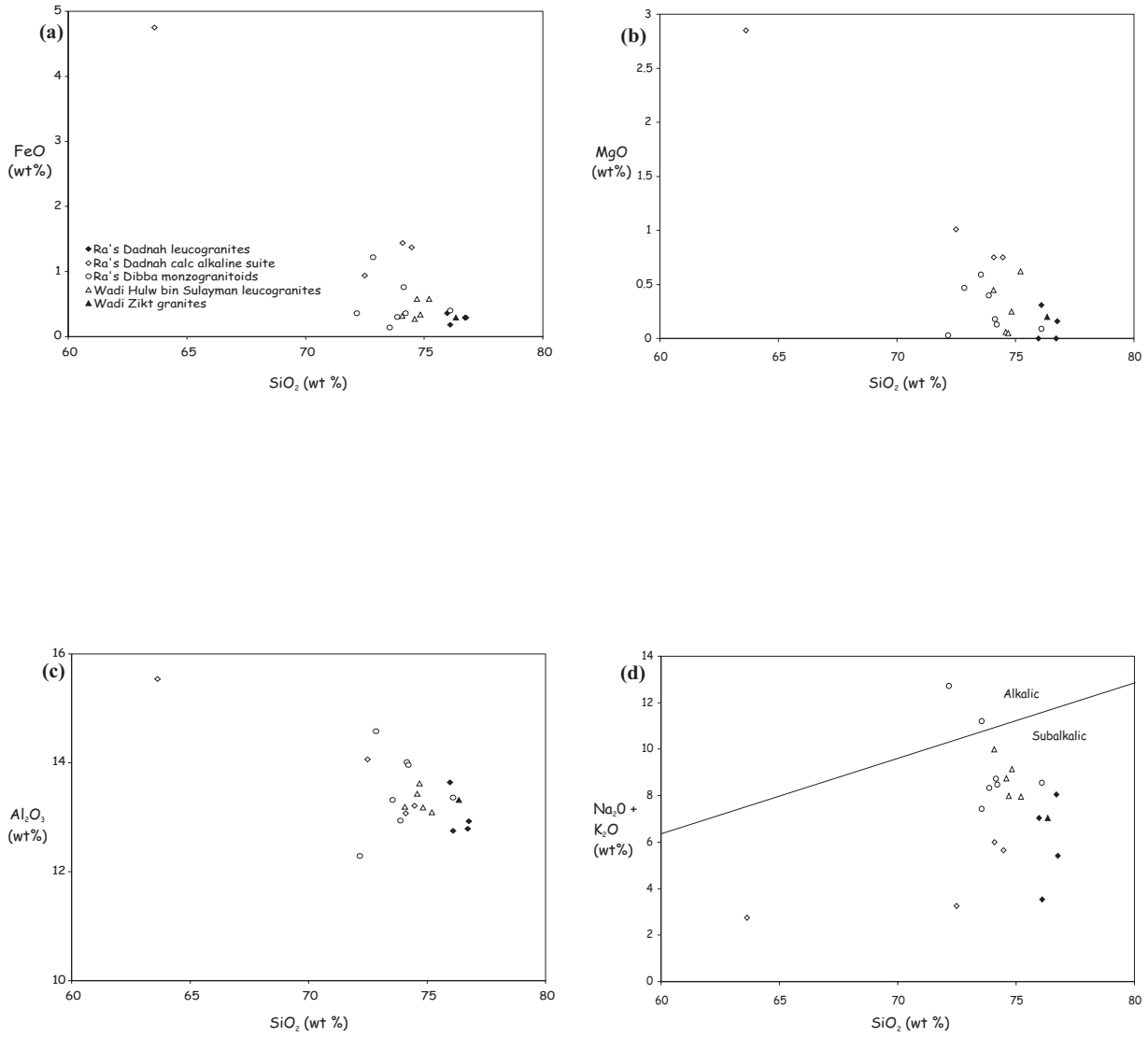


Figure 6.8 Harker SiO_2 variation diagrams for FeO, MgO, Al_2O_3 and total alkalis. Note the low alkali contents of the components of the Ra's Dadnah composite sill which has undergone greenschist facies metamorphism.

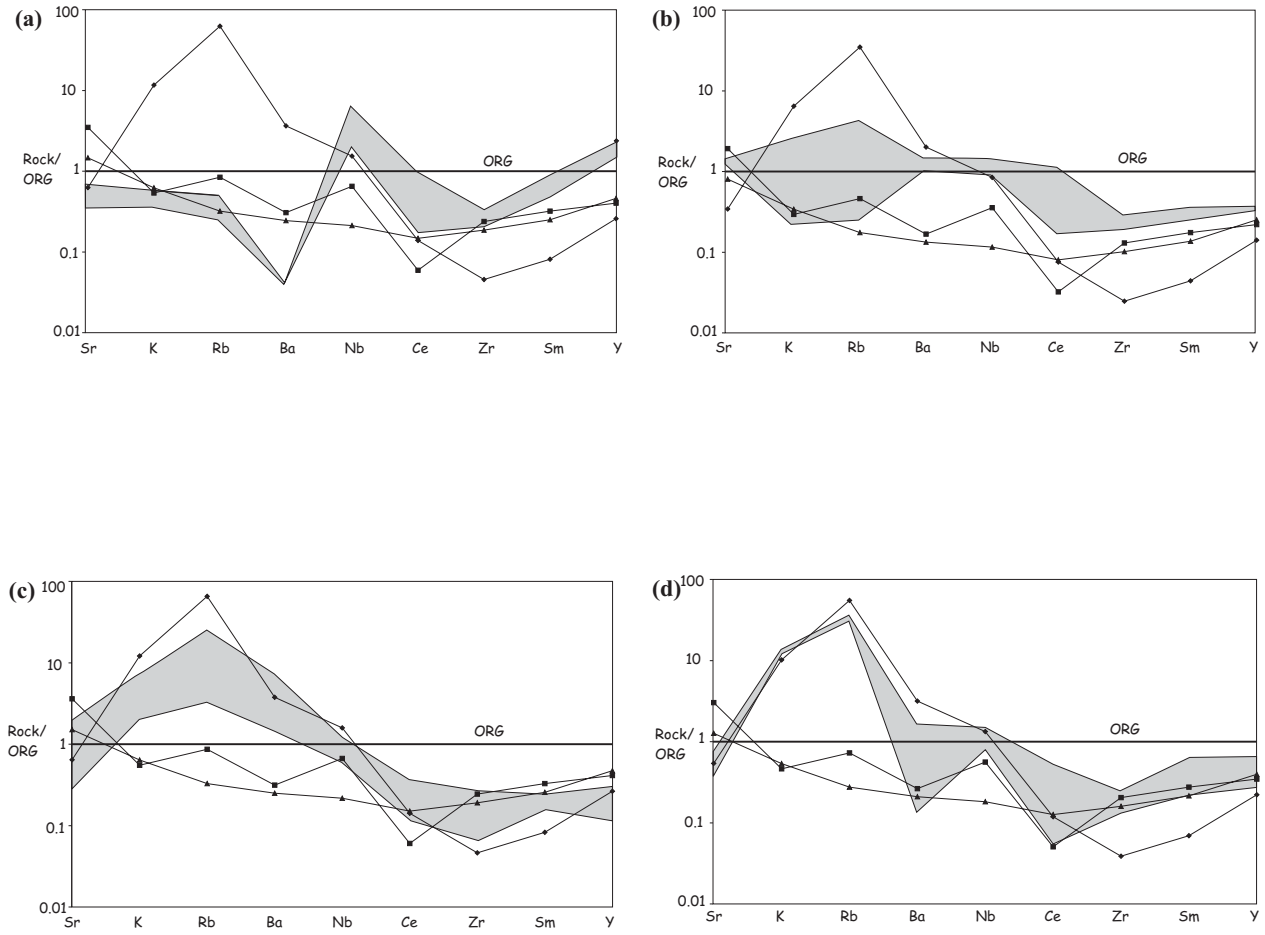


Figure 6.9 ORG normalised trace element patterns of the analysed granitoids from the Khawr Fakkan block. (a) Ra's Dadnah composite sill leucogranites, (b) Ra's Dadnah composite sill calc alkaline components, (c) Ra's Dibba monzogranitoids, (d) Wadi Hulw bin Sulayman leucogranites. All are compared with —◆— a typical Himalayan metasedimentary melt leucogranite (Searle & Fryer 1986), a partial melt —■— from the amphibolite unit of the Semail ophiolite metamorphic sole (Searle & Malpas 1982), and —▲— a late stage trondhjemitic fractionate from the upper crustal units of the Semail ophiolite (Lippard et al. 1986). After Pearce et al. (1984).

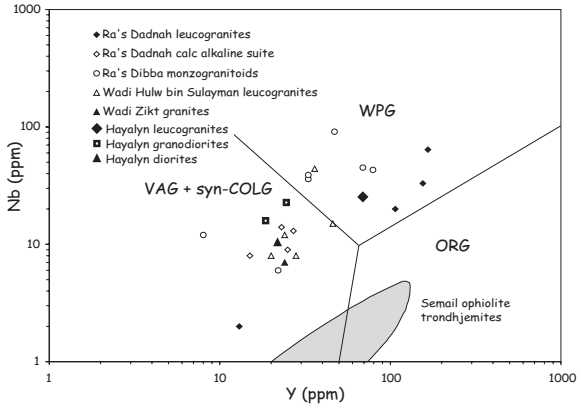


Figure 6.10 Tectonic discrimination diagram plotting Nb and Y concentrations, after Pearce et al. (1984). Syn-COLG: syn-collisional granites; VAG: volcanic arc granites; WPG: within plate granites; ORG: ocean ridge granites. Semail ophiolite trondhjemite data field from Alabaster et al. (1982). The fact that granitoids from higher structural levels plot in the WPG field is indicative of a mantle component in their petrogenesis.

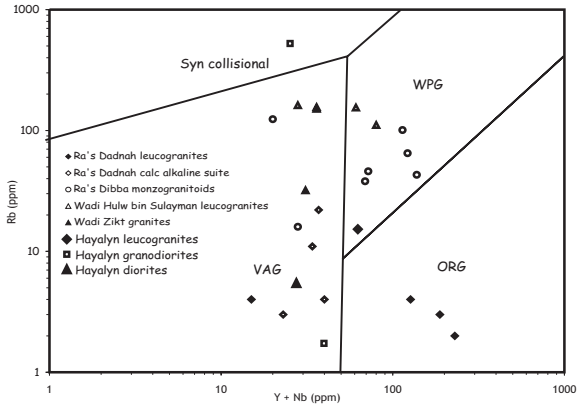


Figure 6.11 Rb-Y tectonic discrimination diagram, after Pearce et al. (1984). Granitoid types as figure 6.10. Granitoids from higher structural levels within the Semail ophiolite plot in the WPG field, consistent with an increasing a mantle component in their petrogenesis.

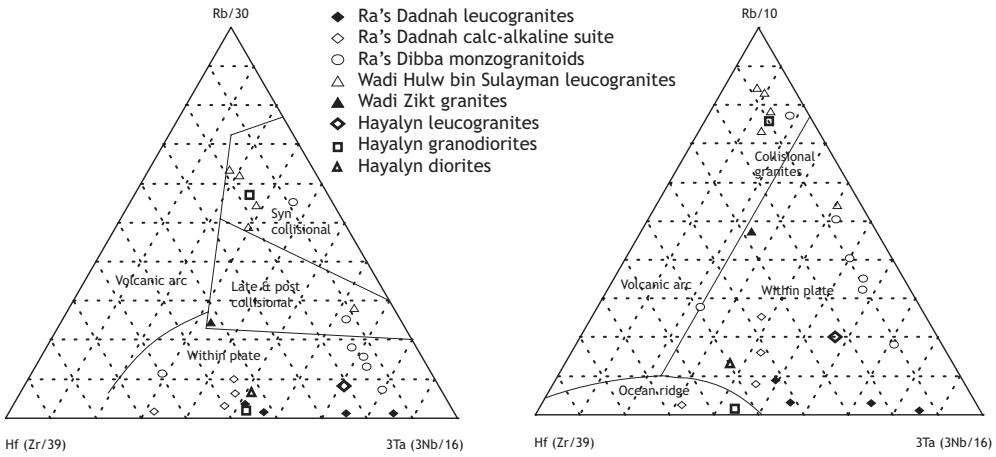


Figure 6.12 Ternary tectonic discrimination diagrams, demonstrating the clear progression from collisional type granitoids at the base of the Khawr Fakkan block mantle sequence to within plate granitoids at the top. After Harris et al. (1986).

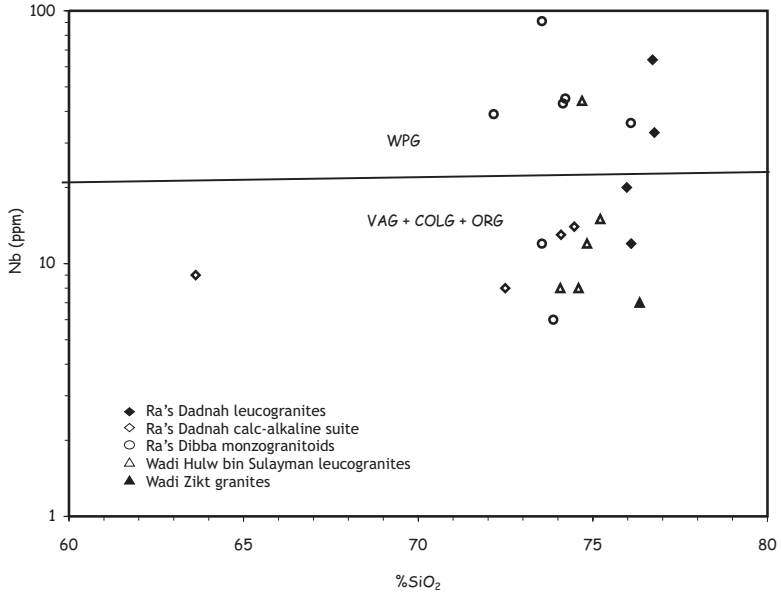


Figure 6.13 Harker style tectonic discrimination diagram plotting Nb against SiO_2, after Pearce et al. (1984). Granitoids from the base of the Khawr Fakkan block of the ophiolite plot in the VAG/COLG/ORG field, while those emplaced at higher structural levels plot in the WPG field.

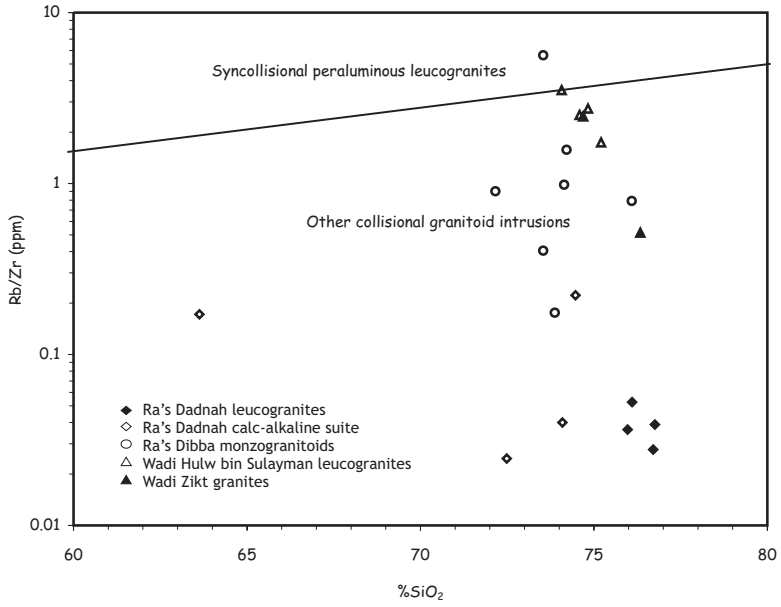


Figure 6.14 Harker style tectonic discrimination diagram plotting Rb/Zr against SiO_2, after Pearce et al. (1984). Although the discrimination displayed in this plot is not as clearly expressed as other techiques, there is again a clear progression from collisional style granitoids at the base of the ophiolite to within plate style granitoids at higher ophiolite structural levels.

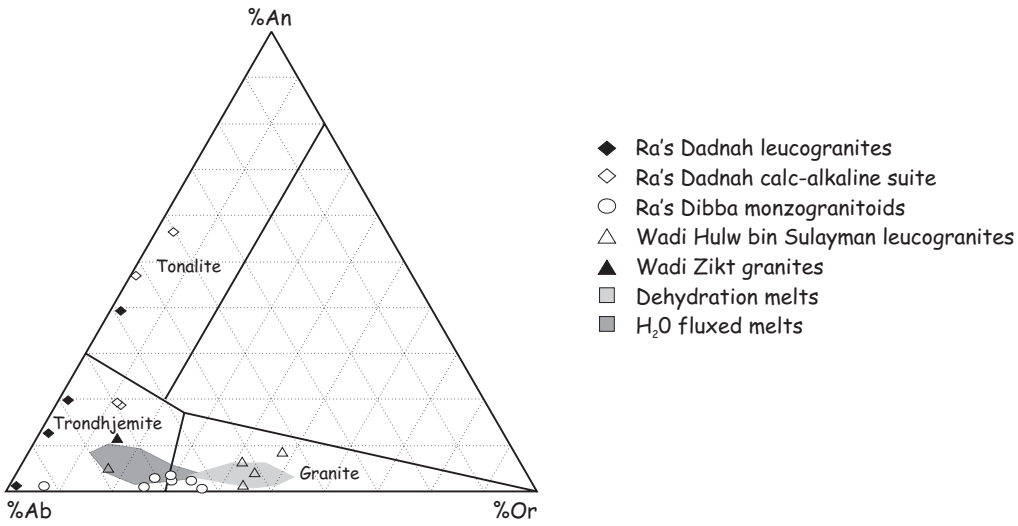


Figure 6.15a CIPW normative classification of the analysed leucogranitic dykes, after Barker (1979). Leucogranites from Wadi Hulw bin Sulayman and Ra's Dibba correlate well with the fields defined by experimentally derived glasses formed from typical Himalayan muscovite-biotite schists (Patiño Douce & Harris 1998). Components of the Ra's Dadnah composite body have undergone metasomatic replacement of potassium feldspar by albite (Briqueu et al. 1991).

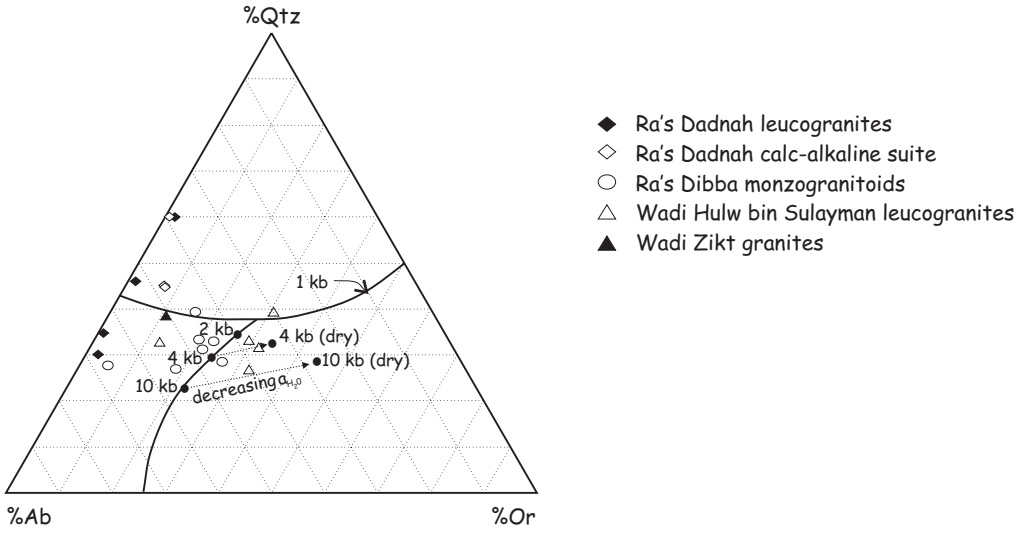


Figure 6.15b Phase relationships and minimum melt compositions in the CIPW normative system quartz-albite-orthoclase ± H_2O ± anorthite ± F. The clustering of the Wadi Hulw bin Sulayman and Ra's Dibba granitoids suggests a minimum melt composition for both domains, with the former suite crystallising at lower H_2O activity. The metasomatic loss of K_2O from the Ra's Dadnah composite dyke components makes any interpretation of their phase relationships equivocal. Experimental minimum melt compositions from Rollinson (1993) and references therein. Data symbols as figure 6.15a.

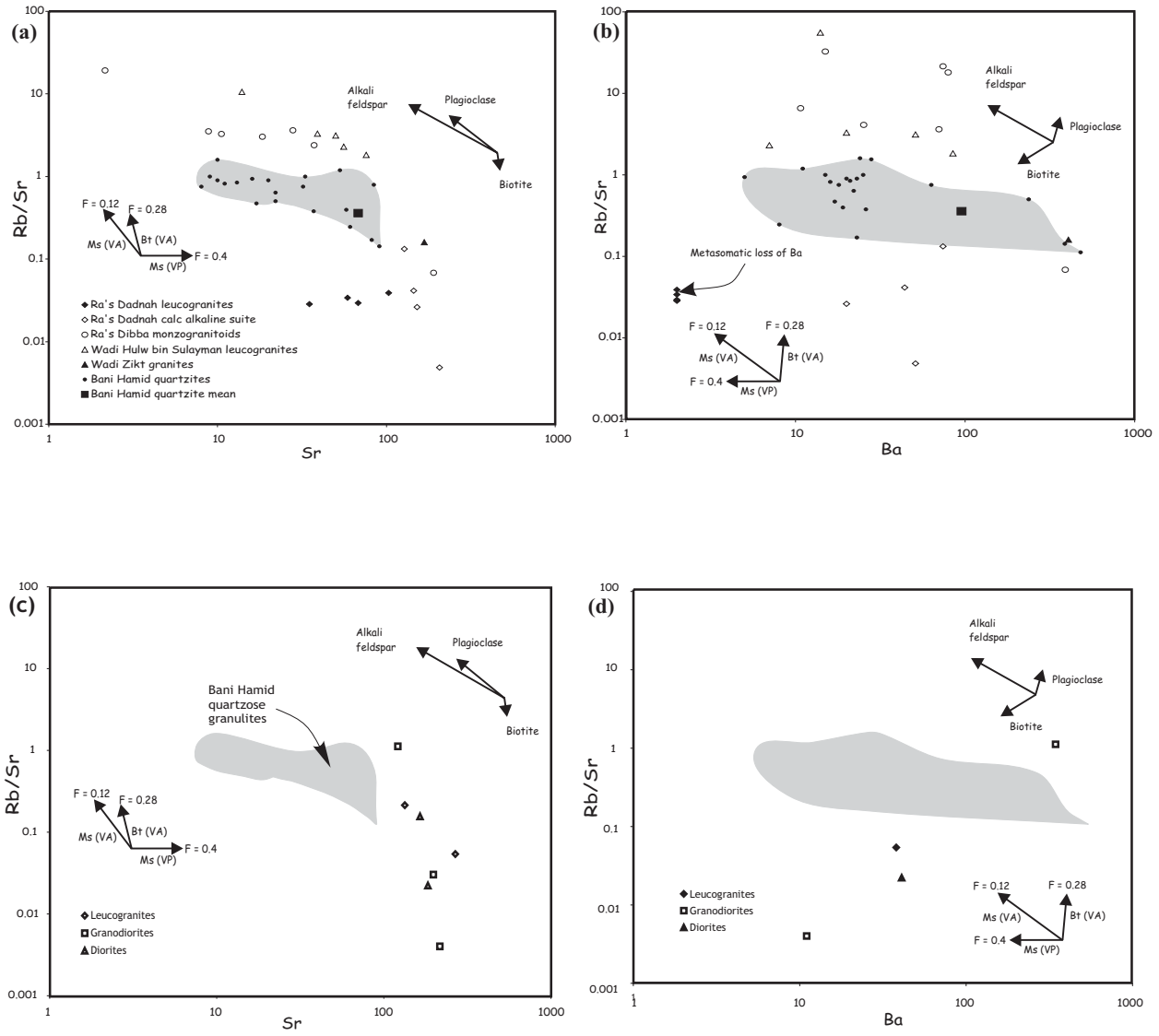


Figure 6.16a-d LILE covariation diagrams for Semail ophiolite leucogranitic dykes and Bani Hamid quartzofeldspathic granulite gneisses. Post emplacement alkali metasomatism of the Ra's Dadnah composite body precludes any clear identification of crystallising phases. Vectors represent 10% crystallisation of phases and partial melting reactions (assuming a source containing 20% muscovite and 10% phlogopite). F = melt fraction, Ms (VA) = vapour absent muscovite melting, Ms (VP) = vapour present muscovite melting, Bt (VA) = vapour absent biotite melting. After Inger & Harris (1993) and references therein. Trends defined by the Wadi Hulw bin Sulayman and Ra's Dibba granitoids correspond to the vapour absent melting of muscovite, from a source region similar to the Bani Hamid quartzofeldspathic granulites (data from Briqueu et al. 1991; Bucher & Kurz 1991). The components of the Hayalyn block (Oman) composite sill exhibit a trend that is consistent with the fractional crystallisation of a source similar in composition to the quartzose granulites of the Bani Hamid sole terrane.

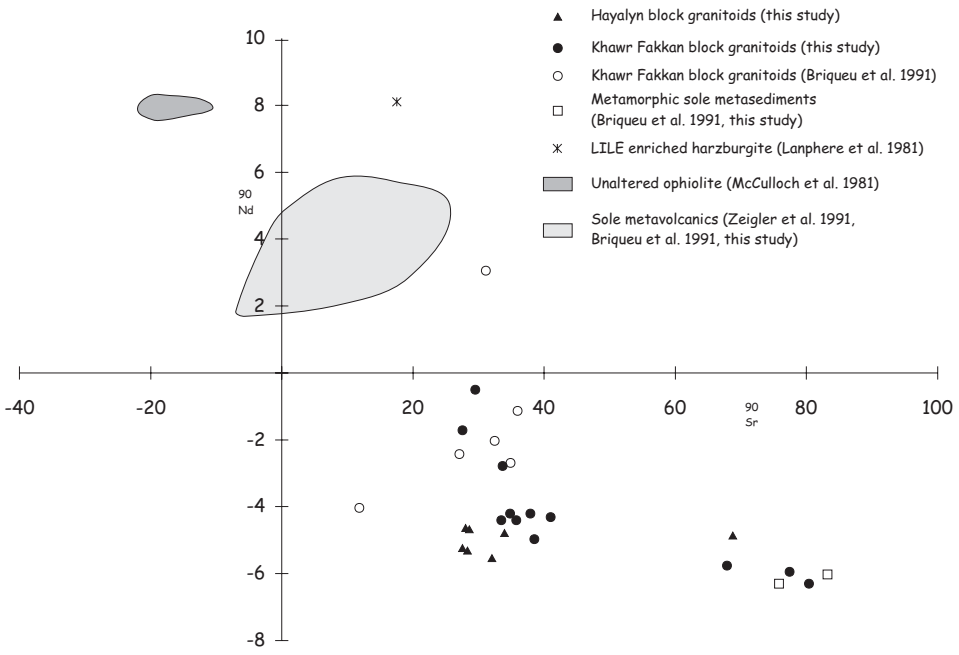


Figure 6.17a ^{90}Nd-^{90}Sr diagram showing the hyperbolic array defined by analyses of granitoid intrusions from the Hayalyn and Khawr Fakkan blocks of the Semail ophiolite. Also shown for comparison are the potential mixing end members discussed in the text.

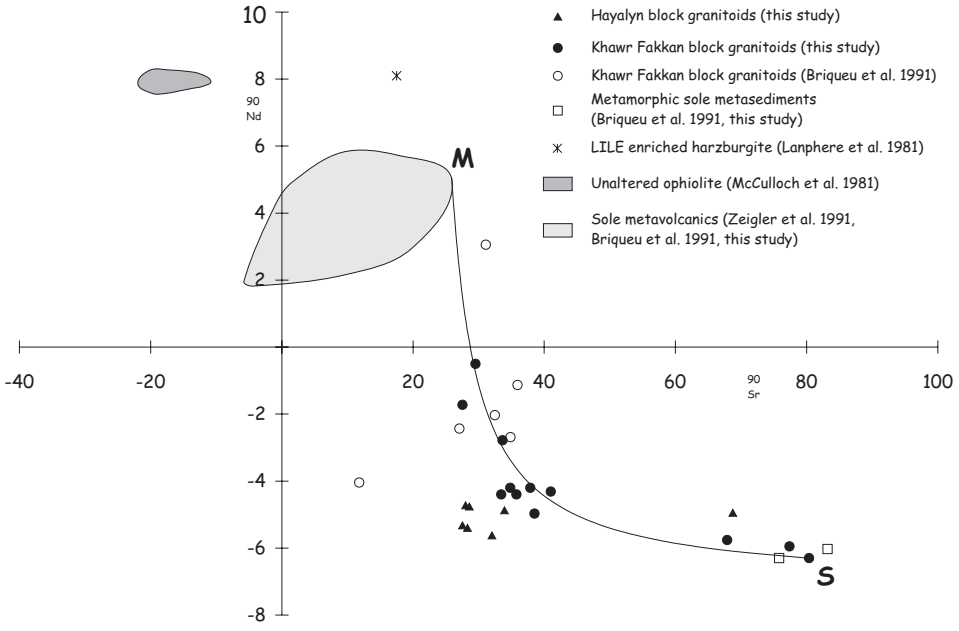


Figure 6.17b $^{143}Nd/^{144}Nd$ versus $^{87}Sr/^{86}Sr$ diagram in which the array defined by the granitoid intrusions is compared with calculated two component mixing. The assumed end-member compositions are represented by an alkali metabasalt from the metamorphic sole (**M**) and a metasedimentary component (Wadi Hulw bin Sulayman leucogranite, **S**). The curvature of the mixing line is controlled only by the Nd/Sr ratios of the two end members. Using values from table 6.6 for **S** and Zeigler et al. (1991) for **M** gives a good fit to the granitoid dyke array and suggests they may have formed by mixing between these two contrasting sources.

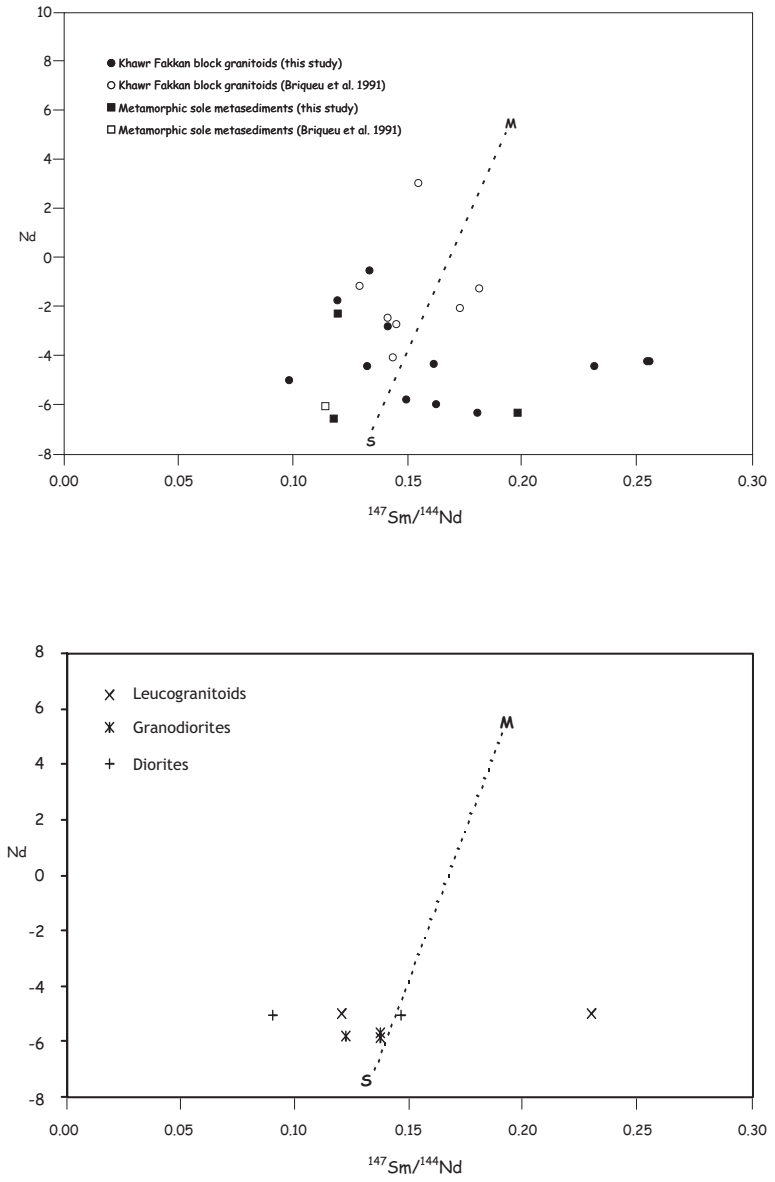


Figure 6.18a,b $_{Nd}$ versus $^{147}Sm/^{144}Nd$ isochron diagrams for the Khawr Fakkan (a) and Hayalyn block (b) granitoids that show Sm-Nd isotope systematics of the granitoid intrusions and its contrasting hypothetical source components. The broken lines represent pure mixing between the Bani Hamid metasediments (**S,** $^{147}Sm/^{144}Nd$ = 0.12 and $_{Nd}$ = -6.0) and the metabasaltic sole components (**M**, $^{147}Sm/^{144}Nd$ = 0.19 and $_{Nd}$ = 5.05, data from Zeigler et al. 1991). Source contamination of the sedimentary melts is implied because the individual dyke suite trends do not converge at the sedimentary component data point. See text for discussion. Data symbols as figure 6.17.

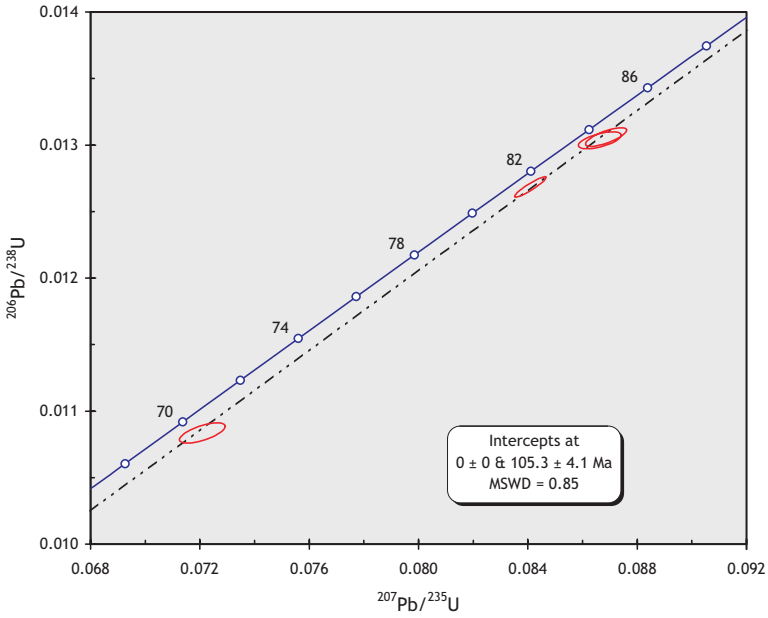


Figure 6.19 U-Pb concordia plot for the Ra's Dadnah leucogranite samples JC 25 and JC 36. The zircon fractions analysed exhibit strongly discordant results and the regression line and the concordia curve become almost parallel at such young ages - which leads to the large uncertainties for the intercept age of 105.3 ± 4.1 Ma, which none the less agrees with the Sm-Nd age of 98.8 ± 9.8 Ma obtained for the adjacent Ra's Dadnah composite sill. See text for discussion.

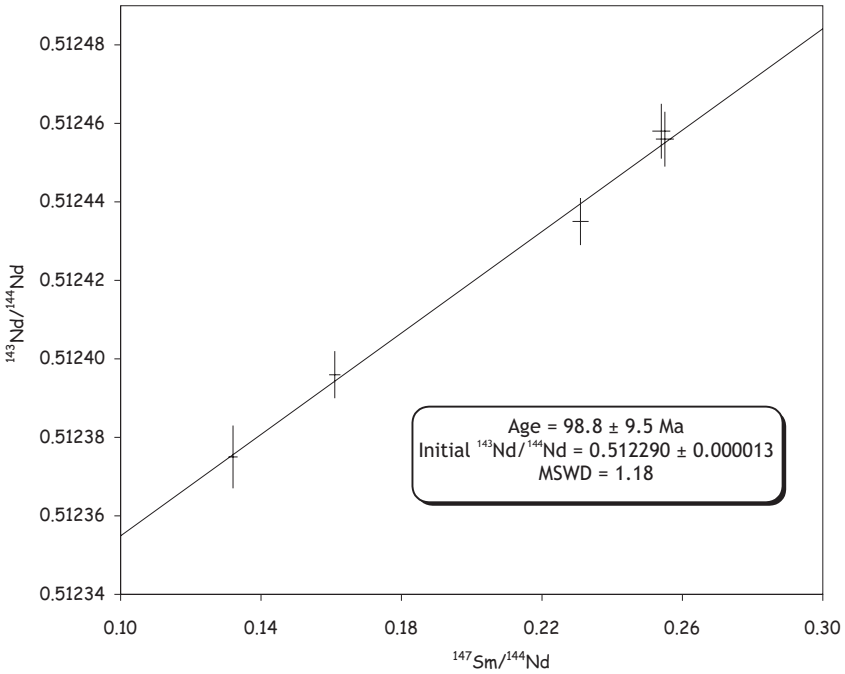


Figure 6.20a Sm-Nd isochron for cogenetic analyses OM 79, OM 85, JC 25, JC 112 and OM 77 (table 6.6), taken from a thick (~75 m) granitoid composite sill intruding mantle transition zone cumulate peridotites and gabbros sequence at Ra's Dadnah, UAE.

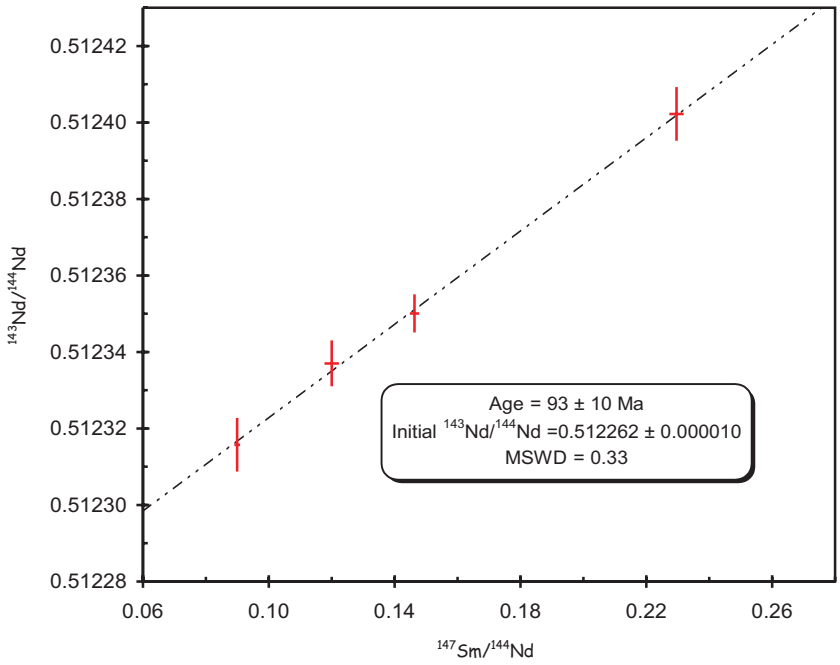
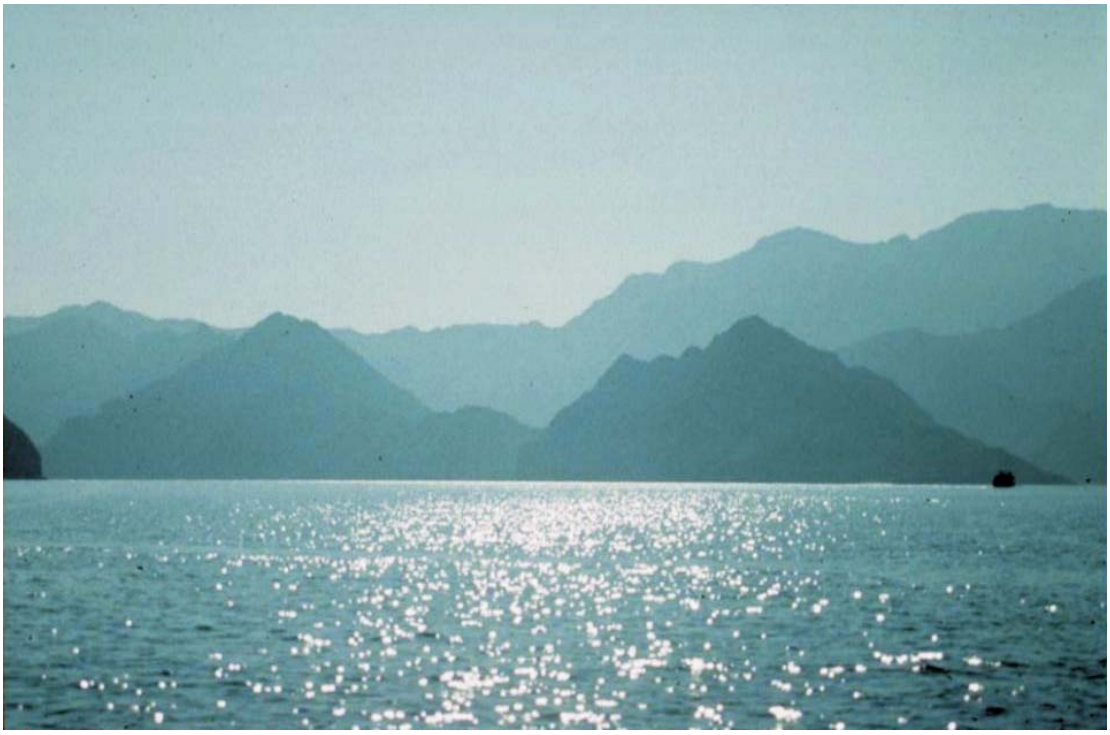


Figure 6.20b. Sm-Nd isochron for cogenetic analyses OM III-1, III-2, III-5 and III-7 (table 6.5), taken from a thick (~100 m) granitoid composite sill intruding lower mantle sequence harzburgites along a NW-SE trending shear zone in Wadi Al Hajar in the NE part of the Hayalyn block of the ophiolite, Oman.

CHAPTER SEVEN : SUMMARY, TECTONIC MODELS AND CONCLUSIONS



Waiting for the dolphins to appear,
Khawr ash Shamm, Musandam

CHAPTER SEVEN : SUMMARY, TECTONIC MODELS AND CONCLUSIONS

7.1 INTRODUCTION

This final chapter draws together and synthesises the material presented and analysed in the preceding chapters of this thesis and uses the evidence outlined in these chapters to produce tectonic models to account for the origin, formation, PT evolution, exhumation and post tectonic history of the contrasting types of igneous and metamorphic rock associated with the emplacement of the Semail ophiolite allochthon. A time chart summarising all the major tectonometamorphic events related to the emplacement of the Semail ophiolite is shown in figure 7.1. Two complementary tectonic models accounting for the subduction-obduction history of the Semail ophiolite are presented in figures 7.2 and 7.3 for the northern Oman-UAE sector of the ophiolite and the SE Oman/Saih Hatat area of the ophiolite belt respectively.

The geodynamic and tectonic origin of the Semail ophiolite remains contentious and there are two competing end member major tectonic settings: a mid-ocean ridge setting (Coleman 1981; Boudier et al. 1985, 1988; Nicolas & Boudier 1995; Hacker 1990, 1991; Hacker et. al. 1996) or a supra subduction zone setting (Searle & Malpas 1980; Pearce et al. 1981; Alabaster et al. 1982; Lippard et al. 1986; Searle & Cox 1999; Cox et al. 1999).

7.2 EVIDENCE FOR THE TECTONIC SETTING OF THE SEMAIL OPHIOLITE: MID OCEAN RIDGE OR SUPRA-SUBDUCTION ZONE?

7.2.1 Constraints from the Semail ophiolite

Resolution of this problem requires evidence from the geochemistry of the ophiolite volcanic sequence and metamorphic sole, the nature and origin of igneous material intruded into the base of the ophiolite, and the timing of ophiolite formation relative to the timing of sole metamorphism. If the Semail ophiolite originated at a mid ocean ridge and obduction was initiated there, then preserved subduction zone footwall components should be the same as the ophiolite itself. However, geochemistry of the garnet diopside amphibolite granulites in the metamorphic sole shows that they are distinct from the Semail ophiolite volcanic sequence and the Haybi alkali volcanic units and closest compositionally to the Triassic Haybi tholeiitic volcanic sequence (Searle 1980; Searle & Malpas 1982) and Neo-Tethyan Masirah ophiolite

MORB crust (*Chapter Three*). The overlap between the ophiolite plagiogranite U-Pb zircon ages and metamorphic sole peak ages of ~96.5 Ma also points to subduction of Neo-Tethyan crust beneath the ophiolite to depths of at least 40 km (Gnos 1998; *Chapter Three*) at the same time as the ophiolite crustal sequence was forming. This configuration is most compatible with a intra-oceanic arc origin for the Semail ophiolite, which must have been formed above a NE dipping (away from the continental margin) subduction zone. The only further possible mechanism would be a transform fault setting. However, this model requires a continental margin parallel transform fault to have formed the site of subduction initiation. There is no evidence for ridge orthogonal transform faulting (MacLeod & Rothery 1992). Hacker et al. (1996) also support the SSZ model by noting that the constraints provided by sole $^{40}Ar/^{39}Ar$ ages and ophiolite crustal sequence U-Pb ages are most compatible with a geometrical arrangement characterised by '*thrusting of the ophiolite away from a more easterly ridge*' – that is, in a SSZ arc with east directed subduction.

The SSZ model is supported by regional tectonic considerations that also suggest that the Semail ophiolite formed by NE directed intra-oceanic subduction within Neo-Tethys. The Mesozoic evolution of the Neo-Tethyan oceanic domain was dominated by N or NE dipping subduction zones (eg Corfield 1998), a process that is still ongoing in the Aegean and Makran.

7.2.2 Constraints from the Semail ophiolite metamorphic sole

Geochemical analysis and tectonic constraints suggest that the Semail ophiolite sole formed from Neo-Tethyan MORB crust similar in composition to the preserved Triassic-Jurassic Haybi tholeiites and Masirah ophiolite crust (*Chapter Three*) that lay between the ophiolite to the NE and the Arabian continental margin to the SW. Similarly, the presence of Neocomian (144-122 Ma) chert and limestone immediately beneath the metamorphic sole led Rabu (1987, 1993) to suggest that the oceanic crust subducted beneath the ophiolite and accreted to its base as the metamorphic sole was ~30-50 Ma old.

The ophiolite metamorphic sole was formed at peak conditions of 840 ± 70°C and 11.6 ± 1.6 kbar (THERMOCALC) and 840-870°C and 11.8-13.9 kbar (thermobarometry) and is characterised by an anticlockwise PTt path. Further PT analysis of lower grade sole material and structural constraints imply an apparent inverted sole gradient of ~2°C m^{-1} and ~3.7 MPa m^{-1} in the Asimah sole terrane. In conjunction with existing sole $^{40}Ar/^{39}Ar$ geochronology, a peak sole exhumation rate of ~12.5 mm yr^{-1} is indicated. Similar peak values have been reported for the exhumation of other recent ophiolite complexes. Existing ages of the metamorphic sole metamorphism are restricted to the $^{40}Ar/^{39}Ar$ hornblende system, which dates sole metamorphism to ~94-95 Ma (Hacker et al. 1996). The closure temperature of hornblende in the $^{40}Ar/^{39}Ar$ system is ~550°C, and utilising metamorphic sole cooling rates of

~200°C Ma^{-1} before 93.5 Ma (Hacker et al. 1996), it can be estimated that peak temperatures of ~850°C in the sole would therefore have been attained at ~96.5 Ma, implying that sole metamorphism, at depths of ~40 km, was synchronous with crystallisation of the ophiolite crustal sequence.

Temperatures at a depth of ~40 km beneath oceanic crust of ~0 Ma are ~1300°C (Parsons & Sclater 1977, assuming T_a = 1300°C and $\kappa = 10^{-6}$). For a peak metamorphic sole temperature of ~850°C, the temperature of the top of the subducted oceanic crust must have been at least (850 x 2) – 1300 = 400°C to produce the observed metamorphic conditions. These conditions could have been achieved by shear heating and conduction effects since the presence of metasedimentary material within even the highest grade parts of the sole suggests that the subducted crust may initially only have been at 0°C.

Using the same equations, oceanic crust at a depth of ~40 km would cool to ~850°C at an age of ~28.5 Ma, which provides an upper age constraint on the age of the mantle wedge crust above the subduction-obduction zone. Using a Semail ridge spreading rate of ~1 cm yr^{-1} (Boudier & Nicolas 1985), this implies that intra-oceanic subduction was initiated at most ~280 km from the Semail ridge.

In the Bani Hamid area of the United Arab Emirates, a sequence of wholly granulite facies material is found and was exhumed along the Bani Hamid thrust that repeats the entire ophiolite mantle sequence. The timing of motion along the Bani Hamid thrust is not well constrained although the extrapolation of existing metamorphic sole cooling rates indicates an age of ~94 Ma, which is similar to the age of the greenschist facies overprint seen throughout the Bani Hamid terrane.

Estimated peak conditions are very similar to the classic sole, while coronae and symplectites in garnet-diopside-scapolite-plagioclase ± wollastonite calc-silicates and marbles are also consistent with an anticlockwise PT evolution. Extrapolation of existing cooling ages, in conjunction with thermobarometry, indicate that the Bani Hamid terrane formed at the same time as the 'classic' metamorphic sole at ~96.5 Ma. Although characterised by a similar PTt path and peak metamorphic conditions, the Bani Hamid terrane formed from subducted oceanic island derived sedimentary and alkaline to carbonatitic igneous material, rather than from subducted oceanic crustal material, due to local palaeogeographical variations.

7.2.3 Melt generation beneath the Semail ophiolite

Leucogranitoid intrusions in the Semail ophiolite mantle sequence are widely, albeit sparsely, distributed and strongly support the SSZ model for the formation of the ophiolite. They are most common in the Khawr Fakkan (United Arab Emirates) and Hayalyn (Oman) blocks

of the ophiolite, and form 10-100 m scale metaluminous to peraluminous granitic intrusions, ranging from cordierite-andalusite-biotite monzogranites to garnet-tourmaline leucogranites, which intrude mantle sequence harzburgites and lower crustal sequence cumulate gabbros, often along shear zones separating mantle sequence harzburgites from crustal sequence cumulate gabbros.

Geochemical and isotopic characteristics of the analysed granitic intrusions indicate that the subducted continental material was derived from oceanic trench fill (Haybi complex) sediments, preserved as greenschist (Asimah area) to granulite facies (Bani Hamid area) ophiolitic metamorphic sole terranes. Sr-Nd isotope systematics indicate that hybrid granitic melts were derived from pre-magmatic mixing of two contrasting, quartzofeldspathic and basaltic subduction zone source components. The latter source may represent volcaniclastic sediments derived from volcanic islands on the subducting continental margin.

Structural and isotopic constraints demand that the subduction of continental sedimentary material beneath the hot proto-ophiolite in an intra-oceanic arc environment led to granulite facies metamorphism and anatexis at the subduction front. Cogenetic units of a composite sill from Ra's Dadnah (United Arab Emirates) yield an Sm-Nd isochron age of 98.8 ± 9.5 Ma, and a similar sill from Wadi Al Hajar (Oman) yields an indistinguishable age of 93.0 ± 10.0 Ma. U-Pb dating of a garnet-tourmaline leucogranite dyke from Ra's Dadnah yields an age of 105 ± 4 Ma and indicates that intra-oceanic subduction was initiated ~10 Ma before the formation of the Semail ophiolite crust.

7.3 SUBDUCTION-OBDUCTION MODELS FOR THE SEMAIL OPHIOLITE

A coherent tectonic model for the subduction and obduction history of the Semail ophiolite must incorporate the processes that produced three distinct tectonic domains: the metamorphic sole, the anatectic granitoids, and the Saih Hatat HP terrane. The metamorphic rocks associated with the Semail ophiolite contain two distinct metamorphic regimes that occur as widely separated outcrops. The classic, HT subophiolitic metamorphic sole records peak conditions of 850 ± 25°C and up to ~14 kbar in the Bani Hamid terrane, whereas the more extensive HP metamorphic terrane of Saih Hatat records peak conditions of 450-550°C and ~20 kbar in eclogites from As Sifah.

The Neo-Tethyan ocean floor that originally lay to the NE of the Arabian continental margin was most likely of mid Triassic to mid Jurassic age, formed after the initiation of rifting in the continental margin. However, very little of this ocean basin has been preserved except in the Neo-Tethyan Masirah and Spongtang ophiolites, and the reconstruction of the geochemistry and tectonics of this basin in the Oman area is based upon limited occurrences of

the Haybi volcanic sequence, preserved in the sub ophiolitic subduction zone, and its greenschist to granulite facies equivalents in the ophiolite metamorphic sole. The age (91 ± 3 Ma; Corfield 1998) of the supra subduction zone Spong arc formed on top of older Jurassic Neo-Tethyan crust in the Himalayan Spongtang ophiolite agrees well with the formation age of the Semail ophiolite, which also exhibits arc related extrusive volcanic units on top of a MORB crust, suggesting that the same intra oceanic subduction zone was responsible for the obduction of both ophiolites.

7.3.1 Northern Oman & United Arab Emirates

Figure 7.2 is a tectonic model for the generation and emplacement evolution of the Khawr Fakkan block leucogranitoid dykes and shows the proto-ophiolite above a NE dipping subduction zone within Tethys, during the Cenomanian (~95 Ma). Initiation of intra-oceanic subduction at ~105-100 Ma (Lippard et al. 1986) and movement along the Semail thrust was followed by the initiation of spreading and the crystallisation of the plagiogranitic components of the ophiolite crustal sequence. The Arabian continental margin thinned towards the NE, and the crust beneath the Hawasina pelagic basin and Haybi trench fill units consisted of attenuated transitional crust containing alkalic ultramafic and basaltic intrusions of Triassic and Jurassic age.

Subduction of this Triassic-Jurassic oceanic crust and its sediment cover, represented by the trench fill components of the Haybi complex (Searle 1980), including Permo-Triassic seamounts and the pelagic marine sediments of the Hawasina basin, led to anatexis by the dehydration melting of muscovite rich sedimentary material at 650-700°C (Peters & Kamber 1994) and 3-5 kbar at the subduction front. The Bani Hamid granulite facies terrane records peak conditions of ~850°C and 10-14 kbar. Minimum melt type granitoids produced in this manner were hybrid melts, containing variable proportions of continental and mantle components; several distinct suites were emplaced up to the base of the ophiolite crustal sequence. A present day section through the Khawr Fakkan block of the Semail ophiolite in the UAE clearly shows the results of SW propagated thrusting of the ophiolite and its metamorphic sole, accompanied by up to 400-500 km shortening within the pelagic (Hawasina), carbonate slope (Sumeini) and shelf (Hajar) sequences of the passive margin. This led to the final emplacement of the cool ophiolite onto the Arabian continental margin by ~78 Ma (Hacker et al. 1996). The presence of a more extensive zone of peraluminous granitoid intrusion at depth within the mantle sequence of the Khawr Fakkan block of the ophiolite is possible, below present erosion levels, as in the Caledonian Karmoy ophiolite of SW Norway (Pedersen & Dunning 1997).

7.3.2 South eastern Oman (Saih Hatat)

A three stage tectonic model for the subduction-obduction and emplacement history of the Semail ophiolite in the Saih Hatat area of the SE Oman mountains is shown in figure 7.3. The Saih Hatat terrane is unique is preserving the record of continental subduction beneath an obducting ophiolite and is characterised by a largely complete HP metamorphic profile through an exhumed portion of Arabian continental crust, which was subducted to depths of ~80 km during the obduction of the Semail ophiolite in the mid Cretaceous (Waters & Martin 1993; Wendt et al. 1993; Searle et al. 1994).

The exact timing of this HP event is the major unresolved issue in the obduction and emplacement history of the Semail ophiolite. The $^{40}Ar/^{39}Ar$ age of the As Sifah eclogites is 96 $\pm$ 2 Ma (Searle et al. 1994), similar to the mean $^{40}Ar/^{39}Ar$ age of 93.5 $\pm$ 0.1 Ma for sole metamorphism in the adjacent Wadi Tayin area (Hacker et al. 1996). This suggests that the HP metamorphism was roughly contemporaneous with the formation of the ophiolite and the metamorphic sole, rather than at ~80 Ma as suggested by Michard et al. (1994). In the northern mountains, the mean age of sole metamorphism is 94.9 $\pm$ 0.2 Ma (Hacker et al. 1996). Here, intra-oceanic subduction resulted in HT metamorphism, and the generation of granitoid melts. In the Saih Hatat area, continental promontory subduction (Searle et al. 1994; Hacker & Gnos 1997) led to HP metamorphism.

The existing geochronological data implies that these two separate metamorphic regimes occurred simultaneously. The processes governing the formation, exhumation and present day distribution of HP rocks in the Saih Hatat window are proposed to have occurred in two distinct stages, with rapid initial exhumation following subduction of the Arabian continental margin, due to relative extension in the subduction zone hanging wall and driven by buoyancy contrasts, followed by a slower erosion. In conjunction with ambiguous existing geochronology, a peak exhumation rate of ~4-12 mm yr^{-1} is indicated for the As Sifah eclogites, followed by erosion at ~0.5 mm yr^{-1}.

7.3.3 Timing and duration of subduction-obduction process

It is proposed that the available geochronological evidence is most compatible with the separate HT and HP metamorphic events being roughly coeval, occurring at around 99-96 Ma. The contemporary distribution of the contrasting terranes along the Oman mountain belt may be related in part to Tertiary deformational events such as the formation of the Musandam culmination and the doming of the Saih Hatat window.

The temporal relationship between the formation of the eclogite facies material and the ophiolite metamorphic sole in the Saih Hatat area is the key to understanding the plate configuration during the obduction process. Since the eclogites reached peak temperatures of ~550°C (Searle et al. 1994; El-Shazly et al. 1997), similar to temperatures in the metamorphic sole at ~94 Ma (Hacker & Gnos 1997), it is unlikely that they formed at the same time in a single subduction zone.

The tectonic model of Searle et al. (1994) is compatible with all the available structural and geochronological evidence and favours the presence of twin subduction zones. It is proposed that the high pressure material formed from continental margin material in a NE dipping subduction zone while the metamorphic sole and related anatectic granitoids formed in an intra-oceanic subduction zone further outboard.

7.3.4 Post obduction tectonics

Peak metamorphic sole pressures imply the exhumation and preservation of Neo-Tethyan oceanic crust accreted to the hanging wall of the Semail thrust at depths of ~40 km, which is much greater than the observed ophiolite thickness of ~5-10 km (Shelton 1984). Sole pressures of only ~2-3 kbar are obtained if simple overburden is assumed. This clear discrepancy may have been due to:

a) Another (structurally repeated) 15-20 km thick ophiolitic thrust sheet above the present ophiolite (Nicolas 1989).

b) The metamorphic sole has been exhumed by normal faulting and juxtaposed against a thinner ophiolite section (Hacker & Gnos 1997).

c) The originally ~40 km thick ophiolite was thinned during the obduction and emplacement process.

Geophysical data (Shelton 1984) limits the structural thickness of the ophiolite to <10 km and negates first two models. There is no evidence for burial of the Semail ophiolite crustal sequence to depths of ~20 km, which would imply the development of greenschist-amphibolite facies assemblages. The presence of late dolerite dykes cutting the Semail thrust in Wadi Tayin (Hacker & Gnos 1997) suggests that thinning related motion was minimal during the early stages of obduction.

Thinning of the ophiolite from ~40 km to <15 km, or by >270%, may have been accommodated by subduction zone 'flattening' (Casey & Dewey 1984). Extensional thinning of

the ophiolite during emplacement is consistent with the common excision of the high grade garnet-diopside amphibolite granulite sole units, the discontinuous sole outcrop, the discontinuous and variable thickness of the 'banded ultramafic unit' basal mantle sequence mylonites, and the variable structural thickness of the wedge shaped ophiolite itself.

Faults and shear zones are abundant throughout the ophiolite mantle sequence. Although many are related (in part at least) to Tertiary thrust culmination and the formation of tectonic windows beneath the Semail thrust, displacements along them are poorly constrained (Kusky et al. 1998) and intra-ophiolitic extension does not appear to have greatly disrupted remnant ophiolite mantle fabrics (eg Ceuleneer et al. 1988). The difficulty in reconciling this apparent absence of clear internal deformation within the ophiolite with the conflicting evidence that may require major intra-ophiolitic extension to exhume the metamorphic sole suggests the model can at best represent a partial solution until the age, nature and extent of intra-ophiolitic extension can be better constrained.

7.4 FUTURE WORK AND UNRESOLVED ISSUES

Further work on the Sr and Nd isotope systematics of the components of the Haybi trench mélange complex and their granulite facies equivalents in the ophiolite metamorphic sole will enable the relationships between the postulated sources of the studied Semail ophiolite granitoids to be more fully understood. The widespread recognition of similar leucogranitic dykes within other ophiolites will help to constrain existing tectonic models of ophiolite obduction and emplacement as well as the relationships between the contrasting types of subduction-obduction related ophiolite metamorphism seen in the Oman mountains.

The clear discrepancy between the estimated depth of subduction beneath the Semail ophiolite of ~40 km, and the <15 km thick preserved ophiolite, suggest than an investigation of the processes that have reduced the ophiolite in thickness during obduction, emplacement and subsequent erosion would greatly elucidate the subduction-obduction history and also have wide applications in other ophiolite complexes and provide insights into the rheology of oceanic lithosphere.

Accurate dating (U-Pb titanite or monazite; garnet Sm-Nd or Lu-Hf) of the peak of high pressure (eclogite facies) metamorphism seen in the Saih Hatat terrane remains the major outstanding issue in the subduction-obduction history of the Semail ophiolite. Similarly, the accurate dating (U-Pb titanite or monazite; garnet Sm-Nd or Lu-Hf) of the peak of the high temperature metamorphism seen in the Semail ophiolite metamorphic sole would complement the existing $^{40}Ar/^{39}Ar$ hornblende cooling ages and facilitate a more accurate history of the Semail ophiolite. A detailed study of the formation age of the Semail ophiolite, widely

accepted to have spanned a narrow range from 97.3 to 93.5 ± 0.25 Ma (Tilton et al. 1981), would better constrain the rates of subduction-obduction processes studied in this work. Accurate, spatially well constrained and widespread dating of the ophiolite using U-Pb or $^{40}Ar/^{39}Ar$ techniques should resolve the true age of the ophiolite clearly.

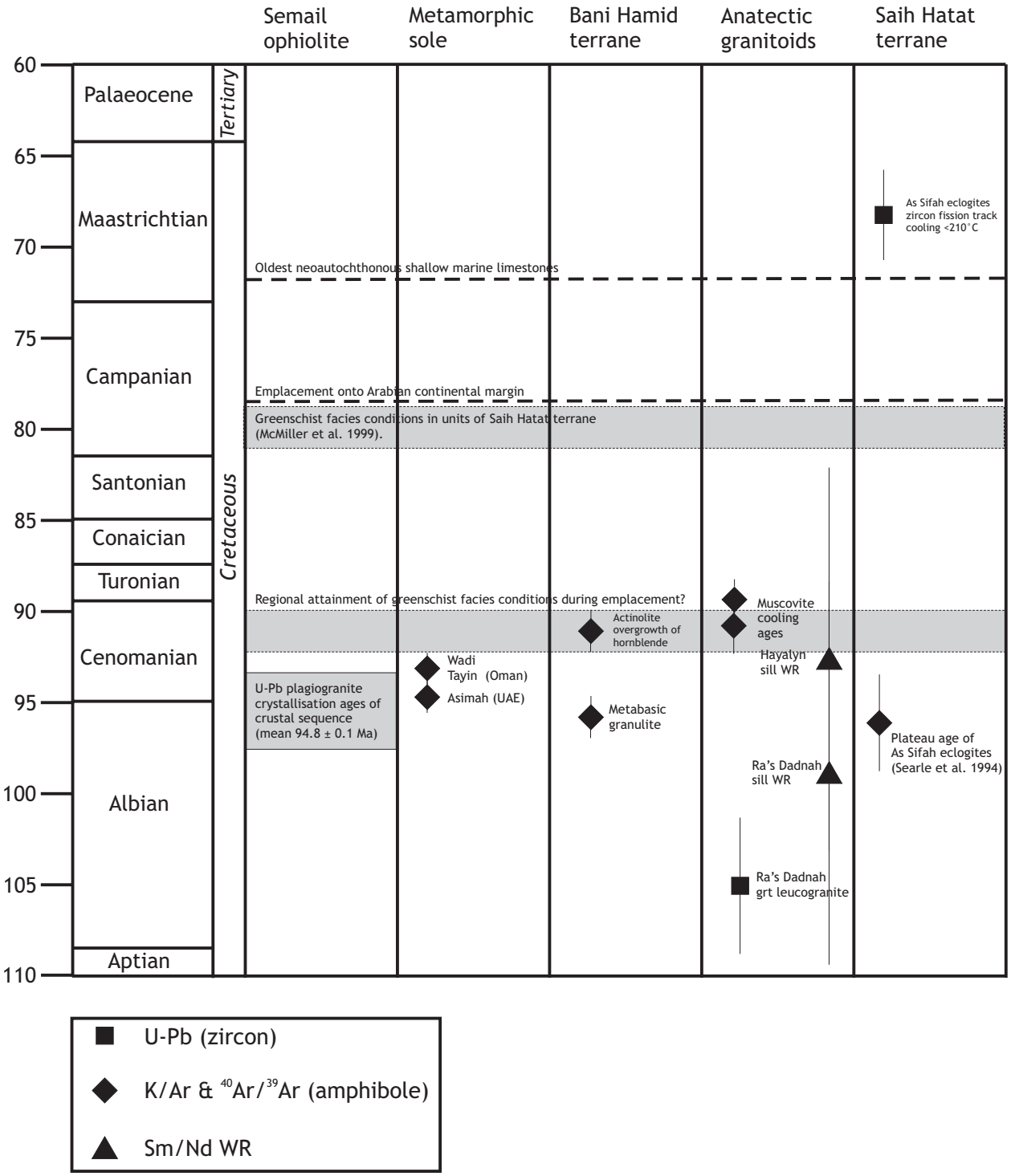


Figure 7.1 Time chart summarising the selected relative and absolute geochronology, both new and from the literature, of all the tectonometamorphic, anatectic and structural events related to the subduction and obduction of the Semail ophiolite. Data from Tilton et al. (1981); Gnos & Peters (1993); Searle et al. (1994); Saddiqi et al. (1995); Hacker et al. (1996) McMiller et al. (1999) and this study. Other published ages have been superceded by this recent accurate data.

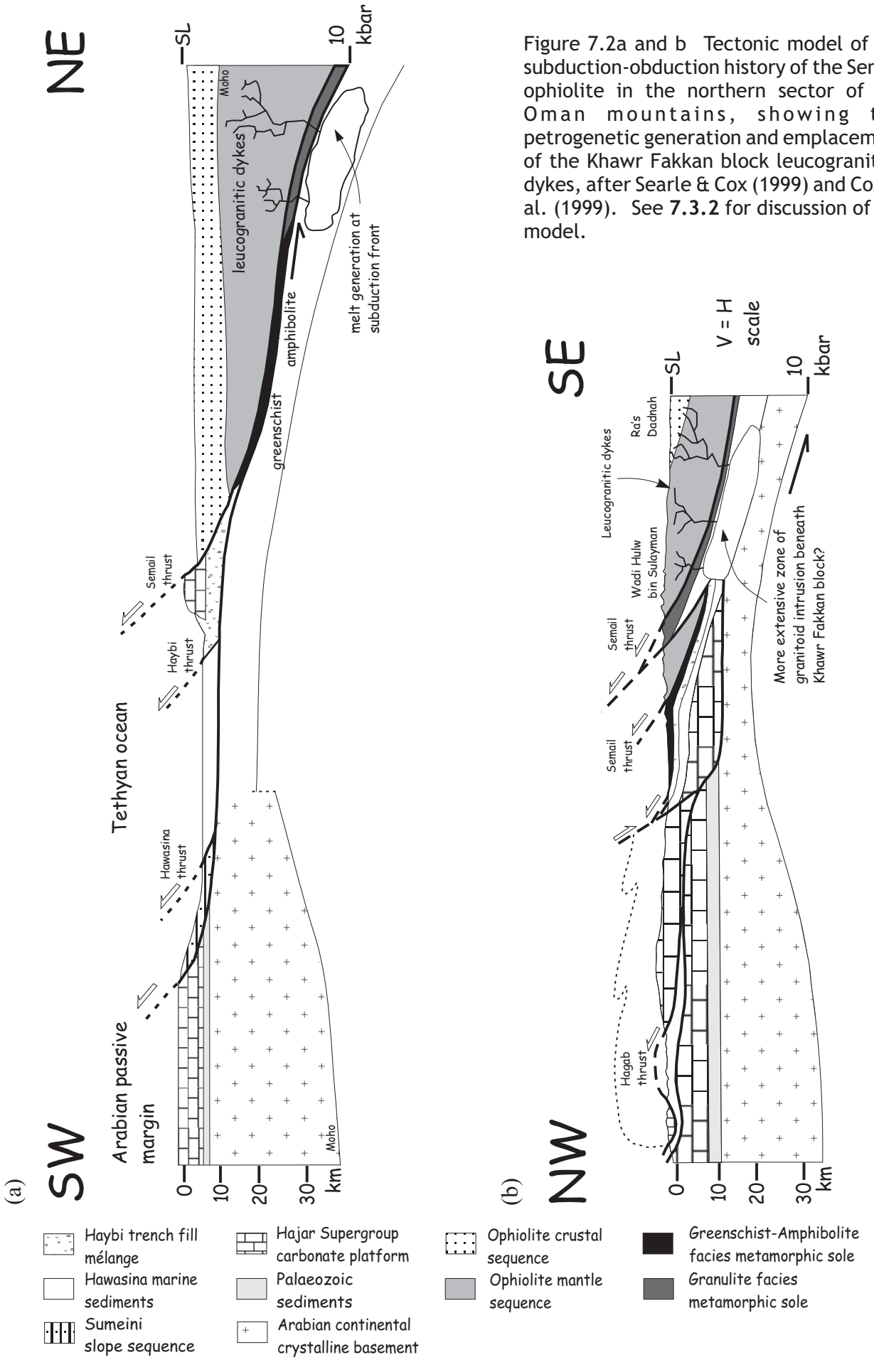


Figure 7.2a and b Tectonic model of the subduction-obduction history of the Semail ophiolite in the northern sector of the Oman mountains, showing the petrogenetic generation and emplacement of the Khawr Fakkan block leucogranitoid dykes, after Searle & Cox (1999) and Cox et al. (1999). See **7.3.2** for discussion of the model.

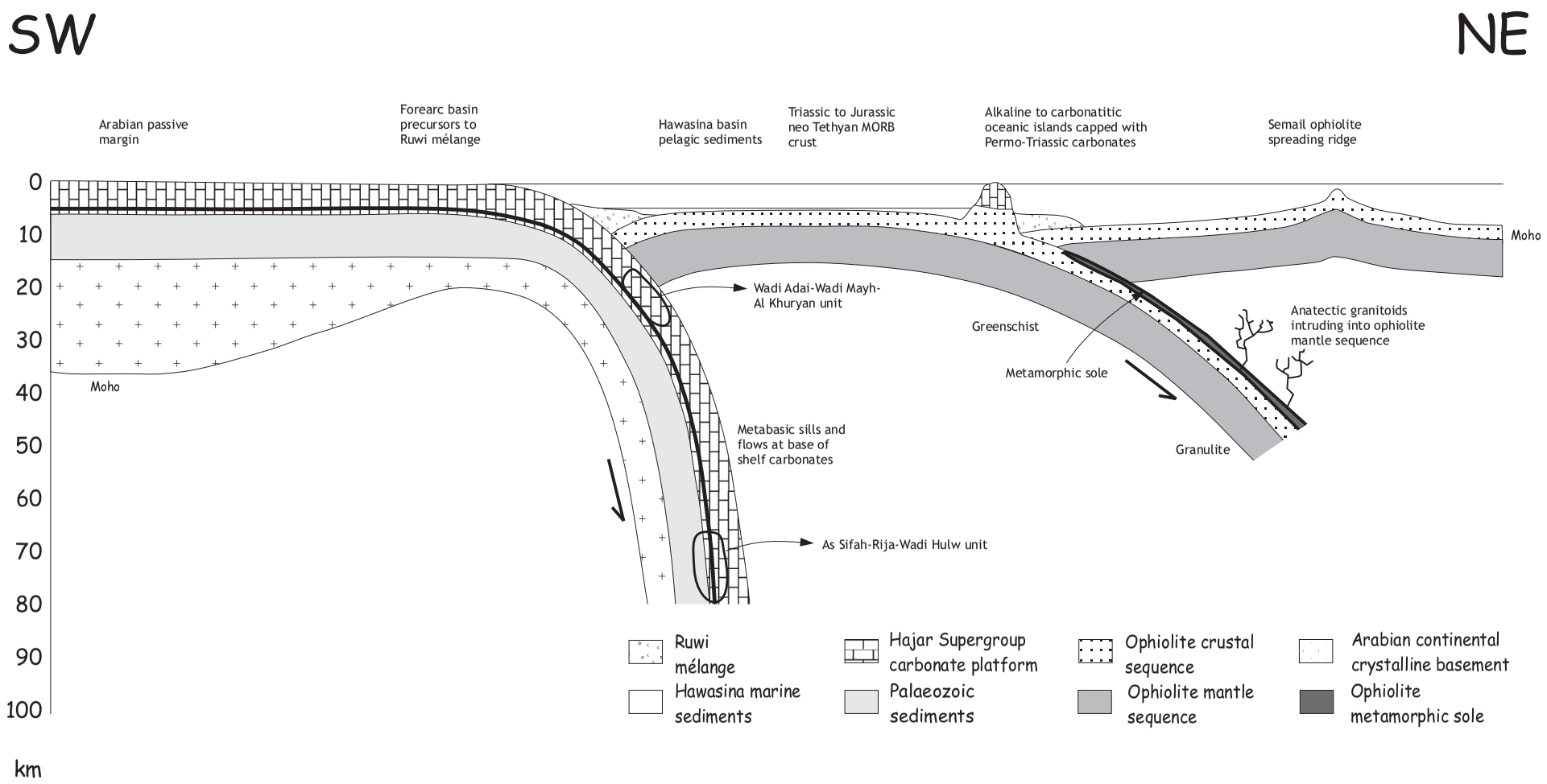


Figure 7.3a Tectonic model for the subduction-obduction history of the Semail ophiolite in the Saih Hatat area of SE Oman in the Cenomanian, ~96 Ma. The presence of anatectic melts within the mantle sequence of the semail ophiolite with crystallisation ages of ~105 Ma (*Chapter Six*) concurs with the Lippard et al. (1986) proposal that intra oceanic arc subduction was initiated at this time. All the new and existing geochronology of metamorphic rocks occurring beneath the Semail ophiolite is consistent with the Saih Hatat HP and the metamorphic sole HT events occurring at the same time at ~96 Ma. See **7.3.3** for discussion of the model. After Searle et al. (1994) and Searle & Cox (1999).

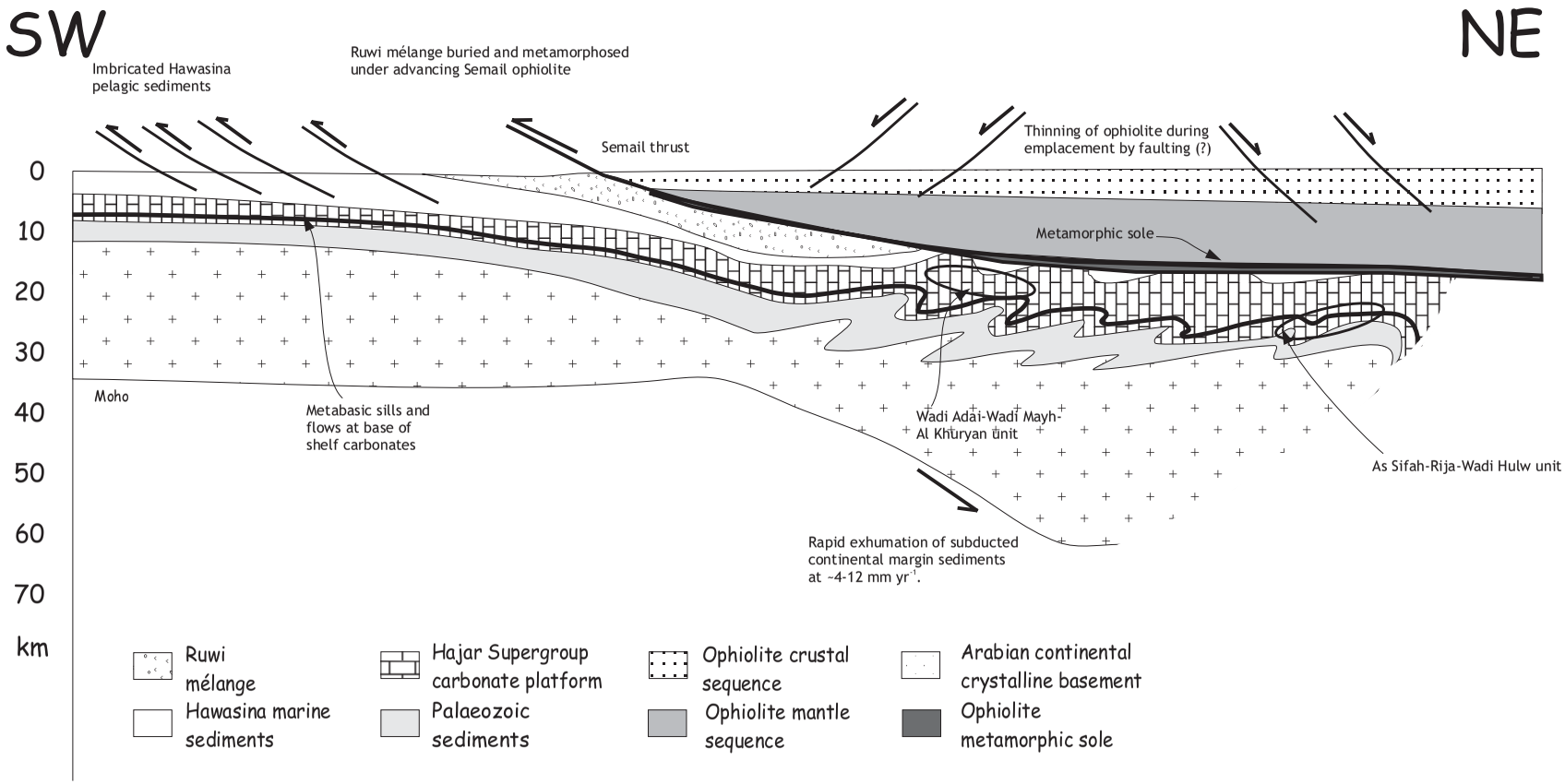


Figure 7.3b Evolution of the subduction-obduction events related to the emplacement of the Semail ophiolite in the Saih Hatat area of the SE Oman mountains by the mid Campanian, ~80 Ma. Rapid exhumation of the highest grade preserved subducted continental margin material (the As Sifah eclogites) proceeded at 4-12 mm yr^{-1} during this period and by ~80 Ma at latest they had attained a structural level equivalent to the greenschist facies. Meanwhile, the SW advancement of the Semail ophiolite thrust sheet buried the forearc mélange sequence to a depth of ~20 km to produce the Ruwi subophiolitic mélange, which has a $^{40}Ar/^{39}Ar$ age of 80.2 ± 0.8 Ma (El-Shazly & Lanphere 1992). See **7.3.3** for discussion of the model. After Searle et al. (1994) and Searle & Cox (1999).

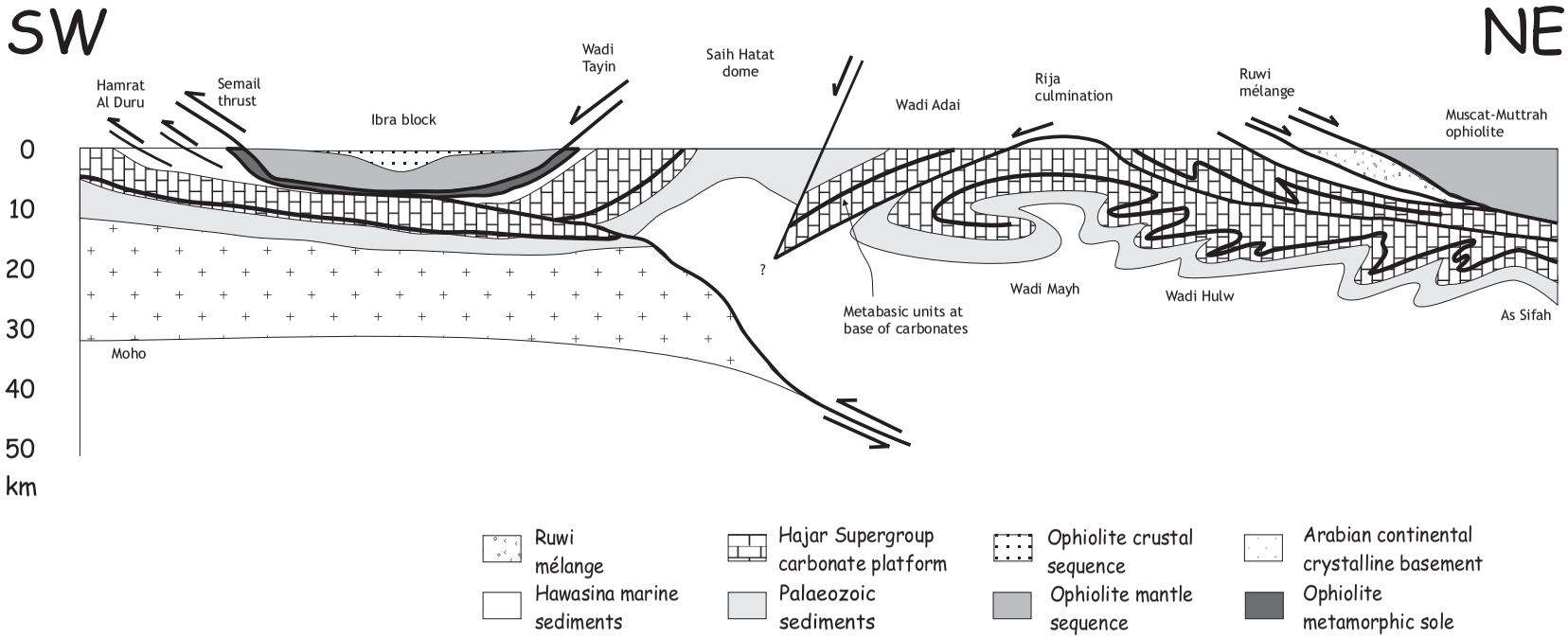


Figure 7.3c Present day cross section through the Semail ophiolite allochthon in the Saih Hatat area of the SE Oman mountains, showing the complete and unmetamorphosed shelf carbonate and pelagic sequences of the SW margin of the Saih Hatat culmination which contrast with their heavily deformed and thickened equivalents in the NE of Saih Hatat, where regional HP assemblages culminate at ~20 kbar and 450-550°C in the As Sifah-Rija-Wadi Hulw structural unit. See **7.3.3** for further discussion of the tectonometamorphic evolution of the Saih Hatat HP terrane.

REFERENCES

Abbotts IL 1978 High potassium granites in the Masirah ophiolite of Oman. Geol Mag 115: p 415-423.

Ahmed Z 1993 Leucocratic rocks from the Bela ophiolite, Khuzdar district, Pakistan. In Treloar PJ, Searle MP (eds). Himalayan Tectonics. Geol Soc Lond Spec Pub: 74 p 89-100.

Ai Y 1994 A revision of the garnet-clinopyroxene Fe^{2+}-Mg exchange geothermometer. Con Min Pet 115: p 467-473.

Alabaster T, Pearce JA, Malpas J 1982 The volcanic stratigraphy of the Oman ophiolite complex. Con Min Pet 81 p 168-183.

Alleman F 1979 Time of emplacement of the Zhob valley ophiolites and Bela ophiolites, Baluchistan (preliminary report). In Farah A, DeJong KA (eds) Geodynamics of Pakistan: p 215-242.

Allemann F, Peters Tj 1972 The ophiolite-radiolarite belt in the north Oman mountains. Eclogae Geolog Hel 65: p 657-697.

Andersen TB, Jamtveit B 1990 Uplift of deep crust during orogenic extensional collapse: A model based on field studies in the Sogn-Sunnfjord region, W Norway. Tectonics 9: p 1097-1111.

Anderson JL, Smith DR 1995 The effects of temperature and f_{O_2} on the Al in hornblende barometer. Am Min 80: p 549-559.

Anonymous 1972 Penrose field conference on ophiolites. Geotimes 17: p 24-25.

Avigad D 1992 Exhumation of coesite-bearing rocks in the Dora Maira massif (western Alps, Italy). Geology 20: p 947-50.

Bailey EH, Hopson CA, Coleman RG, Gregory RT, Pallister JS 1981 Geologic section through the Samail ophiolite and associated rocks along a Muscat-Ibra transect, SE Oman Mountains. J Geophys Res: p 2527-2544.

Barbarin B 1996 Genesis of the two main types of peraluminous granitoids. Geology 24: p 295-298.

Barker F 1979 Trondhjemite: definition, environment and hypotheses of origin. In Barker F (ed). Trondhjemites, dacites and related rocks. Elsevier, Amsterdam: p 1-12.

Béchennec F 1987 Geologie des nappes Hawasina dans les parties orientale et centrale des montagnes d'Oman. Principaux Resultats Scientifiques (BRGM): p 97-98.

Béchennec F, LeMetour J, Rabu D, Villey M, Beurrier M 1988 The Hawasina basin: a fragment of a starved passive continental margin, thrust over the Arabian platform during obduction of the Semail nappe. Tectonophysics 151: p 323-343.

Béchennec F, Tegyey M, LeMetour J, Lemiere B, Lescuyer JL, Rabu D, Milesi JP 1991 Igneous rocks in the Hawasina nappes and Hajar supergroup, Oman: their significance in the birth and evolution of the composite extensional margin of eastern Tethys. In Peters Tj et al. (eds). Ophiolite genesis and evolution of the oceanic lithosphere p 593-611. Kluwer, Amsterdam.

Beck RA, Burbank DW, Sercombe WJ, Khan AM, Lawrence RD 1996 Late Cretaceous ophiolite obduction and Palaeocene India-Asia collision in the westernmost Himalaya. Geodynamica Acta 9: p 114-144.

Berberian M, King GCP 1981 Towards a palaeogeography and tectonic evolution of Iran. Can J Earth Sci 18: p 210-265.

Berberian F, Muir ID, Pankhurst RJ, Berberian M 1982 Late Cretaceous and early Miocene andean-type plutonic activity in northern Makran and central Iran. J Geol Soc Lond 139: p 605-614.

Bhattacharya A, Mohanty L, Maji A, Sen SK, Raith M 1992 Non-ideal mixing in the phlogopite-annite binary: constraints from experimental data on Mg-Fe partitioning and a reformulation of the biotite-garnet geothermometer. Con Min Pet 111: p 87-93.

Bickle MJ, Pearce JA 1975 Oceanic mafic rocks in the Eastern Alps. Con Min Pet 49: p 177-189.

Bohlen SR 1987 Pressure-temperature-time paths and a tectonic model for the evolution of granulites. J Geol 95: p 617-632.

Bohlen SR 1991 On the formation of granulites. J Met Geol 9: p 223-229.

Bowen NL 1927 The origin of ultrabasic and related rocks. Am J Sci 14: p 89-108.

Bowen NL, Tuttle OF 1949 The system MgO-SiO_2-H_2O. GSA Bull 64: p 868-915.

Bowin C, Purdy GM, Johnston C, Shor G, Lawver L, Hartono HMS, Jezek P 1980 Arc-continent collision in Banda Sea region. AAPG Bull 64: p 868-915.

Boudier F, Coleman RG 1981 Cross section through the peridotite in the Semail ophiolite, SE Oman mountains. J Geophys Res 86: p 2573-2592.

Boudier F, Nicolas A 1985 Harzburgite and lherzolite subtypes in ophiolitic and oceanic environments. Earth Planet Sci Lett 76: p 84-92.

Boudier F, Nicolas A (eds) 1988 The ophiolite of Oman. Tectonophysics 151.

Boudier F, Nicolas A 1995 Nature of the Moho transition zone in the Oman ophiolite. J Petrol 36: p 777-796.

Boudier F, Bouchez JL, Nicolas A, Cannat M, Ceuleneer G, Misseri M, Montigny R 1985 Kinematics of oceanic thrusting in the Oman ophiolite: model for plate convergence. Earth Plan Sci Lett 75: p 215-222.

Boudier F, Ceuleneer G, Nicolas A 1988 Shear zones, thrusts and related magmatism in the Oman ophiolite: Initiation of thrusting at an oceanic ridge. Tectonophysics 151: p 275-96.

Brey GP, Kohler T 1990 Geothermobarometry in four phase lherzolites II: new thermobarometers and practical assessment of existing thermobarometers. J Petrol 31: p 1353-1378.

Briqueu L, Mevel C, Boudier F 1991 Sr, Nd and Pb isotopic constraints in the genesis of a calc-alkaline plutonic suite in the Oman ophiolite related to the obduction process. In Peters Tj, Nicolas A, Coleman RG (eds). Ophiolite genesis and evolution of the oceanic lithospher. Kluwer, The Netherlands, p 517-42.

Brongniart A 1813 Essai d'un classification mineralogique des roches melangées. J des Mines, Paris 199: p 5-48.

Browning P 1982 The petrology, geochemistry and structure of the plutonic rocks of the Semail ophiolite. Unpublished Phd thesis, Open University, UK, 405p.

Browning P, Smewing JD 1981 Processes in magma chambers beneath spreading axes; evidence from magmatic associations in the Oman ophiolite. J Geol Soc Lond 138: p 279-280.

Brunn IH 1959 La dorsale medio-atlantique et les epanchments ophiolitiques. Compt Rendues, Soc Geol France 8: p 234-236.

Bucher M 1990 Mineral equilibria in metagabbros: evidence for a polymetamorphic evolution of the Asimah window, northern Oman mountains, United Arab Emirates. In Peters Tj, Nicolas A, Coleman RG (eds). Ophiolite genesis and evolution of the oceanic lithosphere: proceedings of the Ophiolite conference: p 543-572 Kluwer Academic.

Bucher M, Kurz D 1991 The metamorphic series associated with the Oman ophiolite nappe of the Oman mountains in the United Arab Emirates. MSc thesis, University of Bern, 170p.

Casey JF, Dewey JF 1984 Initiation of subduction zones along transform and accreting plate boundaries, triple junction evolution and forearc spreading centres–implications for ophiolitic geology and obduction. In Gass IG et al. (eds). Ophiolites and oceanic lithosphere. Geol Soc Spec Pub 13: p 269-290.

Cassaigneau C 1979 Contribution a l'etude des structures Inde-Eurasie: la zone de suture de Khost dans le SE d'Afghanistan, l'obduction Palaeocene et al tectonique Tertaire. PhD thesis, Univ Sciences & Techniques du Languedoc, Montpellier.

Ceuleneer-G, Nicolas A, Boudier F 1988 Mantle flow patterns at an oceanic spreading centre: the Oman peridotites record. Tectonophysics 151: p 1-26.

Chappell BW, White AJR 1992 I and S type granites in the Lachlan Fold Belt. Trans Roy Soc Edin E Sciences 83: p 1-26.

Chemenda A, Mattauer M, Bokun AN 1996 Continental subduction and a mechanism for exhumation of HP metamorphic rocks: new modelling and field data from Oman. Earth Plan Sci Lett 143: p 173-182.

Chen JH & Pallister JS 1981 Lead isotopic studies of the Semail ophiolite, Oman. J Geophys Res 86: p 2699-2706.

Chopin C 1984 Coesite and pure pyrope in high-grade blueschists of the Western Alps: a first record and some consequences. Con Min Pet 86: p 107-118.

Church WR, Stevens RK 1971 Early Palaeozoic ophiolite complexes of the Newfoundland Appalachians as mantle-oceanic crust sequences. J Geophys Res 76: p 1460-1466.

Cloos M 1982 Flow mélanges: numerical modelling and geological constraints on their origin in the Franciscan subduction complex, California. GSA Bull 93: p 330-344.

Coleman RG 1971 Plate tectonic emplacement of upper mantle peridotites along continental edges. J Geophys Res 76: p 368-378.

Coleman RG 1977 Ophiolites. Springer-Verlag, Berlin-Heidelberg-New York.

Coleman RG 1981 Tectonic setting for ophiolite obduction in Oman. J Geophys Res 86: p 2497-2508.

Coleman RG 1984 The diversity of ophiolites. In Zwart HJ, Hartman P, Tobi AC (eds). Ophiolites and ultramafic rocks: a tribute to Emile Den Tex: p 141-150.

Coleman RG, Hopson CA (eds) 1981 The Oman ophiolite. J Geophys Res 86

Cooper DJW 1988 Structure and sequence of thrusting in deep water sediments during ophiolite emplacement in the south central Oman mountains. J Struct Geol 10: p 473-485.

Cooper DJW 1990 Sedimentary evolution and palaeogeographical reconstruction of the Mesozoic continental rise in Oman: evidence from the Hamrat Duru group. In Robertson AHF, Searle MP (eds). The Geology and Tectonics of the Oman Region. Geol Soc Lond Spec Pub 49: p 361-74.

Corfield RI 1998 Origin and emplacement of the Spongtang ophiolite and crustal shortening processes in the Ladakh-Zanskar Himalaya, NW India. Unpublished DPhil thesis, University of Oxford, 168p.

Corfield RI, Searle MP, Green OR 1999 Photang thrust sheet: an accretionary complex structurally below the Spontang ophiolite constraining timing and tectonic environment of ophiolite obduction, Ladakh Himalaya, NW India. J Geol Soc Lond 156: p 1031-1044.

Cowan DS, Silling RM 1978 A dynamic, scaled model of accretion at trenches and its implications for the tectonic evolution of subduction complexes. J Geophys Res 83: p 5389-5396.

Coward-MP, Windley BF, Broughton RD, Luff IW, Petterson MG, Pudsey CJ, Rex DC, Khan MA 1986 Collision tectonics in the NW Himalayas. In Coward MP, Ries AC (eds). Collision Tectonics. Geol Soc Lond Spec Pub 19: p 185-201.

Cox JS, Searle MP, Pedersen RB 1999 The petrogenesis of leucogranitic dykes intruding the northern Semail ophiolite, United Arab Emirates: field relationships, geochemistry and Sr/Nd isotope systematics. Con Min Pet 137: p 267-287.

Davies HL, Smith IE 1971 Geology of eastern Papua. GSA Bull 82: p 3299-3312.

Den Tex E 1969 Origin of ultramafic rocks, their tectonic setting and history: a contribution to the discussion of the paper 'The origin of ultramafic and ultrabasic rocks' by Wyllie PJ. Tectonophysics 7: p 457-488.

DePaolo DJ, Wasserburg GJ 1976a Nd isotopic variations and petrogenetic models. Geophys Res Lett 3: p 743-746.

DePaolo DJ, Wasserburg GJ 1976b Inferences about magma sources and mantle structure from variations in $^{143}Nd/^{144}Nd$. Geophys Res Lett 4: p 465-468.

DePaolo DJ, Wasserburg GJ 1979 Petrogenetic mixing models and Nd-Sr isotopic patterns. Geochem Cosmochem Acta 43: p 615-627.

De Roever WP 1959 Sind die alpinotypen peridotitmassen vielleicht tektonische verfrachtete bruchstuecke der peridotitschale? Geologische Rundschau 46: p 137-146.

Dewey JF 1976 Ophiolite obduction. Tectonophysics 31: p 93-120.

Dewey JF, Bird JM 1971 Origin and emplacement of the ophiolite suite: Appalachian ophiolites in Newfoundland. J Geophys Res 76: p 3179-3206.

Dewey JF, Pitman WC, Ryan-William BF, Bonnin J 1973 Plate tectonics and the evolution of the Alpine aystem. GSA Bull 84: p 3137-3180.

Eide EA 1995 A model for the tectonic history of HP and UHPM regions in east central China. In Coleman RG, Wang X (eds). Ultra High Pressure Metamorphism. CUP: p 391-427.

Elliott D, Johnson MRW 1980 Structural evolution in the northern part of the Moine thrust belt, NW Scotland. Phil Trans Roy Soc Edin Earth Sci 71: p 69-96.

Ellis DJ 1978 Stability and phase equilibria of chloride and carbonate bearing scapolites at 750°C and 4000 bar. Geochem Cosmochem Acta 42: p 1271-1281.

Ellis DJ, Green DH 1979 An experimental study of the effect of Ca upon garnet-clinopyroxene Fe-Mg exchange equilibria. Con Min Pet 71: p 13-22.

Ellis DJ 1980 Osumilite-sapphirine-quartz granulites from Enderby Land, Antarctica: P-T conditions of metamorphism, implications for garnet-cordierite equilibria and the evolution of the deep crust. Con Min Pet 74: p 201-210.

Ellis DJ 1987 Origin and evolution of granulites in normal and thickened crusts. Geology 15: p 167-170.

El-Shazly AK, Coleman RG 1990 Metamorphism in the Oman Mountains in relation to ophiolite emplacement. In: Robertson AHF, Searle MP, Ries AC (eds). The geology and tectonics of the Oman region. Geol Soc Lon Spec Pub 49: p 475-95.

El-Shazly AK Coleman RG, Liou JG 1990 Eclogites and blueschists from NE Oman: petrology and PT evolution. J Pet 31: p 629-66.

El-Shazly AK, Lanphere MA 1992 Two high pressure metamorphic events in NE Oman: evidence from $^{40}Ar/^{39}Ar$ dating and petrological data. J Geol 100: p 731-51.

El-Shazly AK 1994 Petrology of lawsonite, pumpellyite and sodic amphibole bearing metabasites from NE Oman. J Met Geol 12: p 23-48.

El-Shazly AK, Worthing MA, Jaywardane J, Varne R 1994 Geochemistry of metamorphosed mafic rocks from Saih Hatat: pre-obduction history of NE Oman. J Geol Soc Lond 151: p 999-1016.

El-Shazly AK, Worthing MA, Liou JG 1997 Interlayered eclogites, blueschists and epidote amphibolites from NE Oman: a record of protolith compositional control and limited fluid infiltration. J Pet 38: p 1461-1487.

Encarnacion JP, Essene EJ, Mukasa SB, Hall CH 1995 High-pressure and temperature subophiolitic kyanite-garnet amphibolites generated during initiation of mid-Tertiary subduction, Palawan, Philippines. J Petrol 36: p 1481-1503.

Encarnacion JP, Mukasa SB, Evans CA 1999 Subduction components and the generation of arc-like melts in the Zambales Ophiolite, Philippines: Pb, Sr and Nd isotopic constraints. Chem Geol 156: p 343-357.

England PC, Richardson SW 1977 The influence of erosion upon the mineral facies of rocks from different metamorphic environments. J Geol Soc Lond 134: p 201-213.

Fitzsimons ICW, Harley SL 1994 Garnet coronas in scapolite-wollastonite calc-silicates from East Antarctica: the application and limitations of activity-corrected grids. J Met Geol 12: p 761-777.

Fyfe WS 1973 The granulite facies, partial melting and the Archean crust. Phil Trans Roy Soc Lond A273: p 457-462.

Gass IG 1968 Is the Troodos massif of Cyprus a fragment of Mesozoic ocean floor? Nature 220: p 39-42.

Gass IG 1980 The Troodos Massif; its role in the unravelling of the ophiolite problem and its significance in the understanding of constructive plate margin processes. In Panayiotou-A (ed). Ophiolites. Proc Int ophiolite sym.

Gass IG, Lippard SJ, Shelton AW 1984 (eds) Ophiolites and oceanic lithosphere. Geol Soc Lond Spec Pub 13.

Gass IG, Ries AC, Shackleton RM, Smewing JD 1990 Tectonics, geochronology and geochemistry of the Precambrian rocks of Oman. In Robertson AHF, Searle MP (eds). The Geology and Tectonics of the Oman Region. Geol Soc Lond Spec Pub 49: p 585-599.

Gealey WK 1977 Ophiolite obduction and the geological evolution of the Oman mountains and adjacent areas. GSA Bull 88: p 1183-1191.

Gealey WK 1980 Ophiolite obduction mechanisms. In Panayiotou A (ed). Ophiolites. Proc Int ophiolite sym: p 228-243.

Ghent ED, Stout MZ 1981 Metamorphism at the base of the Semail Ophiolite. J Geophys Res 86: p 2557-2571.

Glennie KW, Boeuf MG, Hughes-Clarke MHW, Moody-Stuart M, Pilaar WF, Reinhardt BM 1973 Late Cretaceous nappes in the Oman mountains and their geologic evolution. AAPG Bull 57: p 5-27.

Glennie KW, Boeuf MG, Hughes-Clarke MHW, Moody-Stuart M, Pilaar WF, Reinhardt BM 1974 Geology of the Oman mountains. Verhandelingen Koninklijk Nederlands geologisch mijnbouwkundidg Genootschap 31: 423p.

Gnos E 1992 The metamorphic rocks associated with the Oman Ophiolite (Sultanate of Oman and United Arab Emirates). Unpublished PhD thesis, University of Bern, 120p.

Gnos E 1998 Peak metamorphic conditions of garnet amphibolites beneath the Semail ophiolite: implications for an inverted pressure gradient. Int Geol Review 40: p 281-304.

Gnos E, Peters Tj 1993 K-Ar ages of the metamorphic sole of the Semail ophiolite: implications for ophiolite cooling history. Con Min Pet 113: p 325-332.

Gnos E, Peters Tj 1995 Tephroite-hausmannite-galaxite from a granulite-facies manganese rock of the United Arab Emirates. Con Min Pet 120: p 372-377.

Gnos E, Kurz D 1994 Sapphirine-quartz and sapphirine-corundum assemblages in metamorphic rocks associated with the Semail ophiolite (United Arab Emirates). Con Min Pet 116: p 398-410.

Gnos E, Nicolas A 1996 Structural evolution of the northern end of the Oman ophiolite and enclosed granulites. Tectonophysics 254: p 111-37.

Gnos E, Wyder R, Rothery DA 1991 Comparison between mapping at 1:25000 scale and decorrelation stretched Landsat thematic mapper images in the Wuqbah Block (Oman

mountains). In Peters TJ, Nicolas A, Coleman RG (eds). Ophiolite genesis and evolution of the oceanic lithosphere. Kluwer Academic Publishers: p 875-882.

Gnos E, Armbruster T, Nyfeler D 1996 Kanoite, donpeacorite and tirodite: Mn-Mg-silicates from a manganiferous quartzite in the United Arab Emirates. European J Min 8: p 251-261.

Gnos E, Immenhauser A, Peters Tj 1997 Late Cretaceous/early Tertiary convergence between the Indian and Arabian plates recorded in ophiolites and related sediments. Tectonophysics 271: p 1-19.

Goffé B, Michard A, Kienast KR, LeMer O 1988 A case of obduction related HP-LT metamorphism in upper crustal nappes, Arabian continental margin, Oman: PT paths and kinematic interpretation. Tectonophysics 151: p 363-86.

Gorin GE, Racz LG, Walter MR 1982 Late Precambrian-Cambrian sediments of Huqf Group, Sultanate of Oman. AAPG Bull: p 2609-2627.

Graham GM 1980 Structure and sedimentology of the Hawasina window, Oman mountains. Unpublished PhD thesis, Open University, 468p.

Graham CM, Powell R 1984 A garnet-hornblende thermometer: calibration, testing and application to the Pelona schist, southern California. J Met Geol 2: p 13-31.

Gregory RT, Gray DR, McMiller J 1998 Tectonics of the Arabian margin associated with the formation and exhumation of high pressure rocks, Sultanate of Oman. Tectonics 17: p 657-670.

Hacker BR 1990 Simulation of the metamorphic and deformational history of the metamorphic sole of the Oman ophiolite. J Geophys Res 95: p 4895-4907.

Hacker BR 1991 The role of deformation in the formation of metamorphic gradients: ridge subduction beneath the Semail ophiolite. Tectonics 10: p 455-473.

Hacker BR 1994 Rapid emplacement of young oceanic lithosphere: Argon geochronology of the Oman ophiolite. Science 265: p 1563-65.

Hacker BR, Peacock SM 1995 Creation, preservation, and exhumation of UHPM rocks. In Coleman RG, Wang X (eds). Ultra High Pressure Metamorphism. CUP.

Hacker BR, Mosenfelder JL, Gnos E 1996 Rapid emplacement of the Oman ophiolite: thermal and geochronological constraints. Tectonics 15: p 1230-47.

Hacker BR, Gnos E 1997 The conundrum of Semail: explaining the metamorphic history. Tectonophysics 279: p 215-226.

Hacker BR, Mosenfelder JL 1996 Metamorphism and deformation along the emplacement thrust of the Samail ophiolite, Oman. Earth Plan Sci Lett 144: p 435-51.

Hamilton WB 1979 Tectonics of the Indonesian region. USGS Prof Paper: p 324-325.

Hansen EC, Newton RC, Janardhan AS 1984 Pressures, temperatures and metamorphic fluids across an unbroken amphibolite facies to granulite facies transition in southern Karnataka, India. In Kröner A et al. (eds). Archean Geochemistry, Springer-Verlag: p 161-181.

Hanna SS 1990 The Alpine deformation of the central Oman mountains. In Robertson AHF, Searle MP (eds). The Geology and Tectonics of the Oman Region. Geol Soc Lond Spec Pub 49: p 343-361.

Harley SL 1989 The origins of granulites: a metamorphic perspective. Geol Mag 126: p 215-247.

Harley SL 1998 On the occurrence and characterisation of ultra high temperature crustal metamorphism. In Treloar PJ, O'Brien PJ (eds). What drives metamorphism and metamorphic reactions? Geol Soc Lond Spec Pub 138: p 81-107.

Harley SL, Buick IS 1992 Wollastonite-scapolite assemblages as indicators of granulite pressure-temperature-fluid histories: the Rauer Group, East Antarctica. J Petrol 33: p 693-728.

Harley SL, Fitzsimons ICW, Buick IS 1994 Reactions and textures in wollastonite-scapolite granulites and their significance for pressure-temperature-fluid histories of high-grade terranes. In Raith M, Hoernes S (eds). Tectonic, metamorphic and isotopic evolution of deep crustal rocks, with special emphasis on Sri Lanka. Precambrian Research 66: p 309-323.

Harris NBW, Ayres M 1998 The implications of Sr isotope disequilibrium for rates of prograde metamorphism and melt extraction in anatectic terranes. In Treloar PJ, O'Brien PJ (eds). What drives metamorphism and metamorphic reactions? Geol Soc Lond Spec Pub 138: p 171-182.

Harris NBW, Pearce JA, Tindle AG 1986 Geochemical characteristics of collision zone magmatism. In Coward MP, Ries AC (eds). Collision Tectonics. Geol Soc Lond Spec Pub 19: p 185-201.

Hawkins JW, Batiza R 1977 Petrology and geochemistry of an ophiolite complex: Zambales Range, Luzon, Republic of Philippines. Eos Trans AGU 58: p 1244.

Hensen BJ, Green DH 1973 Experimental study of the stability of cordierite and garnet in pelitic compositions at high pressures and temperatures III: synthesis of experimental data and geological applications. Con Min Pet 38: p 151-166.

Hensen BJ 1986 Theoretical phase relations involving cordierite and garnet revisited: the influence of oxygen fugacity on the stability of sapphirine and spinel in the system Mg-Fe-Al-Si-O. Con Min Pet 92: p 362-367.

Holland TJB, Blundy JD 1994 Non-ideal interactions in calcic amphiboles and their bearing on amphibole plagioclase thermometry. Con Min Pet 116: p 433-447.

Holland TJB, Powell R 1990 An enlarged and updated internally consistent thermodynamic dataset with uncertainties and correlations: the system K_2O-Na_2O-CaO-MgO-MnO-FeO-Fe_2O_3-Al_2O_3-TiO_2-SiO_2-$C0_2$-H_2O. J Met Geol 8: p 89-124.

Holland TJB, Powell R 1998 An internally-consistent thermodynamic data set for phases of petrological interest. J Met Geol 16: p 309-343.

Holtz F, Barbey P 1991 Genesis of peraluminous granites 2: mineralogy and chemistry of the Tourem Complex (north Portugal). Sequential melting vs restite unmixing. J Petrol 32: p 959-978.

Hutchison I, Louden KE, White RS 1981 Heat flow and age of the Gulf of Oman. Earth Plan Sci Lett 56:p 252-262.

Immenhauser A 1996 Cretaceous sedimentary rocks on the Masirah ophiolite: evidence for an unusual bathymetric history. J Geol Soc Lond 153: p 539-551.

Inger S, Harris NBW 1993 Geochemical constraints on leucogranite magmatism in the Langtang valley, Nepal Himalaya. J Petrol 34: p 345-368.

Ishiwatari A 1985 Alpine ophiolites: product of low-degree mantle melting in a Mesozoic transcurrent rift zone. Earth Plan Sci Lett 76: p 93-108.

Ito K, Kennedy GC 1971 An experimental study of the basalt-garnet granulite-eclogite transition. In The Structure and Physical Properties of the Earth's Crust. AGU Geophysical Monograph 14: p 303-314. 1971.

Jacobsen SB, Wasserburg GJ 1984 Sm-Nd evolution of chondrites and achondrites. Earth Plan Sci Lett 67: p 137-150.

Jamieson RA 1981 Metamorphism during ophiolite emplacement; the petrology of the St. Anthony Complex. J Petrol 22: p 397-449.

Jamieson RA 1986 P-T paths from high temperature shear zones beneath ophiolites. J Met Geol 4: p 3-22.

Jayko AS, Blake MC, Harms-Tekla A 1987 Attenuation of the Coast Range Ophiolite by extensional faulting, and nature of the Coast Range "thrust" California. Tectonics 6: p 475-488.

Jenkyns HC 1980 Tethys: past & present. In Papers in honour of PC Sylvester-Bradley. Proc Geol Ass 91: p 107-118.

Juteau T, Ernewein M, Reuber I, Whitechurch H, Dahl R 1988 Duality of magmatism in the plutonic sequence of the Sumail Nappe, Oman. Tectonophysics 151: p 107-135.

Kohn MJ, Spear FS 1990 Two new geobarometer for garnet amphibolites, with applications to south eastern Vermont. Am Min 75: p 89-96.

Kretz R 1983 Symbols for rock forming minerals. Am Min 68: p 277-279.

Krogh EJ 1988 The garnet-clinopyroxene Fe-Mg geothermometer: a reinterpretation of existing experimental data. Con Min Pet 99: p 44-48.

Kusky T, Robinson C, El-Baz F, Considine P, Blanco D, Ledwith M, Ozdogan M 1998 Tertiary and Quaternary faulting in the northern Oman Mountains. Geol Soc Am: 1998 ann meeting.

Lamb WM, Valley JW 1984 Metamorphism of reduced granulites in a low CO_2 vapour free environment. Nature 321: p 56-58.

Lanphere MA 1981 K-Ar ages of metamorphic rocks at the base of the Semail Ophiolite, Oman. J Geophys Res 86: p 2777-2782.

Lanphere MA, Coleman RG, Hopson CA 1981 Sr isotopic tracer study of the Semail ophiolite, Oman. J Geophys Res 86: p 2709-2720.

LeFort P, Cuney M, Deniel C, France-Lanord C, Sheppard SMF, Upreti BN, Vidal P 1987 Crustal generation of the Himalayan leucogranites. J Geophys Res 11: p 10545-10568.

Lees GM 1928 The geology and tectonics of Oman and parts of SE Arabia. Quart J Geol Soc Lond 110: p 121-152.

LeMetour J, DeGramont X, Villey M 1986 Geological map of Masquat and Quryat and accompanying notes. Scale 1:100, 000, Ministry of Petroleum and Minerals, Sultanate of Oman.

LeMetour J, Rabu D, Tegyey M, Béchennec F, Beurrier M, Villey M 1990 Subduction and obduction; two stages in the Eo-Alpine tectonometamorphic evolution of the Oman Mountains. In Robertson AHF, Searle MP (eds). The Geology and Tectonics of the Oman Region. Geol Soc Lond Spec Pub 49: p 327-339.

LePichon X, Angelier J, Sibuet JC 1982 Plate boundaries and extensional tectonics. Tectonophysics 81: p 239-256.

Lindsley DH 1983 Pyroxene thermometry. Am Min 68: p 477-493.

Linthout K, Helmers H 1994 Pliocene obducted, rotated and migrated ultramafic rocks and obduction-induced anatectic granite, SW Seram and Ambon, eastern Indonesia. In Sopaheluwakan J, Utomo EP, Barber AJ (eds). Symposium on the Dynamics of subduction and its products. J SE Asian Earth Sci 9: p 95-109.

Lippard SJ 1983 Cretaceous high pressure metamorphism in NE Oman and its relationship to subduction and ophiolite nappe emplacement. J Geol Soc Lond 140: p 97-104.

Lippard SJ, Rex DC 1982 K-Ar ages of alkaline igneous rocks in the northern Oman mountains and their relations to rifting, passive margin development and destruction of the Oman Tethys. Geol Mag 119: p 497-503.

Lippard SJ, Shelton AW, Gass IG 1986 The Ophiolite of Northern Oman. Blackwell Scientific Publications Oxford: 178p.

Lister GS, Snoke AW 1984 S-C mylonites. J Struct Geol 6: p 617-638

Lockwood JP 1972 Possible mechanisms for the emplacement of Alpine type serpentinites. GSA Memoir 132: p 273-287.

Lotti B 1886 Paragone fra la roccie ofiolitiche terziare italiane e la roccie basiche pare teraziare della Scozia et dell'irlande. Boll R Comitato Geol Italia 76.

Lovelock PER, Potter TL, Walsworth-Bell EB, Wiemer WM 1981 Ordovician rocks in the Oman mountains: the Amdeh Formation. Geologie en Mijnbouw 60: p 487-495.

Liu J, Bohlen SR, Ernst WG 1996 Stability of hydrous phases in subducting oceanic crust. Earth Plan Sci Lett 143: p 161-171.

MacLeod CJ, Rothery DA 1992 Ridge axial segmentation in the Oman Ophiolite; evidence from along-strike variations in the sheeted dyke complex. In Parson LM, Murton BJ, Browning P (eds). Ophiolites and their modern oceanic analogues. Geol Soc Spec Pub 60: p 39-63.

Mahmood K, Boudier F, Gnos E, Monie P, Nicolas A 1995 $^{40}Ar/^{39}Ar$ dating of the emplacement of the Muslim Bagh ophiolite, Pakistan. Tectonophysics 250: p 169-181.

Malpas J 1979 Two contrasting trondhjemite associations from transported ophiolites in western Newfoundland; initial report. In Barker F (ed) 1979. Trondhjemites, dacites and related rocks. Elsevier, Amsterdam: p 465-487.

Malpas J, Stevens RK, Strong DF 1973 Amphibolite Associated with Newfoundland Ophiolite; Its Classification and Tectonic Significance. Geology 1: p 45-47.

Mann A, Hanna SS 1990 The tectonic evolution of the pre-Permian rocks of the central and SE Oman mountains. In Robertson AHF, Searle MP (eds). The Geology and Tectonics of the Oman Region. Geol Soc Lond Spec Pub 49: p 307-325.

McCaig AM 1983 P-T conditions during emplacement of the Bay of Islands ophiolite complex. Earth Plan Sci Lett 63: p 459-473.

McCulloch MT, Gregory RG, Wasserburg GJ, Taylor HP 1981 Sm-Nd, Rb-Sr and $^{18}O/^{16}O$ isotopic systematics in an oceanic crustal section: evidence from the Samail ophiolite. J Geophys Res 86: p 2721-2736.

McKenzie D, Bickle MJ 1988 The volume and composition of melt generated by extension of the lithosphere. J Petrol 29: p 625-679.

McMiller J, Gray DR, Gregory RT 1998 Exhumation of high pressure rocks in north eastern Oman. Geology 26: p 235-238.

McMiller J, Gregory RT, Gray DR, Foster DA 1999 Geological and geochronological constraints on the exhumation of a high pressure terrane, Oman. In Ring U, Brandon MT, Lister GS, Willett SD (eds). Exhumation processes: normal faulting, ductile flow and erosion. Geol Soc Lond Spec Pub 154: p 241-260.

Mercier JCC 1980 Single pyroxene thermobarometry. Tectonophysics 70: p 1-37.

Meschede M 1986 A method of discriminating between different types of mid ocean ridge basalts and continental tholeiites using the Nb-Zr-Y diagram. Chem Geol 56: p 207-218.

Meyer J, Mercolli I, Immenhauser A 1996 Off ridge alkaline magmatism and seamount volcanoes in the Masirah ophiolite, Oman. Tectonophysics 267: p 187-208.

Michard A, Bouchez JL, Ouazzani TM 1984 Obduction-related planar and linear fabrics in Oman. In Hancock PL, Klaper EM, Mancktelow NS, Ramsay JG (eds). Planar and linear fabrics of deformed rocks; a selection of papers delivered at an international conference held at ETH. J Struct Geol: p 39-49.

Michard A, Le-Mer O, Goffé B, Montigny R 1989 Mechanism of the Oman mountains obduction onto the Arabian continental margin, reviewed. In Geologie de l'Oman: Seance specialisee de la Societe Geologique de France. Bull Soc Geologique de France, 8th Serie: p 241-252.

Michard A, Goffé B, Oberhansli R, Wendt AS 1994 Late Cretaceous exhumation of the Oman blueschists and eclogites: a two stage extensional mechanism. Terra Nova 6: p 404-13.

Michard A, Goffé B, Chopin C, Henry C 1996 Did the western Alps develop through an Oman-type stage? The geotectonic setting of HP metamorphism in two contrasting Tethyan transects. Eclog Geol Helv 89: p 43-80.

Miller CF 1985 Are strongly peraluminous magmas derived from pelitic sedimentary sources? J Geol 93: p 673-689.

Miyashiro A 1973 The Troodos ophiolite complex was probably formed in an island arc. Earth Plan Sci Lett 19: p 218-224.

Moecher DP, Essene EJ, Anovitz LM 1988 Calculation and application of clinopyroxene-garnet-plagioclase-quartz geobarometers. Con Min Pet 100: p 92-106.

Montigny R, Le Mer O, Thuziat R, Whitechurch H 1988 K-Ar and $^{40}Ar/^{39}Ar$ study of the metamorphic rocks associated with the Oman ophiolite. Tectonophysics 151: p 345-362.

Moore DE 1984 Metamorphic history of a high grade blueschist exotic block from the Franciscan complex, California. J Petrol 25: p125-160.

Moores E 1970 Ultramafics and orogeny, with models of the US Cordillera and Tethys. Nature 228: p 837-842.

Moores E 1982 Origin and emplacement of ophiolites. Rev Geophys Space Physics: 20 p 735-760.

Moores E, Vine FJ 1969 Troodos massif, Cyprus as deep ocean floor: preliminary structural and petrologic evidence. Eos transaction, AGU 50: p 333.

Moores E, Vine FJ 1971 Troodos massif, Cyprus and other ophiolites as oceanic crust: evaluation and implications. Phil Trans Roy Soc Lond A268: p 443-466.

Morton DM 1959 The geology of Oman. 5th World Petrol Cong New York Proc, section 1: p 277-294.

Mukasa SB, Ludden JN 1987 Uranium-lead isotopic ages of plagiogranites from the Troodos ophiolite, Cyprus, and their tectonic significance. Geology 15: p 825-828.

Nagler TF, Frei R 1994 Production of acidic rocks by pure differentiation of a depleted mantle source: a combined U-Pb (zircon) and Pb-Nd isotope study on the Masirah ophiolite. Abstracts ICOG 8 Berkeley Geol Surv Circ 1107: p 230.

Nagler TF, Frei R 1997 True K feldspar granites in oceanic crust (Masirah ophiolite, Oman): a U-Pb and Sm-Nd study. Chem Geol 138: p 119-126.

Newton RC 1972 An experimental determination of the high-pressure stability limits of magnesian cordierite under wet and dry conditions. J Geol 80: p 398-420.

Nicolas A 1989 Structures of ophiolites and dynamics of oceanic lithosphere. Kluwer Academic, Amsterdam.

Nicolas A, Jackson ED 1972 Repartition en deux provinces des peridotites des chaines alpines logeant la Mediterranee: implications geotectoniques. Schweiz Mineral Petrogr Mitt 52: p 479-495.

Nicolas A, Girardeau J, Wang Xi bin, Cao Yougong, Zheng Haixiang 1981 Complete ophiolitic sequences in southern Xizang (Tibet): discovery of cumulates, dike and sill layers. Geol Review 27: p 457-459.

Nicolas A, Reuber I, Benn K 1988 A new magma chamber model based on structural studies in the Oman ophiolite. Tectonophysics 151: p 87-105.

Ohnenstetter M, Ohnenstetter D, Vidal P, Cornichet J, Hermitte D, Mace J 1981 Crystallization and age of zircon from Corsican ophiolitic albitites; consequences for oceanic expansion in Jurassic times. Earth Plan Sci Lett 54: p 397-408.

Okay A, Xu-Shutong, Sengor- AMC 1989 Coesite from the Dabie Shan eclogites, central China. European J Min 4: p 595-598.

Okay A, Sengor AMC 1992 Evidence for intra-continental thrust related exhumation of ultrahigh pressure rocks in China. Geology 20: p 411-14.

Oxburgh ER 1972 Flake Tectonics and Continental Collision. Nature 239: p 202-204.

Pallister JS, Hopson CA 1981 Samail ophiolite plutonic suite: field relations, phase variation, cryptic variation and layering, and a model of a spreading ridge magma chamber. J Geophys Res 86: p 2593-2644.

Parsons B, Sclater JG 1977 An analysis of the variation of ocean floor bathymetry and heat flow with age. J Geophys Res 82: p 803-827.

Patiño Douce AE, Harris NBW 1998 Experimental constraints on Himalayan anatexis. J Petrol 39: p 689-710.

Patiño Douce AE, Beard JS 1995 Dehydration melting of biotite gneiss and quartz amphibolite from 3 to 15 kbar. J Petrol 36: p 707-738.

Pattison DRM, Newton RC 1989 Reversed experimental calibration of the garnet-clinopyroxene Fe-Mg geothermometer. Con Min Pet 101: p 87-103.

Pearce JA 1983 Role of the sub-continental lithosphere in magma genesis at active continental margins. In Hawkesworth CJ, Norry MJ (eds). Continental basalts and mantle xenoliths; papers prepared for a UK Volcanic Studies Group meeting at the University of Leicester: p 230-249. Shiva Publ Nantwich, UK.

Pearce JA 1989 High P/T metamorphism and granite genesis beneath ophiolite thrust sheets. Ofioliti 14: p 195-211.

Pearce JA, Cann JR 1971 Ophiolite origin investigated by discriminant analysis using Ti, Zr and Y. Earth Planet Sci Lett 12: p 339-349.

Pearce JA, Cann JR 1973 Tectonic setting of basic volcanic rocks using trace element analyses. Earth Planet Sci Lett 19: p 290-300.

Pearce JA, Alabaster T, Shelton AW, Searle MP 1981 The Oman ophiolite as a Cretaceous arc-basin complex: evidence and implications. Phil Trans Roy Soc Lond A300: p 299-317.

Pearce JA, Harris NBW, Tindle AG 1984 Trace element discrimination diagrams for the tectonic interpretation of granitic rocks. J Petrol 25: p 956-983.

Pedersen RB, Malpas J 1984 The origin of oceanic plagiogranites from the Karmoy ophiolite, Western Norway. Con Min Pet 88: p 36-52.

Pedersen RB, Dunning GR 1997 Evolution of arc crust and relations between contrasting sources: U-Pb (age), Nd and Sr isotope systematics of the ophiolitic terrain of SW Norway. Con Min Pet 128: p 1-15.

Peters Tj, Nicolas A, Coleman RG (eds) 1991. Ophiolite genesis and the evolution of oceanic lithosphere. Kluwer Academic, Amsterdam.

Peters Tj, Immenhauser A, Mercolli I, Meyer J 1996 Geological map of Masirah north and Masirah south with explanatory notes. Sheet K768 north and south scale 1:50,000. Directorate General of Minerals, Oman Ministry of Petroleum and Minerals.

Peters Tj, Kamber BS 1994 Peraluminous, potassium-rich granitoids in the Semail ophiolite. Con Min Pet 118: p 229-38.

Pilgrim G 1908 Geology of the Persian Gulf and adjoining portions of Persia and Arabia. Ind Geol Surv Mem 34: p 1-77.

Pin C, Briot D, Bassin C, Poitrasson F 1994 Concomitant separation of strontium and samarium-neodynium for isotope analyses in silicate samples, based on specific extraction chromatography. Anal Chim Acta 298: p 209-217.

Platt JP 1986 Dynamics of orogenic wedges and the uplift of high pressure metamorphic rocks. GSA Bull 97: p 1037-1053.

Platt JP 1987 The uplift of high pressure, low temperature metamorphic rocks. Phil Trans. Royal Soc Lond A321: p 87-103.

Platt JP 1993 Exhumation of high pressure rocks: a review of concepts and processes. Terra Nova 5: p 119-33.

Poli S 1993 The amphibolite-eclogite transformation; an experimental study on basalt. Am J Sci 293: p 1061-1107.

Pollack HN, Chapman DS 1977 The flow of heat from the Earth's interior. Sci Am 237: p 73-76.

Potts PJ 1987 A handbook of silicate rock analysis. Blackie Academic & Professional, London: 622 p.

Potts PJ, Tindle AG, Isaacs MC 1983 On the precision of electron microprobe data: a new test for the homogeneity of mineral standards. Am Min 68: p 1237-1242.

Powell R 1985 Regression diagnostics and robust regression in geothermometer/geobarometer calibration: the garnet-clinopyroxene geothermometer revisited. J Met Geol 3: p 231-243.

Rabu D 1987 Geologie de l'autochtone des montagnes d'Oman; la fenetre du Jabal Akhdar; la semelle metamorphique de la nappe de Samail dans les parties centrale et orientale des montagnes d'Oman: une revue. BRGM Principaux Resultats Scientifiques 1987: p 96-97.

Rabu D 1993 Stratigraphy and structure of the Oman mountains. Doc BRGM 221.

Ramsey MH, Potts PJ, Webb PC, Watkins P, Watson JS, Coles BJ 1995 An objective assessment of analytical method precision: comparison of ICP-AES and XRF for the analysis of silicate rocks. Chem Geol 124: p 1-19.

Rapp RP, Watson EB, Miller CF 1991 Partial melting of amphibolite/ eclogite and the origin of Archean trondhjemites and tonalites. In Haapala I, Condie KC (eds). Precambrian granitoids; petrogenesis, geochemistry and metallogeny. Precambrian Research 51: p 1-25. Elsevier. Amsterdam.

Ravaut P, Bayer R, Hassani R, Rousset D, Al-Yahyaey A 1997 Structure and evolution of the northern Oman margin: gravity and seismic constraints over the Zagros-Makran-Oman collision zone. Tectonophysics 279: p 253-280.

Reinhardt BM 1969 On the genesis and emplacement of ophiolites in the Oman mountains geosyncline. Schweiz Mineral Petrogr Mitt 49: p 1-30.

Richard P, Shimizu N, Allégre CJ (1976) $^{143}Nd/^{146}Nd$, a natural tracer: an application to oceanic basalts. Earth Plan Sci Lett 31: p 269-278.

Robertson AHF 1987a Upper Cretaceous Muti Formation: transition of a Mesozoic carbonate platform to a foreland basin in the Oman Mountains. Sedimentology 34: p 1123-1142.

Robertson AHF 1987b The transition from a passive margin to an Upper Cretaceous foreland basin related to ophiolite emplacement in the Oman Mountains. GSA Bull 99: p 633-653.

Robertson AHF 1994 Role of the tectonic facies concept in orogenic analysis and its applications to Tethys in the eastern Mediterranean region. Earth Sci Reviews 37: p 139-213.

Robertson AHF, Searle MP, Ries AC (eds) 1990. The geology and tectonics of the Oman region. Geol Soc Lond Spec Pub 49: 845 p.

Robertson AHF, Searle MP 1990 The northern Oman Tethyan continental margin: stratigraphy, structure, concepts and controversies. In Robertson AHF, Searle MP (eds). The geology and tectonics of the Oman region. Geol Soc Lond Spec Pub 49: p 361-74.

Rollinson HR 1993 Using geochemical data: evaluation, presentation, interpretation. Longman Scientific & Technical, London: 352 p.

Rubie DC 1984 A thermal-tectonic model for high pressure metamorphism and deformation in the Sesia Zone, W. Alps. J Geol 92: p 21-36.

Saddiqi O, Poupeau G, Michard A, Goffé B, Oberhænsli R 1995 Exhumation des roches metamorphiques HP-BT d'Oman: datation par traces de fission sur zircons. CR Acad Sci Paris Ser II 320: p 1071-1077.

Sandiford MA, Powell R 1986 Deep crustal metamorphism during continental extension: modern and ancient examples. Earth Plan Sci Lett 79: p 151-158.

Sarwar G 1992 Tectonic setting of the Bela ophiolites, southern Pakistan. Tectonophysics 207: p 359-381.

Searle MP 1980 The metamorphic sheet and underlying volcanic rocks beneath the Oman ophiolite in the northern Oman mountains of Arabia. Unpublished PhD thesis, Open University, UK 213 p.

Searle MP, Malpas J 1980 Structure and metamorphism of rocks beneath the Semail ophiolite of Oman and their significance in ophiolite obduction. Trans Roy Soc Edin Earth Sci 71: p 247-262.

Searle MP, Lippard SJ, Smewing JD, Rex DC 1980 Volcanic rocks beneath the Semail Ophiolite Nappe in the northern Oman Mountains and their significance in the Mesozoic evolution of Tethys. J Geol Soc Lond 137: p 589-604.

Searle MP, Graham GM 1982 "Oman exotics": oceanic carbonate build-ups associated with the early stages of continental rifting. Geology 10: p 43-49.

Searle MP, Malpas J 1982 Petrochemistry and origin of sub ophiolitic metamorphic rocks in the Oman mountains. J Geol Soc Lond 139: p 235-248.

Searle MP 1984 Alkaline peridotite, pyroxenite and gabbroic intrusions in the Oman mountains, Arabia. Can J Earth Sci 21: p 396-406.

Searle MP, Stevens RK 1984 Obduction processes in ancient, modern and future ophiolites. In Gass IG, Lippard SJ, Shelton AW (eds). Ophiolites and oceanic lithosphere. Geol Soc Spec Pub 13: p 303-319.

Searle MP 1985 Sequence of thrusting and origin of culminations in the northern and central Oman mountains. J Struct Geol 7: p 129-143.

Searle MP 1986 Structural evolution and sequence of thrusting in the High Himalayan, Tibetan-Tethys and Indus suture zones of Zanskar and Ladakh, western Himalaya. J Struct Geol 8: p 923-936.

Searle MP, Fryer BJ 1986 Garnet, tourmaline and muscovite bearing leucogranites, gneisses and migmatites of the Higher Himalaya from Zanskar, Kulu, Lahoul and Kashmir. In Coward MP, Ries AC (eds). Collision Tectonics, Geol Soc Lond Spec Pub 19: p 185-201.

Searle MP, Cooper DJW 1986 Structure of the Hawasina Window culmination, central Oman mountains. Trans Roy Soc Edin Earth Sci 77: p 143-156.

Searle MP, James NP, Calon TJ, Smewing JD 1983 Sedimentological and structural evolution of the Arabian continental margin in the Musandam Mountains and Dibba Zone, United Arab Emirates. GSA Bull 94: p 1381-1400.

Searle MP, Windley BF, Coward MP, Cooper DJW, Rex AJ, Rex D, Li Tingdong, Xiao Xuchang, Jan MQ, Thakur VC, Kumar S 1987 The closing of Tethys and the tectonics of the Himalaya. GSA Bull 98: p 678-701.

Searle MP, Waters DJ, Martin HN, Rex DC 1994 Structure and metamorphism of blueschist-eclogite facies rocks from the north eastern Oman Mountains. J Geol Soc Lond 151: p 555-76.

Searle MP, Cox JS 1999 Tectonic setting, origin and obduction of the Oman Ophiolite. GSA Bull 111: p 104-122.

Searle MP, Waters DJ, Dransfield MW, Stephenson BJ, Walker JD, Walker CB, Rex DC 1999 Thermal and mechanical models for the structural and metamorphic evolution of the

Zanskar high Himalaya. In MacNiocaill C, Ryan PD (eds). Continental Tectonics, Geol Soc Lond Spec Pub 164: p 139-156.

Sengor AMC 1979 Mid Mesozoic closure of Permo-Triassic Tethys and its implications. Nature 279: p 590-593.

Sengor AMC 1990 Plate tectonics and orogenic research after 25 years: a Tethyan perspective. Earth-Sci Reviews 27: p 1-201.

Sengor AMC, Natal BA, Burtman VS 1993 Evolution of the Altaid tectonic collage and Palaeozoic crustal growth in Eurasia. Nature 364: p 299-307.

Shearman DJ 1976 The geological evolution of southern Iran. Geograph J Lond 142: p 393-404.

Shelton AW 1984 Geophysical studies of the northern Oman ophiolite. Unpublished PhD thesis, Open University 353p.

Smewing JD, Simonian KO, Elboushi IM, Gass IG 1977 Mineralized fault zone parallel to the Oman ophiolite spreading axis. Geology 5: p 534-538.

Smewing JD, Abbotts IL, Dunne LA, Rex DC 1991 Formation and emplacement ages of the Masirah ophiolite, Oman. Geology 19: p 453-456.

Smith DC 1984 Coesite in clinopyroxene from the Caledonides and its implications for geodynamics. Nature 310: p 641-644.

Spear FS 1981 An experimental study of hornblende stability and compositional variability in amphibolite. Am J Sci 281: p 697-734.

Staudigel H, Bryan WB, Thompson G 1979 Chemical variation in glass-whole rock pairs in IPOD holes 417D and 418A. Eos AGU Transactions 60: p 409.

Steiger RH, Jager E 1977 Submission on geochronology: convention on the use of decay constants in geo- and cosmochronology. Earth Plan Sci Lett 36: p 359-362.

Steinmann G 1927 Die ophiolithischen zonen in den Mediterranean Kettengebirgen. 14th Int Geol Congress 2: p 637-668.

Stössel F, Zeigler URF 1985 The metamorphic series associated with the Semail ophiolite nappe of the Oman mountains in the United Arab Emirates. Unpublished MS thesis, University of Berne, Switzerland.

Streckeisen A 1976 To each plutonic rock its proper name. Earth-Sci Reviews 12: p 1-33.

Thompson AB 1982 Dehydration melting of pelitic rocks and the generation of H_2O-undersaturated granitic liquids. Am J Sci 282: p 1567-1595.

Tilton GR, Hopson CA, Wright JE 1981 U-Pb isotopic ages of the Samail ophiolite, Oman with application to Tethyan ocean ridge tectonics. J Geophys Res 86: p 2763-2775.

Tippit PR, Pessagno EA, Smewing JD 1981 The biostratigraphy of sediments in the volcanic unit of the Samail Ophiolite. J Geophys Res 86: p 2756-2762.

Touret J 1977 The significance of fluid inclusions in metamorphic rocks. In Fraser DG (eds) Thermodynamics in Geology. Dordrecht, Reidel Pub Co: p 203-227.

Treloar PJ, Rex DC, Guise PG, Coward MP, Searle MP, Windley BF, Petterson MG, Jan MQ, Luff IW 1989 K-Ar and Ar-Ar geochronology of the Himalayan collision in NW Pakistan: constraints on the timing of suturing, deformation, metamorphism and uplift. Tectonics 8: p 881-909.

Treloar PJ, Brodie KH, Coward MP, Jan MQ, Khan MA, Knipe RJ, Rex DC, Williams MP 1990 The evolution of the Kamila shear zone, Kohistan, Pakistan. In Salisbury MH, Fountain DM (eds). Exposed cross-sections of the continental crust p 175-214. Reidel Pub Co. Dordrecht-Boston.

Treloar PJ, Petterson MG, Jan MQ, Sullivan MA 1996 A re-evaluation of the stratigraphy and evolution of the Kohistan Arc sequence, Pakistan Himalaya; implications for magmatic and tectonic arc-building processes. J Geol Soc Lond 153: p 681-693.

Vidal O, Goffé B, Theye T 1992 Experimental study of the stability of sudoite and magnesiocarpholite and calculation of a new petrogenetic grid for the system FeO-MgO-Al_2O_3-SiO_2-H_2O. J Met Geol 10: p 603-614.

Vidal O, Theye T/El-Shazly AK 1996 Petrology of Fe-Mg carpholite bearing metasediments from NE Oman: Discussion and reply. J Met Geol 14: p 381-97.

Vine FJ, Moores E 1972 A model for the gross structure, petrology and magnetic properties of oceanic crust. GSA Memoir: Studies in Earth & Space Sciences: 132 p 195-205.

Vry JK, Brown PE, Valley JW 1990 Cordierite volatile content and the role of CO_2 in high-grade metamorphism. Am Min 75: p 71-88.

Vuagnet M 1963 Remarques sur la trilogie serpentinites-gabbros-diabases dans le bassin de la Mediterranee occidentale. Geologische Rundschau 53: p 336-357.

Wang X, Liou JG, Mao HK 1989 Coesite bearing eclogites from the Dabie mountains in central China. Geology 17: p 1085-1088.

Warren RG, Hensen BJ, Ryburn RJ 1987 Wollastonite and scapolite in Precambrian granulites from Australia and Antarctica. J Met Geol 5: p 213-223.

Waters DJ 1988 Partial melting and the formation of granulite facies assemblages in Namaqualand, South Africa. J Met Geol 6: p 387-404.

Waters DJ, Martin HN 1993 Geobarometry in phengite-bearing eclogites. Terra Abstracts 5: p 410-411.

Watts KF, Garrison RE 1986 Sumeini Group, Oman: evolution of a Mesozoic carbonate slope on a South Tethyan continental margin, in Mullins HT & Cook HE (eds). Carbonate aprons versus submarine fans. Sedimentary Geology 48: p 107-168.

Wells PRA 1977 Pyroxene thermometry in simple and complex systems. Con Min Pet 62: p 129-139.

Wendt AS, D'Arco P, Goffé B, Oberhansli R 1993 Radial cracks around α-quartz inclusions in almandine: constraints on the metamorphic history of the Oman mountains. Earth Plan Sci Lett 114: p 449-61.

Williams H, Smyth WR 1973 Metamorphic aureoles beneath ophiolite suites and alpine peridotites; tectonic implications with west Newfoundland examples. Am J Sci 273: p 594-621.

Wilson HH 1969 Late Cretaceous eugeosynclinal sedimentation, gravity tectonics and ophiolite emplacement in the Oman mountains, SE Arabia. AAPG Bull 53: p 626-671.

Wolf MB, Wyllie PJ 1994 Dehydration-melting of amphibolite at 10 kbar: the effects of temperature and time. Con Min Pet 115: p 369-383.

Wood DA 1980 The application of a Th-Hf-Ta diagram to problems of tectonomagmatic classification and to establishing the nature of crustal contamination of basaltic lavas of the British Tertiary volcanic province. Earth Plan Sci Lett 50: p 11-30.

Woodcock NH, Robertson AHF 1982a The upper Batinah Complex, Oman; allochthonous sediment sheets above the Semail ophiolite. Can J Earth Sci 19: p 1635-1656.

Woodcock NH, Robertson AHF 1982b Stratigraphy of the Mesozoic rocks above the Semail ophiolite, Oman. Geol Mag 119: p 67-76.

Wursten F, Flisch M, Michalski I, Le-Metour J, Mercolli I, Matthaus U, Peters Tj 1991 The uplift history of the Precambrian crystalline basement of the Jabal J'alan (Sur area). In Peters Tj, Nicolas A, Coleman RG (eds). Ophiolite genesis and evolution of the oceanic lithosphere: proceedings of the Ophiolite conference. p 613-626 Kluwer Academic.

Wyllie PJ, Wolf MB 1993 Garnet growth during amphibolite anatexis: implications of a garnetiferous restite. J Geol 101: p 357-373.

Yardley BWD 1989 An introduction to metamorphic petrology. Longman Scientific & Technical, London 248p.

Zeigler URF, Stoessel GFU, Peters Tj 1990 Metacarbonatites in the metamorphic series below the Semail ophiolite in the Dibba zone, northern Oman mountains. In Peters Tj et al. (eds). Ophiolite genesis and evolution of the oceanic lithosphere p 627-645. Kluwer, Amsterdam.

Zeigler URF, Stoessel GFU, Peters Tj 1991 Isotopic (Rb-Sr & Sm-Nd) and geochemical studies of the metamorphosed volcanic rocks in the metamorphic series below the Semail ophiolite in the Dibba zone (United Arab Emirates). Schweiz Mineral Petrogr Mitt 71: p 19-33.

Zeitler PK, Tahirkheli RAK, Naeser CW Johnson NM, Lyons J 1981 Preliminary fission track ages from the Swat valley, northern Pakistan. Geol Bull Uni Peshawar 13: p 23-29.

APPENDIX A : ELECTRON MICROSCOPE MINERALOGY AND THERMOBAROMETRY

A.1 PROBE SPECIFICATIONS AND OPERATING CONDITIONS

Minerals were analysed on 30 μm thick polished thin sections coated with a 20 nm thick layer of carbon to counteract charge build up. All analyses were conducted in the Department of Earth Sciences, Oxford, under the supervision of Norman Charnley, using a Cambridge Instruments Microscan 9 electron microprobe, with two wavelength dispersive spectrometers controlled by a Cambridge Instruments Microscan 9 DOS software package.

The electron microprobe was calibrated before each session to within 2σ error for the elemental array, largely the 'usual nine' of Si, Al, Ti, Fe, Mg, Na, K, Mn, and Ca. A ZAF correction was applied to each set of element concentrations measured to correct for differences between the matrix of the unknown analysed minerals and the standards.

The usual operating conditions were:

1. Beam diameter: 0.5 μm
2. Beam current: 40 nA
3. Accelerating potential: 20 kV

Under these operating conditions, the excitation volume of the target has a maximum diameter of 3 μm. Depending on the element, routine counting periods of between 10 and 30 seconds were used.

A.2 ERRORS IN ELECTRON MICROPROBE ANALYSIS

Electron microprobe measurements are based on the rate of production of electron beam induced X ray count rates characteristic to individual elements. The detection of an element and determination of its concentration in an analysed mineral grain therefore relies on the generation of a detectable X Ray: background count ratio during the counting period. The lowest concentration of specific elements (the limit of determination) that can be

quantitatively determined under normal operating conditions has been estimated by Potts (1987).

The precision of electron microprobe analyses presented below were determined using replicated analyses on a single specimen of DSDP basaltic glass (Potts et al. 1983). For elements present in significantly higher concentrations than their limit of determination, the coefficient of variation (CV = 100 [standard deviation/mean analysis]) was typically 0.5-2%. An estimation of the accuracy of the data by comparison between the Potts et al. (1983) results and the consensus results, from independent chemical analyses (Staudigel et al. 1979) of the same specimen of DSDP basaltic glass. For elements present in significantly higher concentrations than their limit of determination, the relative deviation (RD = 100 [measured consensus/consensus]) was typically 1-2%.

Furthermore, a numerical estimate of uncertainty in electron microprobe analyses can be derived from the variation in X ray counts at the characteristic peak for each element using the Cambridge Instruments Microscan 9 DOS software package. In this study, these error estimates have a 2σ variation of <2%.

Table A.1 Elemental oxide limits of determination in electron microprobe analysis under normal operating conditions (Potts 1987).

Oxide	Limit of determination (wt %)
SiO_2	0.05
TiO_2	0.05
Al_2O_3	0.06
Fe_2O_3	0.06
MnO	0.06
MgO	0.07
CaO	0.03
Na_2O	0.07
K_2O	0.04

A.3 THERMOBAROMETRIC ANALYSIS

A variety of techniques have been employed to constrain the PT conditions of formation of the metamorphic and igneous rocks studied during this work. Assemblages (prograde, peak and retrograde) showing petrographic evidence of equilibrium were identified and minerals were analysed by electron microscopy as described above. Where possible, adjacent mineral

grains were analysed. Alternatively, multiple analyses of matrix mineral grains were performed.

In order to minimise electron microprobe counting errors, replicate analyses of mineral grains were performed and averaged. Mineral chemistry analysis of 'typical' grains, to select those used in thermobarometric analysis, was undertaken using the plots shown in *Chapter Three*. Analysed grains with anomalous mineral chemistry were discarded from the thermobarometric datasets.

Two complementary techniques were used to compute PT values: conventional thermobarometry (eg the amphibole-garnet-plagioclase-quartz barometer of Kohn & Spear 1991) and the DOS program THERMOCALC (v 2.75; Holland & Powell 1998) that uses the self consistent thermodynamic dataset of Holland & Powell (1998). In conventional thermobarometry, mineral activity coefficients are calculated individually using the models prescribed in the references, whereas in THERMOCALC, the GUI program AX (Holland 1998), was used to compute mineral activities.

A.4 ERRORS IN THERMOBAROMETRIC ANALYSIS

Quantitative thermobarometry is subject to many errors, most fundamental of which is 'geological error' – the assumption that the selected mineral analyses represent grains that crystallised under equilibrium conditions. Other sources or error may include:

1. Analytical errors (described above). These originate from the analytical uncertainty of electron microprobe analyses.
2. Calibration errors. These are reaction specific and are greatly reduced when multiple equilibria are used, a major advantage of THERMOCALC.
3. Activity calculation errors. These generally form the bulk of final PT estimate errors.

All these sources of errors are propagated through the PT calculations and can be constrained to give a quantitative estimate of the errors, in terms of standard deviations, of any individual PT figure. THERMOCALC errors are stated at the $1<\sigma<2$ level and are typically ± 20-40°C and ± 1 kbar.

APPENDIX B : X RAY FLUORESCENCE ANALYSIS

B.1 XRF SPECIFICATION AND OPERATING CONDITIONS

All the analytical data presented in this thesis is the result of work carried out at the Department of Geology at the University of Bergen, Norway, under the guidance of Rolf Pedersen, and also in part by John Watson at the Open University (samples OM 63, OM 71, OM 3-1, OM 3-3, OM 3-5 and OM 3-7 only). Major and trace elements analyses were determined by X ray fluorescence (XRF) wave dispersive spectrometry (Philips PW 1404, Bergen; ARL 8420+, Open University) using glass beads and pressed-powder pellets respectively, with an accuracy of 1% for major elements and ± 10 ppm for trace elements (Philips PW 1404, Bergen) and as shown in tables B.1 and B.2 (ARL 8420+, Open University).

Table B.1, 2 Limits of determination for major and trace element XRF analysis, Open University.

Oxide	Limit of determination (ppm)
SiO_2	500
TiO_2	50
Al_2O_3	500
Fe_2O_3	50
MnO	50
MgO	300
CaO	100
Na_2O	400
K_2O	100
P_2O_5	100

Trace element	Limit of determination (ppm)
Sr	2
Rb	2
Y	2
Zr	2
Nb	1.5
Ba	12
Pb	5
Th	4
U	3
Sc	5
V	5
Cr	4
Co	2
Ni	3
Cu	3
Zn	3
Ga	3
Mo	2
As	5
S	50

% FeO was determined from total Fe (as Fe_2O_3) by standard titration methods (Bergen University) and total Fe was expressed as Fe_2O_3 (Open University).

The precision of XRF analyses conducted at the Open University is evaluated in Ramsey et al. (1995).

B.2 SAMPLE PREPARATION

For each sample, a minimum of 100 g of fresh, unaltered rock was washed twice in a sonic bath for 10 minutes, using deionised water that was discarded after each bath, and then dried for 24 hours in an oven at 50°C. Crushing of this material in a jaw crusher produced a coarse crush that was processed in a tungsten carbide swing mill to produce the powder used for XRF analysis. Major element analyses were performed on fused glass beads. Beads contained 1 g of rock powder and 5 g of $LiBO_4$ as flux. This resultant mixture was weighed, heated at 1000°C for 12 hours and reweighed to compute the Loss on Ignition (wt% of H_2O+). The dried rock powder and flux were then heated in a Pt-Au alloy crucible at 1200°C for 7.5 minutes and periodically homogenised before being poured into a bead mould and quenched in air. Bead moulds were then cleaned by boiling in a mixture of HCl and HF. Trace element analyses were performed on pressed powder pellets, composed of 10 g of rock powder and 1 ml of glue, mixed using an agate pestle and mortar. The pellets were produced in a hydraulic press subjected to 6 tonnes pressure for 30 seconds before being dried in an oven at 60°C for 12 hours.

B.3 ERRORS IN XRF ANALYSES

XRF measurements are based on the count rates of characteristic X rays emitted by specific elements, and the detection of any element and determination of its concentration therefore relies on the generation of a detectable X Ray: background count ratio during the counting period. Tables B.1 and B.2 show the limits of determination for the Open University ARL 8420+ XRF machine (Watson JS, pers. comm. 1999), and Potts (1987) defined standard limits of determination under normal XRF operating conditions. The accuracy of the Philips PW 1404 XRF machine, Bergen University, is within 1% for major elements and $\pm$ 10 ppm for trace elements (Pedersen RB, pers. comm. 1999).

B.4 ANALYTICAL DATA

Major and trace element analyses obtained by XRF spectroscopy during the course of this thesis and used for geochemical analysis and further techniques in *Chapter Three* and *Chapter Six* are presented in table 3.1 and 3.2 (samples OM 63, OM 71; *Chapter Three*) and tables 6.1, 6.2, 6.3 and 6.4 (granitoid samples, *Chapter Six*).

APPENDIX C : ISOTOPIC GEOCHEMICAL ANALYSIS

C.1 MASS SPECTROMETER SPECIFICATION AND OPERATING CONDITIONS

Rb-Sr and Sm-Nd isotopes were measured at the University of Bergen on a Finnigan MAT 262 RPQ mass-spectrometer. Sr was loaded on a double filament and analysed in static mode. Sm and Nd were loaded on a double filament and analysed in static and dynamic mode respectively. Nd isotopic ratios were corrected for mass fractionation using a $^{146}Nd/^{144}Nd$ ratio of 0.7219. Sm and Nd concentrations were determined using a mixed $^{150}Nd/^{149}Sm$ spike.

C.2 SAMPLE PREPARATION

For each sample, a minimum of 100 g of fresh, unaltered rock was washed twice in a sonic bath for 10 minutes, using deionised water that was discarded after each bath, and then dried for 24 hours in an oven at 50°C. Crushing of this material in a jaw crusher produced a coarse crush that was processed in a tungsten carbide swing mill to produce the powder used for Rb-Sr and Sm-Nd isotopic analysis. The chemical processing was carried out in a clean-room environment with HEPA filtered air supply and positive pressure, and the reagents were purified in two bottle Teflon stills. Samples were dissolved in a mixture of HF and HNO_3. Sr and Rb were separated by specific extraction chromatography using the method described by Pin et al. (1994). REE were separated by specific extraction chromatography using the method described by Pin et al. (1994). Sm and Nd were subsequently separated using a modified version of the method described by Richard et al. (1976).

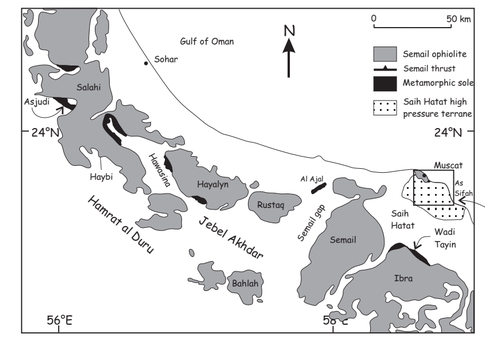
C.3 ERRORS IN ISOTOPIC ANALYSES

Repeated measurements of the NBS 987 Sr standard at the time of this study yielded an average of 0.710252 $\pm$ 19 (2σ) (n = 30); the accepted value is 0.710240. Repeated measurements of the Johnson and Matthey Nd_{203} oxide (batch #S819093A) at the time of this study yielded an average $^{143}Nd/^{144}Nd$ ratio of 0.511120 $\pm$ 10 (2σ) (n = 17).

ENCLOSURE 1:GEOLOGICAL MAP OF THE NORTHERN SAIH HATAT HIGH PRESSURE TERRANE, NE OMAN

JON COX, DEPARTMENT OF EARTH SCIENCES, OXFORD UNIVERSITY, APRIL 2000

Mapped in January-March 1997, February 1998 & May 1999 by the author with additional material from LeMetour et al. (1986) and Searle et al. (1994). The extent of the structural data indicates the coverage of this work. Based on 1:20,000 aerial photography courtesy of the Ministry of Petroleum & Minerals, Sultanate of Oman. Stratigraphic framework is after Glennie et al. (1974) and nomenclature of tectonometamorphic units and boundary shear zones after Searle et al. (1994). Boxes indicate locations of more detailed structural maps of specific areas.



AREA OF MAP COVERAGE

Enclosure 2

Enclosure 3

Figure 4.8

Line of section

GULF OF OMAN

Muttrah
Muscat
Sidab
Ruwi
Bustan
Qantab
Bander Jissah
Wadi Adai
Khawr Yiti
Khawr Yenkit
Bander Khuryan
Yenkit shear zone
Al Khuryan
Al Khuryan shear zone
Al Amarat
Wadi Mayh
Wadi Hulw
Al Wudya shear zone
As Sheik
Rija
As Sifah
Wadi Diqdah
To Quryat

STRATIGRAPHY

Maastrichtian - Palaeocene neoautochthonous shallow water limestones and dolomites; basal conglomerate contains ophiolitic and shelf carbonate clasts. Unconformably overlies all units of the Semail ophiolite allochthon

Semail ophiolite mantle sequence. Dominantly serpentinised harzburgites with subordinate dunite layers defining a strong mylonitic fabric, dipping ~45-50° NE

Ruwi mélange. Syndepositional foreland basin deposit, dominated by pelagic cherts, shales and lime muds with alkali and tholeiitic volcanic blocks. Displays a low grade (lawsonite-pumpellyite/carpholite) facies HP metamorphic assemblage

Hawasina cherts & turbidites. Hawasina basin pelagic sediments and associated tholeiitic to alkaline volcanics

Triassic Mahil Formation limestones and dolomites, typically fine grained,thinly bedded and grey

Permian Saiq Formation limestones & dolomites

Metabasic units within Saiq Formation. Mostly thin tholeiitic sills and volcanoclastic sequences

Amdeh quartzites. Thick sequence of white to grey quartzites and schists of Ordovician age (Lovelock et al. 1981)

Hijam dolomite. White to yellow stromatolitic dolomites and grey limestones of uncertain age (Proterozoic to Cambrian?)

STRUCTURAL FEATURES

- Geological boundary
- Anticlinal axis
- Synclinal axis
- Thrust fault
- Thrust fault reactivated as extensional fault
- Extensional fault
- Line of section
- Strike and dip
- Strike and dip of overturned unit
- Vertical dip
- Horizontal dip

TOPOGRAPHIC FEATURES

- 4WD track
- Paved road
- Village/Town
- Major wadi

0 4 km

N

NNW

Khawr Yiti

E

As Sifah

Deformation concentrated in N dipping, S facing shear zones, parallel to regional stretching lineation and allochthon transport direction

Isoclinally folded NE verging deformation under blueschist-eclogite facies conditions and subsequent large scale nappe formation at lower, greenschist (?) metamorphic grades

TRUE SCALE, SCALE AS MAIN MAP

GEOLOGICAL MAP OF RUWI AREA, NORTHERN SAIH HATAT HIGH PRESSURE TERRANE, NE OMAN

JON COX, DEPARTMENT OF EARTH SCIENCES, OXFORD UNIVERSITY, APRIL 2000

Mapped in February-March 1997 by the author with additional supplementary material from El-Shazly (1994) and Searle et al. (1994). The extent of the structural data indicates the coverage of this work. Based on 1:20,000 colour aerial photography courtesy of the Ministry of Petroleum & Minerals, Sultanate of Oman. Stratigraphic framework is after Glennie et al. (1974) and nomenclature of tectonometamorphic units and boundary shear zones after Searle et al. (1994).

Tertiary ophiolitic/carbonate sandstone

Maastrichtian - Palaeocene neoautochthonous shallow water limestones and dolomites; basal conglomerate contains ophiolitic and shelf carbonate clasts. Unconformably overlies all units of the Semail ophiolite allochthon

Semail ophiolite mantle sequence. Dominantly serpentinised harzburgites with subordinate dunite layers defining a strong mylonitic fabric, dipping ~45-50° NE

Ruwi mélange. Syndepositional foreland basin deposit, dominated by pelagic cherts, shales and lime muds with alkali and tholeiiticvolcanic blocks. Displays a low grade (lawsonite-pumpellyite/carpholite) facies HP metamorphic assemblage

- Marly slate
- Banded marble
- Mélange
- Thin bedded limestone
- Lawsonite schist
- Carpholite schist
- Metabasaltic blocks
- Quartz chlorite schist

Haybi mélange complex serpentinites (?)

Hawasina cherts & turbidites. Hawasina basin pelagic sediments and associated tholeiitic to alkaline volcanics

Sahtan group limestoness

Triassic Mahil Formation limestones and dolomites, typically fine grained,thinly bedded and grey

Permian Saiq Formation limestones & dolomites

Metabasic units within Saiq Formation. Mostly thin tholeiitic sills and volcanoclastic sequences

Amdeh quartzites. Thick sequence of white to grey quartzites and schists of Ordovician age (Lovelock et al. 1981)

Hijam dolomite. White to yellow stromatolitic dolomites and grey limestones of uncertain age (Proterozoic to Cambrian?)

STRUCTURAL FEATURES

- Geological boundary
- Anticlinal axis
- Synclinal axis
- Thrust fault
- Thrust fault reactivated as extensional fault
- Extensional fault
- Line of section
- Strike and dip
- Strike and dip of overturned unit
- Vertical dip
- Horizontal dip

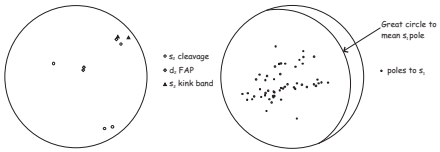
TOPOGRAPHIC FEATURES

- 4WD track
- Paved road
- Village/Town
- Major wadi

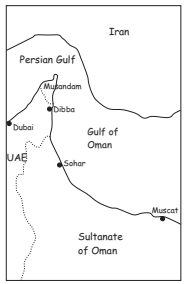
0 1000 m

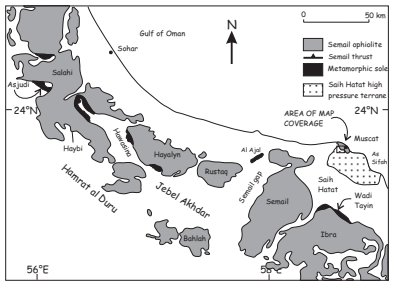
N

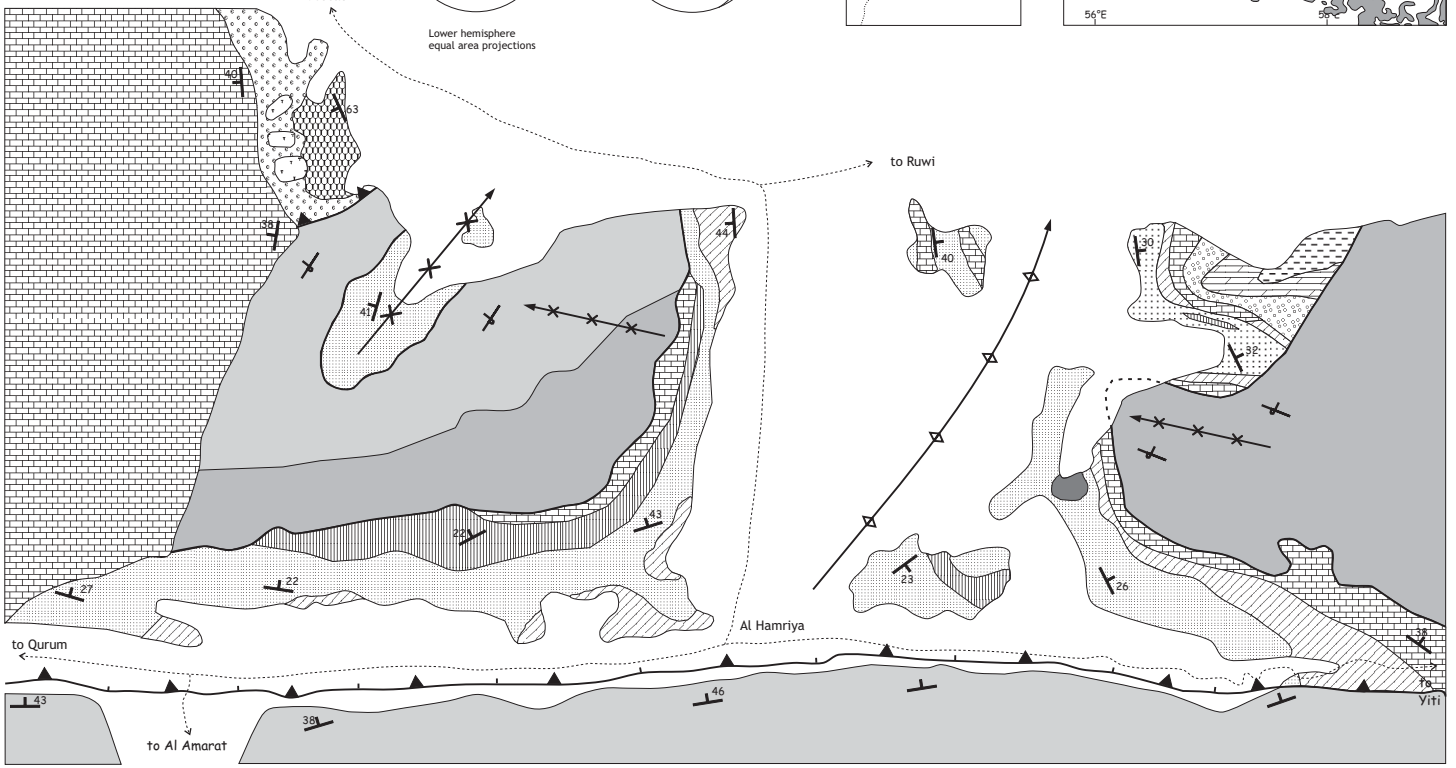
Structural Orientation

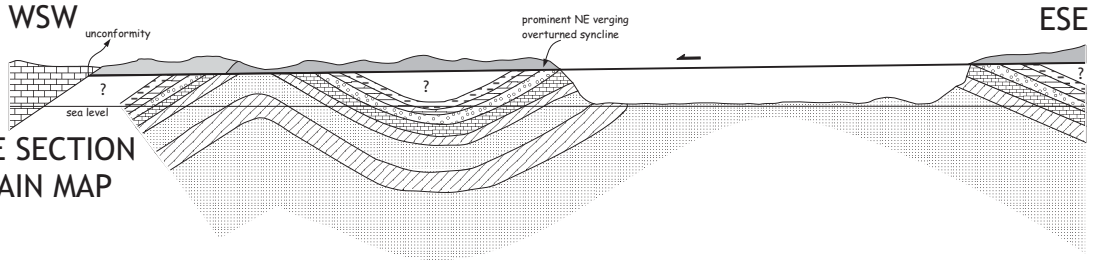


Lower hemisphere equal area projections









TRUE SCALE SECTION
SCALE AS MAIN MAP

ENCLOSURE 3: GEOLOGICAL MAP OF WADI MAYH, NORTHERN SAIH HATAT HIGH PRESSURE TERRANE, NE OMAN

JON COX, DEPARTMENT OF EARTH SCIENCES, OXFORD UNIVERSITY, APRIL 2000

Mapped in January-March 1997, February 1998 by the author with additional material from LeMetour et al. (1986) and Searle et al. (1994). The extent of the structural data indicates the coverage of this work. Based on 1:20,000 aerial photography courtesy of the Ministry of Petroleum & Minerals, Sultanate of Oman. Stratigraphic framework is after Glennie et al. (1974) and nomenclature of tectonometamorphic units and boundary shear zones after Searle et al. (1994).

STRATIGRAPHY

Maastrichtian - Palaeocene neoautochthonous shallow water limestones and dolomites; basal conglomerate contains ophiolitic and shelf carbonate clasts. Unconformably overlies all units of the Semail ophiolite allochthon

Semail ophiolite mantle sequence. Dominantly serpentinised harzburgites with subordinate dunite layers defining a strong mylonitic fabric, dipping ~45-50° NE

Ruwi mélange. Syndepositional foreland basin deposit, dominated by pelagic cherts, shales and lime muds with alkali and tholeiitic volcanic blocks. Displays a low grade (lawsonite-pumpellyite/carpholite) facies HP metamorphic assemblage

Hawasina cherts & turbidites. Hawasina basin pelagic sediments and associated tholeiitic to alkaline volcanics

Triassic Mahil Formation limestones and dolomites, typically fine grained,thinly bedded and grey

Permian Saiq Formation limestones & dolomites

Metabasic units within Saiq Formation. Mostly thin tholeiitic sills and volcanoclastic sequences

Quartz-phengite schists (Amdeh quartzites?). Thick sequence of white to grey quartzites and schists of Ordovician age (Lovelock et al. 1981)

Calcite-dolomite-phengite-quartz schists, derived from Saiq Formation limestones & dolomites.. Equivalent to similar lithologies exposed at As Sifah?

Hijam dolomite. White to yellow stromatolitic dolomites and grey limestones of uncertain age (Proterozoic to Cambrian?)

STRUCTURAL FEATURES

Geological boundary

Anticlinal axis

Synclinal axis

Thrust fault

Thrust fault reactivated as extensional fault

Extensional fault

Line of section

Strike and dip

Strike and dip of overturned unit

Vertical dip

Horizontal dip

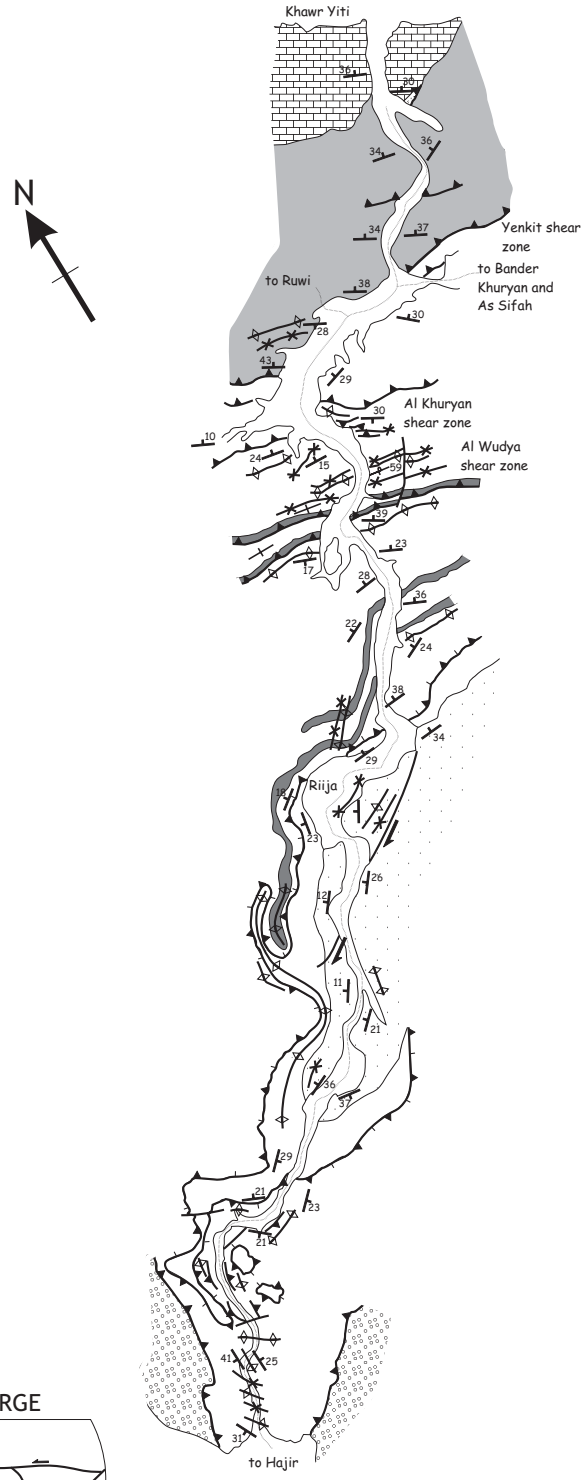
0 1000 2000 m

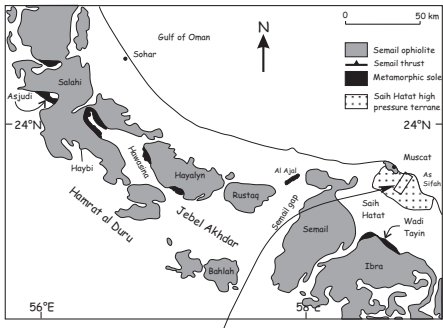
TOPOGRAPHIC FEATURES

4WD track

Village/Town

Major wadi

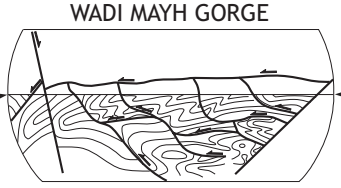




COVERAGE OF ENCLOSURE 3



WADI MAYH GORGE



TRUE SCALE SECTION, SCALE AS MAIN MAP

